Mesoscale Characteristics of Cumulus Convection
A Mesoscale Budget Study of Convection in the NHRE Network

By
Alan L. McNab

Department of Atmospheric Science
Colorado State University
Fort Collins, Colorado

Research report supported by the National Science Foundation under
Grant OCD72-01406.
Principal investigator: A.K. Betts
February 1976

Colorado State University

Department of Atmospheric Science

Paper No. 242

MESOSCALE CHARACTERISTICS OF CUMULUS CONVECTION

A Mesoscale Budget Study of Convection in the NHRE Network

by

Alan McNab

Research report supported by the

National Science Foundation

under Grant OCD72-01406

(Principal Investigator A. K. Betts)

Department of Atmospheric Science

Colorado State University

Fort Collins, Colorado

80523

February 1976

Atmospheric Science Paper No. 242

ABSTRACT

MESOSCALE CHARACTERISTICS OF CUMULUS CONVECTION

Water and energy budget descriptions of four broad classifications of summertime, cumulus convection occurring over the National Hail Research Experiment (NHRE) area are calculated from NHRE rawinsonde data. The convection classifications are based on radar and precipitation data.

A budget equation designed for use with mesoscale data from the NHRE area is derived. The equation uses a normalized pressure coordinate to facilitate calculations at the sloping lower boundary. The environmental variables appear as functions of horizontal position and the time and space averaging scales are made explicit in order to aid the interpretation of the budget results. The change of cloud storage term (usually neglected) is retained for use during intervals of rapid convection development.

The budget calculations are based on data for 39 intervals (about three hours long) occurring over 14 days. The data processing takes into account downwind sonde drift and time differences in the data due to sonde rise time and launch time differences.

The presence or absence of radar echoes and/or precipitation is used to classify the convection as (1) weak, suppressed, (2) weak, developing, (3) moderate, (4) precipitating. The weak, suppressed average budgets are generally similar to budgets calculated for "undisturbed" synoptic situations. The NHRE vertical velocities, however, are several times larger than the earlier undisturbed values. The weak, developing average budget shows the importance of retaining the change of cloud storage term in the budget equation. The moderate and precipitating average budgets show an introduction of relatively dry air into the subcloud layer. The precipitating convection also produces a sink of moist static

energy in the subcloud layer. In general, the fluxes show a systematic variation with the trend of the convective classification.

A cloud model is used to show that weak, suppressed convective fluxes can be expressed as the product of a single convective mass flux times a cloud-environment difference of s_ℓ or h. The water and energy transports are shown to be approximately closely coupled.

Another cloud model is used to approximate the change of cloud storage. This term is shown to be as large as the convective flux terms during periods of rapid cumulus convection development.

General conclusions are drawn on the quantity and quality of the data needed to generate a useful mesoscale convective budget.

ACKNOWLEDGEMENTS

The author expresses his sincere appreciation to Dr. Alan K. Betts for his valuable suggestions and kind encouragement. The author is also indebted to Professors Lewis Grant, David Krueger, and Wayne Schubert for their services on the candidate's committee. The author thanks Dr. Stephen Cox for kindly supplying the radiation program used in this research.

Many thanks go to Richard Miller who assisted in much of the programming, to Pauline Martin who did the data reduction, and to Susan Kuehl who typed the manuscript. The author also wishes to thank his wife, Linda, for her continuous encouragement.

The author is indebted to the National Hail Research Experiment personnel who supplied most of the data used in this research.

This research was supported by the Global Atmospheric Research Program, National Science Foundation, Grant OCD72-01406; and with the additional support of the National Science Foundation Grant No. ERT71-01885. However, any opinions, findings, conclusions or recommendations expressed herein are those of the author and do not necessarily reflect the views of the National Science Foundation.

TABLE OF CONTENTS

TABLE OF CONTENTS - Continued

LIST OF TABLES

LIST OF FIGURES

LIST OF FIGURES - Continued

I. INTRODUCTION

1. Statement of the Problem

The influence of cumulus convection extends well beyond the time and space scales associated with the immediate environment of an individual cumulus cloud. The combined action of all the clouds in a given large scale area produces an important contribution to the large scale circulation. Considerable research has been focused on quantitatively describing cumulus convection in terms of this input to larger scales of motion.

The basic problem involved in obtaining this type of large scale description of convection is the impracticality of directly measuring the total convective input into the larger scale. This problem can be overcome by using a budget approach to make the desired "measurements" indirectly. A budget calculation for a large, given volume is simply the algebraic sum of the measured inflow, outflow, and storage terms of a chosen quantity set equal to a source term plus a contribution due to flows that are not resolved by the measurements. The unresolved flows are assumed to be due to the cumulus convection occurring in the given volume.

The general objective of this thesis is to use a budget approach, as mentioned above, to describe summertime cumulus convection occurring over the National Hail Research Experiment (NHRE) data area. Four specific problems are addressed within the framework of this general objective.

First, a general budget equation designed for use with midlatitude, continental, mesoscale data (see diagram of NHRE area, Fig. 1) will be derived. The equation deals with a sloping lower boundary, pronounced

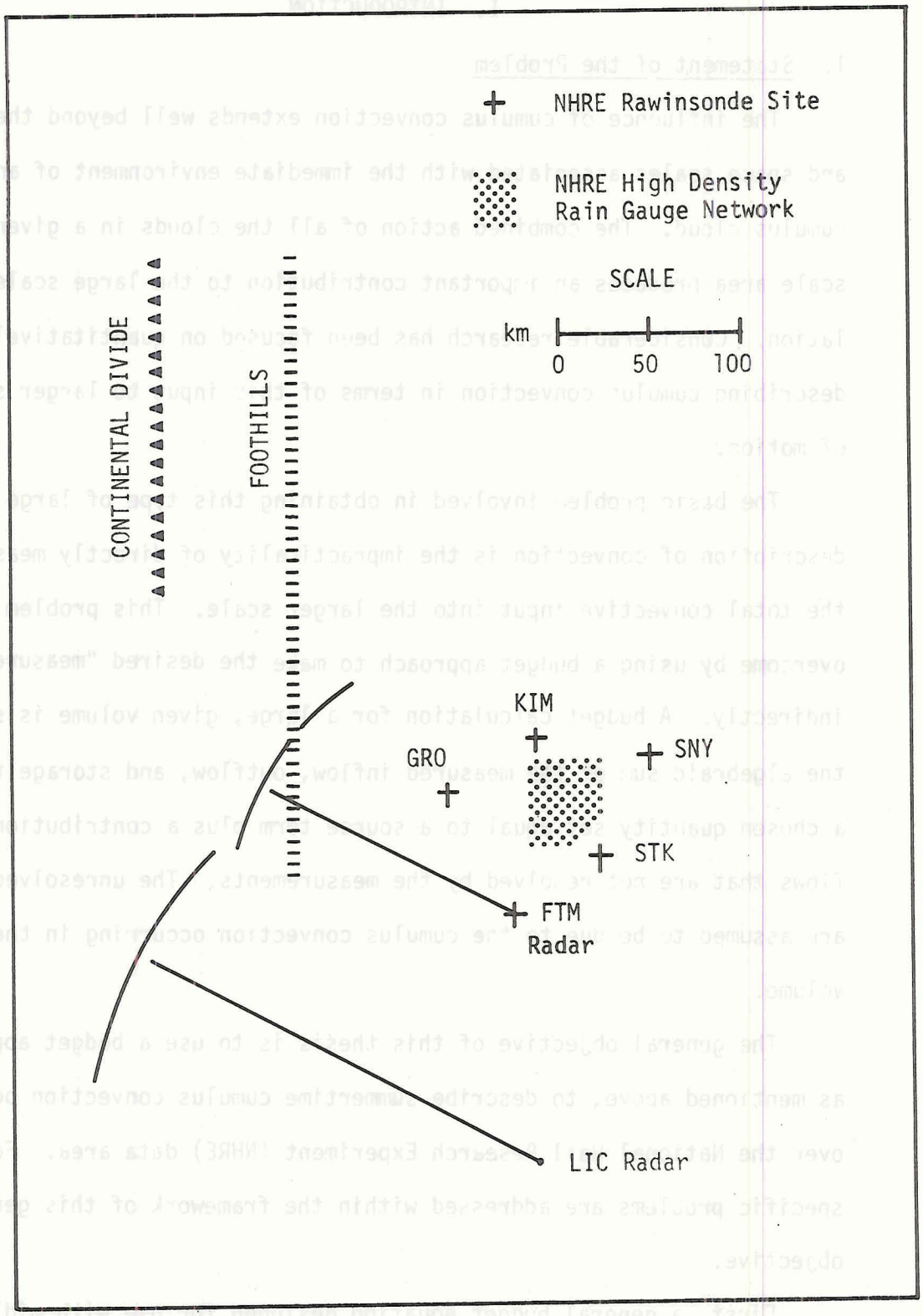

Figure 1. National Hail Research Experiment (NHRE) Data Area

horizontal gradients in the data, and the possibility of rapid cumulus convection development. Also, the time and space averaging scales are made explicit in order to aid the interpretation of the budget results.

Second, the budget equation is used to calculate the cloud transfer properties of the convection for a variety of mesoscale conditions. The mesoscale environment of the convection over the NHRE area has considerably different characteristics (sharper horizontal gradients and time change, for example) than the environments of most of the previous budget studies. Consequently, this budget calculation will provide a useful addition to the current store of budget results.

Third, the calculated descriptions of cumulus convection (the cloud transfer properties) will be stratified and averaged according to a simple radar description of the convection. The radar classification of convection used in this thesis is more detailed than most of the convection descriptions used in other budget studies. This additional detail considerably helps in the interpretation of the budget results.

Fourth, a consistent and reasonable interpretation of the budget calculations is presented in terms of simplified models. Although the value of this interpretation is directly tied to the choice of the model, the use of a model is a key step in understanding the relations between cumulus convection and larger scale circulations.

2. Historical Background

Many researchers have attempted to quantitatively assess the role of cumulus convection on larger scale circulations by using a budget approach. Reed and Recker (1971), Gray (1972), and Yanai, Esbensen and Chu (1973) have used synoptic scale, tropical, oceanic data averaged over many days

for such studies. Pearce (1968), Augstein, et al (1973), Holland and Rasmusson (1973), Nitta and Esbensen (1974), and Nitta (1975) have presented budget studies using Atlantic data gathered (except for Pearce) during ATEX and BOMEX. The ATEX and BOMEX data used in these last four studies were taken on a scale of 750 km and 500 km, respectively, over tropical ocean areas. The results were averaged over one to five days. Williams (1970) used a compositing technique to study tropical cloud clusters on a scale of about 400 km. Ninomiya (1974) did a 200 km mesoscale budget study using data from an oceanic network located at 30°N near Japan. Recently, Lewis (1975) presented a budget study using data from a 180^2 km^2 continental area. These studies clearly point out the importance of convection as a vertical transport mechanism for heat and moisture. The calculations by Williams (1970), Reed and Recker (1971), and Pearce (1968) suggest that cumulus clouds also transport vorticity. Holland and Rasmusson (1973) present a momentum budget. However, the eddy vorticity and momentum transports are noted to contain considerable error. A summary of previous budget studies is presented in Appendix I.

The first problem this thesis addresses is the derivation of a budget equation suitable for use in a mid-latitude, mesoscale area. The above studies were based on budget equations in which the resolved or large scale components were expressed in terms of area average values. The unresolved components were considered deviations from the area averages. Several authors included short remarks that suggested the assumptions relating the measured data to the required averages. Augstein, et al (1973) and Reed and Recker (1971) state that their analysis procedure implies horizontally linear changes of the mass flux as well as of other meteorological values. Yanai, et al (1973) point out that their data

region could be too large to properly represent the required averages because of substantial horizontal variations of large scale parameters and because of the existance of short-lived mesoscale convection regions. Ninomiya (1974) remarked that he was using mesoscale data because cumulus clouds are not always distributed uniformly over a large area. Such remarks are particularly pertinent to this thesis, because the NHRE data have strong horizontal gradients and these gradients are explicitly retained and discussed in the budget derivation in Chapter II.

The second problem addressed in this thesis is the calculation of cloud-transfer properties of the convection within the NHRE data network for a variety of mesoscale conditions. Most of the previously cited budget studies were based on circulations characteristic of low latitude, oceanic regions. Cho and Ogura (1974) state that more budget studies are needed to increase the confidence in the conclusions drawn from previous studies. Yanai et al (1973) stress the need not only for more diagnostic budget studies but also for such studies to be carried out on smaller (they suggest 300 km) areas. Both this study and the study by Lewis (1975) use data taken over mid-latitude, continental, mesoscale areas (the NHRE and NSSL data networks, respectively). These data are quite different than the previously used low latitude, oceanic data. Further, the NHRE data used in this thesis are characteristic of convection periods considerably different than the prefrontal squall line period used by Lewis (1975). The results of the budget calculations and their interpretations (see Chapter V and VI) will consequently be a useful addition to the current store of budget results.

The third problem considered in this research is the averaging of the calculated cloud-transfer properties based on radar descriptions of the

convection. In most of the previously cited studies, the calculated convective contributions to the mean flow were grouped in terms of some general characteristics of the cumulus clouds. In the largest scale studies, the convection was mostly classified in a way that directly corresponded to the synoptic situation, that is, disturbed or undisturbed conditions. Reed and Recker (1971) and Cho and Ogura (1974) discussed the convection in terms of eight sectors of a composite, tropical large scale wave disturbance. Holland and Rasmusson (1973) and Augstein, et al (1973) presented results only for periods when convection was weak or absent. Williams (1970) and Gray (1972) used ATS-3 satellite data to classify the convection in terms of six categories of cloud clusters. Only Ninomiya (1974) and Lewis (1975) were able to use a more detailed description of convection supplied by radar data. The radar description of convection used in this thesis is slightly more detailed than that used by Ninomiya (1974). Lewis' (1975) radar description of convection is quite specific because he deals with only a single case study of a squall line.

The fourth problem approached in this thesis is the presentation of a consistent and reasonable interpretation of the budget calculations in terms of simplified models. The need to interpret cumulus budget studies in terms of conceptual convective transport models was recently emphasized by Betts (1975). Pearce (1968), Gray (1972) and Augstein, et al (1973) used extremely idealized convection models to demonstrate that their calculated eddy transports of moisture, energy and vorticity could be reasonably accomplished by cumulus clouds. Ogura and Cho (1973) and Nitta (1975) used a spectral cloud ensemble model developed by Arakawa and Schubert (1974) to interpret budget calculations in terms of model cloud populations.

Lewis (1975) used a similar model to interpret his results. Betts (1975) interpreted some of the BOMEX data for periods of weak convection by using a single cloud type model that entrains and detrains at all levels during its life cycle. The same model is used in this research to interpret weak convection results over the NHRE area. A second simple model is used to show that the cloud storage term of the budget equation is important in cases of developing convection.

II. BUDGET EQUATION

1. Frequently Used Forms and Terminology

In order to facilitate later comparisons of results in this thesis with those found in the literature and in order to establish a point of reference for the budget equation used in this thesis, a frequently used form of a budget equation will be presented. This short derivation is mainly based on a presentation by Yanai (1971), and is particularly useful in pointing out the role convection plays in influencing the large scale circulation. Let

χ = any scalar

Q = source/mass of χ

The Lagrangian and Eulerian forms of a budget equation for χ are, respectively:

$$\frac{d\chi}{dt} = Q$$

$$\frac{\partial \rho\chi}{\partial t} + \nabla\cdot\chi\rho\vec{V} + \frac{\partial \chi\rho w}{\partial z} = \rho Q$$

Next, define an area averaging operator ($\overline{\quad}$) that will be used over a horizontal area which is large enough to contain the ensemble of clouds but is small enough so that the area can still be viewed as a fraction of the large scale motion. Applying this operator and denoting deviations from the average by primes we obtain:

$$\frac{\partial \overline{\rho\chi}}{\partial t} + \nabla\cdot\overline{\chi\rho\vec{V}} + \frac{\partial \overline{\chi}\,\overline{\rho w}}{\partial z} = \rho\overline{Q} - \frac{\partial \overline{\chi'(\rho w)'}}{\partial z} \qquad (1)$$

$\rho\overline{Q} - \frac{\partial \overline{\chi'(\rho w)'}}{\partial z}$ is called the apparent source of χ and $\overline{\chi'(\rho w)'}$ is the vertical eddy flux of χ.

Yanai (1971) summarizes how the eddy flux term can be related to the cumulus convection:

Let χ and ρw have the average values χ_c and $(\rho w)_c$ inside cumulus clouds and $\tilde{\chi}$ and $\widetilde{(\rho w)}$ in the environment (clear air). A fraction, γ, of the horizontal area is covered by cumulus clouds. Then

$$\overline{\chi} = \gamma \chi_c + (1 - \gamma)\tilde{\chi} \qquad \overline{\rho w} = \gamma(\rho w)_c + (1 - \gamma)\widetilde{(\rho w)}$$

For quantities such as temperature and static energy, $\overline{\chi} = \gamma(\chi_c - \tilde{\chi}) + \tilde{\chi} \simeq \tilde{\chi}$. However, $\overline{\rho w} \neq \widetilde{\rho w}$. Define a cloud mass flux, M_c, as follows $M_c = \gamma(\rho w)_c$. Then

$$\overline{\chi'(\rho w)'} \simeq M_c(\chi_c - \tilde{\chi}). \qquad (2)$$

That is, the eddy flux term is directly related to the cloud mass flux and the excess value of χ_c above the environmental value $\tilde{\chi}$.

The researchers mentioned in section 2 of Chapter I carried out budget calculations using this or very similar approaches. The interpretation of their budget calculations is closely connected to two types of averages and corresponding deviations. The first kind of averaging is obviously the area average defined by the bar ($\overline{\quad}$) operator. The second is a time average. Even though the time average does not appear explicitly, substantial time averaging is used when data are inserted into Eq. 1.

A more explicit treatment of the time averaging would be of use for two reasons. First, in this and the previously cited research a budget equation is being used to study convection, and an important aspect of convection is its transience. Equations 1 and 2, however, contain very little explicit comment on the transience of the source term or eddy flux term. Second, all the average terms on the LHS of Eq. 1 are also functions of time. The treatment of this time dependence and its relation to the cloud time scale does not readily follow from the formalism of Eq. 1. Fraedrich (1973, 1974), Arakawa and Schubert (1974), and Betts (1975) have commented on the importance of distinguishing the average and perturbation time scales in the interpretation of budget calculations.

A slight change in the area averaging procedure used in Eqs. 1 and 2 would also be useful. As long as there is no strong horizontal gradient of the environmental values of χ, χ' and $(\chi_c - \tilde{\chi})$ can be closely related to an excess value of χ in a cloud compared to some environmental value of χ near the cloud. This physical interpretation of χ' or $(\chi_c - \tilde{\chi})$ is somewhat obscured in the presence of a strong horizontal gradient of χ. The problem is illustrated schematically in Fig. 2.

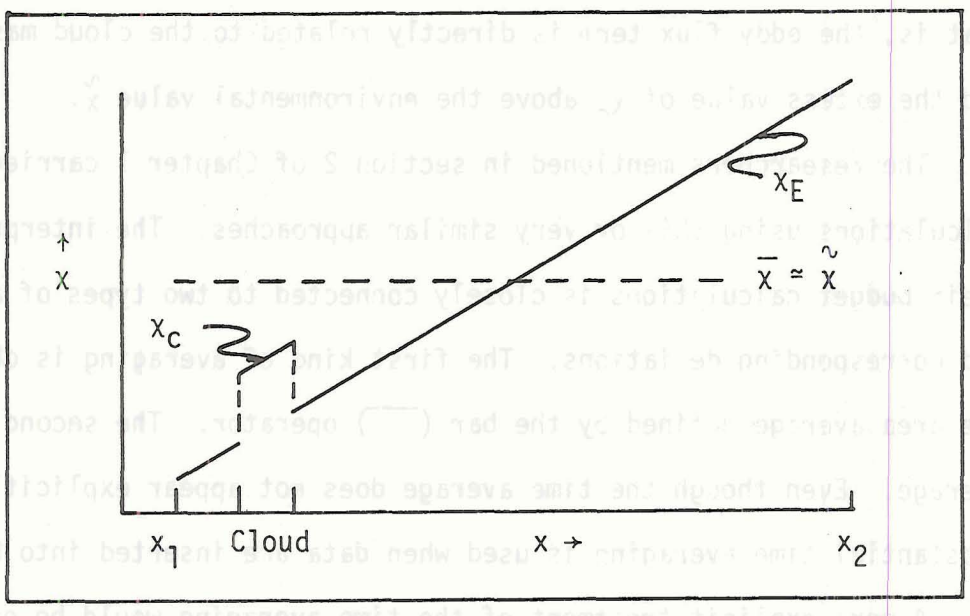

Figure 2. Schematic Representation of χ_E With a Strong Horizontal Gradient.

The quantities $\bar{\chi}$ and $\tilde{\chi}$ are single constant values determined for the entire averaging area ($x_2 - x_1$ in Fig. 2). The quantities χ' and $\chi_c - \tilde{\chi}$ are deviations from $\bar{\chi}$ or $\tilde{\chi}$. They are not directly related to a simple cloud-local environment difference, $\chi_c - \chi_E$ ($\chi_E \equiv$ environmental values of χ).

A formulation of a budget equation that addresses the above problems is presented in the next section. The time averaging is made explicit.

The simple concept of a cloud having an excess value of χ compared to the local environment is retained in the presence of horizontal gradients of χ. Additionally, a general vertical coordinate is used to facilitate calculations over the sloping lower boundary of the data volume used in this research.

2. Budget Formulation Used in This Thesis

A. Total Budget

It is often not convenient to use pressure or height as a vertical coordinate when the lower boundary is not level. In Chapter III, a normalized pressure vertical coordinate will be used in order to make the sloping lower boundary of the NHRE area a coordinate surface. The following derivation will be kept slightly more general by using an arbitrary vertical coordinate, s. Following Kasahara (1974), the Eulerian form of a budget equation for a scalar, χ, in an x, y, s coordinate system is

$$\frac{\partial}{\partial t}\left(\rho\chi \frac{\partial z}{\partial s}\right)\Big|_s + \nabla_s\cdot\left(\rho\chi \frac{\partial z}{\partial s} \vec{V}\right) + \frac{\partial}{\partial s}\left(\rho\chi \frac{\partial z}{\partial s} \dot{s}\right) = \rho \frac{\partial z}{\partial s} Q$$

$\frac{\partial}{\partial t}(\ )\big|_s$ and $\nabla_s\cdot(\ )$ are the standard operators except s is held constant. $\dot{s}$ is the vertical velocity in the s coordinate system. $\vec{V}$ is the horizontal velocity vector with components u, v in the x, y directions, respectively. ρ and z are the usual density and height above sea level. Q is a source per unit mass of the scalar quantity χ.

Even though we want to deal with the effects of convection, we will use the hydrostatic approximation. This is reasonable because the time and space scales of non-hydrostatic effects are probably very much smaller than the scale which we will eventually integrate over. With this approximation, the budget equation becomes

$$\frac{\partial}{\partial t}\left(\frac{\partial p}{\partial s}\chi\right) + \nabla_s\cdot\left(\chi \frac{\partial p}{\partial s} \vec{V}\right) + \frac{\partial}{\partial s}\left(\chi \frac{\partial p}{\partial s} \dot{s}\right) = \frac{\partial p}{\partial s} Q \qquad (3)$$

The $\frac{\partial p}{\partial s}$ factor is simply related to the mass between two adjacent s surfaces. If $\chi = 1$, $Q = 0$ we have a budget equation for mass, that is, the continuity equation. In the following development, $\frac{\partial p}{\partial s}$ and $\vec{V}$ are often considered together because $\frac{\partial p}{\partial s}\ \vec{V}$ has the straightforward interpretation of a horizontal mass flux.

As it now stands, Eq. 3 is valid for any arbitrary "point". In the previous derivation (section 1) an area averaging bar operator was applied to this equation. However, this procedure causes problems when there is an average horizontal gradient of the data. Instead, we proceed by remembering the budget calculation is to be valid for the particular volume for which we have data. The specific extent of this volume will be discussed later; for now we simply integrate over a horizontal area, A, and a depth from s_H to s. The lower limit of integration, s_H, can be considered as either the next lower s surface or it can be considered as the lower boundary. In the latter case, s_H is generally not a coordinate surface and will change as a function of position and time. The integrated equation is

$$\int_A \int_s \frac{\partial}{\partial t}\left(\frac{\partial p}{\partial s}\ \chi\right) ds\ dA + \int_A \int_s \nabla_s \cdot \left(\chi\ \frac{\partial p}{\partial s}\ \vec{V}\right) ds\ dA + \int_A \left[\left(\chi\ \frac{\partial p}{\partial s}\ \dot{s}\right)_s - \left(\chi\ \frac{\partial p}{\partial s}\ \dot{s}\right)_{s_H}\right] dA = \int_A \int_s \frac{\partial p}{\partial s}\ Q\ ds\ dA \tag{4}$$

We have three choices concerning the final form of Eq. 4, none of which would matter if we had four dimensional, correct, analytic data. The first decision concerns the s integration - it can be performed either before or after the $\frac{\partial}{\partial t}$ and $\nabla_s \cdot$ operators are applied. If it is brought inside the $\frac{\partial}{\partial t}$ and $\nabla_s \cdot$ operators, the terms generated because s_H is a function of x, y and t, will cancel with the $\chi\ \frac{\partial p}{\partial s}\ \dot{s}_H$ term. Finite

difference forms for both $\frac{\partial}{\partial t}\left(\int_s \frac{\partial p}{\partial s}\,\chi\,ds\right) + \nabla_s\cdot\left(\int_s \chi\,\frac{\partial p}{\partial s}\,\vec{V}\,ds\right)$ and $\int_s \frac{\partial}{\partial t}\left(\frac{\partial p}{\partial s}\,\chi\right) ds + \int_s \nabla_s\cdot \chi\,\frac{\partial p}{\partial s}\,\vec{V}\,ds$ have been tried, and neither seemed to produce better results than the other. In the following, we will keep the s integration outside of the $\frac{\partial}{\partial t}$ and $\nabla_s\cdot$ operators.

The second choice concerns the time derivative. A time integration could be performed before the volume integration is carried out. This method requires instantaneous values of $\frac{\partial p}{\partial s}\,\chi$ at the beginning and end of the integration interval and time average values of the second and third flux divergence terms in Eq. 4. If the time integration is not performed, instantaneous values of the flux divergences are required. The measurement of the divergence of the flux of χ is more susceptible to error than the measurement of χ and, therefore, averaging the divergence terms instead of χ could help reduce the error. In addition to these computational advantages, the time integration helps to make the data averaging time scale explicit and will later emphasize the transient nature of the convective quantities. The time integration approach is used in this research.

The third choice in Eq. 4 concerns whether or not the term $\int_A \nabla_s\cdot\left(\chi\,\frac{\partial p}{\partial s}\,\vec{V}\right) dA$ is to be transformed by use of the divergence theorem. The proper choice is related to the particular configuration of the data network used in the budget calculations. In this research, the data network is composed of five rawinsonde sites located at the corners of a pentagon about 100 km across (see Chapter III and Fig. 4). Many researchers have taken the approach of changing the term into a line integral. Once this is done, the area being considered is strongly tied

to the plane figure formed by connecting the data points with straight lines. The problem with using this approach is that the rising sondes trace out a volume that is substantially tilted because of the downwind sonde drift. A vertically standing volume cannot be constructed such that the data measurements (or even interpolated measurements) occur along the walls of the volume. As previously mentioned, the line integral approach is closely tied to having the measurements represent perimeter values of the flux of χ. In this thesis the line integral approach is not used; the area integration is retained. This is reasonable because the interpolated data do not represent measurements taken on the sides of a given well defined volume, but rather, are more representative of an area average. It is not necessary to precisely define the area of integration that appears in Eq. 4 if the integrands vary linearly across the area. That this is true can be seen by considering a linear function $H = ax + by + c$. The area integral of this function per unit area is given by

$$\left[\int_0^x \int_0^y H \, dx \, dy\right] / \left[\int_0^x \int_0^y dx \, dy\right] = H\left(\frac{x}{2}, \frac{y}{2}\right).$$

The problem of defining both the size and location of the area has been replaced by the problem of just defining the location (midpoint) of the area. In this thesis, not only will the area integrations be retained, but the integrands also will be assumed to vary linearly across the integration area. This procedure will be discussed further in section 3 and also in Chapter III.

In the above derivation of the budget equation, Eq. 4, we have retained the time and space integrations explicitly, chosen the order of differentiations and integrations, and retained an area integration

instead of using the divergence theorem. This procedure has been motivated by the desire to obtain a budget equation which emphasizes the time averaging of all the budget terms and also facilitates the introduction and discussion of data containing horizontal gradients. A general vertical coordinate and lower boundary have been used in order to cope with the problem of a lower boundary that is not level. Equation 4 is a budget of the total flow of χ. We next separate out the cumulus contribution to this budget.

B. Budget Decomposition

The idea that clear air (environmental) quantities vary smoothly over the mesoscale data network, and that the major perturbations to these background fields are caused by small, localized disturbances related to convection is one of the main assumptions of this thesis. The budget formulation presented in section 1, following Yanai (1971) and several others, makes use of this idea when the characteristic $\tilde{\chi}$ and χ_c quantities were introduced. In this research, however, the environmental quantities (corresponding to $\tilde{\chi}$) are explicitly allowed to vary linearly in the horizontal directions.

Conceptually, divide the area of integration, A, appearing in budget equation 4 into A_E and $A_c = \sum_i^N A_i$. The environmental area, A_E, is the area where the data will later (section 3, and Chapter III) be assumed to vary linearly across the network. The A_i are the areas affected by convection. They include both updraft and downdraft areas and occur both in clouds and below clouds. A_E and the A_i are functions of time and height. In the lower portion of the subcloud layer, the A_i should also include areas of strong dry convection. Applying this area decomposition and the time

integration mentioned in section 2a, to Eq. 4, we examine each resulting term. The notation $]_{t_1}^{t_2}$ means evaluation at the limits t_1, t_2. The first term becomes

$$\int_A \int_s \int_{t_1}^{t_2} \frac{\partial}{\partial t}\left(\frac{\partial p}{\partial s}\chi\right)dt\ ds\ dA = \int_{A_E} \int_s \left[\left(\frac{\partial p}{\partial s}\chi\right)_E ds\ d A_E\right]_{t_1}^{t_2} + \int_{A_c} \int_s \left[\left(\frac{\partial p}{\partial s}\chi\right)_c ds\ dA_c\right]_{t_1}^{t_2}$$

Recalling that we plan to linearly approximate the observed environmental data, we extend the environmental integration (first term on the RHS) over the entire area A ($A = A_E + A_c$) by symbolically assigning linearly interpolated values to the integrand $\left(\frac{\partial p}{\partial s}\chi\right)_E$ in the cloud areas where it was not previously defined. The same term is subtracted in the integration over A_c.

$$\int_A \int_s \int_t \frac{\partial}{\partial t}\left(\frac{\partial p}{\partial s}\chi\right)dt\ ds\ dA = \int_A \int_s \left[\left(\frac{\partial p}{\partial s}\chi\right)_E\right]_{t_1}^{t_2} ds\ dA + \int_{A_c} \int_s \left[\left(\left(\frac{\partial p}{\partial s}\chi\right)_c - \left(\frac{\partial p}{\partial s}\chi\right)_E\right)ds\ dA_c\right]_{t_1}^{t_2}$$

The expression $\left(\frac{\partial p}{\partial s}\chi\right)_c - \left(\frac{\partial p}{\partial s}\chi\right)_E$ is the excess value of χ in clouds compared to the value of χ in the local environment of each cloud. It is a measure of the extra storage of χ due to clouds. The second term on the RHS of the above equation is the time change of the cloud storage of χ. Although this term is not measured, it is usually neglected, because A_c is small compared to A (typically 1-10%) and is fairly constant in time. In this research, it is assumed negligible in three out of the four average budget calculations presented in Chapter V. However, it makes an important contribution to the one budget calculation performed during periods of developing convection (section 4B, Chapter V). A model of the cloud storage term is presented in Chapter VI. The recognition of the importance of this term in developing convection situations is a significant contribution of this research.

The second term in Eq. 4 becomes

$$\int_A \int_s \int_t \nabla_s \cdot (\chi \frac{\partial p}{\partial s} \vec{V}) ds\, dA\, dt = \int_{A_E} \int_s \int_t \nabla_s \cdot (\chi \frac{\partial p}{\partial s} \vec{V})_E\, ds\, dA_E\, dt + \int_{A_c} \int_s \int_t \nabla_s \cdot (\chi \frac{\partial p}{\partial s} \vec{V})_c\, ds\, dA_c\, dt$$

For the moment, we apply the divergence theorem to the RHS of this equation and for clarity examine only the area integration. Also, for the moment, assume the boundaries of the A_i which make up A_c are all within the boundary of A_E (see Fig. 3).

$$\int_{A_E} \nabla_s \cdot (\chi \frac{\partial p}{\partial s} \vec{V})_E\, dA_E + \sum_i \int_{A_i} \nabla_s \cdot (\chi \frac{\partial p}{\partial s} \vec{V})_i\, dA_i$$

$$= \int_{\ell_E} (\chi \frac{\partial p}{\partial s} \vec{V})_{\ell_E} d\ell_E - \sum_i \int_{\ell_i} (\chi \frac{\partial p}{\partial s} \vec{V})_{\ell_i} d\ell_i + \sum_i \int_{\ell_i} (\chi \frac{\partial p}{\partial s} \vec{V})_{\ell_i} d\ell_i .$$

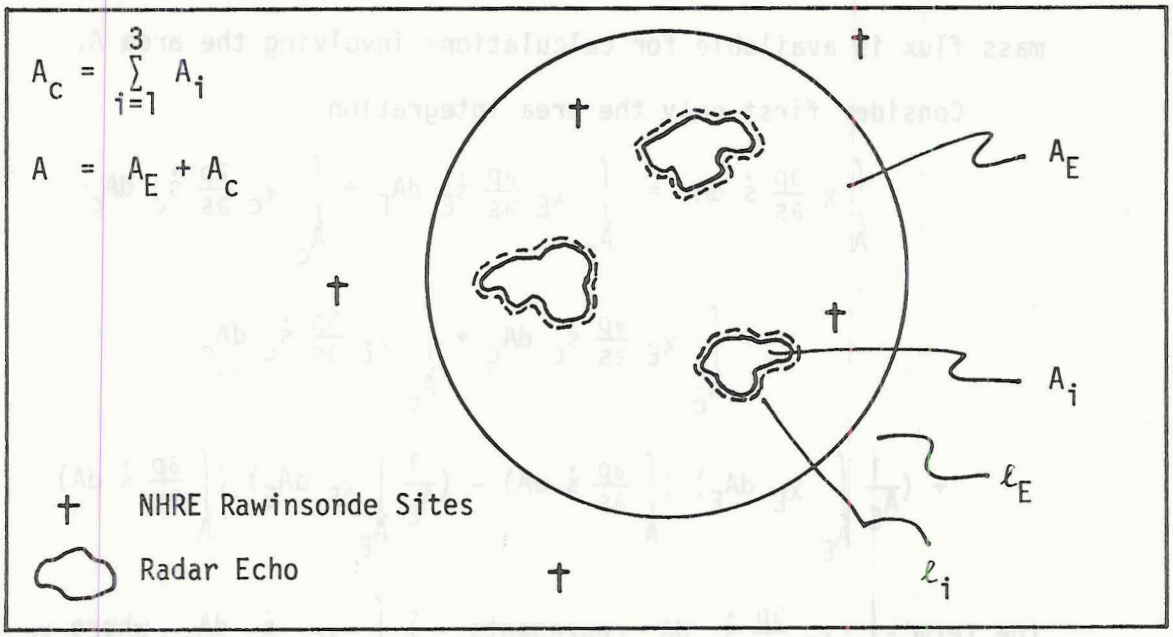

Figure 3. Budget Area Decomposition

The ℓ_E is the outer environmental boundary. The ℓ_i are the inner common boundaries between area A_E and areas A_i. This use of the divergence theorem simply shows that the outward fluxes at the inner boundaries of

the environmental integration are equal and opposite to the outward fluxes of the cloud area integrations. That is, any net divergence within the area A will be accounted for at the outer boundary of A_E (assumed the same as the boundary of A). The presence of clouds on the outer boundary of A will produce a contribution to the budget if there is a net inflow or outflow of the local cloud excess of χ during the period of the time integration. The data presented in Chapter IV suggest this contribution can be neglected in this research. With this one approximation, the second term of Eq. 4 can be written

$$\int_A \int_s \int_t \nabla_s \cdot (\chi \frac{\partial p}{\partial s} \vec{V}) \, ds \, dA \, dt = \int_A \int_s \int_t \nabla_s \cdot (\chi \frac{\partial p}{\partial s} \vec{V})_E \, ds \, dA \, dt.$$

Some manipulation (addition and subtraction of the same term) is needed to obtain the desired expression for the third term in Eq. 4. This manipulation is based on the idea that only the average vertical mass flux is available for calculations involving the area A.

Consider first only the area integration.

$$\int_A \chi \frac{\partial p}{\partial s} \dot{s} \, dA = \int_{A_E} \chi_E \frac{\partial p}{\partial s} \dot{s}_E \, dA_E + \int_{A_c} \chi_c \frac{\partial p}{\partial s} \dot{s}_c \, dA_c$$

$$- \int_{A_c} \chi_E \frac{\partial p}{\partial s} \dot{s}_c \, dA_c + \int_{A_c} \chi_E \frac{\partial p}{\partial s} \dot{s}_c \, dA_c$$

$$+ \left(\frac{1}{A_E} \int_{A_E} \chi_E \, dA_E\right) \left(\int_A \frac{\partial p}{\partial s} \dot{s} \, dA\right) - \left(\frac{1}{A_E} \int_{A_E} \chi_E \, dA_E\right) \left(\int_A \frac{\partial p}{\partial s} \dot{s} \, dA\right)$$

the term $-\int_{A_c} \chi_E \frac{\partial p}{\partial s} \dot{s}_c \, dA_c$ represents $-\sum_i \int_{A_i} \chi_{E_i} \dot{s}_c \, dA_{c_i}$ where χ_{E_i} is a very localized average value of χ_E around the i^{th} cloud. On the time and space scale of the i^{th} cloud, χ_{E_i} is nearly a constant. The value of the

constant would depend on the x, y position of the i^{th} cloud. Using this approximation and decomposing the last integral $\int_A \frac{\partial p}{\partial s} \dot{s}\, dA$ we obtain:

$$\int_A \chi \frac{\partial p}{\partial s} \dot{s}\, dA = (\frac{1}{A_E} \int_{A_E} \chi_E\, dA_E)(\int_A \frac{\partial p}{\partial s} \dot{s}\, dA) + \int_{A_c} (\chi_c - \chi_E) \frac{\partial p}{\partial s} \dot{s}_c\, dA_c$$

$$+ \int_{A_E} \chi_E \dot{s}_E\, dA_E - (\frac{1}{A_E} \int_{A_E} \chi_E\, dA_E)(\int_{A_E} \dot{s}_E\, dA_E)$$

$$+ \sum_i \{[\chi_{E_i} - (\frac{1}{A_E} \int_{A_E} \chi_E\, dA_E)] \int_{A_{c_i}} \dot{s}_{c_i}\, dA_{c_i}\}$$

The above equation is an expansion of the third term of Eq. 4. It is the only term that requires an approximation that is specifically connected to letting the environmental field, χ_E, have horizontal gradients. The second pair of terms on the RHS of the above equation would cancel if χ_E was constant. The terms would also cancel if the environmental vertical mass flux, $(\frac{\partial p}{\partial s} \dot{s})_E$, was horizontally constant (no restirction on χ_E in this case). The sum of these terms will be neglected in this study under the second assumption. That is, the clear air between the strong convective updrafts and downdrafts is assumed to rise or rink uniformly across the data area.

The last term on the RHS of the above equation is a measure of how uniformly the clouds are distributed over the area A. The first term of this product, $[\chi_{E_i} - (\frac{1}{A_E} \int_{A_E} \chi_E\, dA_E)]$, is the deviation of χ_E associated with the i^{th} cloud from an average value of χ_E. The magnitude and sign of the deviation depends on the x, y position of the i^{th} cloud. The sum of these deviations would be zero is the clouds were "evenly" distributed.

However, this deviation is part of a product including the total mass flux of the i^{th} cloud. Each deviation of χ_{E_i} from the average χ_E is weighted by the vertical mass flux associated with the i^{th} cloud. In this research, the convection will be assumed to be uniformly distributed in the sense that the sum of these weighted deviations is nearly zero. Of course the distribution of the clouds would not matter if χ_E was constant because $\chi_{E_i} - (\frac{1}{\chi_E} \int \chi_E \, dA_E)$ is zero in that case.

The two approximations discussed above can be combined into the following more general approximation:

$$\int_A [\chi_E - (\frac{1}{A_E} \int_{A_E} \chi_E \, dA_E)] \frac{\partial p}{\partial s} \dot{s} \, dA = 0$$

The vertical velocity field in area A is assumed to be uncorrelated with the deviation of χ_E from its average value.

The final expression for the third term of Eq. 4 is, therefore,

$$\int_t \int_A [\chi \frac{\partial p}{\partial s} \dot{s}]_{s_H}^{s} \, dA \, dt = \int_t [(\frac{1}{A_E} \int_{A_E} \chi_E \, dA_E) (\int_A \frac{\partial p}{\partial s} \dot{s} \, dA)]_{s_H}^{s} \, dt$$

$$+ \int_t [\int_{A_c} (\chi_c - \chi_E) (\frac{\partial p}{\partial s} \dot{s})_c \, dA_c]_{s_H}^{s} \, dt$$

The terms resulting from the above decomposition (less the neglected portions) will now be combined to give the budget equation used in this thesis. Equation 5 describes the budget for a scalar, χ, over a budget volume defined by area, A, and vertical estent, s_H to s. The budget is valid over the time interval t_1 to t_2.

$$\int_A \int_s [(\frac{\partial p}{\partial s} \chi)_E]_{t_1}^{t_2} \, ds \, dA + \int_A \int_s \int_t \nabla_s \cdot (\chi \frac{\partial p}{\partial s} \vec{V})_E \, dt \, ds \, dA$$

$$+ \int_t [(\frac{1}{A_E} \int_{A_E} \chi_E \, dA_E) \int_A \frac{\partial p}{\partial s} \dot{s} \, dA]_{s_H}^{s} \, dt = \qquad (5)$$

$$\int_A \int_s \int_t \frac{\partial p}{\partial s} Q \, dt \, ds \, dA - \int_t \left[\int_{A_c} (\chi_c - \chi_E) \left(\frac{\partial p}{\partial s} \dot{s}\right)_c dA_c \right]_{s_H}^{s} dt$$

$$- \int_{A_c} \int_s \left[\left(\left(\frac{\partial p}{\partial s} \chi\right)_c - \left(\frac{\partial p}{\partial s} \chi\right)_E\right) ds \, dA_c \right]_{t_1}^{t_2}$$

This thesis is based on Eq. 5. Environmental processes have been separated to the LHS of the equation and will be calculated from rawinsonde data taken over the NHRE area (Chapter III). Convective processes plus the source term, on the RHS of the equation, will be calculated as a residual. Equation 5 contains two approximations. First, any net inflow of clouds into the area, A, during the budget interval is neglected. Second, the vertical mass flux field is assumed to be uncorrelated with the deviation of χ_E from its average value. The use of linear approximations for the integrations have been mentioned in this section and will be used in Chapter III, but this linearity has not been used in Eq. 5.

The formalism of Eq. 5 is different than that of the frequently used budget equation 1. First, a general vertical coordinate, s, is used. Second, the environmental variables, χ_E, are functions of horizontal position. Third, the time and space integrations are explicit. Fourth, the cloud storage term has been retained. A discussion of these features and the linear approximations to be applied to the input data in Chapter III will be presented in the next section.

3. Discussion of the Budget Equation

A. Formalism and Linear Approximations

A particular form of a budget equation has been presented in section 2 (Eq. 5). In Chapter III the data to be used in this equation are approximated by linear time and space functions. These two choices

affect the results of the residual calculation and the interpretation of all the terms in the budget. The implications of these choices will be discussed in this section.

A general vertical coordinate is used in Eq. 5 in order to facilitate the use of a normalized pressure coordinate (σ) in the calculations. The σ system is useful over the sloping NHRE are because the ground is a coordinate surface (see section 1, Chapter III). Computations of the vertical velocity are simplfied because $\dot{\sigma}$(surface) = 0. The choice of the σ coordinate system, however, has another consequence. The vertical velocities and vertical fluxes of χ must now be interpreted as motion relative to slanting σ surfaces (see section 1, Chapter III and section 1A, Chapter VI for this discussion).

The horizontal spatial dependence of χ_E is retained. Consequently, the cloud storage term, which is based on the quantity $\chi_c - \chi_E$, can be modeled as a cloud excess of χ above a local environmental value. The treatment of the net inflow or outflow of clouds into the budget area would also contain this type of local cloud excess term (in this research, however, the term is neglected). When χ_E has a pronounced horizontal gradient it is much more straightforward to model the quantity $\chi_c - \chi_E$ than $\chi_c - \tilde{\chi}$. The quantity $\chi_c - \tilde{\chi}$ is not directly related to a local cloud excess (see Fig. 2).

The consideration of data that have horizontal gradients and the desire to attain a particular final form of term 3 in Eq. 4 (section 2B) has prompted the assumption that the vertical motion of the environmental air is horizontally uniform. This assumption would appear in the derivation of Eq. 2 if $\tilde{\chi}$ was not set to a horizontally constant value.

The explicit use of time and space integrations is an important part of the formalism of Eq. 5. The general consequence of this approach is the explicit appearance of both the time and space averaging scales that are used in the calculations. The emphasis on the area integration prompted the computational decision to not use the divergence theorem in the calculation of the flux divergence term (see discussion in section 2A). One consequence of the time integration is the use of time averaged values of the horizontal divergence of mass flux and χ flux. This averaging is beneficial because these quantities are typically quite noisy. The explicit time integration in the apparent source term also emphasizes the need to account for the transience of individual clouds in the interpretation of the calculated budget residual (see section 2, Chapter VI).

The three particular choices of formalism discussed above filter the information input to the budget equation in an indirect manner. In Chapter III the very direct filter of approximating the data as linear time and space functions is applied. This procedure has two general implications. The first is simply that the interpretation of the budget calculations will be incorrect to the extent that small nonconvective features such as fronts enter the budget volume. The second is an implied assumption that the total influence of the convection will not produce any strongly nonlinear changes in the environment. Such uniform influences on the environment could be accomplished by having the clouds distributed uniformly (in time and space) over the budget area or by having the clouds influence an area of substantial size compared to the budget area. The first possibility goes along with the discussion in section 2 and with Ninomiya's (1974) remark that he used mesoscale budget data because cumulus clouds are not always distributed uniformly over a large area.

B. Budget Residual

The RHS of Eq. 5 will be calculated as a residual. This in no way means that it is the "dependent variable" in the budget equation. In Chapter V, calculations for all of the terms in the budget equation will be presented and discussed. However, because it is not a directly measured quantity, its component parts will now be briefly discussed.

The change of cloud storage (third term on the RHS of Eq. 5) has a straightforward physical interpretation as the change in the excess amount of χ stored in clouds (see sections 2B and 3A). It is zero below cloud base and above cloud tops, and is assumed negligible except in the case of developing convection. In the one case of developing convection it is removed from the apparent source term by the application of a cloud storage model (Chapter VI).

There are two types of sources (first term on the RHS of Eq. 5) for quantities considered in this research. The first is radiation. It is modeled on the scale of the entire data area (section 5, Chapter III). The model calculations are used to remove this source from the calculated residual. Typically, the radiation divergence is small on the three hour time scale of this study. The second type of source is directly related to the change of phase of water due to individual cloud transports.

The last component is the divergence of the eddy flux of χ (second term on the RHS of Eq. 5). The eddy flux is the transport of χ not resolved by the data. The cloud-environment decomposition of the budget equation implies these fluxes are related to convection. Above the lifting condensation level (LCL) the convection is assumed to be cumulus clouds. Below the LCL the convection is assumed to be updrafts, downdrafts, and dry thermals. Mechanical mixing and diffusion are included near the ground.

The decomposition of the eddy flux term into the quantities

$$\int_t \int_{A_c} \chi_c \left(\frac{\partial p}{\partial s}\dot{s}\right)_c \, dA_c \Big]_{s_H}^{s} dt \quad \text{and} \quad -\int_t \int_{A_c} \chi_E \left(\frac{\partial p}{\partial s}\dot{s}\right)_c \, dA_c \Big]_{s_H}^{s} dt$$

is analogous to that of Yanai (1971) which is presented in section 1 as Eq. 2. This decomposition provides the basic motivation for relating the eddy flux to convection. The first term is the direct convective transport of χ. The second term is the product of the negative total convective mass flux (usually called compensating subsidence) and an environmental value of χ_E. In Chapter VI, the interpretation of one of the simpler (non precipitating) eddy flux calculations is developed by the use of a cloud model (Betts, 1975) that has a form similar to the above two terms.

III. CALCULATION PROCEDURES

1. Vertical Coordinate and Vertical Velocity

The specific vertical coordinate to be used in Eq. 5 was not given in Chapter II. The NHRE area, which is the lower boundary of the budget volume (see Chapter IV), is not horizontal. If the usual height or pressure coordinate is used, this lower boundary will not be a coordinate surface, and the lower limit of integration must be treated as a variable in both time and space. The problem is overcome by the use of a normalized pressure, σ, coordinate system introduced by Phillips (1957):

$$\sigma = \frac{p}{\pi} \quad \text{where} \quad \pi = \pi(x, y, t) = \text{surface pressure}$$

With the generalized vertical coordinate, s, equal to σ, the factor $\frac{\partial p}{\partial s}$ that appeared repeatedly in the budget equation is equal to π. The following physical interpretations can be related to σ surfaces and to $\dot{\sigma}$, the vertical velocity.

In a pressure coordinate system, assuming hydrostatic balance, the mass/area contained between two pressure surfaces is constant. In a σ system, two σ surfaces always enclose a given percent of the total mass/unit area, where the total mass per unit area is proportional to π, the surface pressure. The σ surfaces are closely parallel to the surface topography in the lower and mid-troposphere. The ground below the data volume considered in the research has an east-west slope of approximately -4.0 m/km. At σ = .59 (500 mb) a typical σ surface has a slope of -3.5 m/km, at σ = .18 (150 mb) a typical slope of -2.5 m/km. This tendency of the σ surfaces to parallel the ground is related to a problem that occurs in using this coordinate in numerical weather prediction equations. The height gradient appearing in prediction equations is composed of two terms, each of which contains a large hydrostatic component that must cancel (Kurihara, 1968).

This shortcoming of the σ system does not occur in this research, because the budget equations do not contain a pressure gradient force term.

An expansion of the definition of σ shows how $\dot{\sigma}$ is related to the more familiar $\omega = \frac{dp}{dt}$.

$$\omega = \sigma\dot{\pi} + \pi\dot{\sigma}$$

The difference between ω and $\pi\dot{\sigma}$ is $\sigma\dot{\pi}$, a term associated with the changing surface pressure experienced by a moving parcel. The largest part of $\dot{\pi}$ is $\vec{V}\cdot\nabla\pi$. This term usually increases with height because of the increase of wind speed. The product $\sigma\dot{\pi}$, however, has a magnitude of about 2×10^{-3} mb/sec at all levels because of the decrease of σ. The results of the vertical mass flux calculations are presented as profiles of both $\pi\dot{\sigma}$ and the more familiar ω. The interpretation of the differences between these profiles is discussed in Chapter VI.

There are several methods available to calculate the vertical velocity, or as is required in this research, the total vertical mass flux past a σ surface, $\int_A \int_t \pi\dot{\sigma}\, dt\, dA$. In this thesis, the continuity equation will be used although it is subject to serious error because of errors in the wind data. Alternate solutions such as the adiabatic method or some sort of balance approximation, however, would be quite suspect because of the mesoscale, convective nature of the data. The continuity equation is simply a budget equation with χ = 1, Q = 0. It has the following form in σ coordinates (Kasahara, 1974; or Eq. 4, Chapter II).

$$\int_A \{[\pi]_{t_2} - [\pi]_{t_1}\} (\sigma - \sigma_H)\, dA + \int_\sigma \int_A \int_t \nabla_\sigma \cdot \pi\vec{V}\, dt\, dA\, d\sigma + \int_A \int_t [(\pi\dot{\sigma})_\sigma - (\pi\dot{\sigma})_{\sigma_H}]\, dt\, dA = 0 \qquad (6)$$

The lower boundary condition, $\pi\dot{\sigma} = 0$, at $\sigma = 1.0$ can be used to obtain $\int_A \int_t \pi\dot{\sigma}\, dt\, dA$ at any level by integration.

As a budget equation, all the remarks in Chapter II pertain to its formulation. In particular, an area integration instead of a line integration and a linear approximation of the horizontal mass flux πu, πv will be used in the calculation of $\pi\dot{\sigma}$.

2. Choice of Budget Quantities, χ

In this thesis, we shall be concerned with the following thermodynamic energies: latent energy, dry static energy, and moist static energy. These have the following definitions and source terms.

Latent Energy

$\chi = Lq$

$Q = (e - c)L$

L = heat of condensation = $2.5 \times 10^6 m^2 s^{-2}$

q = water vapor mixing ratio

e = evaporation / (mass time)

c = condensation / (mass time)

No attempt is made to account for the additional latent heat of freezing. This extra heat is surely important in terms of the dynamics of individual clouds. However, it makes only a very small contribution to the latent energy budget residual.

The LHS of Eq. 5 with χ defined as q is equal to the apparent source of water vapor, denoted Q_2 by many authors. The calculated values of Q_2 are presented and discussed (Chapters V and VI) as vertical profiles of the integral $\int_{\sigma}^{\sigma_T} Q_2 \frac{d\sigma}{g}$. The interpretation of this method of presenting Q_2 is discussed in section 5B.

Dry Static Energy

$$\chi = c_p T + gz = s \qquad c_p = 996.\ m^2 s^{-2} deg^{-1}$$

$$g = 9.8\ m\ s^{-2}$$

$$Q = (c - e)L + r \qquad r = \text{radiation heating / (mass time)}$$

As discussed by Betts (1974), with the neglect of $\alpha \frac{\partial p}{\partial t}$ (α = specific volume) the use of dry static energy in a budget equation involves an assumption that the locally generated kinetic energy is entirely dissipated in the volume under study.

The apparent source of s has a definition analagous to Q_2, and is usually denoted Q_1. The calculated values of Q_1 are also presented as profiles of the quantity $\int_{\sigma}^{\sigma_T} Q_1 \frac{d\sigma}{g}$ (see section 5B).

Moist Static Energy

$$\chi = c_p T + gz + Lq = h$$

$$Q = r$$

The moist static energy is the sum of the latent energy and the dry static energy. It is particularly useful because the source terms due to evaporation and condensation in Lq and s cancel. Moist static energy has only a radiation source term and is very nearly a conservative quantity. For further reference we define $Q_3 = Q_1 + Q_2$.

3. Final Equations

A. Apparent Source Calculation

The equations actually used for the calculations are now presented. The data that are input to these equations are first expressed as linear functions of x, y. That is, any variable, say D_j, is available in the form

$$D_j = a_j x + b_j y + c_j$$

where the D_j can be any of the following quantities:

$$Dj = \begin{cases} \pi \\ \chi_i \\ \pi\chi_i \\ \pi u \\ \pi v \end{cases} \qquad \text{where } \chi_i = \begin{cases} Lq \\ c_pT + gz \\ c_pT + gz + Lq \end{cases}$$

The coefficients a_j, b_j, c_j are determined by a least squares plane fit program that is applied to values of D_j measured by the rawinsondes at every data level (except π which is only measured at $\sigma = 1.0$). The data levels begin at $\sigma = 1.0$ and proceed to $\sigma \leq .18$ in increments $\Delta\sigma = .01$. The detailed procedure used to reduce the rawinsonde data to linear functions and a discussion of the quality of the resulting fit is presented in Chapter IV.

The calculation of the vertical mass flux is based on an integration of the continuity equation (6) and is given by

$$\pi\dot{\sigma}_K = \pi\dot{\sigma}_{K=1} - \frac{[\nabla\cdot\pi\vec{V}]_{t_2} + [\nabla\cdot\pi\vec{V}]_{t_1}}{2}(\sigma_K - \sigma_{K-1}) - \frac{[\pi]_{t_2} - [\pi]_{t_1}}{(t_2 - t_1)}(\sigma_K - \sigma_{K-1}) \quad (9)$$

where K denotes the data level. The area integration indicated in Eq. 6 is carried out by evaluating each term at the midpoint x_M, y_M of area A (see section 2A, Chapter II). The procedure used to obtain x_M, y_M will be described in Chapter IV.

The residual (apparent source) defined by the LHS of Eq. 5 for the quantity χ_i for the layer between $\sigma = K$ and $\sigma = K\text{-}1$ is calculated using:

$$\frac{\text{Res}(K \text{ to } K\text{-}1)}{(t_2 - t_1)\,Ag} = \frac{[\pi\chi_i]_{t_2} - [\pi\chi_i]_{t_1}}{(t_2 - t_1)}\frac{(\sigma_K - \sigma_{K-1})}{g} + \frac{[\nabla\cdot\chi_i(\pi\vec{V})]_{t_2} + [\nabla\cdot\chi_i(\pi\vec{V})]_{t_1}}{2}\frac{(\sigma_K\ \sigma_{K-1})}{g}$$

$$+ \frac{\pi\dot{\sigma}_K}{g}\frac{[\chi_i]_{t_2} + [\chi_i]_{t_1}}{2} - \frac{\pi\dot{\sigma}_{K-1}}{g}\frac{[\chi_i]_{t_2} + [\chi_i]_{t_1}}{2} \quad (10)$$

In the term $\nabla\cdot[\chi(\pi\vec{V})]$ the χ is fit by one plane and $\pi\vec{V}$ is fit by another.

B. Vertically Integrated Apparent Source

The calculated values of the apparent source are presented and discussed (Chapters V and VI) as vertical profiles of the finite difference integration

$$F(\sigma_K) = \sum_{i=\sigma_T}^{\sigma_K} \frac{\text{Res } (i+1)}{(t_2-t_1)\ Ag} \ (\sigma_i - \sigma_{i-1}) \qquad (11)$$

The apparent source Res (i + 1) is defined by Eq. 10 for the layer σ = i+1 to σ = i. The first (top) value of Res(σ_{T+1} to σ_T) is defined at the end of this section. $F(\sigma_K)$ is a flux form of the apparent source term. The apparent source can be retreived by taking the vertical derivative of the F profile.

The motivation for this presentation of F comes from considering the third term on the RHS of Eq. 5 as the vertical derivative of a convective flux:

$$\int_t \int_{A_c} \int_\sigma \frac{\partial}{\partial\sigma} \{(\chi_c - \chi_E)\ (\pi\dot{\sigma})_c\}\ d\sigma\ dA_c\ dt$$

$$= \int_t \int_{A_c} \int_\sigma \pi \frac{\partial}{\partial\sigma} (F_\chi)\ d\sigma\ dA_c\ dt$$

However, the RHS of Eq. 5 contains two additional terms and these terms make the interpretation of F as a vertical flux difficult. In order to approach this problem, these two terms are treated as follows. Let the source of $\chi(Q_\chi)$ be expressed as

$$Q_\chi = -\left(\frac{\partial I_\chi}{\partial t} + \frac{\partial F_I}{\partial\sigma}\right)$$

I_χ is the property that can be converted into the property χ. For example, when χ = q, water vapor mixing ratio; $I_q = q_\ell$, the mixing ratio of liquid water. F_I is the vertical flux of I_χ. For example, $F_{q\ell}$ is the vertical flux of liquid water. A horizontal flux has not been introduced for clarity. The radiation source term is associated only with $\partial F_r/\partial\sigma$. Using these definitions, the apparent sources of Lq, s and h (RHS of Eq. 5) become:

$$\text{Apparent source of } Lq = -L \int_t \int_{A_c} \int_\sigma \pi \frac{\partial}{\partial \sigma} (F_q + F_{q_\ell}) \, d\sigma \, dA_c \, dt \qquad (12)$$

$$-L \int_{A_c} \int_\sigma \pi [((q + q_\ell)_c - q_E) \, d\sigma \, dA_c]_{t_1}^{t_2} \qquad (a)$$

$$\text{Apparent source of } s = - \int_t \int_{A_c} \int_\sigma \pi \frac{\partial}{\partial \sigma} (F_s - LF_{q_\ell}) \, d\sigma \, dA_c \, dt$$

$$- \int_t \int_A \int_\sigma \pi \frac{\partial}{\partial \sigma} (F_r) \, d\sigma \, dA \, dt - \int_{A_c} \int_\sigma \pi [((s - Lq_\ell)_c - s_E) \, d\sigma \, dA_c]_{t_1}^{t_2} \qquad (b)$$

$$\text{Apparent source of } h = - \int_t \int_{A_c} \int_\sigma \pi \frac{\partial}{\partial \sigma} (F_h) \, d\sigma \, dA_c dt$$

$$- \int_t \int_A \int_\sigma \pi \frac{\partial}{\partial \sigma} (F_r) \, d\sigma \, dA \, dt - \int_{A_c} \int_\sigma \pi [(h_c - h_E) \, d\sigma \, dA_c]_{t_1}^{t_2} \qquad (c)$$

If the change in cloud storage is neglected, the apparent source term falls naturally into the form of the divergence of a vertical flux.

The quantities $q + q_\ell$ (total water mising ratio), $s - L_{q_\ell}$ (liquid water static energy) and h (moist static energy) have been presented and discussed by Betts (1975) as conservative quantities. It is quite natural that these quantities and their respective fluxes appear in Eqs. 12a, b, and c. The elimination of Q as a source term by redefining it has simply produced conservative variables (variables with no source terms).

The portions of the apparent source terms due to changing cloud storage will either be neglected or in the case of developing convection, removed from the apparent source by modeling (Chapter VI). Similarly the radiation term will be modeled and removed from the apparent source terms or will be neglected (section 5). The remaining portion of the

apparent source terms ($F(\sigma_K)$- F_r - cloud storage, see Eq. 11) will be presented (Chapters V and VI) as vertical profiles of the following convective fluxes

$$F_{q_T} = F_q + F_{q_\ell} \quad \text{(convective flux of total water)}$$

$$F_{s_\ell} = F_s - LF_{q_\ell} \quad \text{(convective flux of liquid water and static energy)}$$

$$F_h = LF_{q_T} + F_{s_\ell} \quad \text{(convective flux of moist static energy)}$$

These fluxes will be set to zero at and above level σ_T (see Eq. 11) by the appropriate choice of Res (σ_{T+1} to σ_T). The magnitudes of the calculated fluxes depend on the choice of σ_T and are, therefore, subject to error involved in choosing σ_T. The choice of σ_T is based on an estimate of cloud top height (see Chapter V).

Two important properties of the above three convective fluxes should be noted. First, two of the three fluxes are independent of one another. This property is used in the development of the diagnostic models presented in Chapter VI. Second, the flux of liquid water, F_{q_ℓ}, is often a large part of F_{q_T} and F_{s_ℓ}. However, in the case of precipitating convection, the liquid water is not carried along with the air. This means q_T and s_ℓ are no longer parcel quantities and it is difficult to measure or model F_{q_T} and F_{s_ℓ}.

4. Integral Constraints

It is possible to partially check the budget calculations because the vertical integral throughout the depth of the atmosphere of water vapor and moist static energy represent quantities that can be estimated independently of the budget data. For $\chi = q$, integrating Eq. 5 from $\sigma = 1.$ to $\sigma = 0.$ and assuming the total mass flux to be zero at $\sigma = 0, 1$ and the convective flux to be zero at $\sigma = 0$, we obtain:

$$\int_A \int_{\sigma=1}^{0} [(\pi q)_E]_{t_1}^{t_2} \frac{d\sigma}{g} dA + \int_A \int_{\sigma=1}^{0} \int_t \nabla_\sigma \cdot (q\pi \vec{V})_E \, dt \frac{d\sigma}{g} dA = -(P + C_2) + E \quad (7)$$

where

$$\int_{\sigma=1}^{0} \int_A \int_t \pi(e-c) \, dt \frac{d\sigma}{g} dA + \int_{A_c} \int_{\sigma=1}^{0} [((\pi q)_c - (\pi q)_E) \frac{d\sigma}{g} dA_c]_{t_1}^{t_2} \equiv -(P + C_2)$$

and $$\int_t [\int_{A_c} (q_c - q_E) (\pi \dot{\sigma})_c \, dA_c]_{\sigma=1} \rightarrow E$$

The first two terms on the RHS of Eq. 7 are sink terms for water vapor. P is the total mass of water that fell from clouds in the given volume during the interval $t_2 - t_1$, and reached the ground without evaporating. C_2 is the increase in the excess total cloud water due to more clouds forming than dissipating. Horizontal losses of water due to a net amount of clouds drifting out of the volume are neglected. The convective flux of water vapor evaluated at the ground (σ=1) has been replaced by the total surface evaporation, E. The replacement is reasonable because even though the convective mass flux at the surface σ=1 is zero, there is a diffusional flux of water vapor analogous to a convective flux. The total evaporation from the σ=1 surface includes evaporation of precipitation at the ground and evapotranspiration.

The measurements needed to calculate the RHS of Eq. 7 are independent of those used in the calculation of the LHS of the equation, and theoretically could be used as a check. However, considering the uncertainty involved in estimating the total precipitation, net cloud formation, surface evaporation and evapotranspiration, this integral constraint probably can offer no more than a qualitative check on the water vapor budget.

The integral constraint for the moist static energy, h, is derived from a similar integration of Eq. 5.

$$\int_A \int_{\sigma=1}^{0} [(\pi h)_E]_{t_1}^{t_2} \frac{d\sigma}{g} dA + \int_A \int_{\sigma=1}^{0} \int_t \nabla\sigma\cdot(h\pi\vec{V})_E \, dt \, \frac{d\sigma}{g} dA = R + C_3 + (S + LE) \tag{8}$$

where $\int_{\sigma=1} \int_A \int_t \pi r \, dt \, dA \, \frac{d\sigma}{g} \equiv R$ and $\int_{A_c} \int_{\sigma=1}^{0} [((\pi h)_c - (\pi h)_E) \frac{d\sigma}{g} dA_c]_{t_1}^{t_2} \equiv C_3$

and $$\int_t [\int_{A_c} (h_c - h_E) (\pi\dot{\sigma})_c \, dA_c]_{\sigma=1} \rightarrow S + LE$$

R is the net radiational heating that occurs throughout the entire volume during the interval $t_2 - t_1$. C_3 is the change in the cloud storage of h. The convection term at the surface has again been replaced by diffusion processes. S is the total flux of sensible heat from the ground and LE is the surface evaporation cooling. Conservation of energy at the ground requires $F_r = G + S + LE$ where F_r is the flux of radiation of all wavelengths at the ground and G is a typically small net storage flux into the ground. An estimate of F_r provides an approximate check on Eq. 8 if R and C_3 are modeled or neglected. Unfortunately F_r is sensitive to the amount of cloud cover and cannot be estimated with assurance. However, the clear sky estimate of $F_r = 725$ kg s^{-3} provided by the radiation computations (see section 5) can be used as an upper bound of the LHS of Eq. 8. Also, the consistency of the trend of the LHS of Eq. 8 for situations with different cloud covers can be checked.

5. Radiation Source Calculation

The apparent sources of dry and moist static energies contain radiation source terms (section 2). This net radiation contribution will

be computed for two of the four average budget calculations discussed in Chapter V. The computation is carried out with the use of two computer programs kindly supplied by Dr. S. K. Cox. One program computes a vertical profile of the long wave radiation divergence (cooling) for any specified vertical distribution of temperature, water vapor, carbon dioxide, and ozone. This model can also do the calculation with any specified cloud layer present. The second program computes a vertical profile of the short wave radiation convergence (heating) for any specified vertical distribution of temperature, water vapor, carbon dioxide, and ozone. This program, however, cannot calculate the effects of clouds. Both programs assume a horizontally homogeneous atmosphere. The following procedure is used to apply these programs to this research.

Two net radiation divergence profiles are calculated. One is for the suppressed and one is for the developing convection average data intervals (see Chapter V for the definition of the convection present in these intervals). Rawinsonde data are used to supply the required temperature and water vapor inputs up to the 100 mb level. Temperature and water vapor lapse rates from the 100 mb level to the 1 mb level are set equal to standard atmosphere values. Standard atmosphere values are also used for the carbon dioxide and ozone inputs from the surface to the 1 mb level.

The effects of cloud cover are approximated in the long wave calculation in the following manner. First, an estimate of the cloud cover for each of the two average intervals is made using standard hourly surface observations near the data area (see Chapter V, section 2). Second, these estimates are used to define a percent area coverage for clear air, cumulus clouds, and cirrus clouds for each average data

interval. The cumulus cloud bases are assumed to be at the lifting condensation level and the cirrus tops at a near tropopause level. Representative values for the cumulus tops and cirrus bases are unknown and are simply approximated subjectively. Third, long wave cooling profiles are calculated (1) with no clouds present, (2) with a cumulus layer present, and (3) with a cirrus layer present for each of the two average data periods. Finally, net long wave cooling profiles are formed by taking an area weighted average of the three profiles valid for different types of sky cover (clear, cumulus, and cirrus).

The long wave radiation program does not calculate the vertical distribution of cooling within the cloud layer. Only a net long wave radiation divergence throughout the depth of the cloud is given. In cumulus clouds this net divergence is usually the sum of a cooling that occurs in the upper part of the cloud and a weaker warming in the lower portion of the clouds. Paltridge (1974) suggests that layer clouds can be assumed to act as black bodies once they have achieved a depth of .5 to 1.0 km. Neglecting the lower level warming, the net calculated cooling within the cumulus cloud will be assumed to occur within the uppermost 1 km. However, unlike the model cloud in the radiation calculation, the real clouds over the NHRE area have many different top heights. Taking account of this, the calculated in-cloud cooling is assumed to be evenly distributed over approximately the upper half of the model cumulus layer. The cooling is set to zero in the lower half. In the case of the cirrus clouds, the divergence is evenly distributed over the entire depth because the model cirrus cloud is relatively thin (50 mb deep).

The two average net radiation divergence profiles are finally formed by adding the respective long and short wave contributions. These

calculated profiles represent a rough estimate of the radiation source term. The treatment of cloud effects is the most serious approximation. The two average data intervals used in this radiation calculation have only weak cumulus convection occurring, and this probably contributes to making the calculated radiation profile appear reasonable. The remaining two average budget intervals have deeper convection occurring and trial radiation calculations produced suspiciously large values. Consequently, the radiation was left as an unknown contribution in the apparent source terms for these latter two cases. Fortunately, the radiation sources in the weak convection cases were small compared to the total apparent sources of s and h. It will be assumed that radiation contribution to the other two average budgets are also small.

IV. DATA REDUCTION

1. Data Network

The budget calculations in this thesis are based on high density rawinsonde measurements taken during the summer of 1973 National Hail Research Experiment (NHRE). These budget calculations are related to radar echo and precipitation occurrence data within the NHRE area. Standard hourly surface observations and hourly precipitation reports from sites within 200 km of the NHRE area are used to supplement the rawinsonde and radar data.

The NHRE area is defined by the five NHRE rawinsonde launch sites. The sites are arranged in a pentagonal shape about 100 km across and centered in northeastern Colorado (Fig. 1). The area is mostly flat grassland with few abrupt elevation changes. The foothills of the Rocky Mountains begin about 80 km from the western most site (Grover). The Continental Divide is about 150 km west of Grover. Elevation values within the NHRE area are used to define the lower boundary ($\sigma = 1$) of the budget volume. Care was taken to approximate this lower boundary by a surface that is representative of the entire NHRE area ground elevation, because the vertical mass flux is set to zero on this boundary. To determine this surface, 144 elevation values were taken from a topography map of the NHRE area at regularly spaced intervals. A plane surface was then fit in the least squares sense to these data. The equation of this $\sigma = 1.0$ plane is

$$z_{\sigma=1} = (-.40082 \times 10^{-2})\, x + (.22741 \times 10^{-2})\, y + 1653.68$$

where z is the elevation (meters) above sea level and $x = 0$, $y = 0$ is located at the Grover site. The standard deviation from this plane is 38.77 meters. Three rawinsonde sites lie below this plane and getting

data valid on the plane involves an interpolation. Two sites are above the constructed plane and getting data on the plane at these locations involves an extrapolation. The details of the interpolation and extrapolation are given in section 2, but the average distance involved in calculation is 29 meters (the maximum extrapolation distance is 40 meters).

Rawinsondes were released approximately simultaneously from the above five sites at two to three hour intervals on several days during the summer of 1973. A summary of the available sounding data is presented in Table 1 . As the sondes rose, they were blown downwind causing the data volume they define to be tilted. At 500 mb, the volume tilts approximately 5 km, at 100 mb, 40 km. The extreme values at 100 mb are 5 km and 65 km. The data along one sounding path is not valid at one single time. The balloon reaches 500 mb about ten minutes after launch and 100 mb about fifty minutes after launch. The paths traced out by two successive sondes usually fall within two kilometers of each other at 500 mb and six kilometers of each other at 100 mb. A set of "simultaneous" ascents were used as data only when at least four of the five rawinsondes reached the $\sigma = .19$ (175 mb) level. Two such successive sets of sonde data are needed to make one budget calculation.

The radar data are obtained from PPI photographs of Ft. Morgan and Limon radars (Fig. 1 and section 3). The FPS-18 radar at Ft. Morgan has a 150 km range and provides data that reach the foothills to the west and extends about 45 km beyond the NHRE point farthest from Ft. Morgan. The Ft. Morgan radar elevation angle is usually increased by 1° each scan until the tops of the highest clouds are reached, giving some vertical structure to the PPI photographs (at 100 km the vertical increment and beam width, each 1°, equal about 1.7 km). During the periods of strong convective activity

Table 1. DATA SUMMARY

Legend

I	echo radius ≤ 10 km
II	echo radius > 10 km
High	echo top > 10,000 m
+	unknown increase in number of echoes
-	no precipitation during interval
Blank	missing data
Y	(yes) precipitation during interval
N	(no) no precipitation during interval
Amount	Precipitation rate (cm/sec average of all operating NHRE raingauges during precipitation period)
B	Precipitating at beginning of interval
M	Precipitation during middle of interval
E	Precipitation at end of interval

Rawinsonde Data						Number of Radar Echoes and Precipitation Reports									
						Max Values for Interval					Development (End - Beginning or Max - Beginning, End - Max)				
Date	Time	Interval		Δt	Number of Sondes	Precip	I	II	Total	High	Precip	I	II	Total	High
0601	1312	1020	1458	278	9	Y1	1	0	1	0	E	1	0	1	0
	1542	1320	1626	186	10	Y1	6	0	6		M	6	0	6	
	1639	1530	1822	172	10	N	6	0	1		-	2, -4	0	2, -4	
	1737	1655	1926	151	10	N	6	0	6		-	-6	0	-6	
0612	1149	1022	1300	158	10	N	0	0	0	0	-	0	0	0	0
	1235	1155	1420	145	10	N	0	0	0	0	-	0	0	0	0
	1403	1320	1549	149	10	N	0	0	0	0	-	0	0	0	0
	1533	1450	1819	209	10	N	0	0	0	0	-	0	0	0	0

Table 1. DATA SUMMARY
Continued

Rawinsonde Data						Number of Radar Echoes and Precipitation Reports								
Date	Time	Interval		Δt	Number of Sondes	Max Values for Interval					Development				
											End - Beginning or Max - Beginning, End - Max				
						Precip	I	II	Total	High	Precip	I	II	Total	High
0629	1741	1620	1855	155	8	N	1	0	1	0	-	1	0	1	0
0704	1211	1020	1414	234	8	.074	7	1	7		E	6, -4	1	6, -3	
	1401	1310	1555	165	8	.074	7	1	7		ME	-4	1	-3	
0709	1233	1020	1459	279	10	N									
	1518	1320	1718	238	9	.081	6	0	6		ME	6	0	6	
	1720	1554	1825	151	8	.081	6	0	6		BME	4, -1	0	4, -1	
	1808	1729	2005	156	8	.081	6	0	6		BM?				
0712	1609	1350	1723	213	9	N	0	0	0	0	-	0	0	0	0
	1735	1620	1850	150	10	N	0	0	0	0	-	0	0	0	0
0713	1153	1020	1325	185	10	N	0	0	0	0	-	0	0	0	0
	1303	1220	1450	150	10	N	0	0	0	0	-	0	0	0	0
	1433	1350	1621	151	10	N	0	0	0	0	-	0	0	0	0
	1604	1520	1752	152	10	N	0	0	0	0	-	0	0	0	0
	1734	1652	1920	148	9	N	0	0	0	0	-	0	0	0	0

Table 1. DATA SUMMARY
Continued

Rawinsonde Data						Number of Radar Echoes and Precipitation Reports								
						Max Values for Interval					Development			
											End - Beginning or Max - Beginning, End - Max			
Date	Time	Interval		Δt	Number of Sondes	Precip	I	II	Total	High	Precip	I	II	Total	High
0716	1344	1220	1452	152	8										
	1433	1350	1615	145	8										
	1603	1520	1748	148	8										
	1733	1650	1935	165	8	N	2	0	2	0	-	2	0	2	0
0717	1217	1020	1314	174	8	N	0	0	0	0	-	0	0	0	0
	1331	1220	1450	150	8	N	0	0	0	0	-	0	0	0	0
	1503	1350	1618	148	8	N	0	0	0	0	-	0	0	0	0
	1637	1523	1818	175	8	.009	3	0	3	Y	ME	3	0	3	+
	1737	1650	1950	180	8	.009	3	0	3	Y	M?	3	0	3	+
0718	1332	1220	1450	150	8		1	3	4			1	2	3	
	1554	1350	1800	250	8		≥3	≥3	≥4						
	1810	1653	1915	142	8										
0723	1147	1020	1310	170	8		0	0	0	0		0	0	0	0
	1332	1220	1446	146	9		0	0	0	0		0	0	0	0
	1502	1350	1630	160	10		0	0	0	0		0	0	0	0
	1603	1520	1809	169	9		0	0	0	0		0	0	0	0

Table 1. DATA SUMMARY
Continued

Rawinsonde Data						Number of Radar Echoes and Precipitation Reports									
						Max Values for Interval					Development (End - Beginning or Max - Beginning, End - Max)				
Date	Time	Interval		Δt	Number of Sondes	Precip	I	II	Total	High	Precip	I	II	Total	High
0724	1148	1012	1323	191	10	Y	Y	Y	Y	Y	?M	<0	<0	<0	<0
	1303	1220	1449	149	10	N	0	0	0	0	-	0	0	0	0
*	1547	1350	1746	236	9	N	1	1	2		-	1	1	1	
	1806	1655	1925	150	8	N	1	1	2		-	1, -1	0	1, -1	
0727	1158	1020	1330	190	10		0	0	0	0		0	0	0	0
	1422	1229	1618	229	10		0	0	0	0		0	0	0	0
	1633	1520	1750	150	10		1	0	1	1		1	0	1	1
	1733	1650	1919	149	9		1	0	1	0		1, -1	0	1, -1	1, -1
0728	1508	1320	1719	239	8	.105	3	0	3	Y	BME	3, -2	0	3, -2	>0?
	1655	1605	1850	165	8	.105	3	0	3	Y	BM?	<0?	0	<0?	
0731	1217	1020	1440	260	10	N	0	0	0	0	-	0	0	0	0
*	1448	1320	1710	230	9	N	0	1	1	Y	-	0	1	1	>0

* Not used - bad rawinsonde data.

only sector scans were made and the elevation angle is stepped by several degrees. Each sweep of the PPI scope was photographed, but numerous difficulties (clock, camera, elevation indicator) have degraded the data significantly. Data were also collected from the Limon WSR-57 radar. This is quite far from the NHRE area and, therefore, the vertical resolution near NHRE is poor. At 200 km, the 2° beam is about 5.2 km wide. Also, the elevation angle is often fixed at 2°. When available, the radar does have good time resolution - PPI photographs are available about every 5-10 minutes.

The precipitation data used in the description of the convection within the NHRE area is obtained from a high density rain gauge network (119 sites spaced approximately 5-10 km apart). However, analyzed hourly values of the total precipitation in the NHRE area are not available, and the author has not attempted the analysis of the very large amount of data himself. Such a detailed analysis for use in comparison with the vertically integrated water vapor budget results is not warranted for two reasons. First, the RHS of the vertically integrated water vapor budget (Eq. 7) is the sum of the precipitation, evaporation, and net cloud formation. An estimate of the last two factors would be extremely crude. Second, although a detailed quantitative estimate of the precipitation is not available, the data offer an excellent record of the occurrence or nonoccurrence of precipitation. This coarse description of the convection, that is, precipitating or nonprecipitating, is compatible with the rather coarse radar echo description of the convection. In light of these factors, the precipitation data has been used to specify whether the convection in the NHRE area is precipitating or nonprecipitating.

Hourly surface observations of temperature, dew point, pressure, wind and sky cover were plotted at eight locations within a 200 km radius circle centered over the NHRE area. Also, hourly precipitation reports from 33 sites within the same area have been plotted. These data were plotted primarily to provide an additional check for the presence of fronts in the NHRE area (other checks for such non linear changes in the rawinsonde data will be described in section 2). Only a few representative analyses will be presented in this thesis (Chapter V, section 2) because there are an extremely large number of them. The recorded sky cover of the stations within a 100 km radius of the NHRE area have been used, in addition to the radar data, to subjectively assign cloud covers to a few typical radiation calculations (Chapter V, section 3).

2. Rawinsonde Data Reduction

The personnel at NHRE kindly supplied the appropriate, processed rawinsonde data on magnetic computer tapes. These consisted of computer and hand checked values of q, T, p, h, x, y, t at contact point pressures and u, v wind components at half minute intervals. A GMD-1a rawinsonde system with ratio theodolite tracking was used. No lag corrections were applied to the data. Recent estimates suggest that at 5 mb^{-1} the thermistor lag is about 5 seconds and the hygristor thermal lag is about 16 seconds (A.K. Betts, personal communication).

The data in each set of four or five "simultaneous" soundings (depending on whether four or five sondes reached at least 175 mb) are interpolated vertically to regularly spaced σ levels and then interpolated to a common time. Finally, at each σ level, linear surfaces are fit in a

least squares sense to the four or five (depending on the number of sondes in the data set) values of each type of data (q, T, p, etc.).

The first step in the above procedure is to make the data available at regularly spaced σ levels. The first σ level (σ = 1.00) is defined as the plane that was fit to the NHRE area elevation data (section 1). For the three sites below the plane, this was accomplished by a linear interpolation between the first and second points for q, p, and T. The u and v were simply set to the first data point value (the observed surface wind). The q, p, and T values for the two sites above the plane were linearly extrapolated to obtain the required values at σ = 1.00. The u and v were again just set to the first data point value. The processing was carefully monitored by hand checking any large interpolation or extrapolation. Most of the interpolations and extrapolations produced changes of only 1-4 mb and about 1°K.

The data (which were in pressure coordinates) had to be changed to coordinates above the first level of the original sounding. This involves division by the surface pressure directly below the sonde. It is important not to divide the pressure by the surface pressure recorded at the sonde site, because a typical upper level balloon drift of 50 km would place the balloon over a surface pressure easily 20 mb different than the site surface pressure because of the ground slope. The x, y position of the balloon was part of the data and the pressure on the lower boundary was approximated by a plane $\pi = ax + by + c$. This enabled the division by the proper surface pressure. The resulting set of q, T, p, h, u, v, x, y, t values were valid at irregularly spaced σ levels. These data were linearly interpolated to σ levels with a regular spacing of $\Delta\sigma$ = 0.01. A linear interpolation was used because

the pressure difference involved in the interpolation was usually less than 5 mb. The 0.01 value for $\Delta\sigma$ was chosen because the resulting number of σ levels was about the same as the original number of data points. This vertical resolution is more detailed than the original wind data warrants, but it does nearly reflect the resolution of the original q, T, and p data.

These data were measured at times varying over a period of about 80 minutes (50 minutes ascent time plus 30 minutes difference in launch time). To obtain data valid at a single time for each set of ascents, the data for each ascent at each level was linearly interpolated with data from the corresponding level of the previous ascent. It was usually possible to choose a time that resulted in the smallest interpolation being done at the low levels. The desired time was chosen so that no extrapolations were performed (only interpolations). This time interpolation is one of the practical reasons that the two sets of ascents making up one final data group always use the same four or five stations for their data. That is, if five sondes reached at least the σ = .19 level for time t_1 but only four sondes reached this level for time t_2, the budget calculation for the period t_2-t_1, would be based on data from only four sondes. A second reason is that it is difficult to assess the effects on the averaged data caused by having a different number of data points at time t_1 than at time t_2. The results of the time interpolation are, therefore, sets of four or five soundings valid at a single time throughout their ascents. The ascents, however, still tilt downwind.

The data for every group of ascents is next approximated, at every level, by linear equations

$$\chi_i = a_i x + b_i y + c_i \qquad \text{where} \qquad \chi_i = \begin{cases} q,\ T,\ h \\ \pi q,\ \pi T,\ \pi h \\ \pi u,\ \pi v \end{cases}$$

The coefficients a_i, b_i, c_i are determined by a standard computer routine to give a least squares fit to the four or five data points available at each data level. The fit (standard deviation) of these planes is a measure of the linearity of the environmental variables. A poor fit could indicate the presence of a front. Examination of the standard deviations show good fits in all cases. In order to check both the plane approximation and the time interpolation, the final data were extrapolated back to their original position and time and compared with the original data. Table 2 summarizes the average absolute differences between the original data and the plane value evaluated at the time and position of the original data.

Table 2. Average Absolute Differences Between Original Data and Plane Values

σ	Δq (gr/kg)	ΔT (°K)	Δz (m)	Δu (m/s)	Δv (m/s)
1.00	.49	.61	1.41	.74	.66
.60	.21	.33	3.81	.77	.84
.20	.00	.30	11.46	1.95	1.61

Algebraic averages all < 0.00 (in above units)

It is necessary to specify the midpoint of the area of integration, A, because the value of the data at this point will be taken to be the area integrated value per unit area (see Chapter III, section 3A). This midpoint could reasonably be taken as the midpoint of the rawinsonde sites, however, the following procedure was used to account for the balloon drift. For each data period, the figure defined by the four or five sondes at their highest data level was traced over the figure

defined by the surface position of these sondes. The upper level figures drawn for all the ascents on any given day were always very similar. Also, the upper level figures always overlapped the surface figure. The midpoint position to be used for an entire day's data was then visually estimated as the centroid of the area common to the upper and lower figures. This procedure assumes that the linear variation used to approximate the measured data is valid over an area extending slightly beyond the area defined by the balloon positions. An example of this procedure is shown in Fig. 4. The procedure has the merit that the resulting vertical structure is always obtained by interpolation, never extrapolation outside the figure formed by the sondes.

Before the final data set was determined, the vertical velocity profiles were calculated using Eq. 9. The vertically integrated results showed unrealistic values of $\pi\dot{\sigma}$ on the order of 7×10^{-3} mb/sec at the highest data levels (about 120 mb). At these near-tropopause levels, it is reasonable to expect the area average value of $\pi\dot{\sigma}$ to be near zero. If deep convection is penetrating the tropopause, this assumption would call for exactly compensating subsidence to occur at these levels within area A. A divergence adjustment technique developed by O'Brien (1970) and used by Fankhauser (1969, 1974) was used to force the $\pi\dot{\sigma}$ to zero at the highest data levels (σ = .12 to .17). In this technique, the divergences are adjusted by an amount linearly proportional to the height. The low level, and presumably more accurate, values are changed very little and less accurate upper level divergences are adjusted more. This adjustment method only describes how to change the total horizontal divergences. The actual velocity components are adjusted by evenly dividing the divergence correction between the x slope of the πu component and the y slope of the πv component.

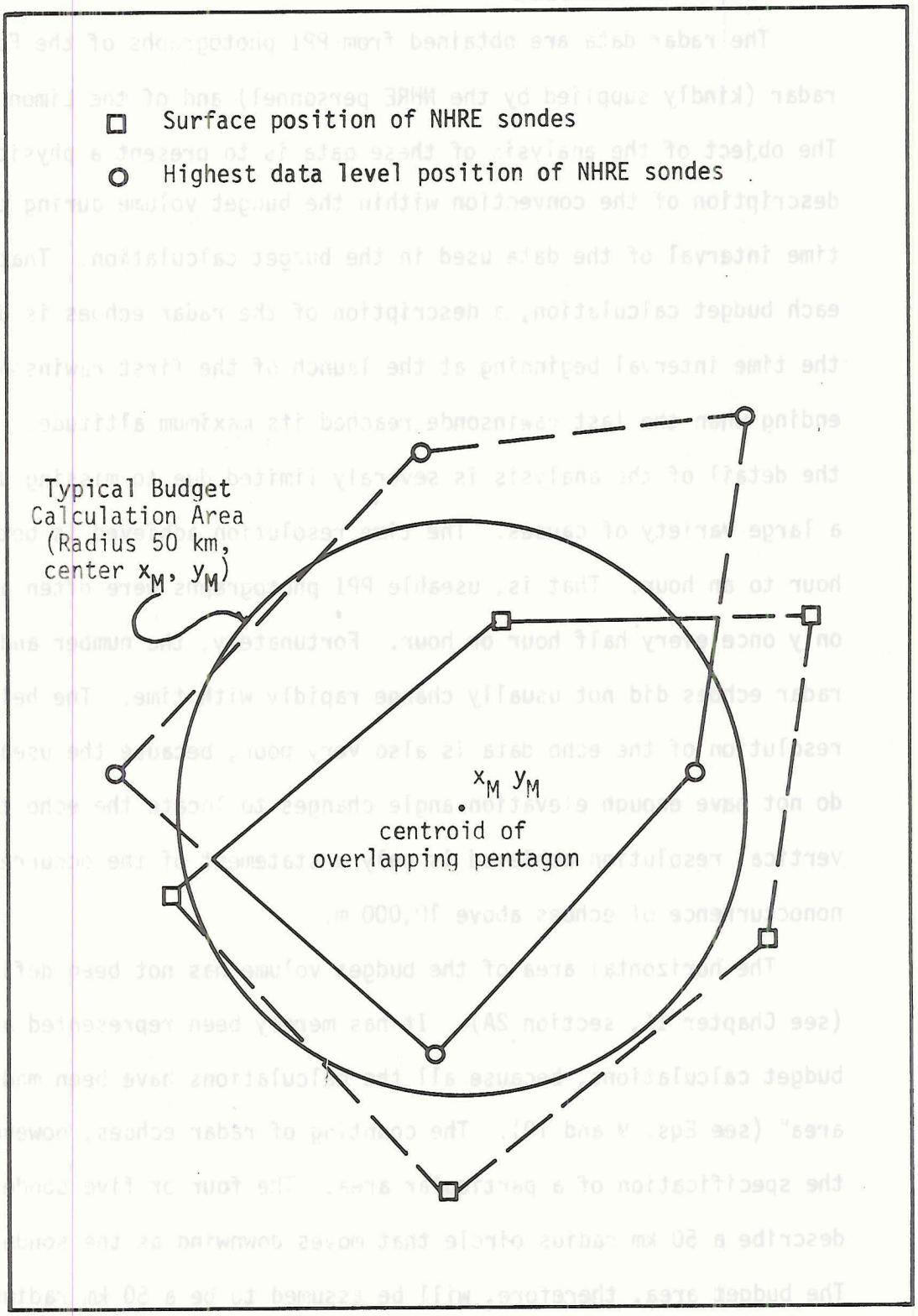

Figure 4. Typical Budget Calculation Area

3. Radar Data Reduction

The radar data are obtained from PPI photographs of the Fort Morgan radar (kindly supplied by the NHRE personnel) and of the Limon radar. The object of the analysis of these data is to present a physical description of the convection within the budget volume during the entire time interval of the data used in the budget calculation. That is, for each budget calculation, a description of the radar echoes is desired for the time interval beginning at the launch of the first rawinsonde and ending when the last rawinsonde reached its maximum altitude. Unfortunately, the detail of the analysis is severaly limited due to missing data due to a large variety of causes. The time resolution achieved is between a half hour to an hour. That is, useable PPI photographs were often available only once every half hour or hour. Fortunately, the number and size of radar echoes did not usually change rapidly with time. The height resolution of the echo data is also very poor, because the useable data do not have enough elevation angle changes to locate the echo tops. The vertical resolution achieved is only a statement of the occurrence or nonoccurrence of echoes above 10,000 m.

The horizontal area of the budget volume has not been defined as yet (see Chapter II, section 2A). It has merely been represented as A in the budget calculations, because all the calculations have been made "per unit area" (see Eqs. 9 and 10). The counting of radar echoes, however, requires the specification of a particular area. The four or five sondes roughly describe a 50 km radius circle that moves downwind as the sondes rise. The budget area, therefore, will be assumed to be a 50 km radius circle centered at x_M, y_M (see section 2 and Fig. 4 for the choice of x_M, y_M).

Fortunately, the choice of A is not critical because almost all of the echoes are clearly inside or outside this area.

The actual analysis of the radar data consisted of first obtaining a representative PPI picture of the radar echoes within the budget area for a given one hour interval. "Representative" means that the number of small, large, and high echoes did not change. Small echoes have an approximate outer contour (17 dbz) radius of less than 10 km; large echoes are greater than 10 km. High echoes extend above 10,000 m. These data were then used to determine the maximum number of echoes in each category for each budget calculation interval. The development of each category (small, large, high) during the defined budget interval was also determined. The "development" of a particular category is defined as the number of echoes at the end of the budget interval minus the number at the beginning. If the maximum number occurs in the middle of an interval, the development is characterized by two differences - the maximum number minus the beginning number, and the final number minus the maximum.

Budget calculations are presented in Chapter V as average budgets for periods that have similar gross radar features. These averages do not use the characteristics of radar echo size, height, or development. (However, the weak, developing average category is concerned with change of non-echo producing clouds into echo producing clouds.) Nevertheless, these features are included in the list of data in order to provide a more complete picture of the individual data that make up each average data period. A complete listing of the data intervals including a description of the rawinsonde characteristics (number of sondes, time interval, etc.) and echo characteristics is presented in Table 1.

V. BUDGET CALCULATION RESULTS

1. Introduction

A. Organization and Presentation of Budget Calculations

This chapter deals with the second and third problems mentioned in Chapter I, section 1: What are the cloud transfer properties (term 5 of Eq. 5) of convection for a variety of mesoscale conditions? How do they compare to a radar description of the convection? The cloud transfer properties will be presented in the context of the entire budget, that is, all the terms in the budget will be discussed. This discussion will be in terms of the physical processes that contribute to each term in the budget.

Latent heat, dry static energy, and moist static energy budgets have been calculated for 39 separate data intervals. The data in these intervals represent a variety of mesoscale conditions. In section 2 these data are introduced by displaying several representative examples set in larger (almost synoptic) scale fields. The main purpose of the presentation in section 2 is to provide a background for the discussion of the mesoscale fields in section 4. In addition to this, however, the larger scale background data in which the mesoscale data are set provides an estimate of sky cover to be used in the radiation calculations presented in section 3. In section 4 the results of all the budget calculations are presented in the form of four average budgets.

B. Average Budgets

In order to compare the budget description of convection to the radar description, the budget calculations are presented in section 4 as average budgets for periods that have similar gross radar features. Average budgets are appropriate for two reasons. First, the resolution

of the radar data is very coarse (see section 3, Chapter IV) and does not warrant budget-radar comparisons for each individual budget calculation. The use of simple gross radar features to describe the convection instead of the use of detailed descriptions of individual echoes is reasonable considering that this is a study of mesoscale characteristics of cumulus convection. Second, the budget results contain considerable variability and noise. Averaging reduces the noise and brings out features that frequently occur. In fact, the discussion of a particular average budget feature generally includes a statement of how frequently the feature occurred in the individual cases making up the average. In addition, the thermodynamic structure (vertical profile of θ, h, and q) of the individual mesoscales input data used in each average budget is also carefully noted.

Four types of convective fields are defined: (1) weak suppressed convection, (2) weak developing convection, (3) moderate convection, and (4) precipitating convection. The data intervals that are used in the calculation of average budgets for each of these convective situations are summarized in Table 3. The specific characteristics of each type of mesoscale convection are defined as follows. (1) weak, suppressed convection is defined as small, non-precipitating clouds that do not produce radar echoes and do not develop into larger echo producing clouds later in the day. Four days (containing fifteen data intervals) have this weak convection that did not develop further during the day. That is, it is certain that on these days no radar echoes (or, of course, precipitation reports) were present in the data volume until approximately 1730 LST when the radar was turned off. (2) a particular data interval is said to contain weak developing convection when no radar echoes or

Table 3. Data Intervals in Each Convective Category

Legend (see Table 1)

Date (1973)	Time (LST)	Number of Radar Echoes and Precipitation Reports									
		Maximum Value for Interval					Development				
		Precip	I	II	Total	High	Precip	I	II	Total	High
Weak, Suppressed Convection											
0612	1149	N	0	0	0	0	-	0	0	0	0
	1235	N	0	0	0	0	-	0	0	0	0
	1403	N	0	0	0	0	-	0	0	0	0
	1533	N	0	0	0	0	-	0	0	0	0
0712	1609	N	0	0	0	0	-	0	0	0	0
	1735	N	0	0	0	0	-	0	0	0	0
0713	1153	N	0	0	0	0	-	0	0	0	0
	1303	N	0	0	0	0	-	0	0	0	0
	1433	N	0	0	0	0	-	0	0	0	0
	1604	N	0	0	0	0	-	0	0	0	0
	1734	N	0	0	0	0	-	0	0	0	0
0723	1147		0	0	0	0		0	0	0	0
	1332		0	0	0	0		0	0	0	0
	1502		0	0	0	0		0	0	0	0
	1603		0	0	0	0		0	0	0	0
Weak, Developing Convection											
0717	1217	N	0	0	0	0	-	0	0	0	0
	1331	N	0	0	0	0	-	0	0	0	0
	1503	N	0	0	0	0	-	0	0	0	0
0724	1303	N	0	0	0	0	-	0	0	0	0
0727	1158		0	0	0	0		0	0	0	0
	1422		0	0	0	0		0	0	0	0
0731	1217	N	0	0	0	0	-	0	0	0	0

Table 3. Continued

Date (1973)	Time (LST)	Number of Radar Echoes and Precipitation Reports									
		Maximum Value for Interval					Development				
		Precip	I	II	Total	High	Precip	I	II	Total	High
Moderate Convection											
0601	1639	N	6	0	1		-	2, -4	0	2, -4	
	1737	N	6	0	6		-	-6	0	-6	
0629	1741	N	1	0	1	0	-	1	0	1	0
0716	1733	N	2	0	2	0	-	2	0	2	0
0724	1547	N	1	1	2		-	1	1	1	
*	1806	N	1	1	2		-	1, -1	0	1, -1	
* 0731	1448	N	0	1	1	Y	-	0	1	1	>0
Precipitating Convection											
0601	1312	Y	1	0	1	0	E	1	0	1	0
	1542	Y	6	0	6		M	6	0	6	
0704	1211	.074	7	1	7		E	6, -4	1	6, -3	
	1401	.074	7	1	7		ME	-4	1	-3	
0709	1518	.081	6	0	6		ME	6	0	6	
	1720	.081	6	0	6		BME	4, -1	0	4, -1	
	1808	.081	6	0	6		BM?				
0717	1637	.009	3	0	3	Y	ME	3	0	3	+
	1737	.009	3	0	3	Y	M	3	0	3	+
0724	1148	Y	Y	Y	Y	Y	?M	<0	<0	<0	<0
0728	1508	.105	3	0	3	Y	BME	3, -2	0	3, -2	>0,
	1655	.105	3	0	3	Y	BM?	<0?	0	<0?	

* Not used - bad rawinsonde data.

precipitation reports are present during the given interval, but echoes and/or precipitation occur later during the day. Seven data intervals are characterized by this type of convection. In each case, echoes and/or precipitation develop in the data volume within two hours of the end of the interval characterized as weak and developing. (3) moderate convection is defined as situations in which radar echoes are present within the data volume, but no precipitation is recorded by the ground collecting instruments. We cannot be sure that the clouds in this category did not precipitate at all, because complete evaporation of precipitation before it reaches the ground is a common occurrence in northeastern Colorado. (4) precipitating convection was present and recorded by the ground collecting instruments in the data volume during twelve data intervals spread over six days.

Each individual budget calculation period with useable radar data is assigned as having one of the above types of convection. A budget calculation is made for each of these 39 individual data intervals. To form an average budget for a given type of convection, each term in an individual budget is averaged with corresponding budget terms for periods of similar convection. Average budgets of latent heat, dry and moist static energies for the above four types of convective fields are presented and discussed in section 4. The average lifting condensation level is mentioned in these discussions. The LCL (based on q and T at σ = .99) is calculated graphically for each individual budget interval and then an average is calculated for each of the four convection types. Henz (1975) notes the close correspondence between LCL and cloud base in the NHRE area.

C. Three Dimensional Flux Divergence

The final budget equation 5 in Chapter II contains four terms: time change of χ_E, "average" horizontal and vertical divergences of the flux of χ_E, and an apparent source of χ. The average horizontal and vertical divergences of the flux of χ_E (for χ = s, h) are the two terms with the largest magnitudes (about 10 times the other two terms). These large magnitudes, however, should not be taken to mean that these terms represent the "cause" or "forcing" of the observed budget. Rather, their magnitudes simply reflect the fact each of the two terms contain part of the total mass circulation. Omitting the integrations, the second terms of Eq. 5 is the sum $\chi_E \nabla\cdot \frac{\partial p}{\partial s} \vec{V} + \frac{\partial p}{\partial s} \vec{V}\cdot\nabla\chi_E$; the third term of Eq. 5 is the sum $\chi_E \frac{\partial}{\partial s} (\frac{\partial p}{\partial s} \dot{s}) + \frac{\partial p}{\partial s} \dot{s} \frac{\partial}{\partial s} (\chi_E)$. The first term in each sum is related to the mass circulation. The sum $\chi_E(\nabla\cdot \frac{\partial p}{\partial s} \vec{V} + \frac{\partial}{\partial s} (\frac{\partial p}{\partial s} \dot{s}))$ is approximately zero by the continuity equation. The mass circulation portion of terms 2 and 3 of Eq. 5 are about ten times larger than the remaining advection portions ($\frac{\partial p}{\partial s} \vec{V}\cdot\nabla\chi_E$ and $\frac{\partial p}{\partial s} \dot{s} \frac{\partial}{\partial s} (\chi_E)$). Consequently, vertical profiles of terms 2 and 3 look almost like mirror images. The sum of terms 2 and 3 is presented in section 4 in order to illustrate the portion of these terms that is not due to the mass circulation. This sum is the three-dimensional divergence of the flux of χ_E. Although this flux contains the environmental value of χ_E, the product $\pi\vec{V}_3\chi_E$ is not an environmental flux of χ because $\dot{s}$ is a vertical velocity averaged over both cloud and environmental areas.

D. Vertically Integrated Apparent Source

In section 4, the apparent source term in the budget equation will be presented in a vertically integrated form. The motivation for this method of presentation was described in Chapter III, section 3B. The actual

calculation of the vertical profile of an integrated apparent source requires a choice of σ_T. The convective fluxes of F_{q_T}, F_{s_ℓ}, and F_h are set equal to zero at and above σ_T and the numerical integration of Eq. 11 proceeds downward from σ_T.

The value of σ_T is set to .30 (250 mb) in the moderate and precipitating convection cases. This corresponds to an approximate tropopause level. The only convective processes that could produce an apparent source of s or h above the tropopause are very large cumuli that overshoot the tropopause. However, the magnitude of the apparent source term above the tropopause is often larger than below even though very few clouds could be assumed to penetrate the tropopause level. It is difficult to relate a real, physical process to these high level, erratic, nonzero apparent sources. However, inaccuracies of upper level rawinsonde winds make it very reasonable to ascribe an apparent source above the tropopause to wind errors.

In the case of weak, developing convection, σ_T is set to .40 (340 mb) and for weak, suppressed convection, σ_T is set to .50 (430 mb). The choice σ_T=.40 is simply a subjective evaluation of the general cloud top level for developing convection. It is slightly below the σ_T for moderate and precipitating convection. The choice of σ_T = .50 eliminates a negative convective flux of moist static energy that is unrealistic in the case of weak, suppressed convection. It also agrees with the general idea of the cloud tops being much lower in a suppressed situation than in the other situations.

Although the convective fluxes have been set to zero above σ_T, the other terms in the budget equation (from which the apparent source is calculated) have not been set to zero above σ_T. Therefore, the assumed error above σ_T can be estimated by visually combining the time change and three-dimensional divergence terms above σ_T.

The choice of σ_T has a large influence on the magnitude of the convective fluxes. The surface ordinate of these fluxes are roughly checked, however, by use of the integral constraints mentioned in Chapter III, section 4.

2. Synoptic Scale Setting for Budget Data

In this section, the mesoscale data used in the budget calculations are introduced by displaying several representative examples set in larger scale flows. This presentation is not meant to give a detailed relation between mesoscale and synoptic scale circulations. Rather, it provides a general setting for the budget data and a rough indication of how smoothly the budget data mesh with nearby surface data and 500 mb synoptic circulations. The following procedure was used to obtain Figs. 5 through 10. Standard NMC 500 mb height analyses at 1800 L (00Z) were checked (and occasionally adjusted subjectively) and interpolated to display isoheights every 20 meters. These analyses were then copied on to a 400 km square map centered over the NHRE are (Fig. 1). Surface data were plotted on a second set of these maps at 1200 and 1800 L (surface wind data at 1500 L were also plotted to aid continuity of the wind data). The data used in the budget calculations were then added to these two sets of maps. These mesoscale values were obtained by evaluating the linearly fit rawinsonde data at the five corners of the NHRE area at the appropriate times. That is, the values plotted at the five squares in Figs. 5 through 10 were constructed from the coefficients described in Chapter IV, section 2. Use of the time derivatives of these coefficients enabled the budget data to be given at 1200 and 1800 L. Two maps (surface and 500 mb) were prepared for each of the fourteen days for which budget data are available. The resulting maps fall into three clear cut categories, and because the object of this section is quite general, only three of the most clearly representative sets of maps are presented.

Legend Figures 5 - 10

Figures 5, 7, and 9 - Surface Maps.

Figures 6, 8, and 10 - 500 mb Maps.

Station Model.

Surface

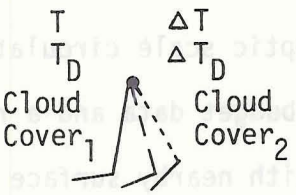

T = temperature (°F) 1200 LST

T_D = dew point (°F) 1200 LST

Cloud Cover$_1$ = cloud cover 1200 LST

Cloud Cover$_2$ = cloud cover 1800 LST

ΔT = T at 1800 - T at 1200

ΔT_D = T_D at 1800 - T_D at 1200

= Wind at 1200 (5 and 10 knot barbs)

= Wind at 1500

= Wind at 1800

● = Surface station (identified on 500 mb map)

□ = NHRE rawinsonde site surface observation (plane fit)

500 mb

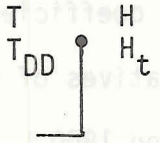

● = 500 mb synoptic station

□ = NHRE observation (plane fit)

T = temperature (°F) 1800 LST

T_{DD} = dew point depression (°F)

H = 500 mb height decameters (Usual isoheight contour 60 m, 20 m used in this analysis.)

H_t = 12 hour height change decameters.

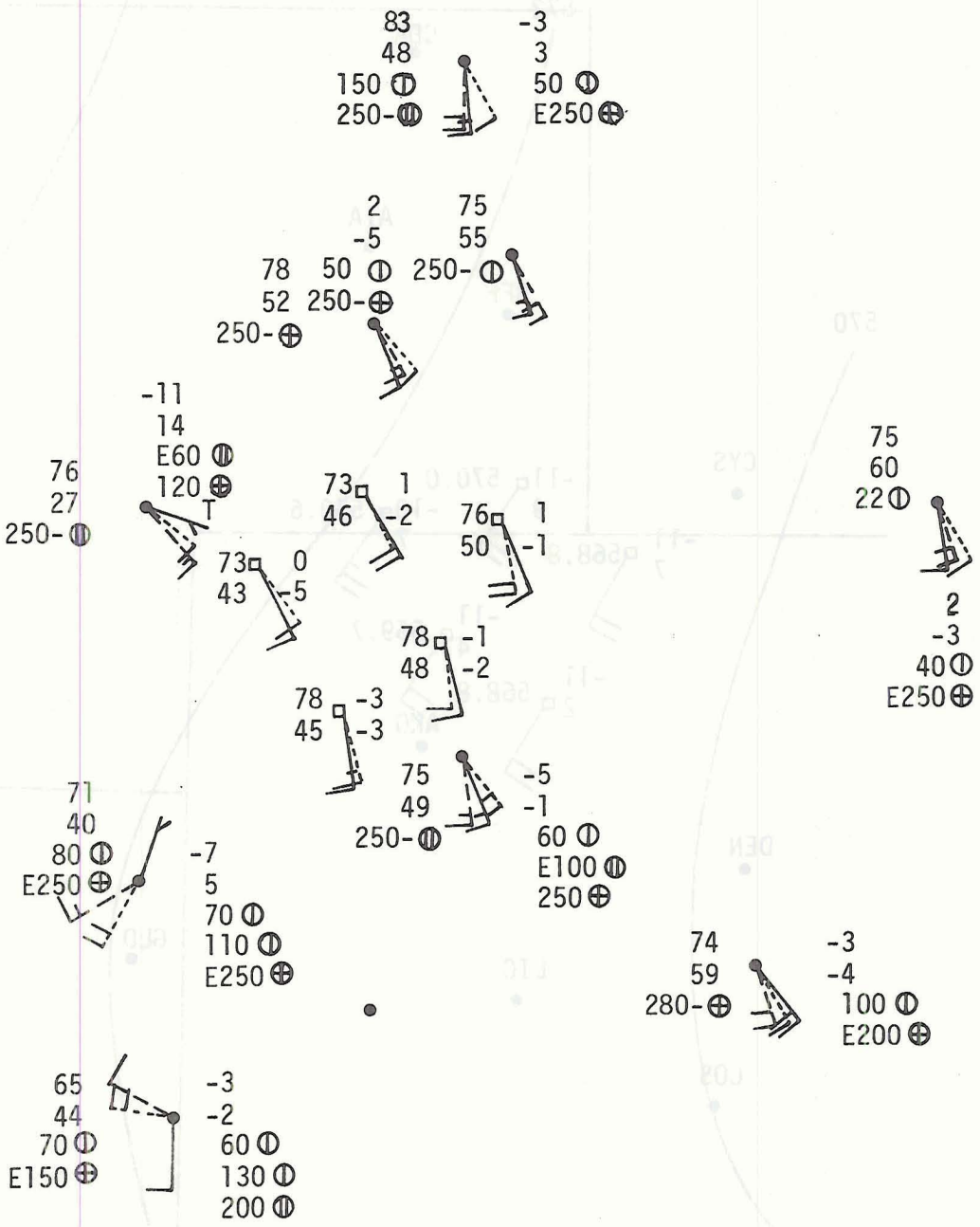

1 June 73 SURFACE MAP.

Station Identifiers and State Boundaries given on 500 mb maps.

Figure 5. 1 June 1973 Surface Map

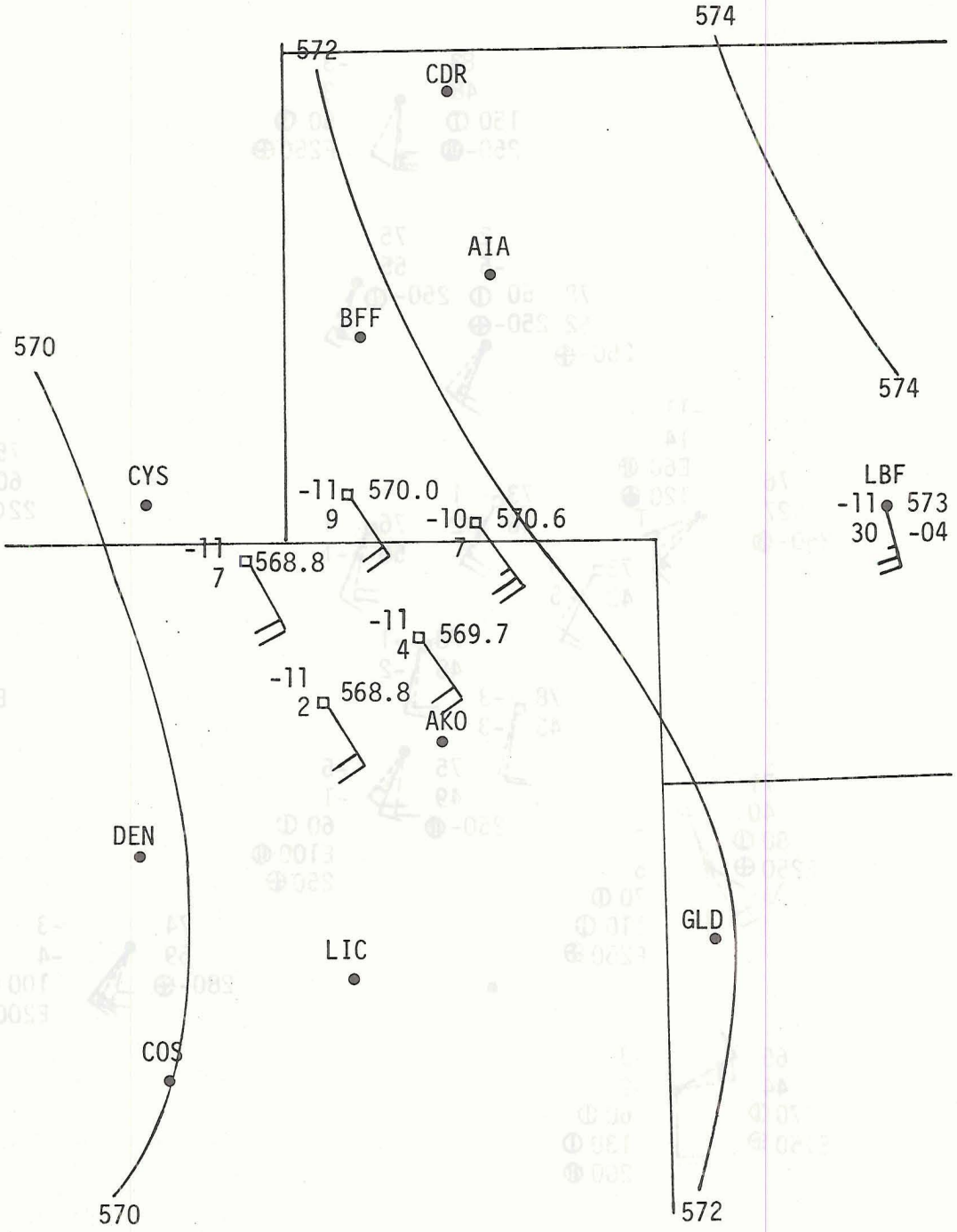

1 June 73. 500mb.
1800

Figure 6. 1 June 1973 500 mb Map

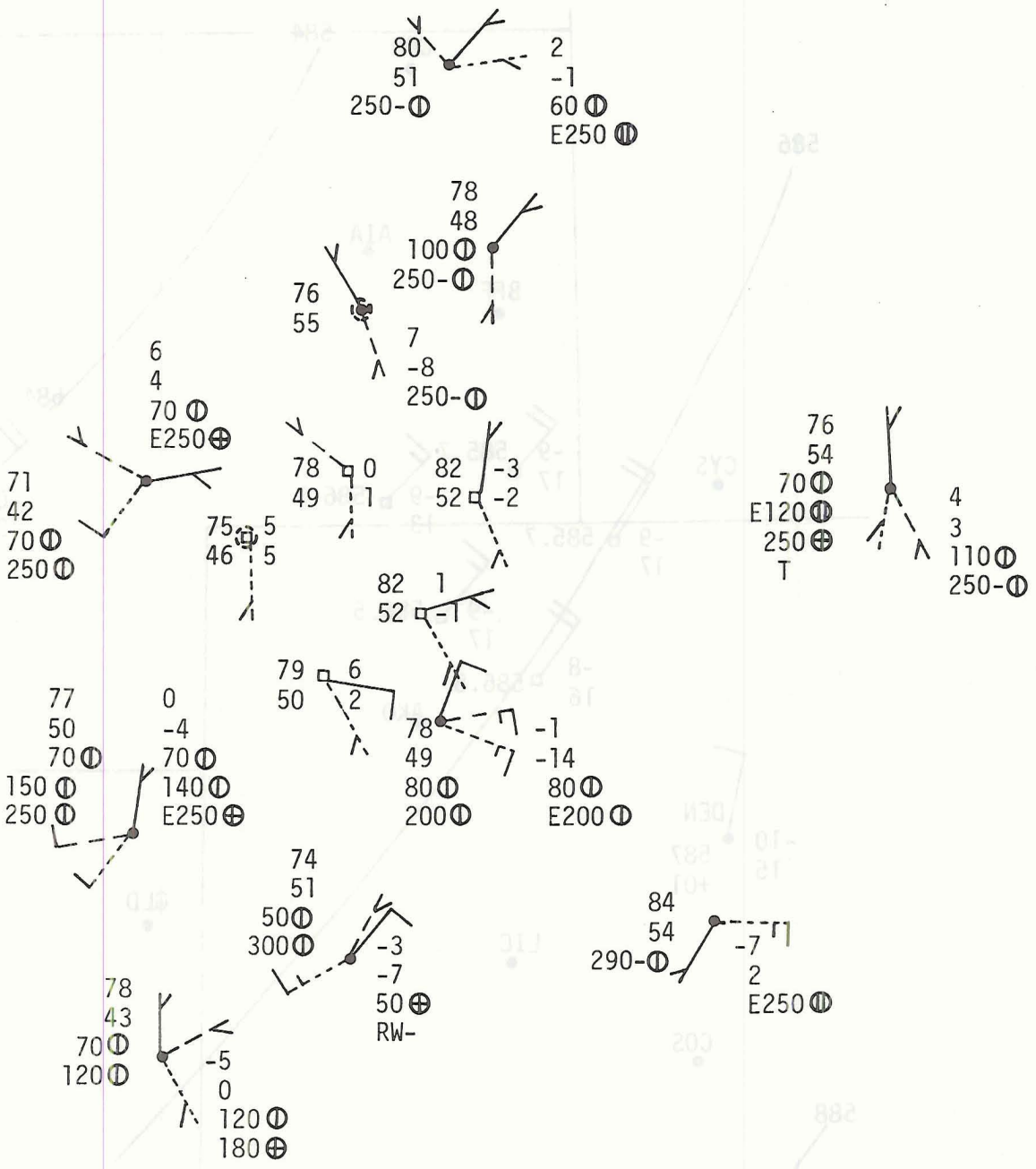

27 July 73. SURFACE MAP.

Figure 7. 27 July 1973 Surface Map

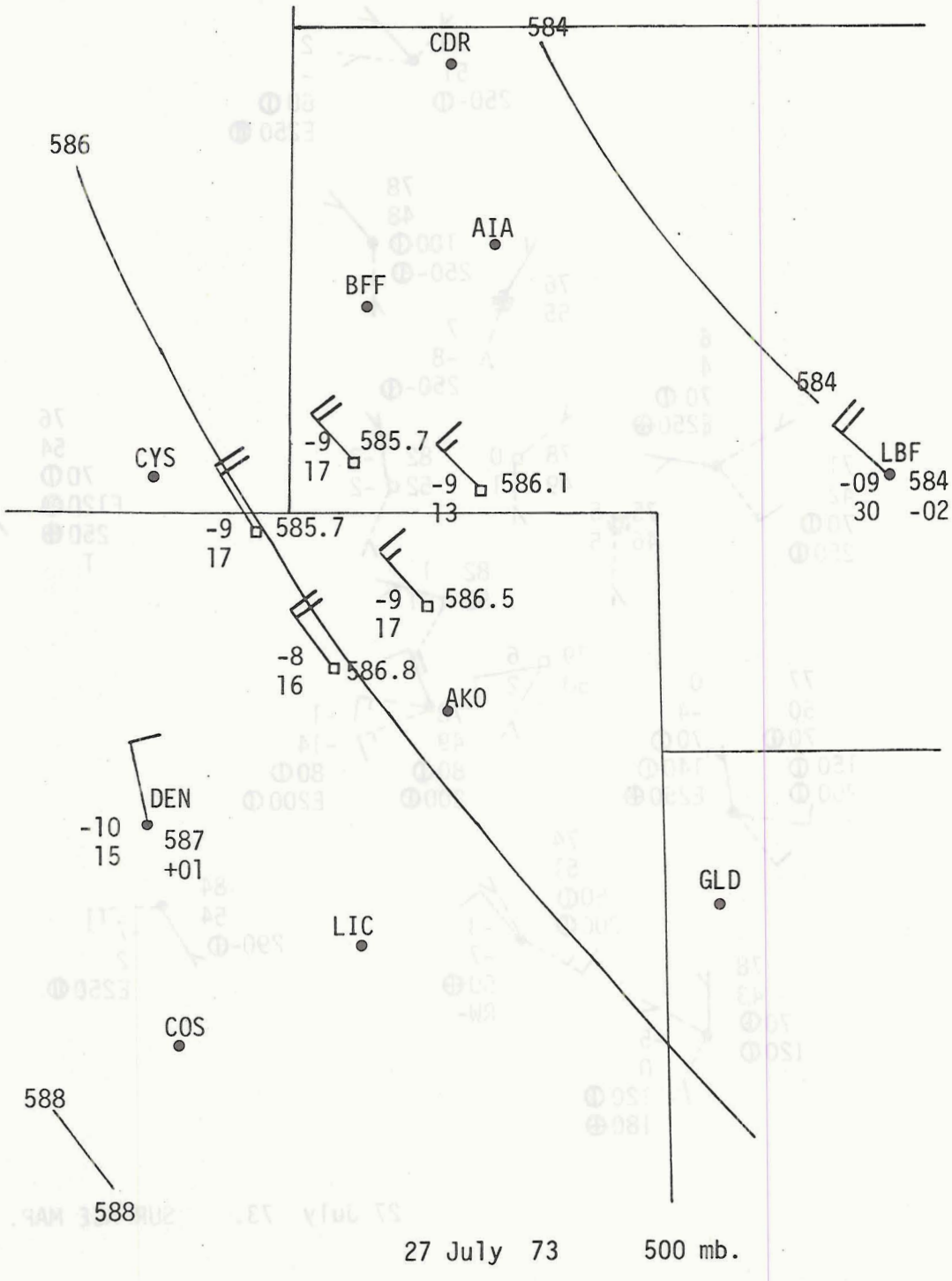

Figure 8. 27 July 1973 500 mb Map

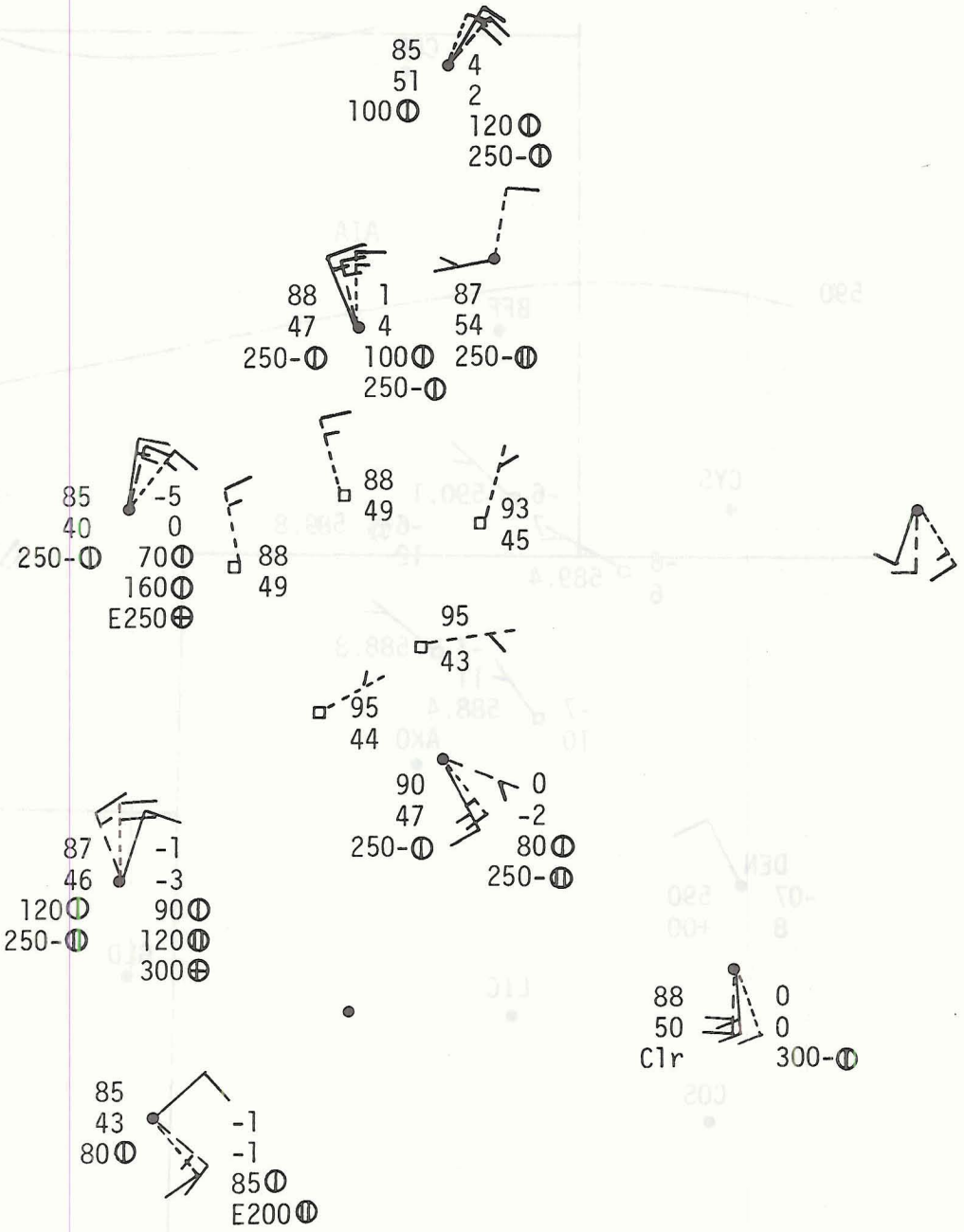

12 July 73. SURFACE MAP.

Figure 9. 12 July 1973 Surface Map

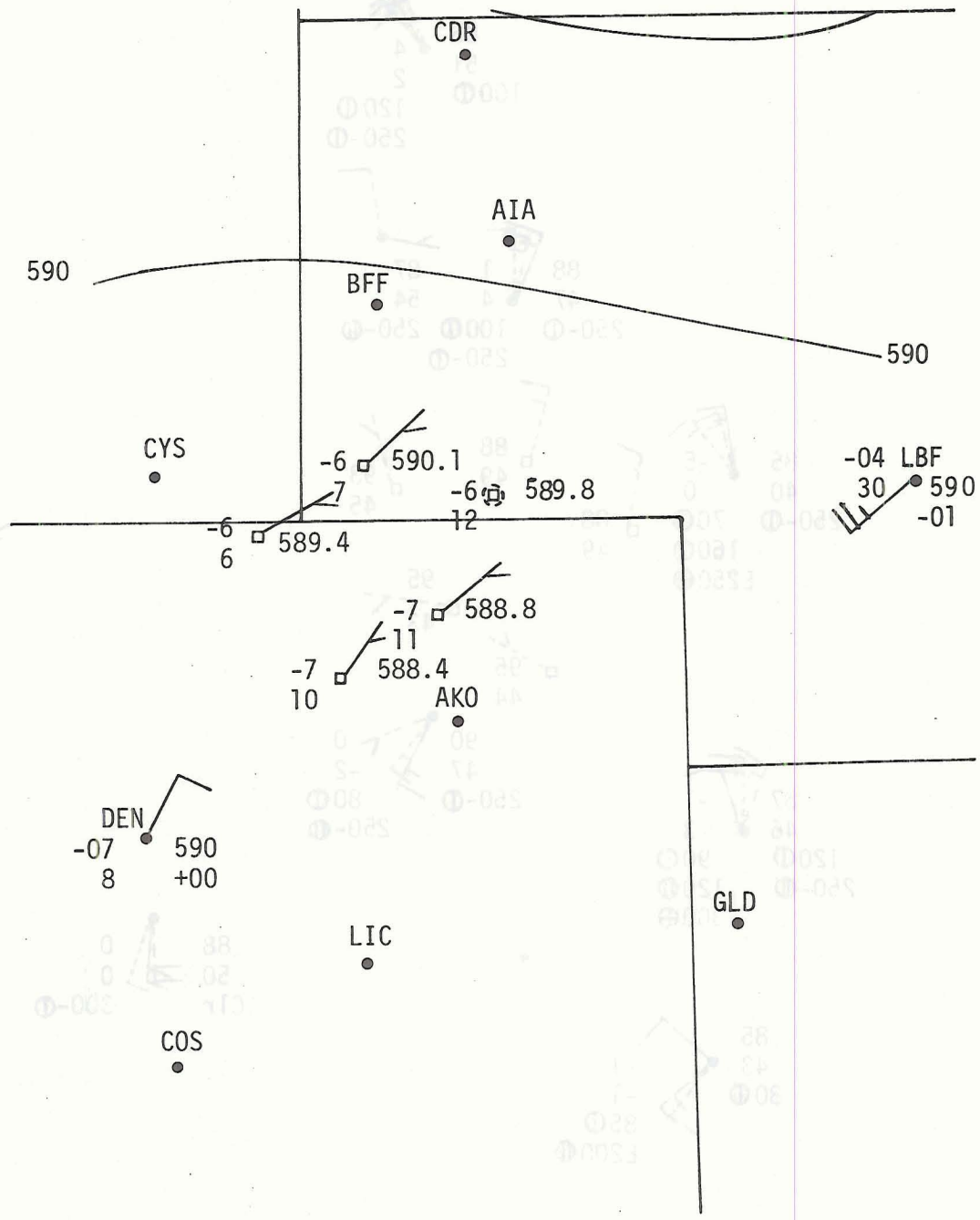

Figure 10. 12 July 1973 500 mb Map

The first set, Figs. 5 and 6, are representative of days 1, 29 June and 9 and 13 July. Almost all the surface wind data show a flow in a well defined direction (SE on 1, 29 June and NE on 9 and 13 July) and this direction is closely aligned with the general flow indicated in the NHRE area. The surface temperatures and dew points vary considerably from station to station and no pattern stands our for comparison with the NHRE surface temperatures and dew points. Figure 6 shows that the 500 mb synoptic analysis and the mesoscale data mesh quite well. The mesoscale wind directions follow the height contours closely and the speeds are similar to those measured at Denver (DEN) and North Platt (LBF). The mesoscale heights differ from the interpolated synoptic isoheights by approximately 20 m. The temperatures are generally within one degree of the DEN and LBF 500 mb temperatures. The dew point depressions are much more erratic, Fig. 6 showing one of the largest differences in dew point depressions.

Figures 7 and 8 are representative of the second category of maps (12 June, and 4, 16, 17, 23, 27, 28, 31 July). The main characteristic of this category is a much less organized surface and low level (below 700 mb) flow. The surface wind speed (5-10 kts) is generally weaker than the wind speeds of the first category (10-15 kts). The direction of the flow is not well defined and the direction changes from 1200 to 1500 to 1800 L are larger than those in the first category. The budget data generally reflect these larger direction differences and direction changes with time. This lack of a well defined flow direction over the entire 400 km square area extends up to about 700 mb. At 500 mb the flow is quite smooth and the mesoscale wind, temperature, and dew point depression data mesh as well with the synoptic scale analysis as in the case of the

first category. The surface temperatures and dew points again show large station to station differences with no clear patterns present. The low level wind direction changes in the NHRE area are somewhat smoother because the data are filtered by applying a linear representation for u and v. This smooth variation might not, however, accurately represent all the low level direction changes suggested by the surrounding surface observations. As pointed out in Chapter II, section 3A, this assumed linear fit could be a source of error. Fortunately, these possibly non-linear flows are not too deep and above them Fig. 8 shows the linear approximation to be quite appropriate.

The third category occurs on only three days, 12, 16 and 24 July. These days have a well defined, low level convergence line running through the NHRE area (Fig. 9). The existence of this line is suggested by both the flow defined by the hourly observations and by the NHRE data. If this convergence zone is on the order of 50 to 100 km wide, the linear variation assumed in the NHRE data could be a good representation. If the zone is very sharp, say 5-10 km, the assumed smooth wind variation would be a source of error. Fortunately, the hourly observations do not show any marked difference in temperature or dew point across the convergence zone that would compound this possible non linearity. This convergence line is also quite shallow. On 16 and 24 July the 500 mb flow again has a single, well-defined direction and the mesoscale pattern meshes as well as the previous two categories with the synoptic pattern. The 12 July case, Fig. 10, displays the weakest of all the 500 mb flows, but the mesoscale data are still consistent with the flat contour data between DEN and LBF.

The above descriptions show that the mesoscale budget data fit very well with the larger scale data in the sense that circulations that are well defined over the 400 km square area are also well defined by the budget data. The hourly observations that show a weak and ill defined flow are echoed by a similar weak flow in the budget area. The hourly surface observations provide another piece of data in addition to the wind, temperature and dew point fields. These observations supply the only visual estimate of the cloud cover over the 400 km square area. The next section will discuss these observations and use them as the basis for several model radiation calculations.

3. Radiation Calculations

A single net radiation divergence profile is calculated for the weak, suppressed and weak, developing average convective situations mentioned in section 1B. The temperature and water vapor profiles that are used in the calculation (see Chapter III, section 5) are described in detail in section 4. The subjective assessment of the cloud cover to be used in the long wave radiation calculation is presented in Table 4.

Table 4. Cloud Cover Used in Long wave Radiation Calculations.

Average Data Interval	Cloud Estimate in Synoptic Code	Values in long wave program	
		Fractional Area Covered	Cloud Base-Top (mb)
1. Weak, Suppressed	6000, 2500	.75	clear
		.125	675-500
		.125	300-250
2. Weak, Developing	7000, 2500	.75	clear
		.125	625-350
		.125	300-250

The estimates of cloud cover in Table 4 given in synoptic code are based primarily on the hourly sky cover observations recorded at the two stations directly north of the NHRE area (BFF and AIA, see Fig. 6) and the one station south of the NHRE area (AKO). The two stations to the west of the NHRE area (CYS and DEN) were afforded somewhat less importance because they are close to the foothills. The cloud model to be used in the radiation program is based on this estimate and on the following factors. The cumulus cloud base levels were approximately adjusted to the appropriate lifting condensation level. The choices of the cumulus tops are approximately at the σ_T level (see section 1D for discussion of σ_T). The cirrus clouds were put at a near tropopause level and assumed to be 50 mb thick. The specific area cloud coverages are within the bounds of synoptic code estimates, but are otherwise arbitrary.

The long, short, and net radiation heating rates are presented in Figs. 11-12. Although the radiation calculation was carried out to the 1 mb level, only the profiles from the 850 mb to 150 mb level are presented. The apparent source of moist static energy is approximately ten times larger than the radiation source.

The net radiation source is much smaller than the contributions due to the individual long and short wave components, and is very much smaller than the apparent source of h. The radiation contributions to the moderate and precipitating average budgets are neglected on the basis of the very small values calculated for weak convection cases. Radiation profiles are not presented for moderate and precipitating cases because the increased cloud cover makes the important short wave contribution suspect (see Chapter III, section 5).

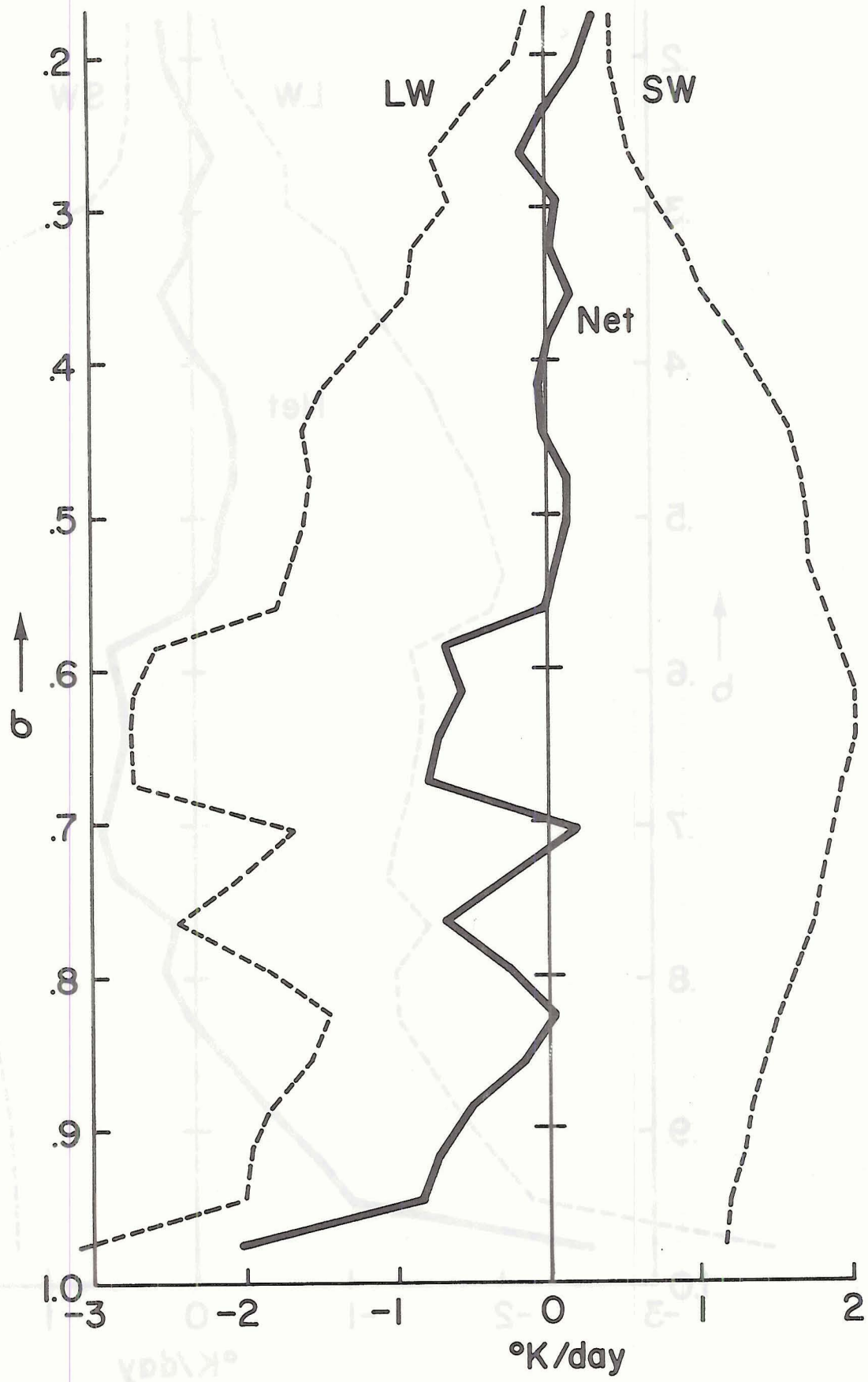

Figure 11. Radiation Source - Weak Suppressed Convection.

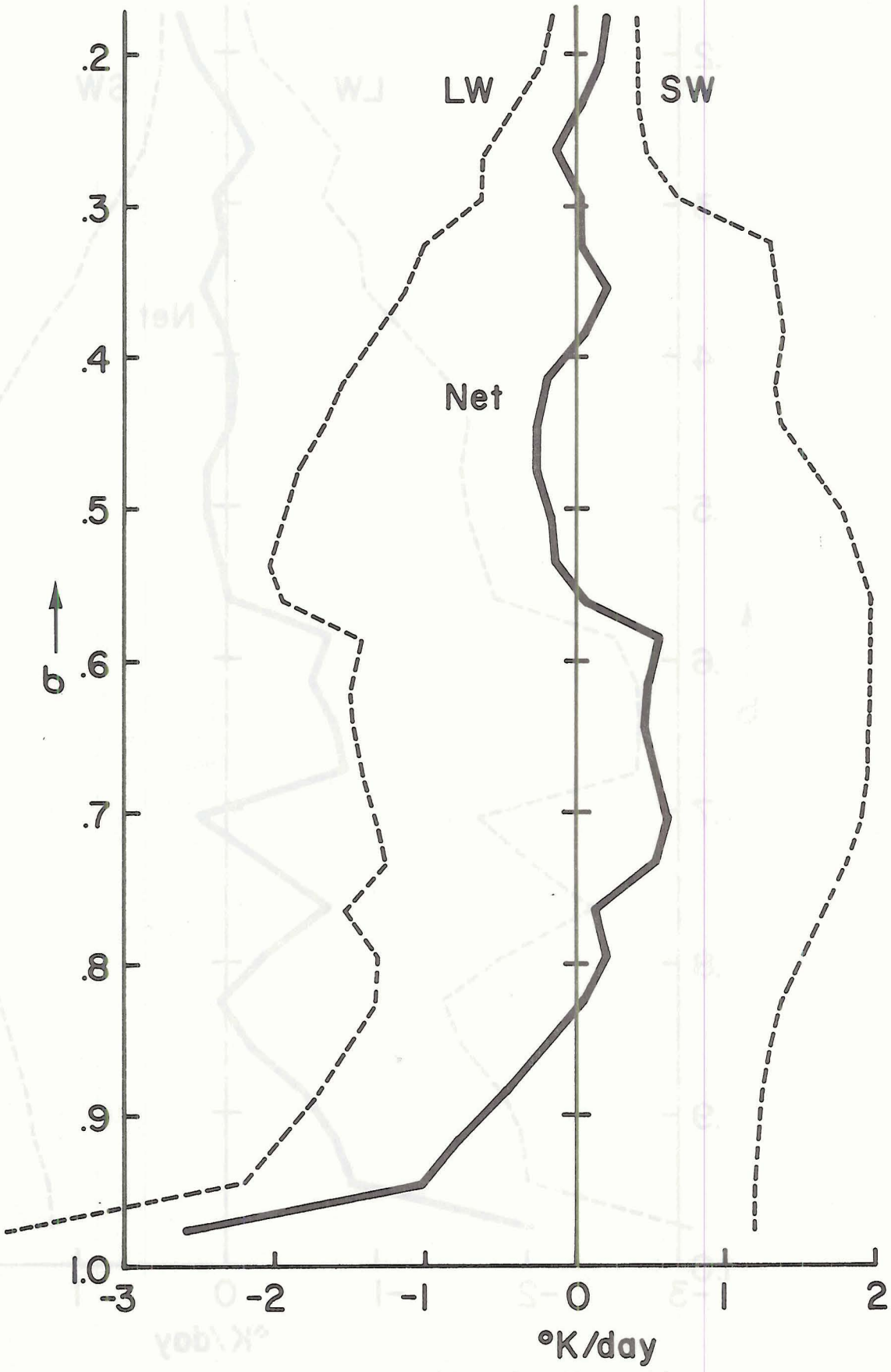

Figure 12. Radiation Source - Weak Developing Convection.

The neglect of the divergence of the radiation flux in the atmosphere does not mean that radiation is unimportant. First, it is the divergence of F_r that is being neglected and not the flux that reaches the ground. The surface radiation flux forces dry low level thermals and evaporates water from the ground. Second, a relatively small magnitude of a term in a diagnostic budget calculation is not a statement that the term has little affect on the larger budget terms. The proper interpretation of radiation effects on mesoscale circulations remains for others to model.

4. Budgets for Various Convective Situations

A. Weak Suppressed Convection

Shallow, non-precipitating clouds that do not produce radar echoes were present during all 39 of the data intervals. There were four days in which this weak convection did not develop any radar echoes during the day. The budget calculations for the fifteen data intervals in these four days have been averaged and will be taken to represent weak, suppressed convection. This classification is a finer division of the "undisturbed" BOMEX period discussed by Holland and Rasmusson (1973), Nitta (1975), Betts (1975); or the "no echo" class of Ninomiya (1974); or "region 8" (ridge region) of Reed and Recker (1971); or the "weak/absent" convective activity period of Augstein, et al (1973).

The general vertical structure of the thermodynamic variables, as represented by θ, q, and h, is presented in Figs. 13a-c. All five data intervals in 13 July contained a distinctly cool lower layer, and inclusion of day 13 July in a single average produced an unrepresentative low level vertical thermodynamic structure. Consequently, two sets of average thermodynamic profiles are presented. One is for 13 July and the other is for the remaining data intervals (see Table 3 for specific dates and

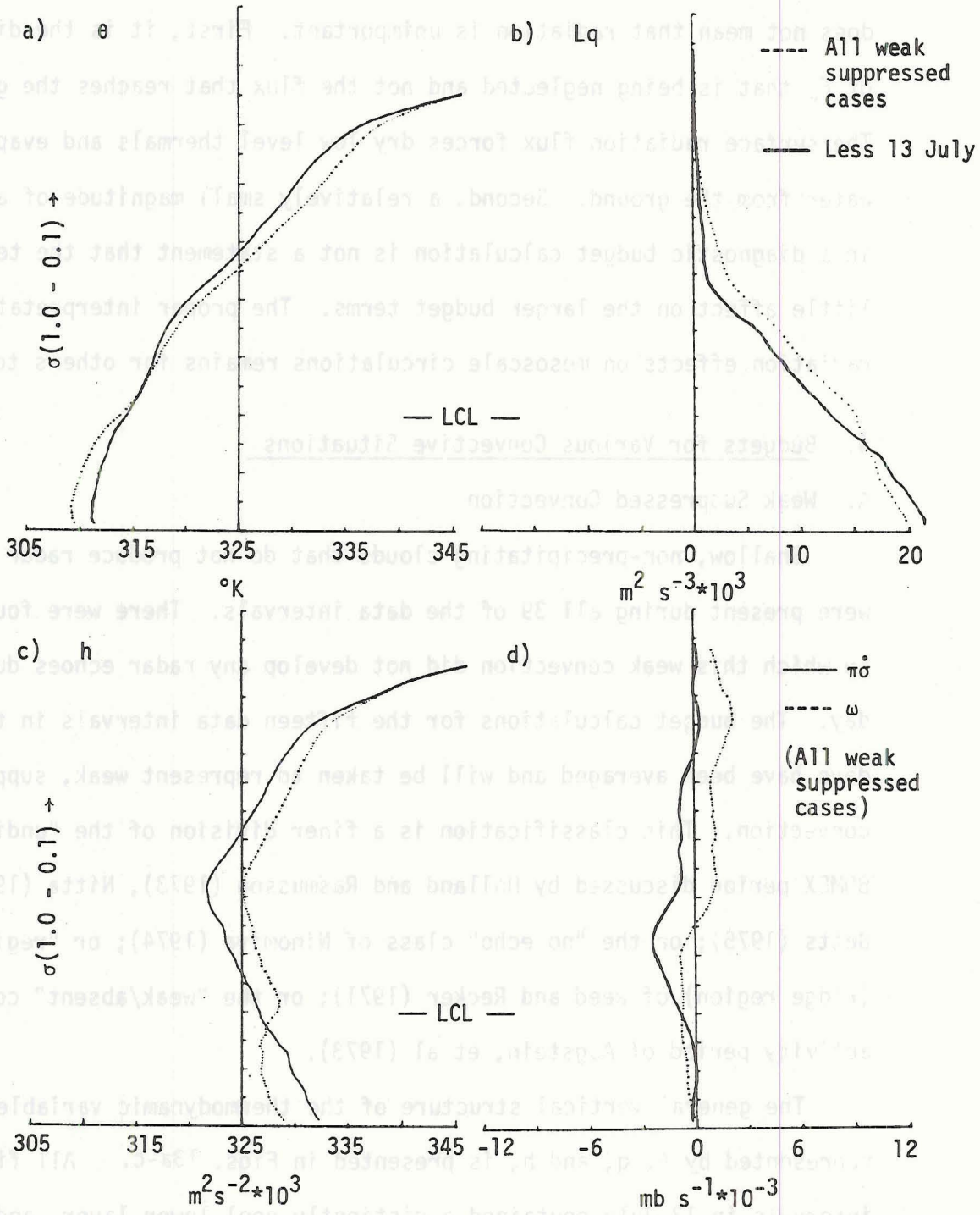

Figure 13. Weak Suppressed Convection Thermodynamic and Vertical Velocity Profiles

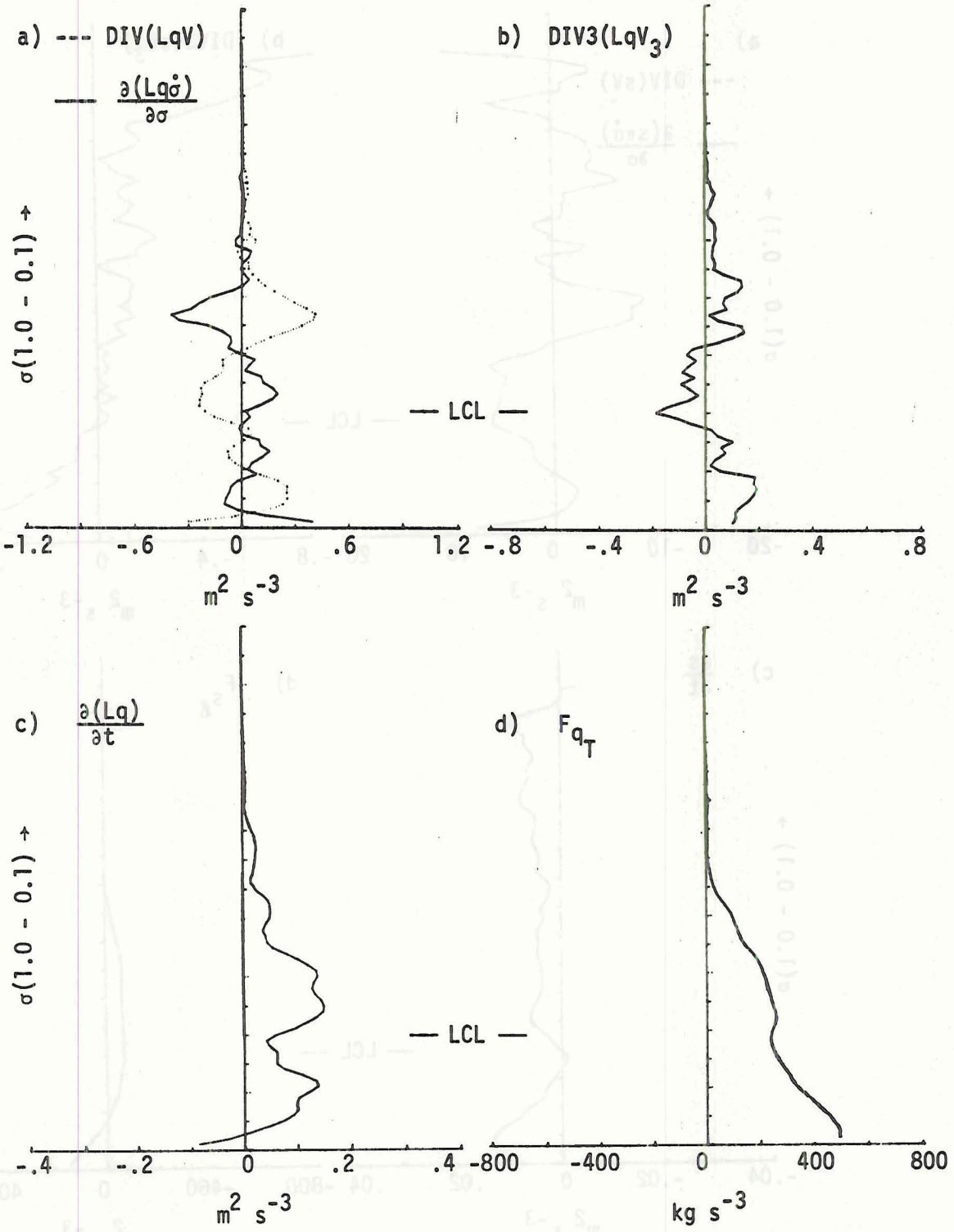

Figure 14. Weak Suppressed Convection Lq Budget

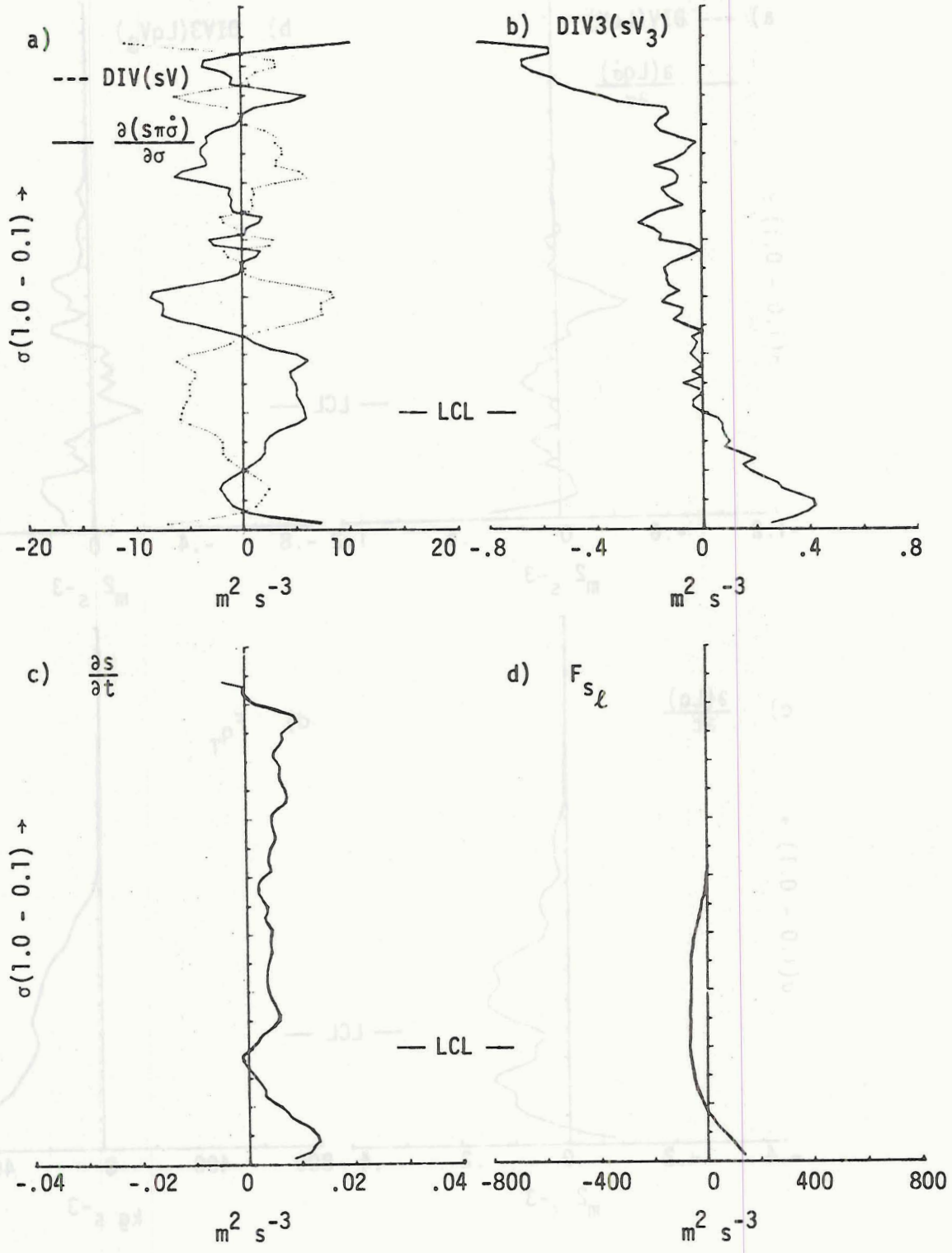

Figure 15. Weak Suppressed Convection s Budget

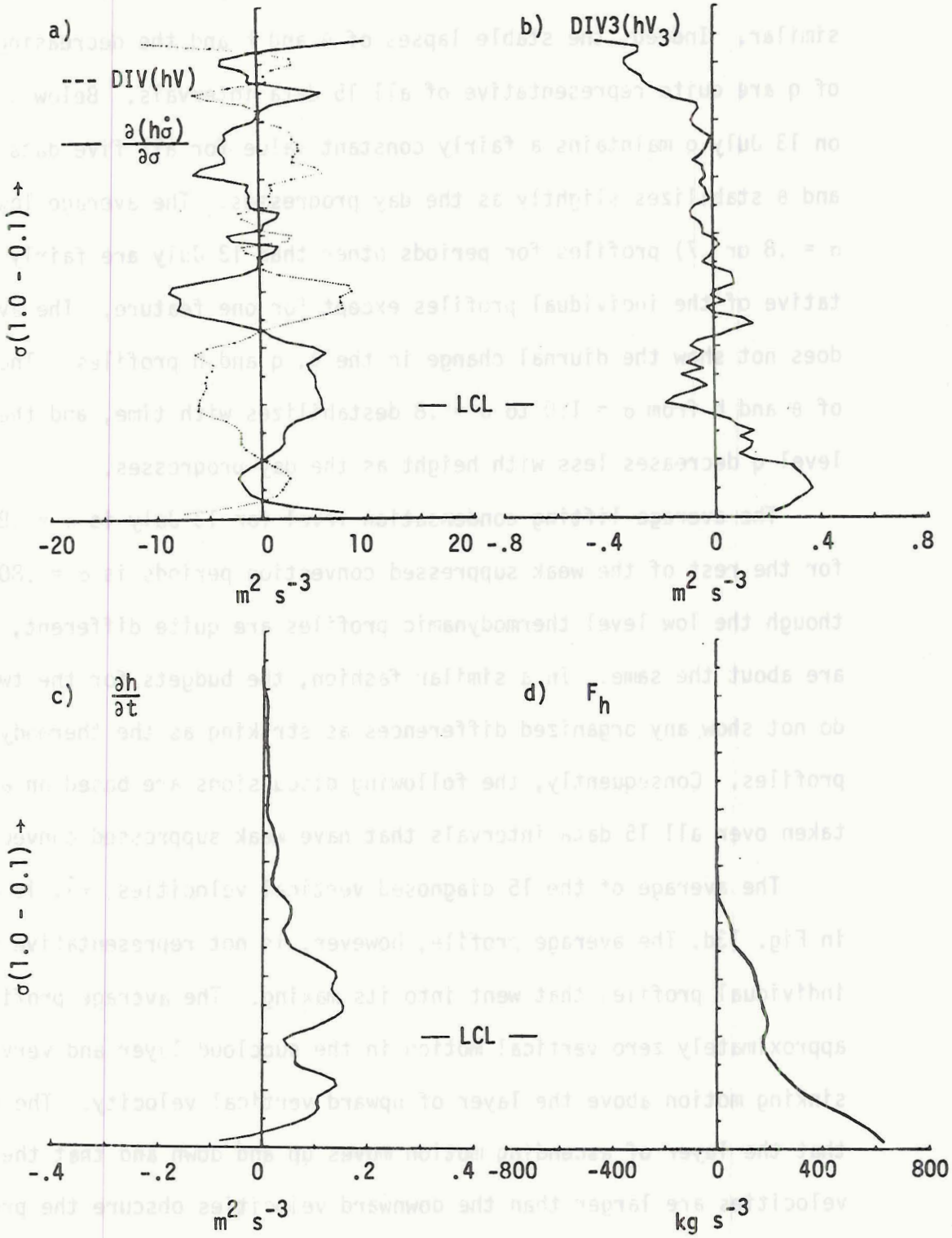

Figure 16. Weak Suppressed Convection h Budget

times). Above the level σ = .70 the average lapses of θ, q, and h are similar. Indeed, the stable lapses of θ and h and the decreasing values of q are quite representative of all 15 data intervals. Below σ = .70 on 13 July q maintains a fairly constant value for all five data periods and θ stabilizes slightly as the day progresses. The average lower (below σ = .8 or .7) profiles for periods other than 13 July are fairly representative of the individual profiles except for one feature. The average does not show the diurnal change in the θ, q and h profiles. The lapse of θ and h from σ = 1.0 to σ = .8 destabilizes with time, and the low level q decreases less with height as the day progresses.

The average lifting condensation level for 13 July is σ = .81 and for the rest of the weak suppressed convection periods is σ = .80. Even though the low level thermodynamic profiles are quite different, the LCL's are about the same. In a similar fashion, the budgets for the two periods do not show any organized differences as striking as the thermodynamic profiles. Consequently, the following discussions are based on averages taken over all 15 data intervals that have weak suppressed convection.

The average of the 15 diagnosed vertical velocities, $\pi\dot{\sigma}$, is presented in Fig. 13d. The average profile, however, is not representative of the individual profiles that went into its making. The average profile shows approximately zero vertical motion in the subcloud layer and very slight sinking motion above the layer of upward vertical velocity. The fact that the layer of ascending motion moves up and down and that the upward velocities are larger than the downward velocities obscure the presence of the sinking motions. In ten out of the fifteen cases, there was subcloud sinking motion of about $2\text{-}3*10^{-3}$ mb/sec. The upper level sinking motion in another (different) ten cases was much more pronounced ($2\text{-}3*10^{-3}$ mb/sec)

than the average profile suggests. These individual layers of sinking average motion are compatible with the occurrence of weak, suppressed convection. Only two intervals do not show a subcloud and/or an upper layer of subsiding motion that would be compatible with the suppressed convection.

The average ω profile is also presented in Fig. 13d. As was discussed in Chapter III, section 1, ω is equal to $\pi\dot{\sigma}$ plus the contribution due to $\sigma\dot{\pi}$. Fig. 13d shows that the average $\sigma\dot{\pi}$ contributes an upward component in the subcloud layer and a downward component above cloud base. This $\sigma\dot{\pi}$ average is quite representative of the individual cases. Thirteen out of fifteen cases show a positive $\sigma\dot{\pi}$ above the LCL and nine cases show a negative $\sigma\dot{\pi}$ below the LCL. The dominant term in $\sigma\dot{\pi}$ is $\vec{V}\cdot\nabla\pi$. This means the positive values are due to a "downhill" (towards higher surface pressure) motion and the negative values are due to an "uphill" motion.

The interpretation of a direct comparison between the ω profile of Fig. 13d and ω profiles calculated for the previously mentioned data sets is complicated by the sloping lower boundary in this research. The other ω profiles are for oceanic regions and have no component of ω due to a sloping lower boundary. This problem is discussed in Chapter VI but no firm conclusions are reached. However, the argument is advanced (Chapter VI, section 1) that at least in the lower portion of the atmosphere $\pi\dot{\sigma}$ is a velocity relative to cloud base level just as in oceanic regions ω is a velocity relative to cloud base level. Therefore, it is reasonable to compare the $\pi\dot{\sigma}$ of this research with the ω of other studies.

A comparison of this $\pi\dot{\sigma}$ with ω calculated from the four data sets mentioned at the beginning of this section shows two general differences

between the profiles. First, the maximum vertical velocities in this case are much larger than in the other four cases. The "undisturbed" BOMEX calculation (which reached only to 500 mb) shows a maximum subsiding motion of about $.5*10^{-3}$ mb/sec; "weak/absent" convection ATEX calculations (which reached only to 700 mb) $.8*10^{-3}$ mb/sec; "region 8" of Reed and Recker data (reached 100 mb) $.3*10^{-3}$ mb/sec; "no echo" class of Ninomiya (reached 300 mb) $1.1*10^{-3}$ mb/sec. These magnitudes are one third to one tenth the magnitude of the subsiding velocities calculated for the weak, suppressed convection average in this research.

The second outstanding difference between this calculated vertical velocity profile (Fig. 13d) and the others is the pronounced layer of average rising motion. The average maximum ascent rate is about $3*10^{-3}$ mb/sec and three cases have maximum values of about $9*10^{-3}$ mb/sec. The four previously mentioned average calculations all show nothing but subsiding average motion. However, the Reed and Recker data have a layer of convergence from 800 mb to 600 mb which diminished the sinking motion from $.3*10^{-3}$ mb/sec to about .0 mb/sec. Also, Ninomiya included all the individual vertical velocity profiles that he used to compute an average "no echo" profile. These individual profiles (which have considerable scatter) show values of rising motion of 3×10^{-3} mb/sec.

The average latent heat (water vapor) balance achieved during periods of weak, suppressed convection is shown in Figs. 14a-d. We first discuss the budget below the lifting condensation level. The condensation source term is zero within this subcloud layer; any evaporation is assumed to occur directly on the lower boundary ($\sigma = 1.$). Figure 14a shows a slight net horizontal divergence of environmental water vapor throughout this layer. As the average vertical mass flux (Fig. 13d) is approximately zero

to slightly negative, the positive values of water vapor divergence indicate a loss of water by advection. That is, the horizontal q gradient is oriented relative to the wind direction in a way that produces a horizontal loss of water vapor. This subcloud divergence of q is also present in the three dimensional divergence of q (Fig. 14b).

In this subcloud layer, the vertically integrated apparent source of water vapor can be interpreted in a straightforward manner as a flux of water vapor, F_q (Fig. 14d), due to dry convection and mechanical mixing. The positive value of F_q at the surface indicates an evaporation of water at the rate of .07 cm/hr. This evaporation rate is large compared to the .01 to .05 cm/hr rates calculated over the four oceanic areas. However, considering that the air near the ground in the NHRE area was very hot and dry (37°C and 8 g/kg compared to 28°C and 18 g/kg in the BOMEX case) it is quite reasonable to expect more vigorous evaporation processes in this situation. Similarly large evaporation rates (.04 cm/hr daytime mean and .05-.06 cm/hr mid-afternoon values) have been calculated from the Great Plains Turbulence Field Program data (Tables 7.3.1 and 7.3a, Lettau and Davidson, 1957). These data were taken in open prairie country near O'Neill, Nebraska during August and September.

F_q decreases with height (decreasing values of σ) throughout most of the subcloud layer. This positive slope of F_q indicates a convergence or source of water vapor (originally supplied by the surface evaporation) due to dry subcloud convection processes. This eddy convergence of q is larger than the three dimensional average divergence of q, and consequently, the local time rate of change of q (Fig. 14c) is positive (approximately .3 (g/kg) / hr. The subcloud layer moistens.

Above cloud base, Fig. 14a indicates a layer of horizontal convergence of q topped by a layer in which the horizontal flux of q diverges. This average profile is quite representative of the individual profiles that make up the average. The corresponding two layer profile above cloud base displayed by the three dimensional average divergence, however, is not so representative of the individual cases.

The F_{q_T} profile above cloud case includes the effects of condensation and evaporation. Except for a thin layer near cloud base, F_{q_T} continues its decrease with height. The shallow layer of converging F_{q_T} is consistent with condensation of water at cloud base and a transport of this water before it can reevaporate. Above this layer, the positive slope of F_{q_T} indicates a net evaporation and convergence of water vapor due to the weak, suppressed cumulus clouds. This convergence of F_{q_T} combines with the three dimensional divergence of q to produce a positive time change of q.

In general, the F_{q_T} profiles calculated from the NHRE data and from the other four sets of data are quite similar in that they all have a fairly constant decrease with height. This decrease means the small cumulus clouds add moisture to the cloud layer. The main difference is the magnitude of this positive slope which determines the value of the surface evaporation.

The average dry static energy balance achieved during periods of weak, suppressed convection is shown in Figs. 15a-d. The first thing that is apparent in the s budget is the strikingly close balance of the apparent source of s and the three dimensional divergence of the average flux of s. That is, the time change of s shown in Fig. 15c is very small (note the scale in Fig. 15c). In both the average and all the individual cases, the

local time rate of change of s is ten to one hundred times smaller than the total divergence and apparent source terms. The atmosphere acts to maintain a characteristic thermal structure.

The profiles that are averaged to produce Fig. 15a, the horizontal divergence of the flux of s, all display many layers of alternating convergence and divergence of the flux of s. However, when these rather erratic patterns are added to the vertical divergence of s, both the average and most of the individual profiles of the three dimensional divergence of the average flux of s assume the two layer profile shown in Fig. 15b. In the subcloud layer there is a net divergence of the average flux of s just as there was a net divergence of the average flux of q. Also similar to the q budget, there is a convergence of F_{s_ℓ} in the subcloud layer. The dry, subcloud upward convergent eddy transport of both dry static energy and water vapor can reasonably be pictured as representing the addition of energy by mechanical mixing and unsaturated thermals. Above cloud base there is a net divergence of F_{s_ℓ}. Recalling the apparent source of water vapor indicated in Fig. 14d, the negative slope of F_{s_ℓ} above cloud base suggests a net evaporation of cloud water during all the data intervals containing weak suppressed convection.

There are several similarities and differences between the apparent source of s (less the radiation contribution: Q_1-r) calculated for weak, suppressed convection over the continental mesoscale area studied in this research and Q_1-r calculated for the three larger, oceanic areas (Ninomiya, 1974, did not calculate an s budget). The BOMEX and ATEX calculations both show low level convergence of F_{s_ℓ} and an upper level divergence of F_{s_ℓ} (the data extend only to 500 mb and 700 mb, respectively) which is similar to the pattern of Fig. 15d. However, in the case of the NHRE data,

the convergence of s occurs below cloud base while the BOMEX and ATEX calculations show this convergence well into the cloud layer. The third calculation of Q_1 by Cho and Ogura (1974) using the Reed and Recker (1971) data would produce an F_{s_ℓ} profile that would have subcloud convergence and divergence of s above, except for the layer from 700 mb to 500 mb where slight convergence is indicated. The magnitude of Q_1-r from the NHRE data is larger than the magnitude calculated in the other three cases.

The average moist static energy budget achieved during periods of weak, suppressed convection is shown in Figs. 16a-d. These graphs are the sums of the respective s and Lq graphs. The horizontal divergence of the flux of h (Fig. 16a) is mainly determined by the s flux divergence contribution. Below cloud base the three dimensional average flux divergence of both Lq and s produce a very clear net divergence of the average flux of h (Fig. 16c). Above cloud base the Lq and s flux divergences generally cancel. The time change of h (Fig. 16b) is due almost entirely to the time change of water vapor.

The convective flux of h, F_h (Fig. 16d), can be interpreted in a straightforward manner because the apparent source of h has no condensation/evaporation source term. Below cloud base, F_h has a definite positive slope indicating a convergence of the dry convective and mechanically induced flux of moist static energy. This convergence continues to the level $\sigma = .49$, and above cloud base is associated with the weak cumulus convection. The cloud layer profile of both F_h and F_{s_ℓ} are interpreted further in section 2 of Chapter VI with the use of a simple diagnostic cumulus convection model.

The magnitude of F_h calculated for the NHRE data is larger than that calculated in the previously mentioned studies. The surface value of F_h shown in Fig. 16d is 631 kg s^{-3} compared to a value of approximately 180 kg s^{-3} noted by Betts (1975). The value 631 kg s^{-3} does not exceed the 725 kg s^{-3} figure noted as an upper limit in Chapter III, section 4, but is probably somewhat too large, because the upper limit refers to a clear sky. In addition to the large magnitude, the profile of F_h in Fig. 16d has its maximum positive slope (convergence) in the subcloud layer. The other studies have layers of maximum slope of F_h within the cloud layers. The F_h profile of Fig. 16d does, however, show a somewhat similar feature in the sharply increasing slope from $\sigma = .7$ to $\sigma = .6$.

The budget description of weak, suppressed convection presented in this section is summarized in Chapter VII.

B. Weak, Developing Convection

Shallow, non-precipitating clouds that did not produce radar echoes during given data periods, but later developed into echo and/or precipitation producing clouds occurred during seven data intervals. That is, there were no echoes present during these seven data intervals. The budgets for the seven intervals (occurring over four days) have been averaged and the average is taken to represent weak, developing convection.

The main feature of this classification is the idea that the convection is developing. The radar data show that the clouds are developing in the sense that some become large enough to produce radar echoes. In addition, the convection is probably developing in the sense that the number and/or size of the non echo producing clouds are also increasing. This general increase of cloudiness makes the change of cloud storage term (see Eq. 5) important in the budget calculations.

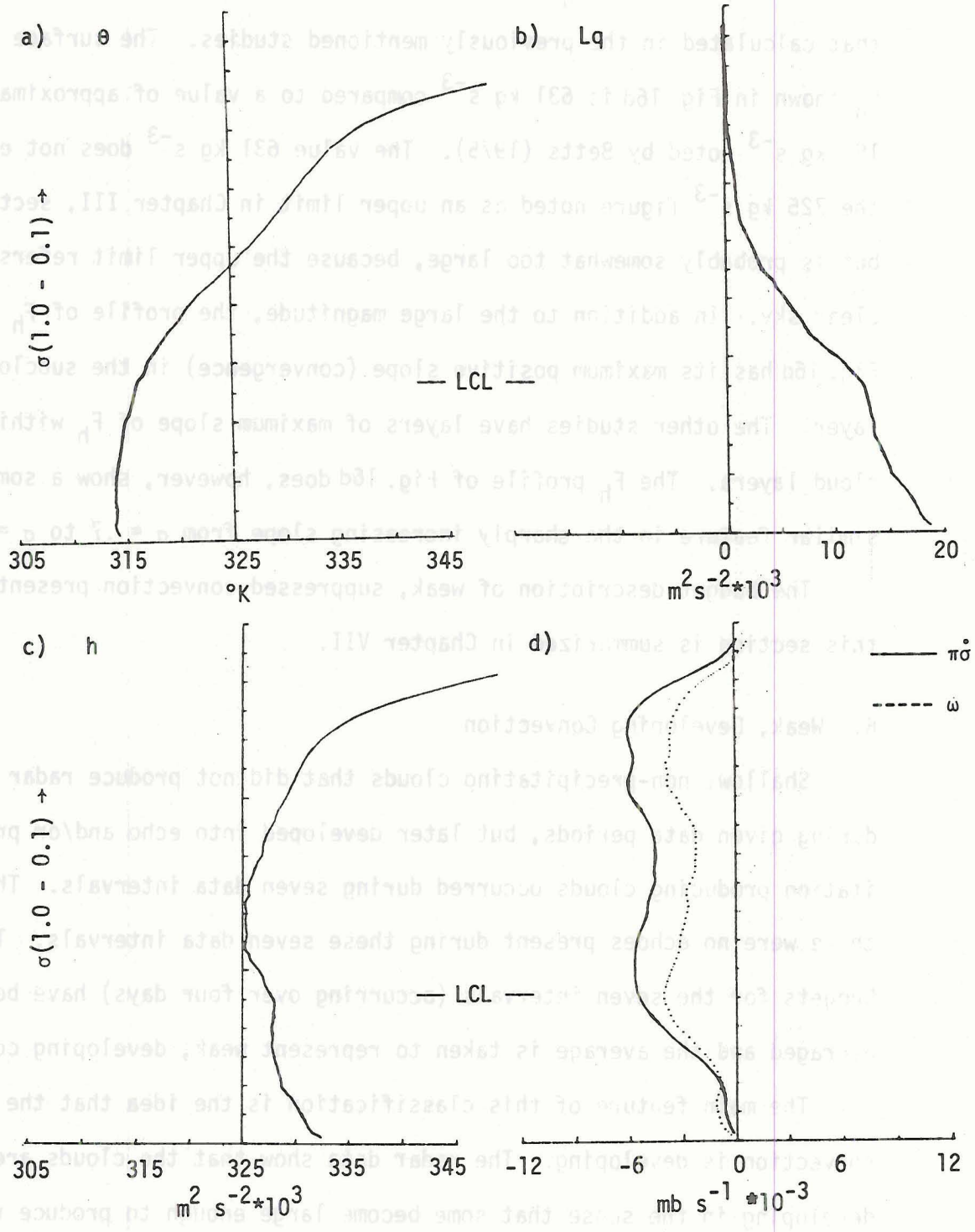

Figure 17. Weak Developing Convection Thermodynamic and Vertical Velocity Profiles

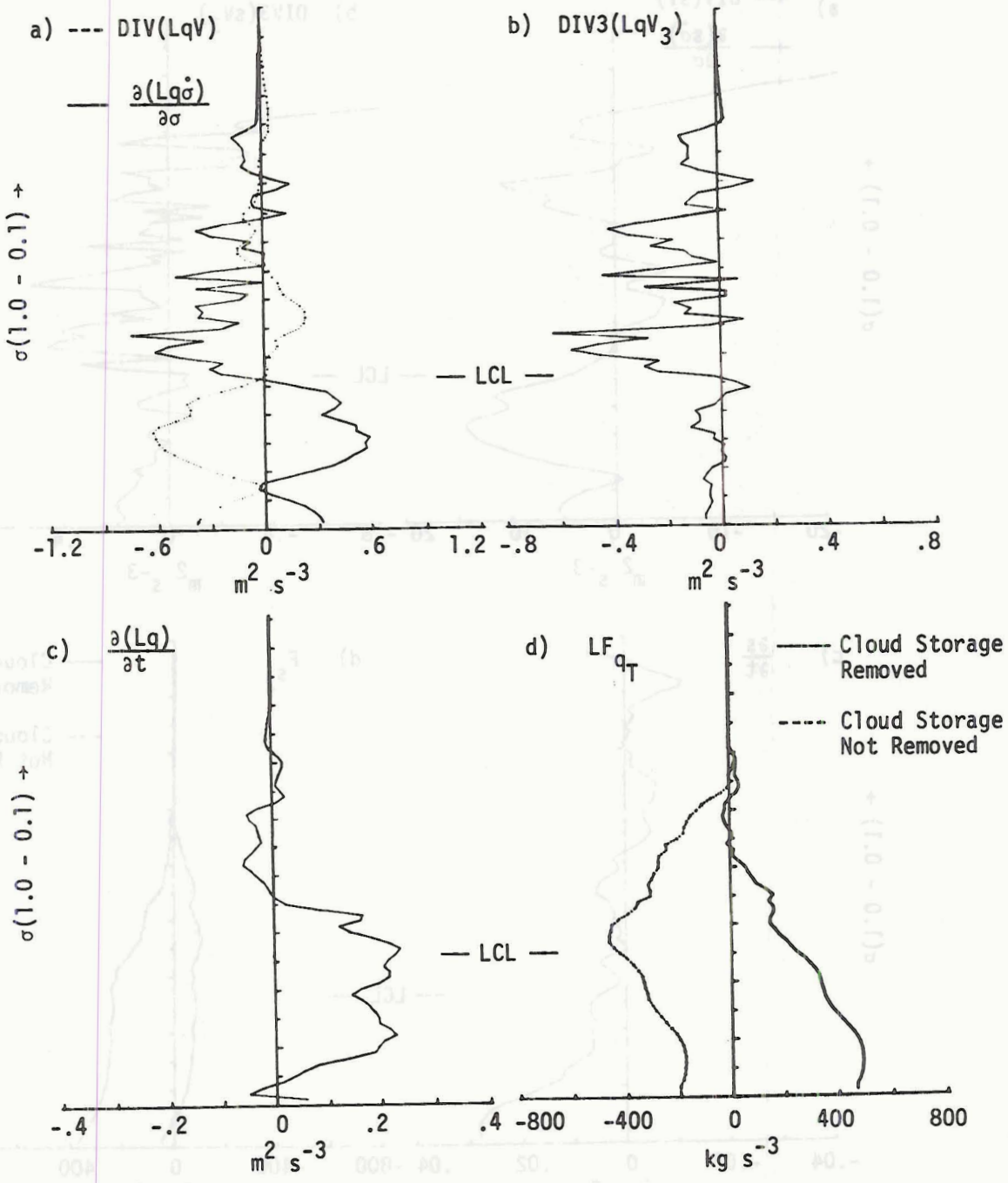

Figure 18. Weak Developing Convection Lq Budget

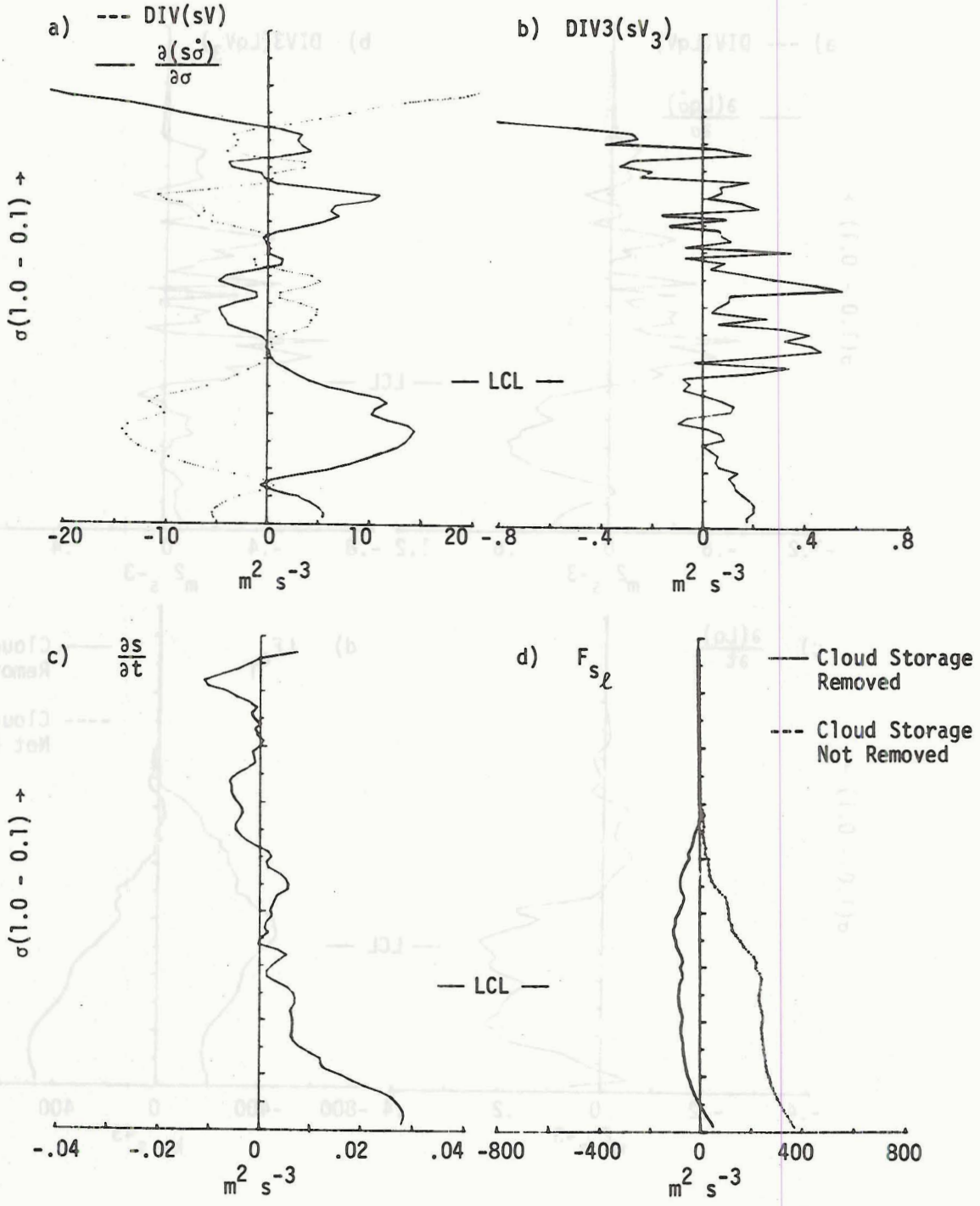

Figure 19. Weak Developing Convection s Budget

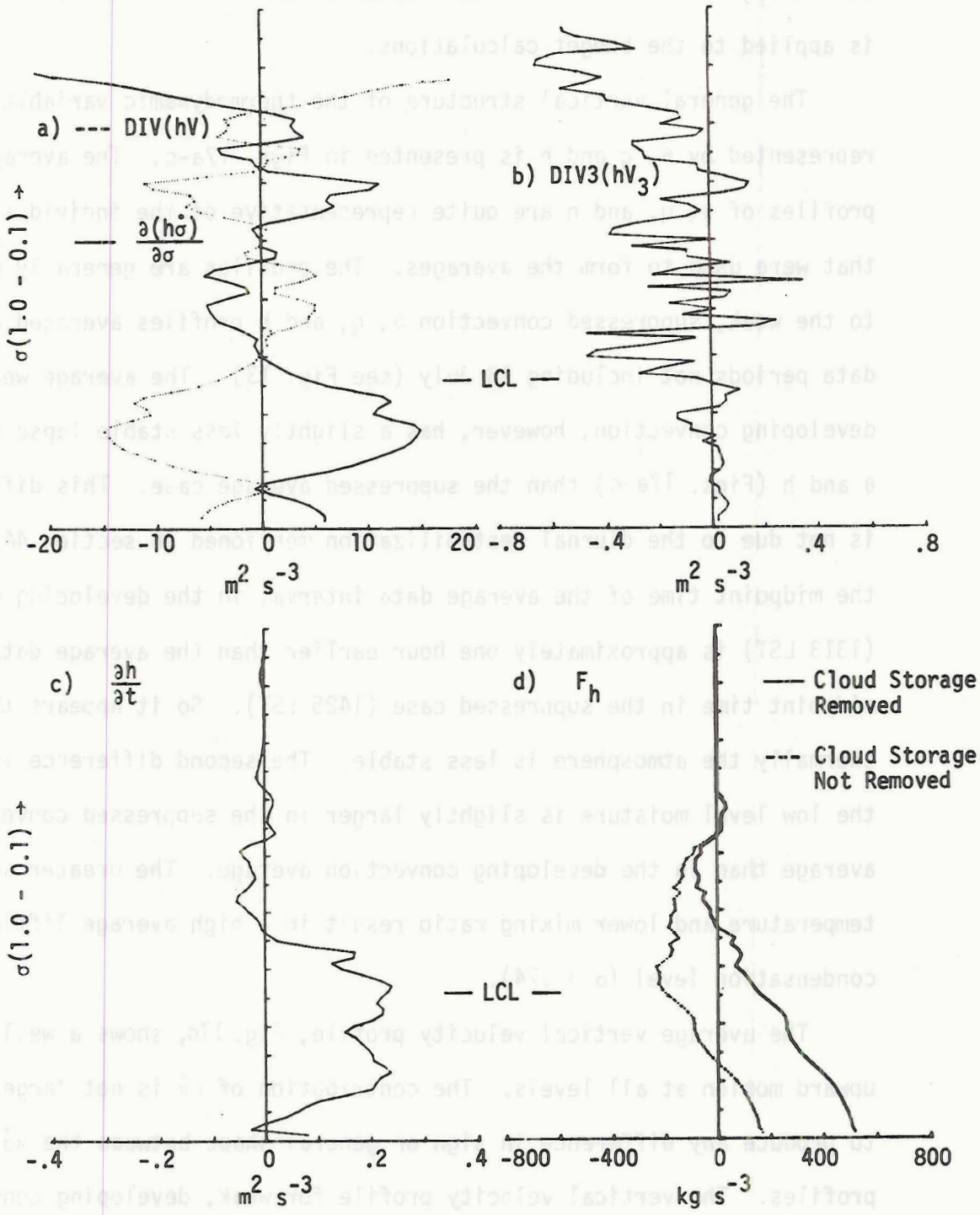

Figure 20. Weak Developing Convection h Budget

The storage term is modeled in Chapter VI and in this section the model is applied to the budget calculations.

The general vertical structure of the thermodynamic variables, as represented by θ, q and h is presented in Figs. 17a-c. The average profiles of θ, q, and h are quite representative of the individual profiles that were used to form the averages. The profiles are generally similar to the weak, suppressed convection θ, q, and h profiles averaged over data periods not including 13 July (see Fig. 13). The average weak, developing convection, however, has a slightly less stable lapse rate of θ and h (Figs. 17a-c) than the suppressed average case. This difference is not due to the diurnal destabilization mentioned in section 4A, because the midpoint time of the average data interval in the developing case (1313 LST) is approximately one hour earlier than the average data interval midpoint time in the suppressed case (1425 LST). So it appears that thermally the atmosphere is less stable. The second difference is that the low level moisture is slightly larger in the suppressed convection average than in the developing convection average. The greater surface temperature and lower mixing ratio result in a high average lifting condensation level (σ = .74).

The average vertical velocity profile, Fig. 17d, shows a well defined upward motion at all levels. The contribution of $\sigma\dot{\pi}$ is not large enough to produce any difference in sign or general shape between the $\pi\dot{\sigma}$ and ω profiles. The vertical velocity profile for weak, developing convection is clearly different than that for weak, suppressed convection.

The average $\pi\dot{\sigma}$ profile is representative of four of the seven individual cases. One of the intervals (24 July) has weak descending motion in the subcloud layer with ascending motion above cloud base. Two

cases (27 July) have a mid level layer of descending motion, but this region of descending motion becomes shallower and weaker as day 27 July progresses. It is absent in the later intervals containing echoes. The average profile indicates the largest upward mass flux change (i.e., largest convergence) occurs in the subcloud layer. This feature is clearly present in five out of the seven individual $\pi\dot{\sigma}$ profiles.

The magnitude of the calculated $\pi\dot{\sigma}$ is much larger than the magnitude of the mass flux per unit area calculated in the "disturbed" BOMEX period ($.1 \times 10^{-3}$ mb/sec) or any of the easterly wave regions studied by Cho and Ogura (1974) (1×10^{-3} mb/sec), or the "weak echo" average ($.3 \times 10^{-3}$ mb/sec) calculated by Ninomiya (1974). The magnitude of $\pi\dot{\sigma}$ for weak, developing convection is, however, about the same as that calculated by Ninomiya (1974) for an average echo cluster. These large magnitudes are discussed in Chapter VI in terms of a cloud-environment mass flux imbalance.

The average water vapor balance achieved in the case of weak developing convection is presented in Figs. 18a-d. As contrasted to the suppressed convection average, both the horizontal and three dimensional average fluxes of water vapor have convergent vertical profiles (Figs. 18a, b) throughout most of the atmosphere.

The profile of the vertically integrated apparent source of water vapor is presented as the dotted line in Fig. 18d. The apparent source includes the previously neglected cloud storage term. This dotted profile indicates a cloud layer sink of q_T and a negative surface value of F_q. An interpretation of this profile in terms of net condensation and precipitation is clearly inconsistent with the absence of observed radar echoes or precipitation. The dotted profile and the description of the convection

as "developing" does suggest, however, an interpretation in terms of the previously neglected change of cloud storage.

The amount of water used to increase the cloud storage is modeled in Chapter VI. This modeled loss of water has been subtracted from the dotted profile to form the convective flux F_{q_T} (solid line, Fig. 18d). The profile of F_{q_T} in the cloud layer (solid line, Fig.18d) is closely related to the cloud layer F_{q_T} for weak, suppressed convection (see Chapter VI, section 3). In addition, the details of the developing convection F_{q_T} profile (for example, the small negative values near mid-cloud level) are strongly influenced by the choice of cloud storage model. Consequently, it will simply be noted that above the LCL the F_{q_T} profile generally indicates a moistening of the environment by convection.

The slope of the F_{q_T} profile below the LCL is not affected by the cloud storage model. The surface value of F_{q_T}, however is strongly dependent upon the cloud storage model. Fig. 18d shows dry convection and mechanical mixing also act to moisten the environment.

The dry static energy budget for weak, developing convection is presented in Figs. 19a-d. As in the budget for suppressed convection, a very near balance between the three-dimensional average s flux and the convective s flux is indicated by the near zero value of the time change of s (Fig. 19c). This balance occurs in both the average and individual profiles.

There is a strong horizontal convergence of s (Fig. 19a) below cloud base unlike the suppressed average. However, this convergence is not large enough to produce a convergence of the three-dimensional average flux of s below cloud base (Fig. 19b). There is a net average flux of s divergence below cloud base as there was in the suppressed case. This

average s flux divergence continues into the cloud layer in contrast to the convergent DIV3($s\vec{V}_3$) profile for weak, suppressed convection.

The integrated apparent source of s (dotted line, Fig. 19d) contains the cloud storage term. This dotted profile shows convective warming throughout almost all of the cloud layer. The importance of the cloud storage term explains how this heating can occur in the absence of precipitation. The solid line in Fig. 19d is the profile of F_{s_ℓ} and is formed by subtracting the modeled cloud storage term from the dotted profile. Again this cloud layer profile of F_{s_ℓ} is closely related to the cloud layer F_{s_ℓ} for weak, suppressed convection (see Chapter VI, section 3). Consequently, it will simply be noted that above the LCL the F_{s_ℓ} profile generally indicates a cooling of the environment by convection. The slope of the F_{s_ℓ} profile below the LCL is independent of the cloud storage model. A general warming by dry convection and mechanical mixing is indicated below cloud base.

The moist static energy budget for weak, developing convection is presented in Figs. 20a-d. The subcloud convergence of the horizontal flux of h (Fig. 20a) is nearly compensated by the diverging vertical average flux of h. The result is a near zero three dimensional convergence of the average flux of h (Fig. 20b) in the subcloud layer. The three-dimensional flux and the apparent source of h combine to produce a positive time change of s in the subcloud layer (similar to the suppressed convection case). In six out of seven cases, however, shortly above the LCL the time change of h (Fig. 20c) falls to near zero (in contrast to the positive time change throughout the suppressed case cloud layer).

Below the LCL the convective flux of h (solid line, Fig. 20d) shows a net addition of moist static energy to the environment by dry convection

and mechanical mixing. The surface value of F_h is strongly affected by the cloud storage model. The profile of F_h above the LCL is also closely related to the cloud storage model. The profile has a positive (convergent) slope in the lower half of the cloud layer and this represents an addition of h to the environment by convection. The divergent F_h profile of the upper half of the cloud layer is present for most reasonable model cloud storage values (see Chapter VI, section 3). This negative slope of F_h indicates an introduction into the environment of relatively small values of h by convection, and is probably erroneous.

The budget description of weak, developing convection presented in this section is summarized in Chapter VII.

C. Moderate Convection

Cumulus convection that produced radar echoes but no measured precipitation occurred in the data volume during seven data intervals (see Table 1). Two of these data intervals (24 July 1806, 31 July 1448) will be excluded from this data set, because of extremely unrealistic F_h profiles. The very large divergent slopes and negative surface values of these two F_h profiles are not realistic. Their large magnitude and the fact that they represent two-sevenths of the average budget produces unrealistic average F_h profiles. The five remaining data intervals occur on four different days. This convection is probably in the mature or dissipating stages. Three of the data intervals show a decreasing number of radar echoes in the interval or a decrease in a subsequent interval. The remaining two data intervals have only one or two echoes present in the data volume and the intervals end late in the afternoon (after 1800 LST).

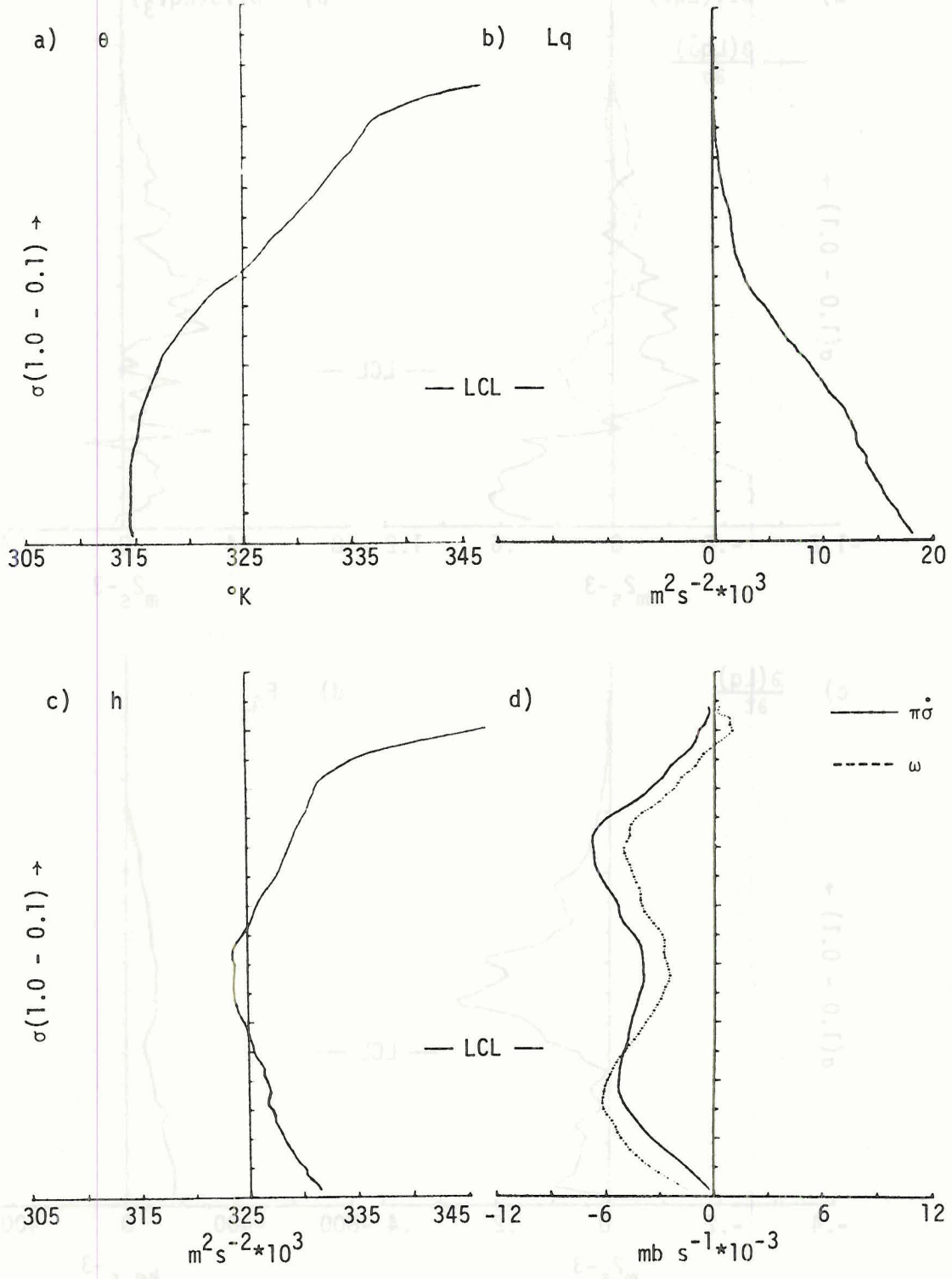

Figure 21. Moderate Convection Thermodynamic and Vertical Velocity Profile

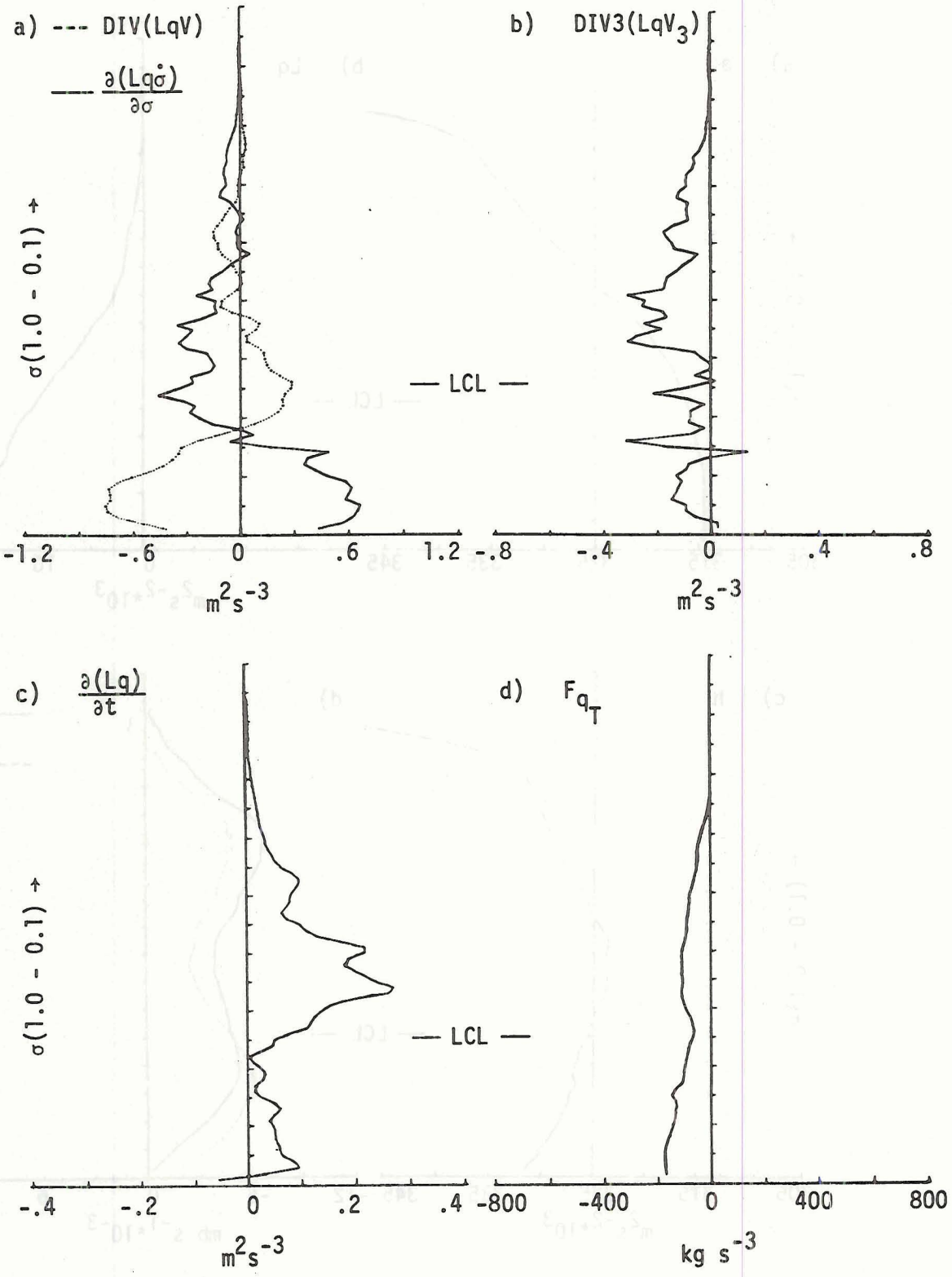

Figure 22. Moderate Convection Lq Budget

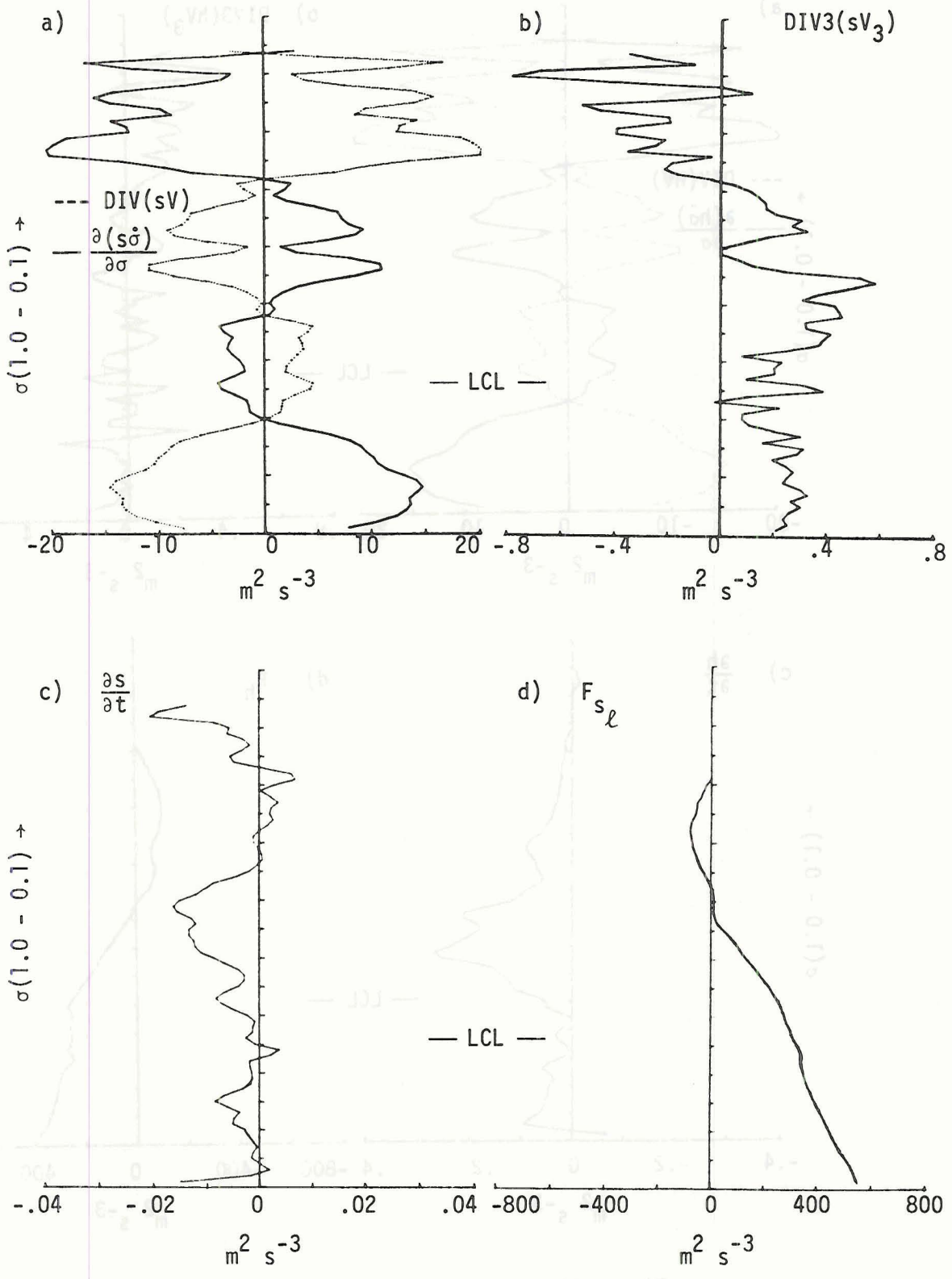

Figure 23. Moderate Convection s Budget

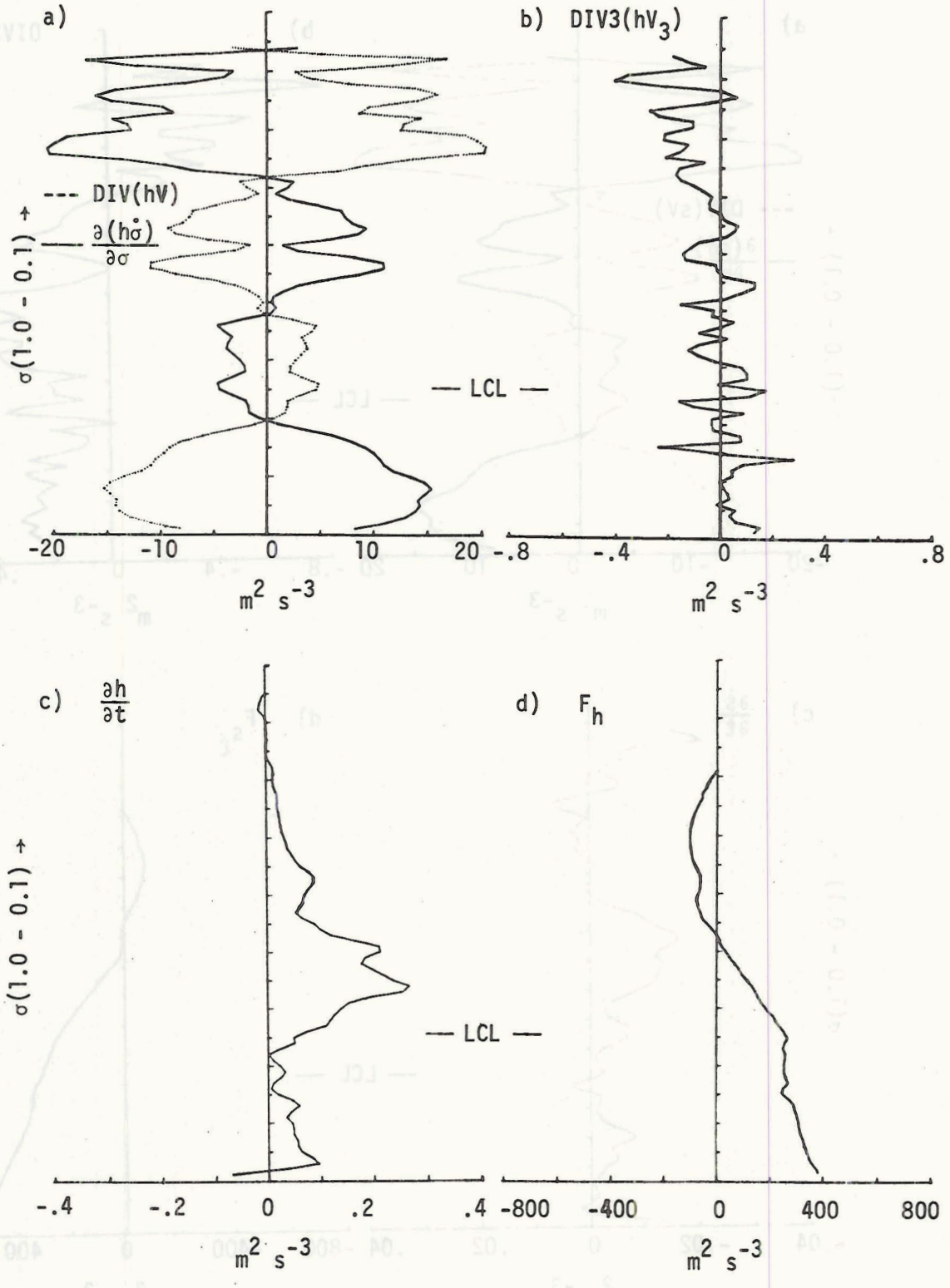

Figure 24. Moderate Convection h Budget

The possible occurrence of precipitation (even though none was recorded) is another characteristic of these data intervals. The complete evaporation of precipitation in the subcloud layer is a common occurrence in northeastern Colorado. However, the absence of recorded precipitation does suggest that no heavy precipitation occurred. The average of these five budgets will be described simply as moderate (because radar echoes were produced) cumulus convection. The convection is probably in its mature to dissipating stages and some evaporating precipitation could be present. This classification of the convection is much more detailed than the previously cited budget studies have used, and it is not clear whether the convection is more like the disturbed or undisturbed classification. The average budget discussed in this section will be compared mostly with other average budgets calculated in this research.

The general vertical structure of the thermodynamic variables, as represented by θ, q, and h, is presented in Figs. 21a-c. The profile of θ in Fig. 21a is quite representative of the individual θ profiles. The only pronounced difference occurs on 24 July. The θ profile in this interval has a stable subcloud lapse of θ. The other intervals are characterized by adiabatic subcloud layers. All of the data intervals (including the one with the stable subcloud lapse of θ) occur in the late afternoon. The constantly decreasing q profile (Fig. 21b) is generally representative of the individual profiles. Only two intervals have shallow layers in which q changes abruptly. The average h profile (Fig. 21c) is representative of most of the individual h profiles. The one exceptional case (24 July) has a shallow abrupt stable h lapse from σ = .84 to σ = .78. The average lifting condensation level defined by these various thermodynamic profiles is at σ = .74. The range of the individual LCL's (σ = .68

to σ = .79) is similar to the range of LCL's that occur in the other three average cases.

The average of the five diagnosed mass fluxes, $\pi\dot{\sigma}$, is presented in Fig. 21d. Four of the five individual $\pi\dot{\sigma}$ profiles show a net upward motion with magnitudes similar to the average magnitude ($5*10^{-3}$ mb/sec). Only one case (24 July) exhibits any net downward motion, and this net sinking occurs from about cloudbase to σ = .52. There is strong net ascent above this layer. The average net ascent (Fig. 21d) is quite realistic considering that the cumulus clouds in these data intervals were able to produce radar echoes. The magnitude of the $\pi\dot{\sigma}$ profiles is similar to the developing convection average magnitude and to the ω values for "echo clusters" (Ninomiya, 1974). The contribution of $\sigma\dot{\pi}$ is not large enough to produce any difference in sign or general shape between the calculated $\pi\dot{\sigma}$ and ω profiles.

The average water vapor balance achieved in the case of moderate convection is presented in Figs. 21a-d. The horizontal flux of water vapor converges in the lower part of the subcloud layer, but then clearly becomes divergent just below and just above cloud base (Fig. 22a). This average profile is representative of four of the five individual cases. The profile of the three dimensional average flux of q (Fig. 22b) is also convergent throughout most of the atmosphere. Three of the individual profiles exhibit this marked convergence, while only one shows any clear divergence (the fifth profile has near zero three-dimensional average q flux convergence).

The average profile of the subcloud, horizontal water vapor flux convergence for moderate convection forms a pattern or reasonable sequence with the corresponding average profiles for weak, developing

and weak, suppressed convection. The horizontal subcloud flux of q for weak, suppressed convection is slightly convergent (Fig. 14a). The weak, developing convection average profile (Fig. 18a) is strongly convergent. The moderate convection average is clearly divergent around cloud base and convergent below. This type of profile is consistent with the idea that the moderate convection is not generally developing, but rather is either mature or decaying.

The convective flux of total water, F_{q_T} (Fig. 22d), shows a weak, but generally divergent slope. The small negative surface value (-.02 cm/hr) indicates a net removal of water from the atmosphere by precipitation. This indication of precipitation stands opposed to the earlier statement that no surface precipitation was measured, although radar echoes were observed.

Four of the five individual F_{q_T} profiles show an apparent sink of water in the upper portion of the cloud layer (above σ = .58 in Fig. 22d). This, combined with the occurrence of radar echoes, is a good indication of a loss of water from the layer above σ = .58 by precipitation. From σ = .58 to the LCL the slope of F_{q_T} shows that the environment was moistened by the convection. This is consistent with the idea of evaporating cloud water suggested by the mature to dissipating radar echoes. Below cloud base the negative slope of F_{q_T} indicates the introduction of relatively dry air by downdrafts (see section 4D) for a discussion of subcloud downdrafts). The interpretation of F_{q_T} in the above terms of evaporating cloud water and dry downwrafts is reasonable but must be considered somewhat tentative. Only three individual cases clearly display the above mentioned features, and the entire average consists of only five cases.

The average dry static energy balance achieved in the case of moderate convection is presented in Figs. 22a-d. The average convergence and divergence of the horizontal s flux (Fig. 23a) is not particularly representative of the individual DIV($s\vec{V}$) profiles, because the individual profiles have many alternating layers of strong convergence and divergence of the horizontal s flux. The pronounced low to mid level divergence of the three dimensional average flux of s (Fig. 23b) is representative only of three of the five individual profiles.

As in the case of the previous average budgets the time change of s (Fig. 23c) is very small compared to the other budget terms. This means that the apparent source of s closely balances the three dimensional average flux divergence of s. There is a marked convergence of F_{s_ℓ} above cloud base and a net upward convective transport of s_ℓ by the cumulus clouds. Both processes are compatible with the observed moderate convection. The subcloud convergence of F_{s_ℓ} is less than the cloud layer convergence. The condensation source of s is not present in the subcloud layer. In this moderate convection average, possible evaporation of precipitation can work to further decrease the convergent slope of F_{s_ℓ}.

The average moist static energy budget for moderate convection is presented in Figs. 24a-d. The divergence of the horizontal flux of h (Fig. 24a) is quite similar to that of s (Fig. 23a), because the horizontal s divergence is much larger than the horizontal Lq divergence ($h = s + Lq$). Both profiles have sharply changing features. The Lq contribution to the three dimensional average flux of h, however, is clearly evident. The DIV3($s\vec{V}_3$) profile is divergent below $\sigma = .40$, but DIV3(hV_3) alternated about zero (Fig. 24b). Below $\sigma = .40$, the DIV3(hV_3) profile is also more representative of the individual profiles than

DIV3(sV_3). For levels where $\sigma < .40$ both the horizontal and three dimensional average flux divergence of h (and s) have large erratic values and consequently are somewhat suspect.

The distinct increase of h with time above cloud base that appears in Fig. 24c is representative of all the individual cases in this average. It reflects the contribution due to water vapor, because the time change of s is very small. The small negative convective flux of h (Fig. 24d) above $\sigma = .40$ is suspect because of the previously mentioned erratic DIV3($h\vec{V}_3$) profile above $\sigma = .40$. Indeed, the slope of F_h is slightly negative above $\sigma = .40$. An upper level divergence (negative slope) of F_h indicates a convective sink of h, that is, some sort of cumulus overshooting process. This is not realistic because the cumuli in this average are probably for the most part mature or decaying.

The F_h profile for moderate convection is similar to those for weak, suppressed and developing convection in that they generally show an addition of moist static energy to the environment by convection. In the case of moderate convection, however, the cloud layer apparent source of h is larger than the subcloud apparent source (the slope of F_h becomes steeper at the LCL). The situation is reversed in the suppressed convection case.

The budget description of moderate convection presented in this section is summarized in Chapter VII.

D. Precipitating Convection

Precipitation was recorded within the NHRE area during 12 data intervals. These 12 intervals occur over six different days (see Table 3). The average budgets for these intervals are taken to represent precipitating

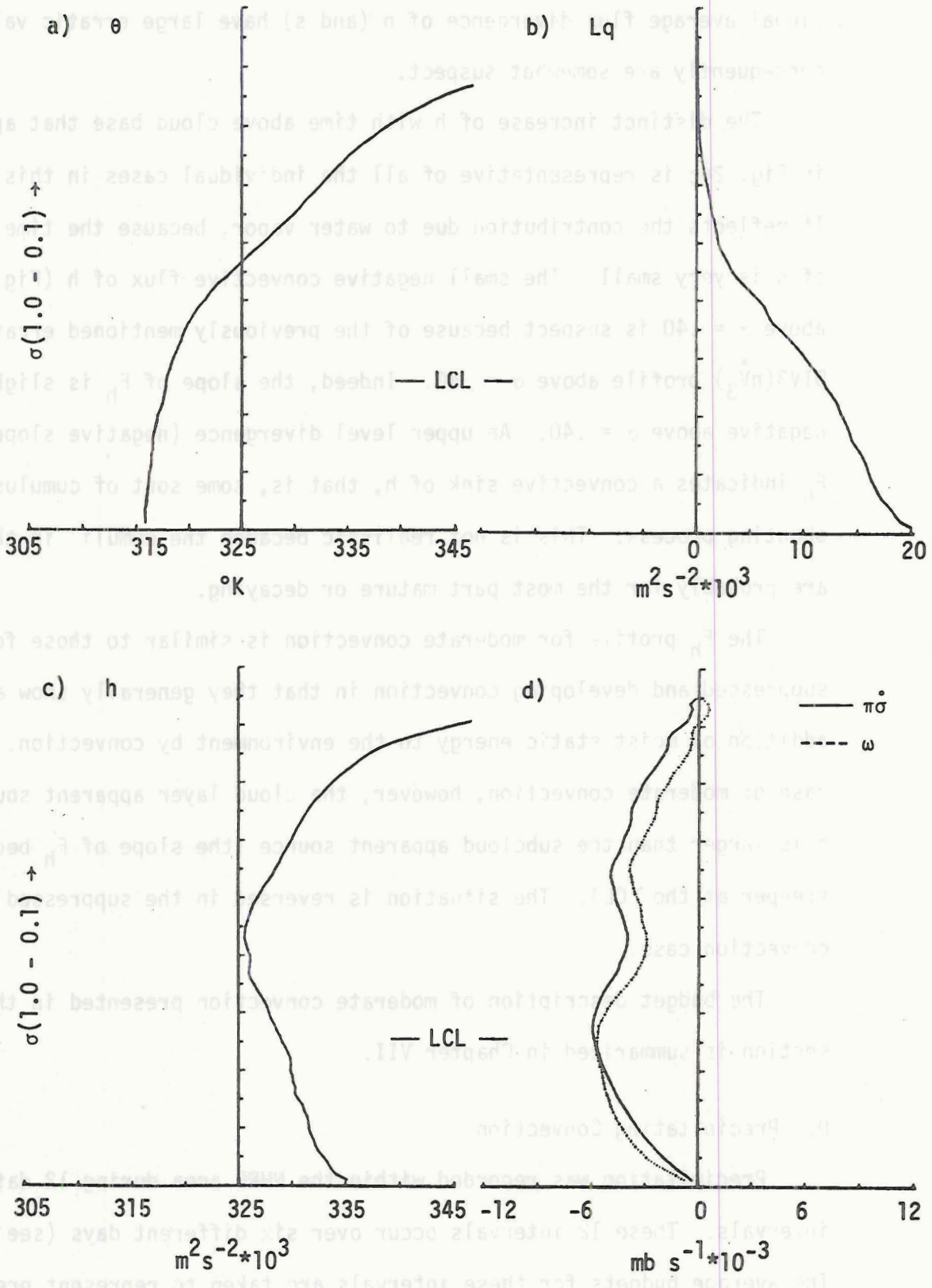

Figure 25. Precipitating Convection Thermodynamic and Vertical Velocity Profiles.

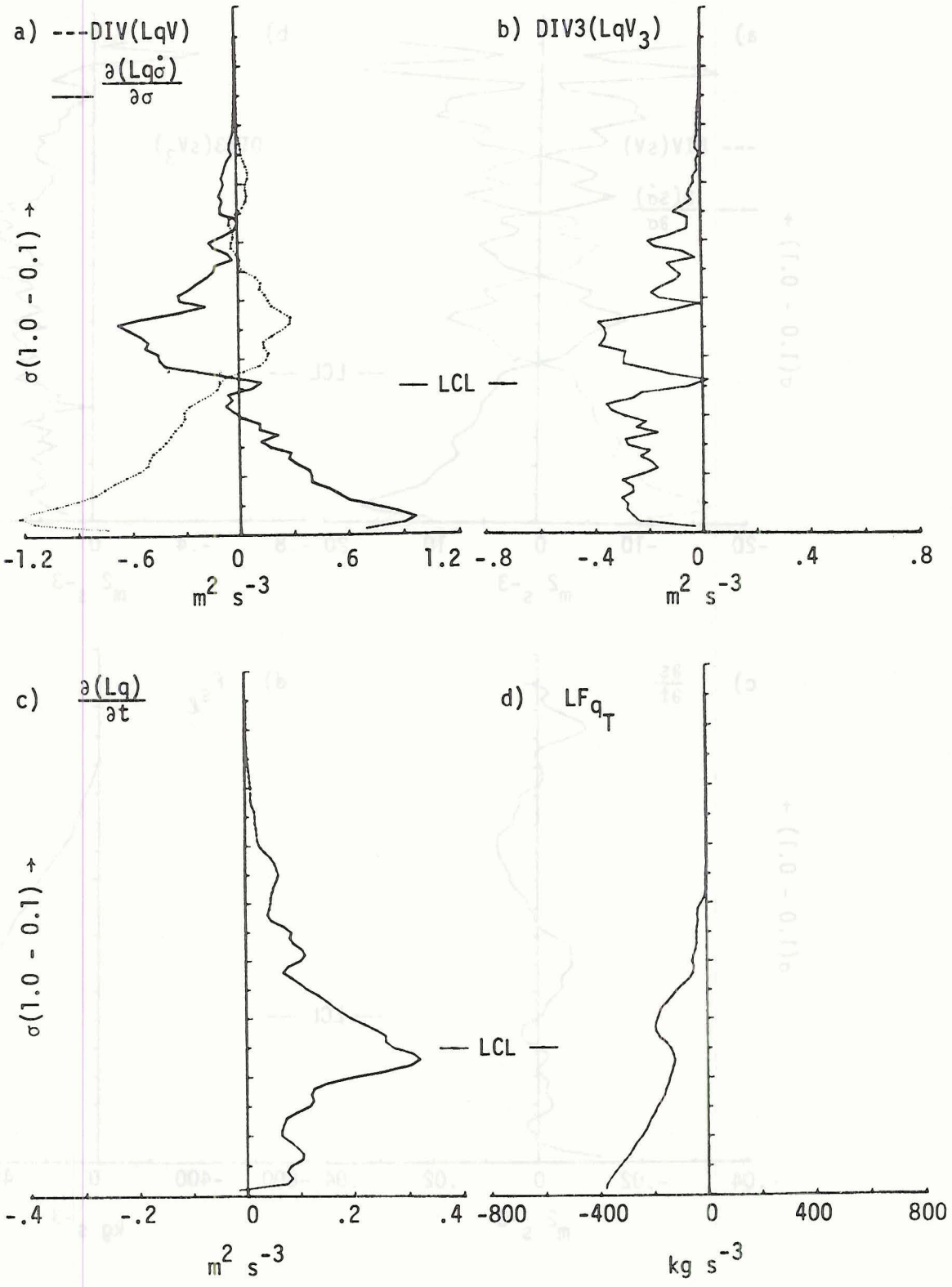

Figure 26. Precipitating Convection Lq Budget

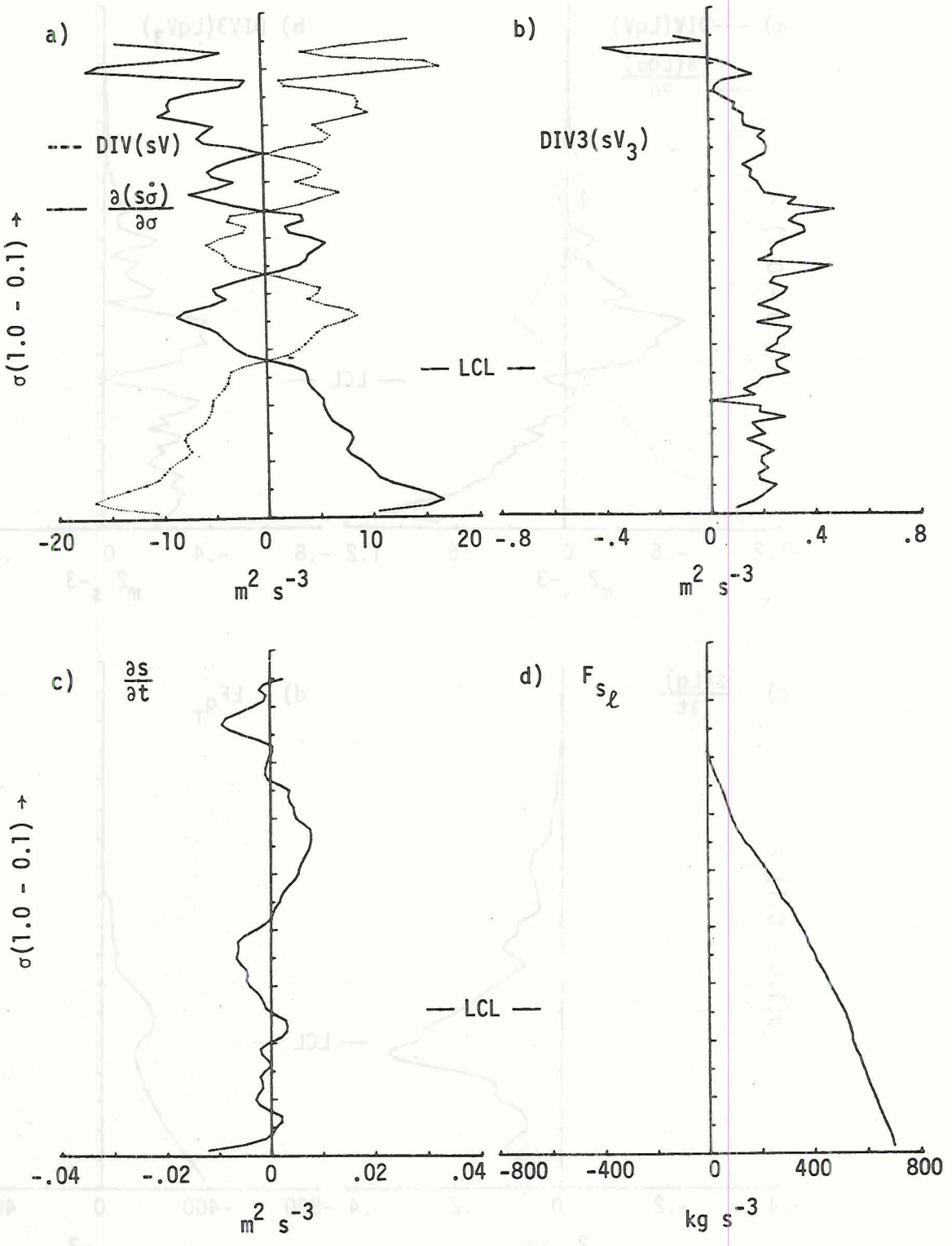

Figure 27. Precipitating Convection s Budget

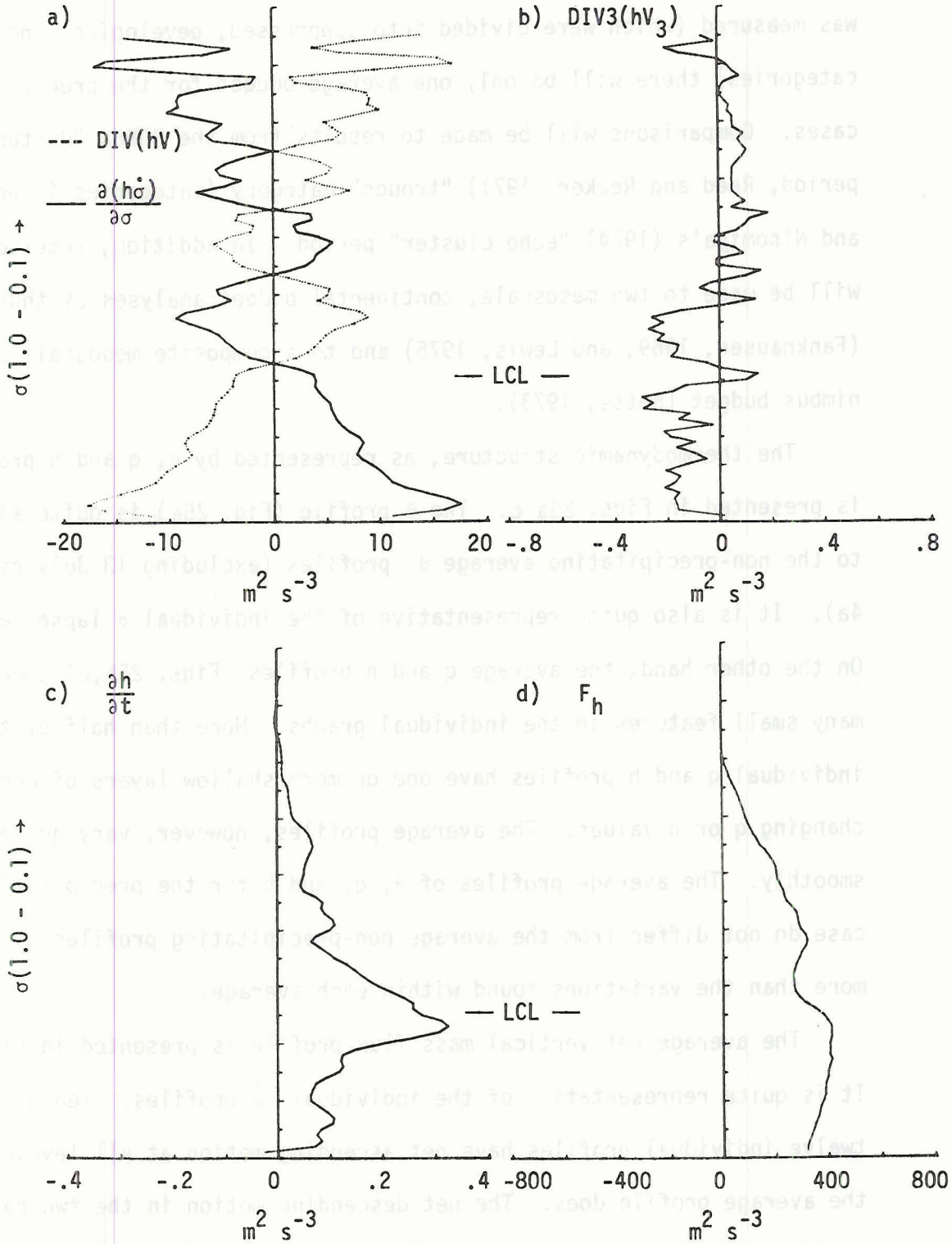

Figure 28. Precipitating Convection h Budget

cumulus convection. Unlike the average periods in which no precipitation was measured (which were divided into suppressed, developing, and moderate categories) there will be only one average budget for the precipitation cases. Comparisons will be made to results from the BOMEX "disturbed" period, Reed and Recker (1971) "trough" category (categories 4 and 5) and Ninomiya's (1974) "echo cluster" period. In addition, some comparisons will be made to two mesoscale, continental budget analyses of thunderstorms (Fankhauser, 1969; and Lewis, 1975) and to a composite mesoscale cumulonimbus budget (Betts, 1973).

The thermodynamic structure, as represented by θ, q and h profiles, is presented in Figs. 25a-c. The θ profile (Fig. 25a) is quite similar to the non-precipitating average θ profiles (excluding 13 July of section 4a). It is also quite representative of the individual θ lapse rates. On the other hand, the average q and h profiles (Figs. 25b,c) smooth out many small features in the individual graphs. More than half of the individual q and h profiles have one or more shallow layers of abruptly changing q or h values. The average profiles, however, vary quite smoothly. The average profiles of θ, q, and h for the precipitating case do not differ from the average non-precipitating profiles by any more than the variations found within each average.

The average net vertical mass flux profile is presented in Fig. 25d It is quite representative of the individual $\pi\dot{\sigma}$ profiles. Ten of the twelve individual profiles have net ascending motion at all levels as the average profile does. The net descending motion in the two cases is confined to shallow layers. The $\sigma\dot{\pi}$ contribution to $\pi\dot{\sigma}$ is relatively small and consequently the ω profile is similar to the $\pi\dot{\sigma}$ profile. In addition to the indication of generally ascending net motion, the average $\pi\dot{\sigma}$

profile shows a strong subcloud horizontal mass convergence and then a clear divergence just above cloud base. (σ_{LCL} = .74). This local maximum of $\pi\dot{\sigma}$ near cloud base is clearly present in eight of the twelve individual mass budgets.

This mass budget is not similar at all to that calculated for the BOMEX disturbed period (Nitta and Esbensen, 1974). The vertical mass flux in that period was upward only in the subcloud layer. The net descending motion above could reflect the fact that the data area is in the trade wind regime or it could simply indicate a data problem. The Reed and Recker data for the trough regions (presented by Cho and Ogura, 1974) yields an upward vertical mass flux at all level, but the magnitude is much smaller ($1*10^{-3}$ mb/sec) than the $\pi\dot{\sigma}$ of Fig. 25d ($5*10^{-3}$ mb/sec). Also, the local maximum of vertical mass flux is not evident in those data. The average ω profile calculated by Ninomiya (1974) for echo cluster periods exhibits a stronger similarity to Fig. 25d. The magnitude of the echo cluster ω is about $5*10^{-3}$ mb/sec. Although there is considerable scatter, almost all of his individual echo cluster profiles are upward (just as ten out of twelve $\pi\dot{\sigma}$ profiles here were upward at all levels). The average ω profile, however, does not have a local maximum around the cloud base level. Ninomiya's presentation of the individual values of ω at given levels does not reveal whether or not any individual profiles had this feature.

Three different continental, mesoscale vertical mass flux calculations show a marked similarity to the average $\pi\dot{\sigma}$ profile calculated for the precipitating convection periods. Two of the calculations are based on National Severe Storm Laboratories (NSSL) data (a mesoscale network about 200 km square with rawinsondes spaced about 85 km apart). Fankhauser (1969)

calculated an average ω profile for four points around a thunderstorm. The points were spaced 20 km apart, but the data that were used to calculate ω at these points were spaced about 85 km apart. Lewis (1975) calculated an average ω profile for the entire NSSL area. Part of a prefrontal squall line was in the data area during the calculation interval. The third calculation (Betts, 1973) is based on a composite mesoscale mass budget for a small (25 km diameter) mesoscale area "surrounding" a cumulonimbus. The squall line analysis (Lewis, 1975) and composite cumulonimbus analysis have average ω magnitudes of about $30\text{-}50*10^{-3}$ mb/sec. This is considerably larger than the $5*10^{-3}$ mb/sec calculated in this budget, but the difference is reasonable considering one case deals with a squall line and the other deals with a small area around a cumulonimbus. The analysis by Fankhauser (1969) shows an average magnitude of about $10\text{-}15*10^{-3}$ mb/sec. All three analyses depict net upward motion at all levels just as Fig. 25d does.

All three of the above profiles also have the local ω maximum near cloud base that is present in both the average $\pi\dot{\sigma}$ profile and eight of twelve individual $\pi\dot{\sigma}$ profiles. The occurrence of this local maximum in four independent data sets suggests that this feature is a general characteristic of precipitating mesoscale convection.

The average latent heat (water vapor) budget achieved during periods of precipitating convection is presented in Figs. 26a-d. There is strong average horizontal convergence of q flux below cloud base (Fig. 26a). About half of the individual profiles are similar to the horizontal q flux convergence for the developing convection average (section 4B). That is, the convergence clearly extends throughout the depth of the subcloud layer. The other half of the individual precipitating profiles are similar to the

moderate (mature to dissipating) convection average (section 4c). These profiles show a definite horizontal divergence of q flux just below cloud base (Fig. 26a). The three dimensional average q flux (Fig. 26b) is convergent up to σ = .40. While the individual profiles often have layers of positive (diverging) DIV3($Lq\vec{V}_3$), the average profile is quite representative in the sense that only one case (24 July) exhibits strong three dimensional divergence from the surface to σ = .40.

The three dimensional convergence of the average flux of q is larger than the mostly diverging convective flux of q_T(F_{q_T}, Fig. 26d), and consequently the time change of the water vapor (Fig. 26c) is positive. Except for a thin layer immediately above cloud base, the F_{q_T} profile has a negative (divergent) slope. In the cloud layer, this apparent sink of water vapor indicates a net loss of water vapor by condensation and the loss (precipitation) of this liquid water before it evaporates. Ten out of the twelve individual F_{q_T} profiles indicate either a convective sink (divergent slope of F_{q_T}) throughout the cloud layer or a divergent F_{q_T} layer above cloud base and a convergent (negative slope) layer above that.

Below cloud base the average F_{q_T} indicates an apparent sink of water vapor. The surface value of F_{q_T} indicates a net average precipitation of .05 cm/hr. Only evaporation (a source) and not condensation occurs below cloud base, which means the apparent loss of water vapor is due to the addition of relatively dry air into the subcloud layer by convection processes. As will be discussed, downdrafts are quite consistent with this subcloud eddy sink of water vapor even though the downdrafts are driven in part by evaporation of precipitation. Seven out of twelve individual F_{q_T} profiles have a negative (divergent) slope in the subcloud layer.

Three out of the remaining five individual cases that have positive subcloud slopes occur just before data intervals that have negative subcloud slopes. That is, later development of a dominating downdraft feature is indicated. The shallow convergent layer just above cloud base that is surrounded by divergent F_{q_T} profiles is not found in any of the individual F_{q_T} profiles. It appears in the average F_{q_T} because of individual F_{q_T} profiles that are convergent below (and sometimes above) cloud base.

The BOMEX data for disturbed periods (Nitta and Esbensen, 1974) show an apparent source of moisture throughout most of the 500 mb extent of the data. There is only a shallow (100 mb thick) layer containing an apparent moisture sink. Nitta and Esbensen, 1974, remark on the problem of unrepresentative and/or erroneous data present during the disturbed periods. Ninomiya's (1974) echo cluster calculations show an apparent sink of q from the 300 mb level to the 900 mb level. A weak apparent source of q is present below 900 mb, that is, below cloud base. The Reed and Recker (1971) trough region data discussed by Cho and Ogura (1974) show a clear apparent moisture sink throughout all data levels. The midlatitude calculation of Lewis (1975) has a net apparent q sink above cloud base (the net being composed of alternating weak source and sink layers) and a maximum apparent q sink below cloud base. Although Lewis (1975) notes that the squall line is in the mature stage, no mention of downdrafts is made in relation to the large subcloud value of Q_2.

Betts (1975) presents a F_{q_T} profile derived from continental (Venezuelan) composite mesoscale data. The profile has a definite negative (divergent) slope from 300 mb to the surface. Betts (1976) presents the following model and explanation of the subcloud divergent

F_{q_T} profile. Downdrafts originating above cloud base are driven by evaporating precipitation. However, the air that descends into the subcloud layer is originally much drier than the subcloud air. Consequently, even though the air is moistened by evaporation, it is relatively dry (compared to the subcloud air) and appears in a budget calculation as an apparent sink of q. The generally divergent slope of F_{q_T} in this precipitating average (Fig. 26d) is similar to the calculations by Cho and Ogura (1974), Ninomiya (1974), Betts (1975), and Lewis (1975) and is quite consistent with the downdraft discussion presented by Betts (1976).

The average dry static energy balance achieved in the case of precipitating convection is presented in Figs. 27a-d. The average convergence and divergence of the horizontal s flux (Fig. 27a) is not particularly representative of the individual DIV($s\vec{V}$) profiles, because the individual profiles have many alternating layers of strong convergence and divergence of the horizontal flux of s. The three dimensional average s flux divergence (Fig. 27b) is representative of the individual profiles. Even though most individual profiles have one or more convergence layers, the convergent layers are shallow compared to the divergent layers.

As in the other average convection cases, both the individual and average time changes of s (Fig. 27c) are very small compared to the other terms in the budget equation. That is, the three dimensional average divergence of s closely balances the apparent source of s at all data levels. The average convective flux of s_ℓ, F_{s_ℓ} (Fig. 27d), is quite representative of the individual F_{s_ℓ} profiles below $\sigma = .50$. Nine of the twelve F_{s_ℓ} profiles have either a positive (convergent) slope up to $\sigma = .30$ or a positive slope to at least $\sigma = .50$ and a shallow divergent slope above. These positive or convergent slopes show that convection is acting to add dry static energy to the atmosphere.

The average F_{s_ℓ} profile for precipitating convection is generally similar to those for moderate convection (Fig. 23d). However, the precipitating and moderate averages generally show cloud level warming in contrast to the cloud level cooling shown in the weak convection averages. Some upper level cooling does appear in the moderate case, but none is shown in the precipitating case.

The subcloud slope of F_{s_ℓ} in the precipitating and moderate convection cases is as great as in the developing and suppressed average cases. This suggests that not only are the previously mentioned downdrafts drier than their surroundings, but they are also about as warm as their surroundings. Such downdrafts could be driven by very weak evaporative cooling or by an overshoot process. In the overshoot process, the downdrafts descend below the equilibrium level set by evaporative cooling. Downdrafts in some midlatitude convection have been known to warm the environment.

Cho and Ogura's (1974) Q_1 (apparent source of s) calculation using data from Reed and Recker's (1971) trough regions shows a continuous source of s as does Fig. 27d. However, the precipitating convection average (Fig. 27d) has a rather uniform slope and does not indicate a maximum warming near 400 mb as the Cho and Ogura (1974) calculations indicate. The calculation by Lewis (1975) also shows an upper level (250 mb) maximum of Q_1. Above cloud base, Betts' (1975) F_{s_ℓ} profile is nearly unfirom as is the F_{s_ℓ} of Fig. 27d. Below cloud base both Betts' (1975) and Lewis' (1975) F_{s_ℓ} profiles show some divergence, that is, eddy cooling by the convection. In contrast, Fig. 27d shows a continued convergence or warming due to convection

below cloud base. This convective contribution does not produce any substantial net temperature change (see Fig. 27c), because the three dimensional average s flux is divergent (see Fig. 27b for DIV3($s\vec{V}$) and Fig. 27a for the components of DIV3($s\vec{V}$)).

The moist static energy budget for precipitating convection is presented in Figs. 28a-d. The average horizontal h flux divergence (Fig. 28a) is made up of individual profiles that vary considerably, and therefore does not portray any common major features. In the same sense the three dimensional average h flux (Fig. 28b) is only slightly more characteristic of the individual profiles. More than half of the individual DIV3($h\vec{V}_3$) profiles are generally convergent in the low levels, and somewhat more than half are generally divergent in the upper levels. Only four out of twelve, however, have both the negative DIV3($h\vec{V}_3$) values in low levels and positive DIV3($h\vec{V}_3$) values in the upper levels as the average profile does.

The only common feature of the individual time changes of h is the tendency to be generally positive. Nine of the twelve cases that are used to form the average time change of h (Fig. 28c) are positive throughout almost all of the data levels. The negative values of $\frac{\partial h}{\partial t}$ are not related to a diurnal change; they occur during the intervals centered on times 1148, 1401 and 1808 LST. Although the individual $\frac{\partial h}{\partial t}$ and DIV3(hV_3) profiles do not have common features which appear in their respective average profiles, the average F_h profile (Fig. 28d) does look like many of the individual F_h profiles. The convective flux of h, Fig. 28d, has a positive (convergent) slope throughout most of the cloud layer. Below

cloud base the slope is negative. F_h is convergent in most of the cloud layer in nine of the twelve individual calculations. In eight of these nine cases the slope of F_h changes near cloud base from convergent to zero (three cases) or divergent (five cases). The shallow layer from $\sigma = .75$ to $\sigma = .63$ is not a distinct feature present in the individual F_h profiles. It is due to the changing heights and slopes of the characteristic upper and lower layers.

The condensation source term is not present in the convective flux of h. Therefore, the F_h profile is directly related to convective transports of moist static energy. Both the average and individual F_h profiles indicate that precipitating convection produces a net source of moist static energy in the mid to upper cloud levels. Below cloud base, Fig. 28d shows a definite convective sink of moist static energy. This pattern shows precipitating convection acting to increase the environmental values of h in the cloud layer and decrease the subcloud environmental values of h.

The surface value of F_h may be somewhat large (319 kg s^{-3}) considering the general reduction in incoming radiation due to the scattered cumulus and broken cirrus cloud coverage (80◐, 250◍ average sky cover estimated in the same manner as values in Table 4 were estimated). However, this value of F_h is less than that calculated for the moderate convection case (381 kg s^{-3}) and for the weak, suppressed case (631 kg s^{-3}). Also, the value is much less than the maximum possible 725 kg s^{-3} (see Chapter III, section 4).

The two major features of Fig. 28d (cloud layer convergence, subcloud divergence) are clearly present in three of the previously cited budget studies. In the calculations by Cho and Ogura (1974) there is an apparent

h source above the 650 mb level and a sink below in trough category 4, and a source above the 850 mb level and a sink below in the trough category 5. The F_h calculation by Lewis (1975) for a prefrontal squall line situation shows a divergence of F_h below cloud base and a convergence beginning about 100 mb above cloud base. The F_h profile calculated by Lewis (1975) has a maximum value of about 1050 kg s^{-3} at the 600 mb level (cloud base is at the 700 mb level). As is consistent with the other budget quantities calculated by Lewis (1975), this maximum value is considerably larger than the maximum value of 411 kg s^{-3} indicated in Fig. 28d. The shape of the F_h profile calculated by Betts (1975) for Venezuelan cumulonimbus composite data is also similar to that calculated for this precipitating average case. His F_h profile has a positive (convergent) slope beginning about 100 mb above cloud base and a sharply divergent slope below cloud base. Betts (1976) discusses the fact that such a subcloud sink of h can only be due to the action of downdrafts transporting air with relatively low h values into the subcloud layer. A comparison of the four average F_h profiles calculated in this thesis suggests this explanation by Betts (1976) is quite reasonable. Of the four types of convection considered, only the precipitating case has a negatively (divergent) sloped F_h in the subcloud layer. Betts (1976) modeled the downdrafts as being driven by evaporative cooling by precipitation.

The budget description of precipitating convection presented in this section is summarized in Chapter VII.

VI. DISCUSSION AND MODELING

1. Vertical Velocities

A. Comparison of $\pi\dot{\sigma}$ to ω

The σ vertical coordinate system is useful in this research because it simplifies calculations at the sloping lower boundary (Chapter III, section 1). In addition, the related vertical mass flux $\pi\dot{\sigma}$ is useful because it simplifies the comparison of a vertical velocity over sloping terrain to a vertical velocity over level terrain. This latter point is discussed below.

A part of the presentation of results in Chapter V, section 4 involved a comparison of average vertical mass fluxes calculated in this research with those calculated in other budget studies. The point of the comparison was to note the similarities and differences for periods that exhibited generally similar types of convection. However, pressure surfaces in the low to mid atmosphere have a considerable slope with respect to the NHRE terrain (40 mb/100 km in the east-west direction), but are almost parallel to the lower boundaries (oceans) of the other studies. If vertical velocities with respect to pressure surfaces (ω) are compared, the comparison will always have some built in difference related to the sloping terrain in the NHRE area. The following argument suggests that this difference can be partly accounted for by comparing $\pi\dot{\sigma}$ of this research to ω values of the previously mentioned studies.

In studying convection it is reasonable to consider vertical velocities relative to surfaces that are nearly parallel to the cloud base level. Pressure surfaces are nearly parallel to cloud bases over mesoscale areas with level lower boundaries. The lower boundary of the NHRE area, however, slopes considerably. The schematic east-west cross

section of Fig. 29 uses p, T, and q values averaged over all 39 data intervals to show the relation between the p, σ, and LCL surfaces over the NHRE area. The LCL is taken to represent cloud base level (see Chapter V, section 1B).

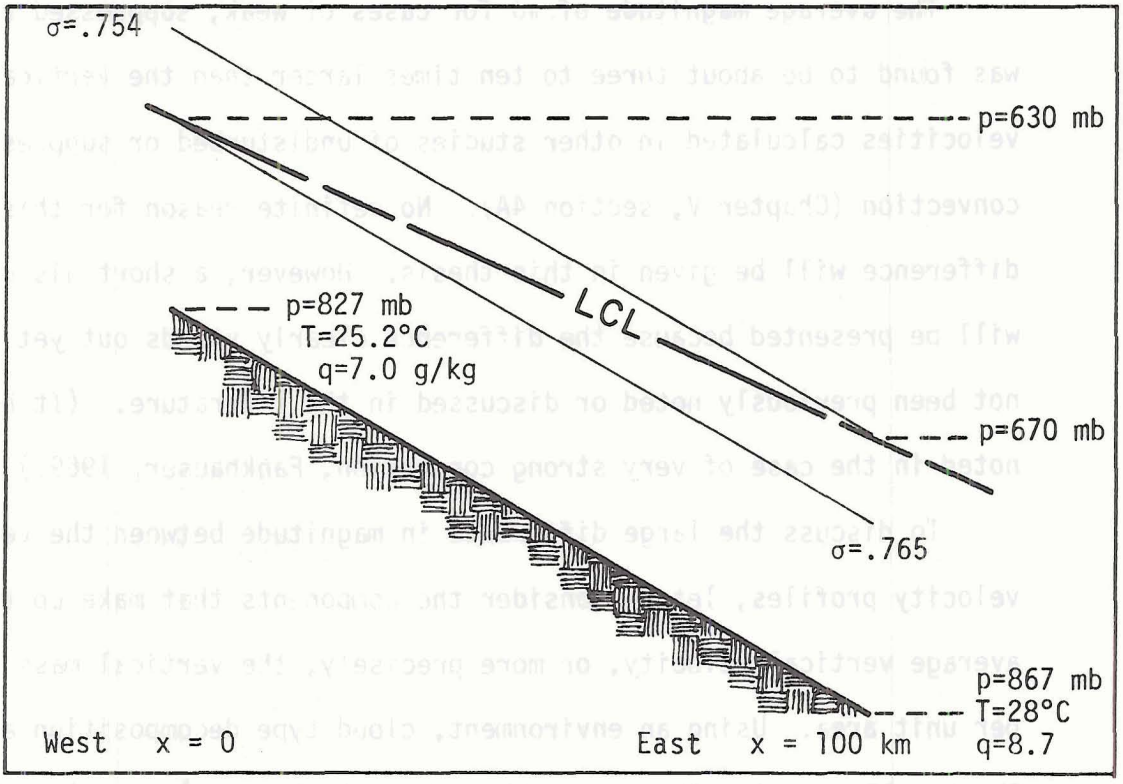

Figure 29. Schematic East-West Cross Section of NHRE Area (Slope Exaggerated)

Figure 29 shows that the cloud base level is nearly parallel to the σ surfaces and not p surfaces. This means that over the NHRE area, $\pi\dot{\sigma}$ is a vertical velocity relative to surfaces nearly parallel to the cloud base level. Consequently, it is reasonable to compare $\pi\dot{\sigma}$ profiles in this study to ω profiles of other studies.

The above argument begins to break down at high levels, because p surfaces begin to slope less with respect to σ surfaces. Also, the significance of the cloud base as a reference level becomes questionable

at high levels. Fortunately, for the discussion in Chapter V, section 4, the difference between $\pi\dot{\sigma}$ and ω is relatively large only in the case of weak, suppressed convection.

B. Magnitude of $\pi\dot{\sigma}$

The average magnitude of $\pi\dot{\sigma}$ for cases of weak, suppressed convection was found to be about three to ten times larger than the vertical velocities calculated in other studies of undisturbed or suppressed convection (Chapter V, section 4A). No definite reason for this difference will be given in this thesis. However, a short discussion will be presented because the difference clearly stands out yet it has not been previously noted or discussed in the literature. (It has been noted in the case of very strong convection, Fankhauser, 1969.)

To discuss the large difference in magnitude between the vertical velocity profiles, let us consider the components that make up the average vertical velocity, or more precisely, the vertical mass flux per unit area. Using an environment, cloud type decomposition as in Chapter II, section 2B, we see that the calculated $\pi\dot{\sigma}$ or ω (recall that $\omega = \pi\dot{\sigma} + \sigma\dot{\pi}$) is the sum of the cloud mass flux plus the environment mass flux for a given data area and time interval. Assuming these fluxes generally are not in the same direction (Yanai, 1971), the large magnitude difference is a statement that cloud-environment mass fluxes in the mesoscale data of this thesis do not balance as well as they do in the other data networks. This larger imbalance could be due to two factors.

First, the weak suppressed convection dealt with in this research could contain many more clouds than the various types of weak convection

present in the other studies. If a certain amount of cloud-environment imbalance is associated with each cloud a larger number of clouds would produce a larger average $\pi\dot{\sigma}$.

Second, the imbalance could be due to stronger mesoscale circulations not directly related to convection. Even though the NHRE area slopes quite smoothly (see Chapter IV, section 1) it contains several small scale topographical features that could produce pronounced local circulations. Mesoscale circulations could also be related to localized surface heating and stronger diurnal temperature changes characteristic of continental areas.

No data are available to indicate which one or more of the two possibilities is related to the large magnitude of the $\pi\dot{\sigma}$ profiles. Nevertheless, the above discussion was presented to emphasize this distinctive feature of weak, continental, mesoscale convection.

2. Model Interpretation of Weak, Suppressed Convective Fluxes

The net contributions of weak, suppressed cumulus convection to the mesoscale budgets of q, s, and h are given by the F_q, F_s and F_h profiles presented in Figs. 14d, 15d, and 16d. In this section these profiles are expressed in terms of a model convective transport process developed and used by Ooyama (1971), Betts (1973, 1975), and Yanai, et al (1973). The discussion of the diagnostically derived convective transports in terms of a model is useful because the derived profiles represent only the final or net result of many complicated processes occurring in and around cumulus clouds (see Chapter II, section 2 for a general description of processes included in the eddy flux term). The model is used to break down the individual profiles into simplified component parts.

The form of the convection model and particularly the interpretation of the individual terms comprising the model will closely follow Betts (1975). The two convective fluxes F_h and F_{s_ℓ} (F_{q_T} is simply the difference $F_h - F_{s_\ell}$) are modeled (Eqs. 11a, b) as the products of single convective mass fluxes times a cloud-environment difference of s_ℓ and h.

$$F_h = \pi\dot{\sigma}_h^*(h_c - h_E) \tag{11a}$$

$$F_{s_\ell} = \pi\dot{\sigma}_s^*(s_{\ell_c} - s_E) \tag{11b}$$

From Chapter III, section 5B, recall that

$$F_h = \int_t \int_{A_c} (h_c - h_E)\, \pi\dot{\sigma}_c\, dA_c\, dt \tag{12a}$$

$$F_{s_\ell} = \int_t \int_{A_c} (s_{\ell_c} - s_E)\, \pi\dot{\sigma}_c\, dA_c\, dt \tag{12b}$$

The environmental quantities in Eqs. 11a, b are to be taken as area and time averaged values as described, for example, by $\int_t \int_A h_E\, dA\, dt \,/\, \int_t \int_A dA\, dt$, and are available from the data. Various types of overbars could have been used in Eq. 11 to describe these integrations but for clarity have been omitted. Representative values of cloud quantities are denoted by h_c and s_{ℓ_c} and are not available from the data. They are modeled by the following simple entraining parcel concept (Eq. 13a, b)

$$\frac{\partial h_c}{\partial \sigma} = \lambda(h_c - h_E) \tag{13a}$$

$$\frac{\partial s_{\ell_c}}{\partial \sigma} = \lambda(s_{\ell_c} - s_E) \tag{13b}$$

The entrainment rate $\lambda(>0)$ will be assumed. For this simple model its value was not found to be critical for either these calculations or for those of Betts (1975).

The model is applied by first integrating Eqs. 13a and b to obtain the representative cloud values h_c and s_{ℓ_c}, and then Eqs. 11a, b are used to determine $\pi\sigma_h^*$ and $\pi\sigma_{s_\ell}^*$. The integration of 13a, b requires given vertical profiles of h_E and s_E and lower boundary values of h_c and s_{ℓ_c}. The calculation of $\pi\sigma^*$ is sensitive to the input profiles of h_E, s_E, and F_h, F_{s_ℓ}, and to the lower boundary values of h_c, s_{ℓ_c}. Once these quantities are determined, the choice of λ is not critical.

The average h_E and s_E profiles for weak, suppressed convection, excluding day 13 July, are used in the integrations of Eqs. 13a, b (see Fig. 30). As described in Chapter V, section 4A, day 13 July had a pronounced moist layer near cloud base. Inclusion of this moist layer in the average profile of h_E produces very large and sometimes negative values of $\pi\dot{\sigma}_h^*$.

The flux profiles averaged over all days including 13 July are used in the calculations of $\pi\dot{\sigma}^*$ in Eqs. 11a, b. The exclusion of 13 July changes F_{s_ℓ} enough to produce negative values of $\pi\dot{\sigma}_s^*$. This arbitrary including and excluding of one day will be discussed later, but for now we proceed with the calculations of $\pi\dot{\sigma}^*$ realizing the sensitivity of the model.

In order to obtain profiles of h_c and s_{ℓ_c} by integrating Eqs. 13a, b the cloud base values of h_c and s_{ℓ_c} are set equal to h_E and s_E at $\sigma = .99$. This is consistent with the procedure used to calculate the lifting condensation level (Chapter V, section 1B). Betts (1975) forced the cloud base value of s_{ℓ_c} to a value that matched the convective mass fluxes at cloud base. In this case the procedure was quite reasonable because the necessary adjustment was well below the accuracy of the instruments. A similar approach was tried in this research, but s_{ℓ_c} at cloud base had to

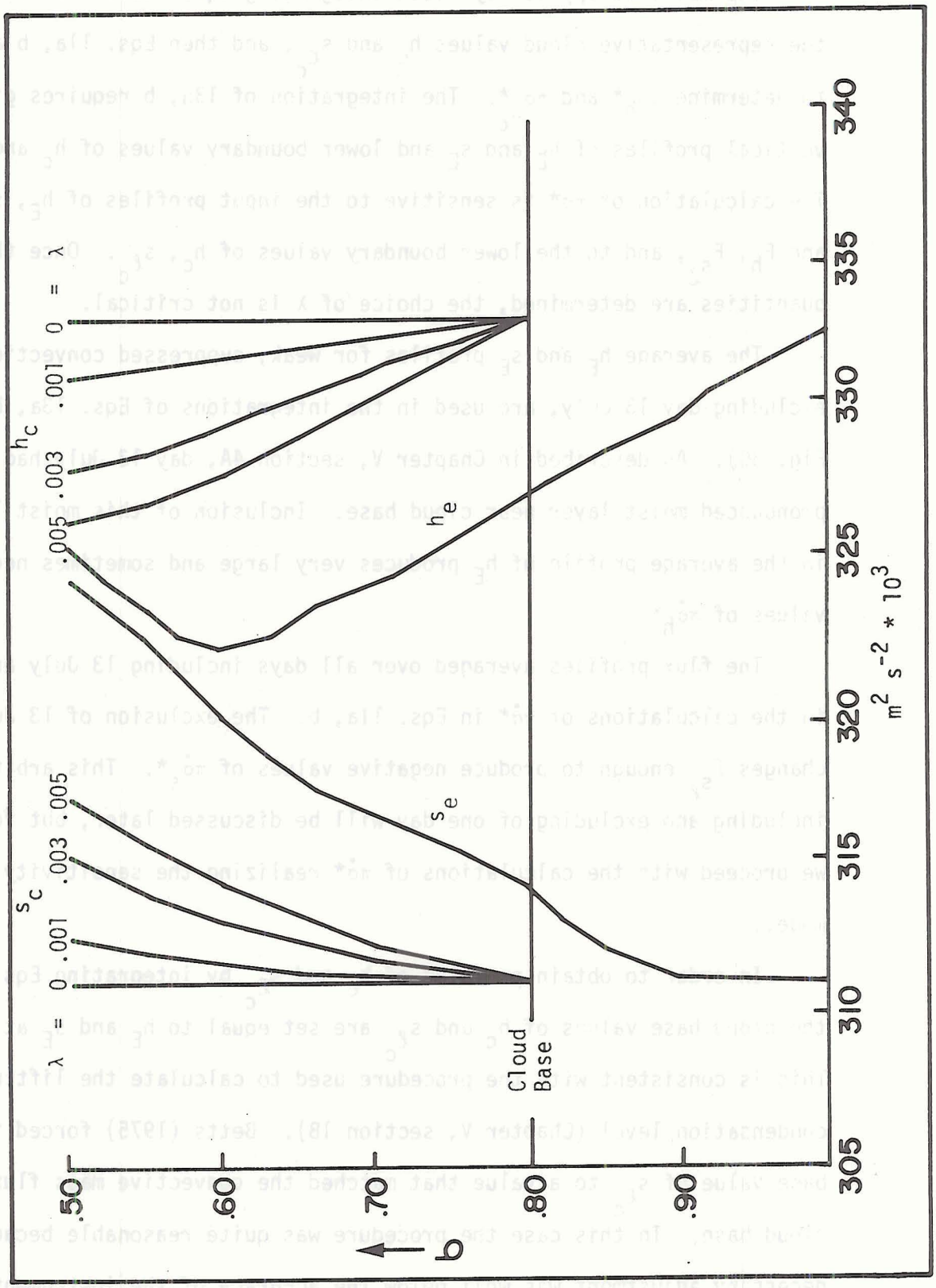

Figure 30. Model Profiles of h_c, s_{ℓ_c} for λ = 0, .001, .003, and .005 mb^{-1}

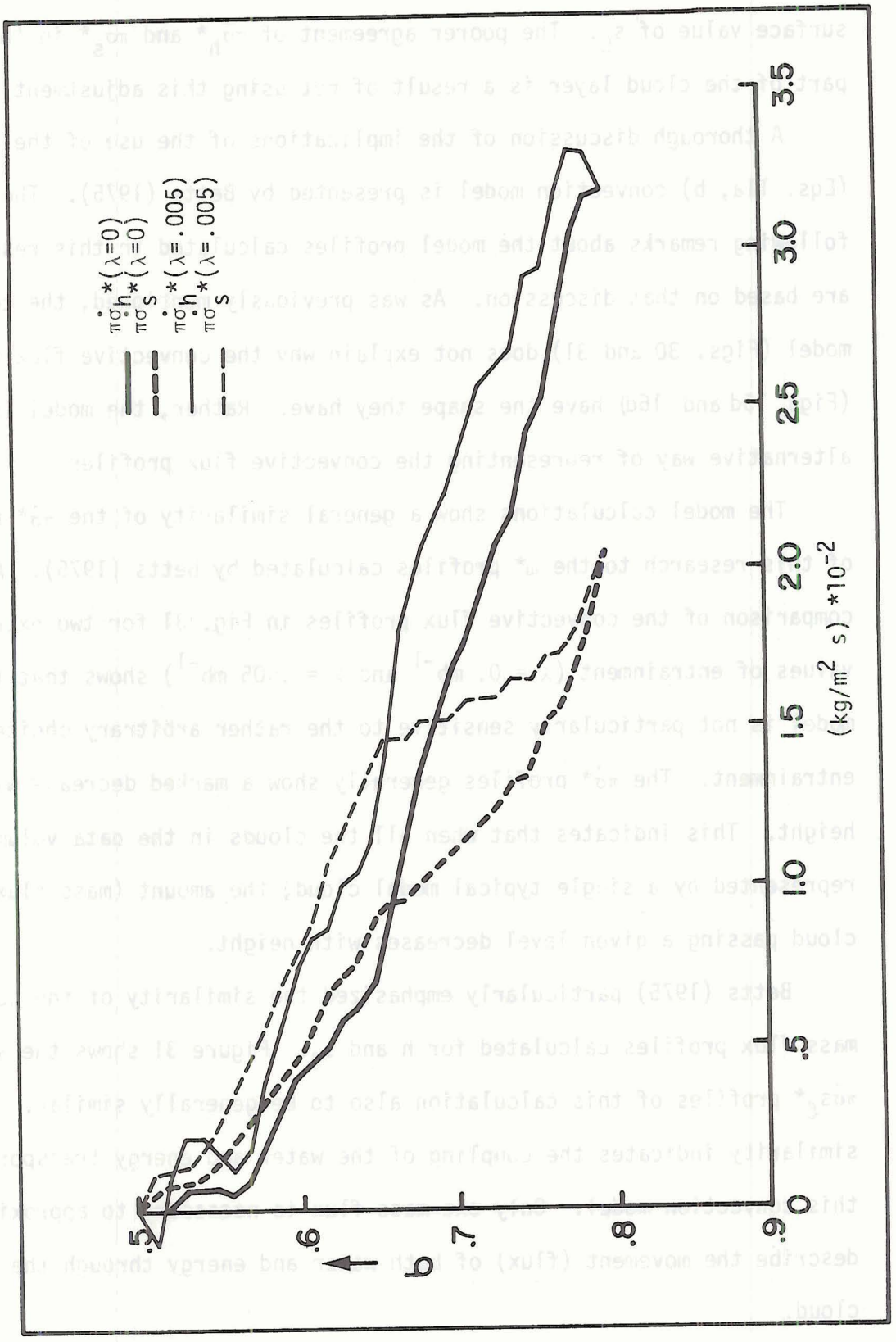

Figure 31. Model Convective Mass Flux Profiles for λ = 0, .005 mb^{-1}

be increased approximately 1×10^3 j/kg (equivalent to 1°K) above the surface value of s_E. The poorer agreement of $\pi\dot{\sigma}_h^*$ and $\pi\dot{\sigma}_s^*$ in the lower part of the cloud layer is a result of not using this adjustment.

A thorough discussion of the implications of the use of the above (Eqs. 11a, b) convection model is presented by Betts (1975). The following remarks about the model profiles calculated in this research are based on that discussion. As was previously mentioned, the convection model (Figs. 30 and 31) does not explain why the convective flux profiles (Figs. 15d and 16d) have the shape they have. Rather, the model is an alternative way of representing the convective flux profiles.

The model calculations show a general similarity of the $\pi\dot{\sigma}^*$ profiles of this research to the ω^* profiles calculated by Betts (1975). A comparison of the convective flux profiles in Fig. 31 for two extreme values of entrainment ($\lambda = 0.\ mb^{-1}$ and $\lambda = .005\ mb^{-1}$) shows that the model is not particularly sensitive to the rather arbitrary choice of entrainment. The $\pi\dot{\sigma}^*$ profiles generally show a marked decrease with height. This indicates that when all the clouds in the data volume are represented by a single typical model cloud, the amount (mass flux) of cloud passing a given level decreases with height.

Betts (1975) particularly emphasized the similarity of the convective mass flux profiles calculated for h and s_ℓ. Figure 31 shows the $\pi\dot{\sigma}_h^*$ and $\pi\dot{\sigma}s_\ell^*$ profiles of this calculation also to be generally similar. This similarity indicates the coupling of the water and energy transports in this convection model. Only one mass flux is necessary to approximately describe the movement (flux) of both water and energy through the model cloud.

The slope of the convective mass flux is related to the detrainment ($\mu = \lambda + \frac{1}{\omega^*} \frac{\partial \omega^*}{\partial p}$, Betts (1975)). As in the calculations made by Betts (1975), these $\pi\dot{\sigma}^*$ profiles indicate that detrainment is large compared to entrainment, and is important even in the case of zero entrainment. Betts proceeds from the idea of detrainment and the calculation of its relatively large magnitude to the concept that the transient character of a cloud (the cloud's life cycle) is an important part of a cloud model. This same interpretation follows nicely in this thesis from the definition of F_h and F_{s_ℓ} (Eq. 12a, b). The time integrations in Eqs. 12a, b indicate that the calculated convective fluxes of h and s_ℓ include the effects of cloud life cycles.

Finally, the application of this model to a new set of data adds credence to the usefulness of the model and also points out problem areas in its use. The calculations of this research show three general features that were found by Betts (1975). First, the cloud mass flux of the single model cloud decreases with height. Second, the convective transports of water and energy are approximately coupled. Third, the detrainment is of the same magnitude as the entrainment.

The main problem area indicated by the calculations is the sensitivity of the model to the input data. Betts (1975) used tropical, oceanic data averaged over five days. In this research, changes in the vertical profiles due to the presence or absence of one day of data can make the model yield unreasonable $\pi\dot{\sigma}^*$ profiles. The noise in the convective flux profiles plus the smoothing of the environmental profiles of h and s indicate the NHRE data are only marginally useful for use with this type of model.

3. Model Interpretation of Weak, Developing Convective Fluxes

Estimates of the net convective transports of q_T, s_ℓ, and h for weak, developing convection were presented in Figs. 18d, 19d, and 20d. These estimates are based on a model computation described in this section. The model is used to account for the change in cloud storage of water and energy due to the development of the clouds in the budget volume.

The original calculations of the flux forms of the apparent sources for q_T, s_ℓ, and h are presented as dotted lines in Figs. 18d, 19d, and 20d. Although the dotted profiles and the profiles presented in Figs. 14d, 15d and 16d both represent weak convection (developing and suppressed, respectively) they are strikingly different. One of the clearest differences is the net apparent sink of q that is indicated by the original (dotted) developing convection profile of F_{q_T}. This sink of water vapor is not due to precipitation because the clouds do not even produce radar echoes during the budget calculation periods. However, it is quite reasonable to ascribe this loss of water vapor to the net increase in the number and/or size of clouds in the budget volume (see Chapter V, section 1B for a description of the developing nature of the convection). The positive (convergent) slope of the original profile of F_{s_ℓ} in Fig. 19d also suggests a net condensation heating due to an increase of cloud water.

A simple model of the change of cloud storage of water and energy for weak, developing clouds will be developed in this section. This model is based on the storage terms that were mentioned and then neglected in the use of the general budget equation 5. These terms will now be reintroduced into the form of the budget equation developed in Chapter III, section 5B.

$$\Delta F_\chi = -\frac{1}{AT}\int_{A_c}\int_{t}\left[-F_I + (\chi_c - \chi_E)\,(\pi\dot{\sigma})_c\right]_{\sigma_1}^{\sigma_2} dA_c\, dt$$

$$-\frac{1}{AT}\int_{A}\int_{\sigma}\left[(\pi I_\chi + (\pi\chi)_c - (\pi\chi)_E)\,\frac{d\sigma}{g}\, dA_c\right]_{t_1}^{t_2} \qquad (14)$$

The LHS, $\Delta F_\chi = F_\chi(\sigma_2) - F_\chi(\sigma_1)$, is the residual in flux form for the layer σ_1 to σ_2. The first term on the RHS, which is an average over area A and time interval T, is the convective term that has been assumed to be the dominant term. The second term on the RHS is the previously neglected change in storage. Recall that I_χ was defined as the property or material than can be converted into χ. For the case of water vapor, q, $I_q = \ell$, where ℓ is the mixing ratio of liquid water. The sum $(I_\chi + \chi_c - \chi_E)$ represents the excess of χ in the clouds over the environmental value of χ. Taking account of the negative sign of $(\sigma_2 - \sigma_1)$, we see that an increase with time of the total cloud excess of χ tends to produce an apparent sink of χ.

The calculated residual F_χ only gives a measure of the sum of the storage term plus the convective transport term. In order to proceed with modeling the storage term, we now make the following important assumption. The convective transport of χ above cloud base in the case of weak, devleoping convection is assumed equal to the convective transport of χ above cloud base calculated for weak suppressed convection. (See Figs. 14d, 15d, 16d, and Chapter V, section 4A.) The validity of this assumption will be discussed later. The direct result of the assumption is that subtraction of the weak, suppressed convective flux profiles ($F_{\chi(supp)}$) from the weak, developing convective flux profiles ($F_{\chi(dev)}$) will yield a measure of the cloud storage term alone:

$$\Delta F'_\chi = -\frac{1}{AT}\int_A\int_\sigma (\pi I_\chi + (\pi\chi)_c - (\pi\chi)_E)\frac{d\sigma}{g}\,dA_c\Big]_{t_1}^{t_2} \qquad (15)$$

where $\Delta F'_\chi = \Delta F_{\chi(dev)} - \Delta F_{\chi(supp)}$ and $\Delta F_\chi = F_\chi(\sigma_2) - F_\chi(\sigma_1)$

It has been assumed that

$$\frac{1}{AT}\int_{A_c}\int_t -F_I + (\chi_c - \chi_E)(\pi\dot{\sigma})_c\Big]_{\sigma_1}^{\sigma_2} dA_c\,dt \text{ (suppressed case)}$$
$$= \frac{1}{AT}\int_{A_c'}\int_t -F_I + (\chi_c - \chi_E)(\pi\dot{\sigma})_c\Big]_{\sigma_1}^{\sigma_2} dA_c\,dt \text{ (developing case)} \qquad (16)$$

Because the suppressed and developing cloud bases are at slightly different levels, the suppressed (lower) convective profiles were simply raised .06 σ levels to make the cloud bases coincide. We next set χ equal to q_T, s_ℓ, and h and omit the integral notation by letting I_χ, χ_c and χ_E be representative values over area A_c, time T, and layer $(\sigma_2-\sigma_1)$ (the usual bar ($\bar{}$) notation is also omitted for clarity):

$$\Delta F_{q_T}' = (\ell + q_c - q_E)\left(\frac{\pi\Delta\sigma}{g}\right)\left\{\frac{1}{T}\left[\left(\frac{Ac}{A}\right)_{t_2} - \left(\frac{Ac}{A}\right)_{t_1}\right]\right\} \qquad (17a)$$

$$\Delta F_{s_\ell}' = (s_c - L\ell - s_E)\left(\frac{\pi\Delta\sigma}{g}\right)\left\{\frac{1}{T}\left[\left(\frac{Ac}{A}\right)_{t_2} - \left(\frac{Ac}{A}\right)_{t_1}\right]\right\} \qquad (17b)$$

$$\Delta F_h' = (h_c - h_E)\left(\frac{\pi\Delta\sigma}{g}\right)\left\{\frac{1}{T}\left[\left(\frac{Ac}{A}\right)_{t_2} - \left(\frac{Ac}{A}\right)_{t_1}\right]\right\} \qquad (17c)$$

The quantities $(\ell + q_c - q_E)$ and $(s_c - L\ell - s_E)$ are representative values of excess total water $(\ell + q_c)$ and liquid water static energy $(s_c - L\ell)$ above the environmental values. The term $\frac{1}{T}\left[\left(\frac{Ac}{A}\right)_{t_2} - \left(\frac{Ac}{A}\right)_{t_1}\right]$ is the change in fractional cloud area over the interval T.

As in the modeling of weak, suppressed convection (Eq. 13, section 2) a simple entraining parcel model will be used to generate representative values of the conservative cloud properties $(\ell + q_c = q_T)$ and $(s_c - L\ell = s_{\ell_c})$:

$$\frac{\partial q_T}{\partial \sigma} = \lambda(q_{T_c} - q_{T_E}) \tag{18a}$$

$$\frac{\partial s_{\ell_c}}{\partial \sigma} = \lambda(s_{\ell_c} - s_{\ell_E}) \tag{18b}$$

In the unsaturated environment $q_{T_E} = q_E$ and $s_{\ell_E} = s_E$. Cloud base values of q_{T_c} and s_{ℓ_c} are chosen to be consistent with the procedure used to calculate the cloud base level (see Chapter V, section 1B). The cloud base values are set to the near surface values: $s_\ell(cB) = s(\sigma = .99)$ and $L(\ell + q)_{cB} = h(cB) - s_\ell(cB) = h(\sigma = .99) - s(\sigma = .99)$. Graphs of the excess total water $(q_{T_c} - q_E)$ and excess liquid water static energy $(s_{\ell_c} - s_E)$ are presented in Fig. 32 for two values of entrainment ($\lambda = 0.$, and $\lambda = .005\ mb^{-1}$).

Equations 17a, b and c model the change of cloud storage of water and energy for weak, developing convection. The excess quantities $(q_T - q_E)$ and $(s_\ell - s_E)$ that appear in Eqs. 17a, b are obtained from Eqs. 18a, b. The change in fractional cloud area is then calculated from the F' profiles. The vertical profile of the change of fractional cloud area that is consistent with (1) the model cloud and (2) the assumption that the convective transport terms for developing and suppressed weak convection are equal will be calculated using both equations 17a and b. Equations 17a and b provide two independent estimates of the change of fractional cloud area.

The agreement of these estimates (as given by the area between the 0-0-0 and x-x-x profiles) does not depend strongly on the choice of λ. The use of $\lambda = 0$ (Fig. 34) produces slightly better agreement than the use of $\lambda = .005\ mb^{-1}$ (Fig. 33). The approximate shape of the time change of cloud area profile (given by --- and —— lines in Figs. 33 and 34) is somewhat more dependent on the choice of λ.

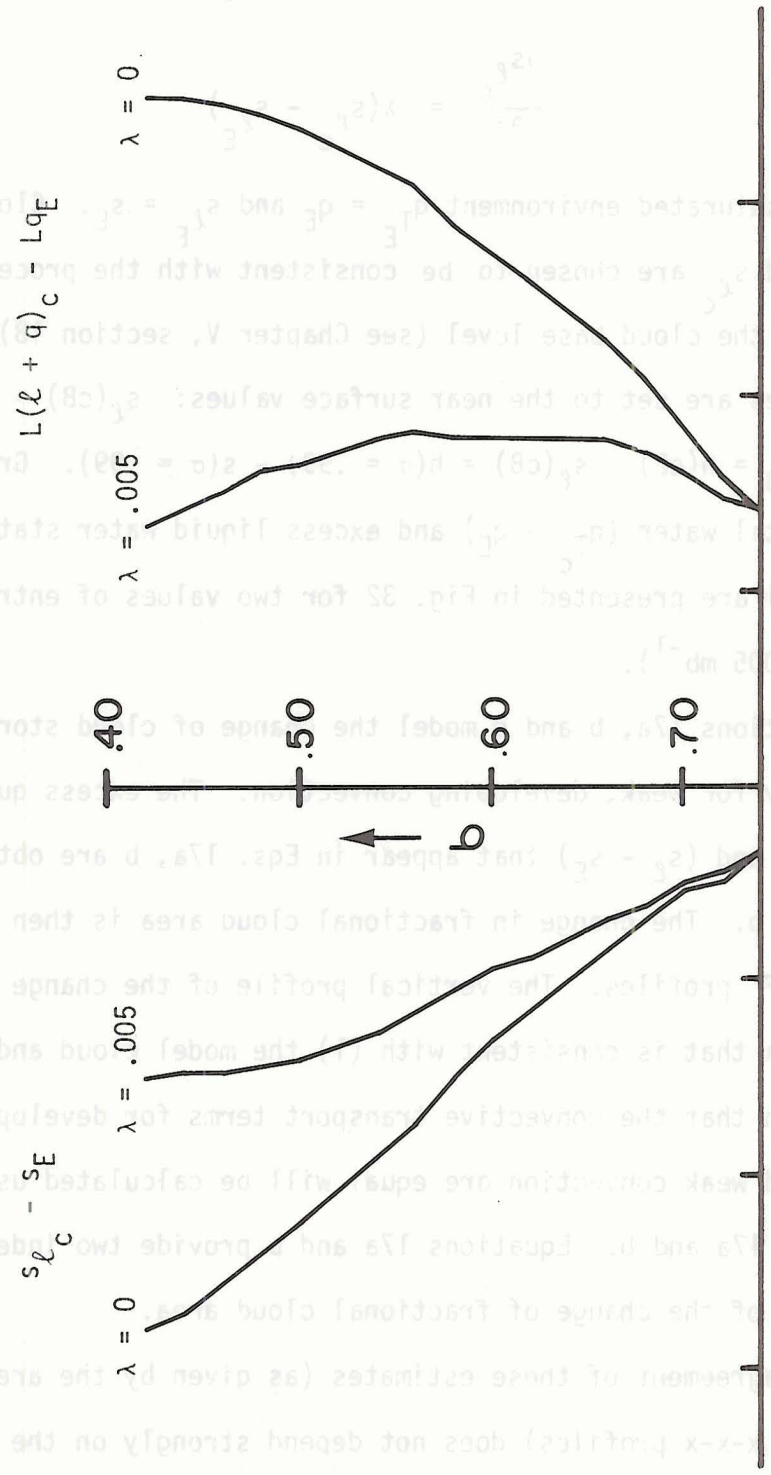

Figure 32. Model Cloud Excess Liquid Water Static Energy and Total Water for λ = 0, .005 mb^{-1}.

Figure 33. Time Change of Fractional Cloud Area, λ = .005 mb^{-1}.

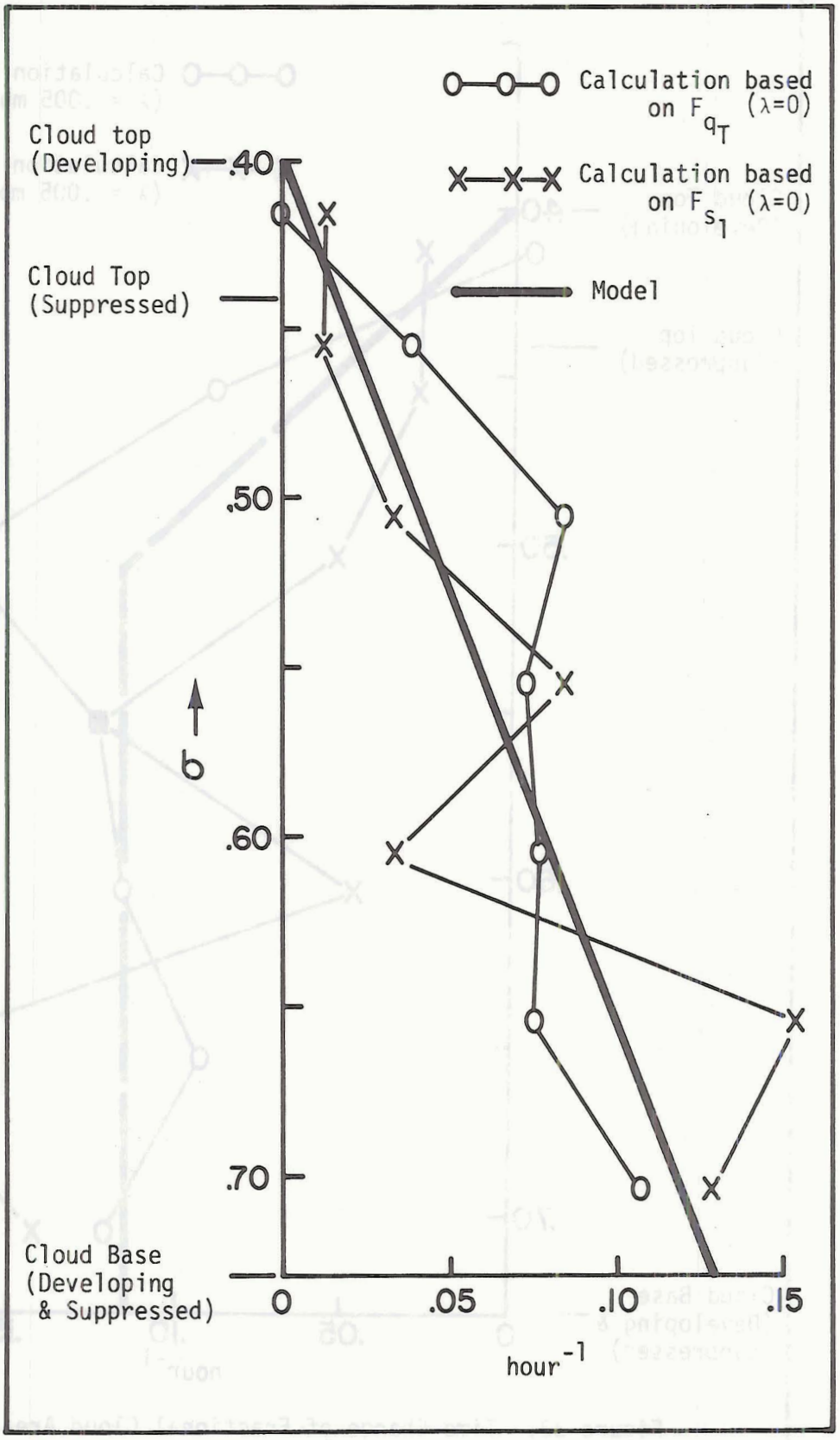

Figure 34. Time Change of Fractional Cloud Area, λ=0 mb^{-1}

Both Fig. 33 and 34 show a time change of fractional cloud area on the order of .1 hr^{-1}. This is a substantial increase, but it is quite consistent with the general developing character of the convection and the fact that it represents development over about a three hour period in the afternoon.

The model of the change of cloud storage of water and energy is completed by approximating the two derived profiles in Fig. 34 by the single, linearly decreasing profile (solid line). This idealized profile of the time change of fractional cloud area and the profile of the excess cloud values of q_T and s_ℓ for $\lambda = 0$ together make up the model of changing cloud storage. This model has been applied to the original (dotted) F_{q_T}, F_{s_ℓ} and F_h profiles for weak, developing convection (Figs. 18d, 19d, and 20d) to produce the final (solid line) profiles that represent just the convective transports of q_T, s_ℓ, and h. Application of the model removes the cloud storage contribution.

Obtaining the convective fluxes (solid lines, Figs. 18d, 19d, and 20d) by subtraction of the modeled cloud storage term from the original apparent source term (dotted lines), however, severely limits the interpretation of the convective fluxes. The two initial estimates of the cloud storage term (0-0-0 and x-x-x lines of Fig. 34) assume the developing convective fluxes are equal to the suppressed case convective fluxes. These two estimates are then idealized to the solid line of Fig. 34 . This means the developing case fluxes F_{q_T}, F_{s_ℓ}, and F_h of Figs. 18d, 19d, and 20d are almost forced to equal the respective suppressed case fluxes of Figs. 14d, 15d, and 16d. However, this equality of the suppressed case and developing case convective fluxes

appears to be a reasonable assumption, because the two independent estimates of the cloud storage term based mainly on this assumption turn out to be nearly equal.

The role of the change of cloud storage has not been emphasized in previous large and mesoscale budget studies. These calculations clearly show that it produces a substantial contribution to the apparent sources of water and energy in a developing convection situation. The recognition and modeling of this cloud storage term are two of the main contributions of this research.

VII. SUMMARY AND CONCLUSIONS

This thesis presents and interprets water and energy budget descriptions for four broad classifications of summertime cumulus convection occurring over the National Hail Research Experiment (NHRE) mesoscale data area. The budgets are calculated from NHRE rawinsonde data. The convection classifications are based on radar and precipitation data. The budget equation, calculation procedure, data, results, and conclusions are summarized here. Suggestions for future research are presented.

A budget equation for an aribtrary scalar quantity, χ, is derived. The most basic assumption in this equation is that clear air (environmental) quantities, χ_E, vary smoothly and the major perturbations to these background fields are caused by small, localized disturbances related to convection with properties χ_c. The environmental terms are separated to the LHS and the convection terms to the RHS of the budget equation. The general goal of the thesis then becomes the calculation of the environmental terms from the data, and the interpretation of both the RHS convection residual and the individual LHS terms.

The budget equation derived in this thesis has several features that aid in the above calculations and interpretations. A normalized pressure (σ) vertical coordinate is used to facilitate calculations over the sloping NHRE terrain. The environmental variables appear as functions of horizontal position. This enables the simple interpretation of $\chi_c - \chi_E$ as a cloud excess even when χ_E has a horizontal gradient. The time and space integrations are explicit in order to emphasize the time and space averaging scales. The change of cloud storage term is retained for use during intervals when it is not negligible. Finally, the source term on

the RHS of the budget equation is written in a flux form. This introduces the fluxes of total water and liquid water static energy which have been used by Betts (1975).

The approximations of the data as linear functions of horizontal position and time are two of the most important steps in the calculation procedure. These approximations act as the main filters of the input data. Fortunately, a comparison of the original data and the linear spatial approximations show small average absolute differences (.5 g/kg, .6°K, 1 m s^{-1} for q, T, u respectively). Another important step in the calculation procedure is the use of the continuity equation to determine the average vertical mass flux ($\pi\dot{\sigma}$). A correction technique developed by O'Brien (1970) is applied to the $\pi\dot{\sigma}$ profile in order to produce a zero vertical velocity at the top (100 mb) data level. Finally, the radiation term on the RHS of the budget equation is modeled using a program supplied by S. K. Cox. The radiation contribution is small compared to the other budget terms and is only applied to the budgets calculated for periods with little convection present.

The budget calculations are based on data obtained from the NHRE rawinsonde network. Five sondes were launched approximately simultaneously at two to three hour intervals in the afternoon on several days during the summer of 1973. The final data set consists of data for 39 intervals occurring over 14 days. The rawinsonde data processing takes into account the downwind drift of the sondes and time differences in the data due to the sonde rise time (about 50 minutes) and launch time differences (about 30 minutes).

Each of the 39 individual budget calculation periods is classified as having one of four types of convection: (1) weak, suppressed, (2) weak,

The slope of the F_{q_T} profile for weak convection shows an addition of water vapor in both the cloud and subcloud layer. Unlike the comparable oceanic studies, this convective source is larger in the subcloud layer than the cloud layer. The moderate convection average shows a weak drying of both cloud and subcloud layers. The precipitating average F_{q_T} profile shows a more pronounced convective sink of water vapor throughout most of the atmosphere. This loss is due to precipitation in the cloud layers which corresponds to the radar/precipitation classification. A convective sink of water vapor is present in the subcloud layer even though no condensation occurs below cloud base. This is due to the introduction of relatively dry cloud-level air into the subcloud layer by downdrafts. Budget studies by other authors show this subcloud sink of moisture in precipitating situations.

The average convective fluxes of liquid-water static energy are presented in Fig. 36. All the profiles show a subcloud warming of approximately the same magnitude. This suggests that the previously discussed downdrafts in the precipitating cases are not very cool relative to the subcloud air. Both weak evaporative cooling and convective overshooting may be acting to drive such downdrafts.

The cloud layer slopes of F_{s_ℓ} again display a very reasonable progression from the weak to the precipitating classification. Weak convection cools the upper portion of the cloud layer by net evaporation. In contrast, moderate and precipitating convection warm the cloud layer by net condensation.

The average convective fluxes of moist static energy are presented in Fig. 37. Weak, moderate, and precipitating convection are all shown to generally add moist static energy to the cloud layer. The surface

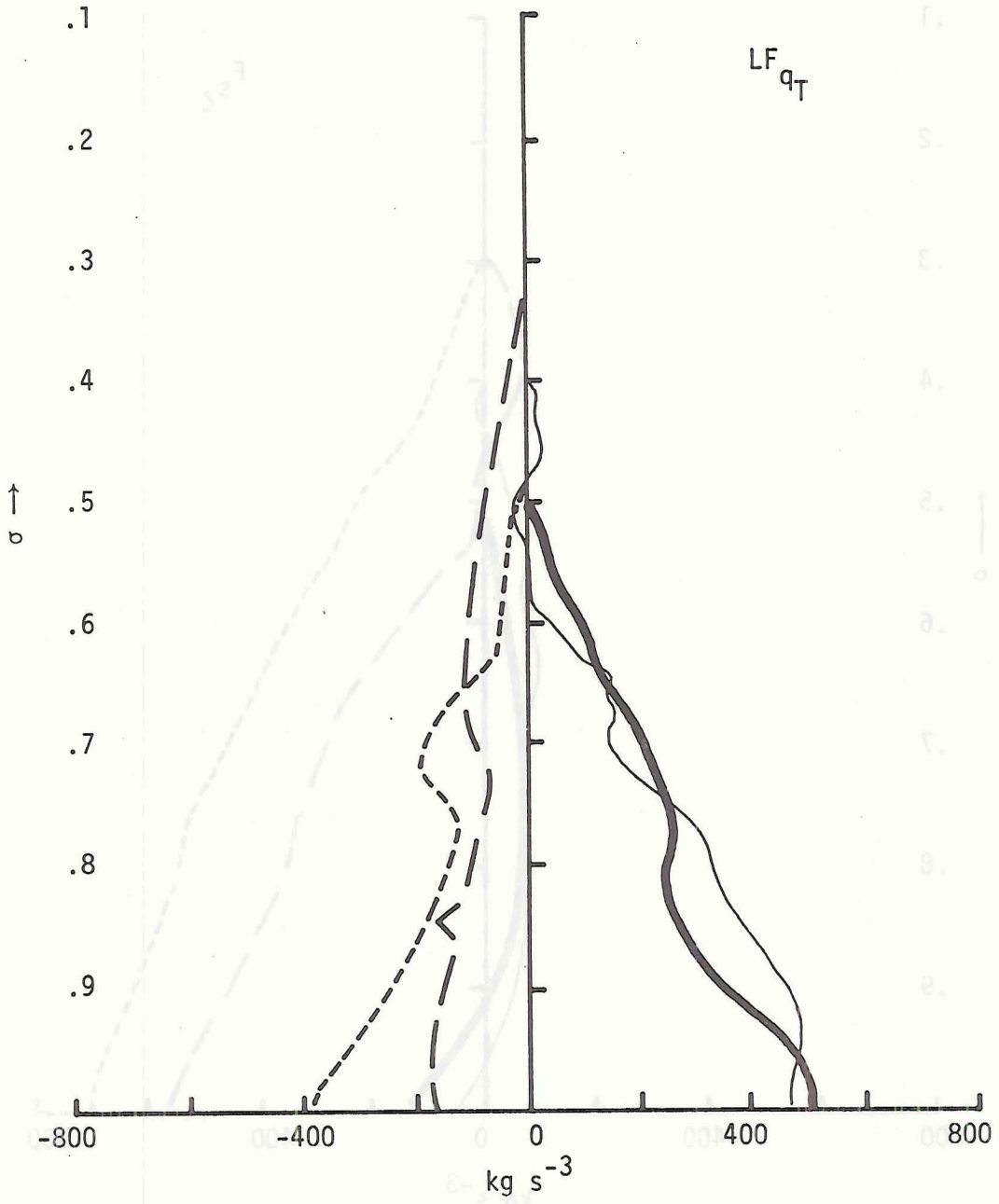

Figure 35. Convective Flux of Total Water (F_{q_T}).

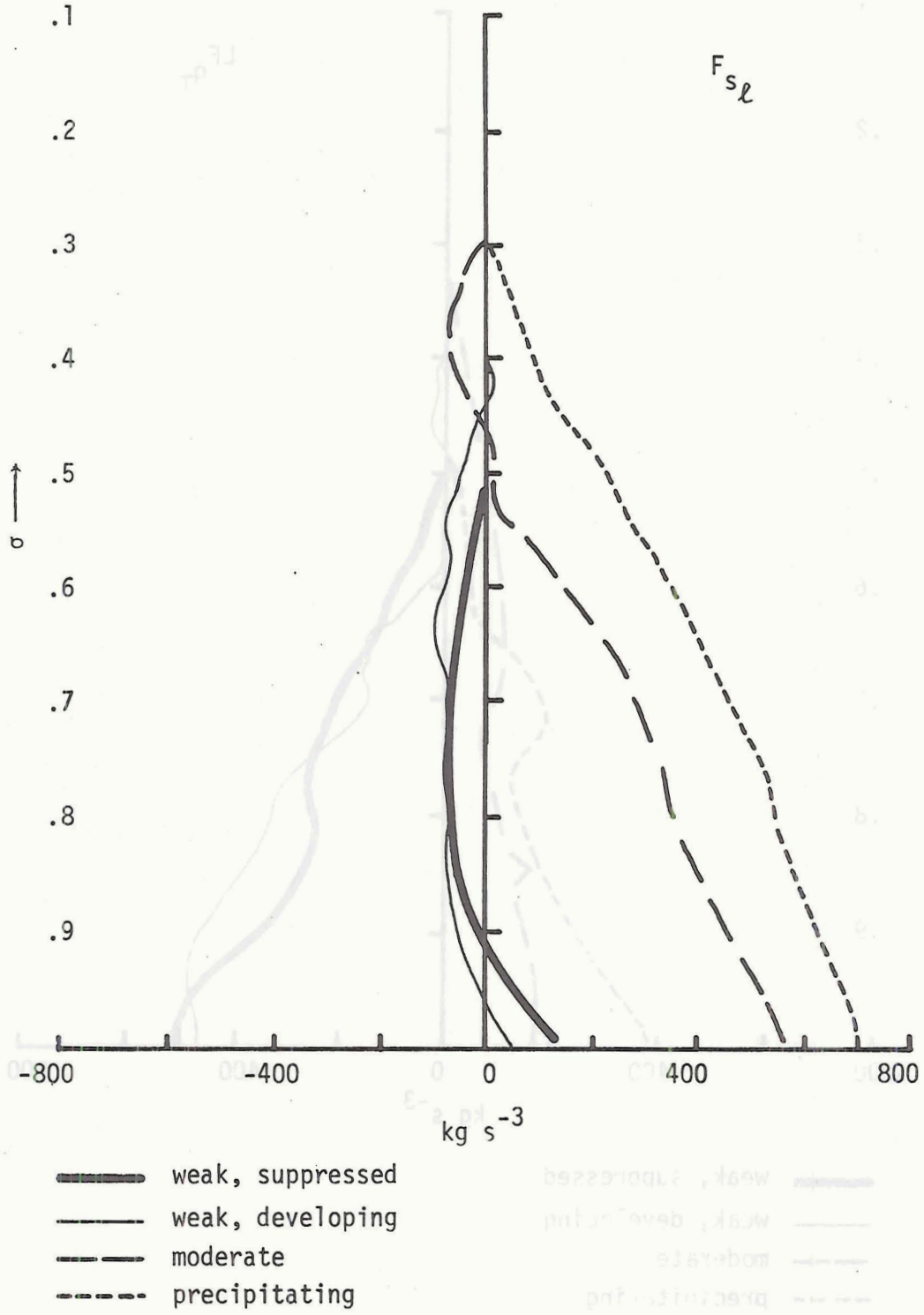

Figure 36. Convective Flux of Liquid Water and Static Energy (F_{s_ℓ})

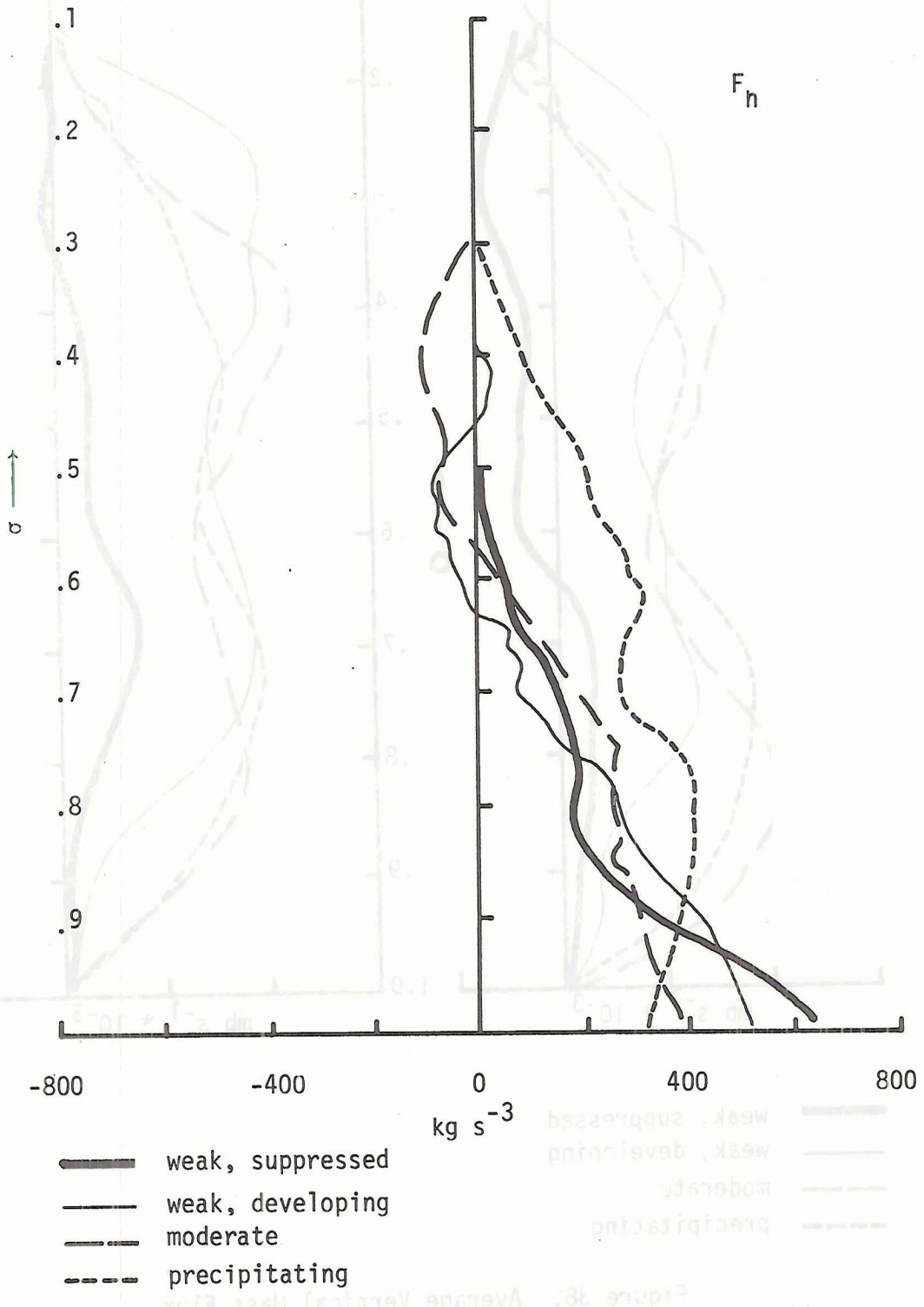

Figure 37. Convective Flux of Moist Static Energy (F_h).

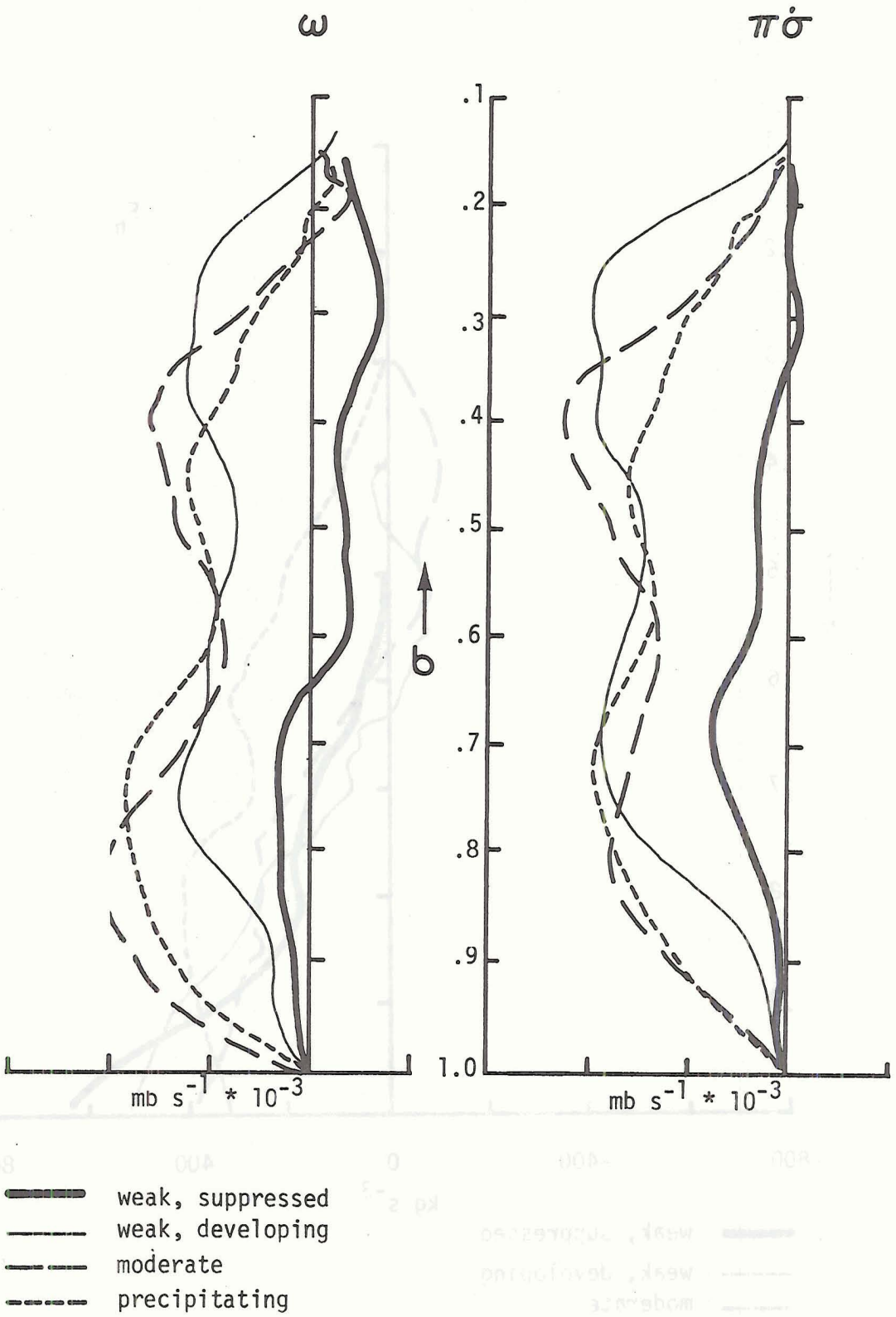

Figure 38. Average Vertical Mass Flux

values of F_h decrease from the weak to the moderate to the precipitating convection case. This progression is quite realistic, because the surface value of F_h is approximately equal to the net surface radiation which decreases as the cloudiness increases.

The subcloud slope of F_h for weak convection indicates a strong convective source of moist static energy. In contrast to comparable oceanic studies, the subcloud convective source of h is larger than the cloud layer convective source. The subcloud slopes of the F_h profiles also show a progression from the weak to the precipitating cases. Dry convection and mechanical mixing add moist static energy to the subcloud layer during periods of weak convection. This source is considerably weaker in the case of moderate convection. Precipitating convection produces a subcloud sink of h. This convective sink is due to the introduction of higher level air by downdrafts. Three other budget studies have shown this subcloud convective sink of moist static energy.

The average vertical mass flux as represented by either $\pi\dot{\sigma}$ or ω (Fig. 38) clearly shows two types of profiles. The $\pi\dot{\sigma}$ profile for the weak, suppressed convection indicates weak net ascent in the cloud layer with descent above and/or below the cloud layer. Other budget studies of "undisturbed" convection do not show this layer of net ascent. Also the magnitude of ω in these similar studies is much smaller than the $\pi\dot{\sigma}$ magnitude for weak, suppressed convection.

Developing, moderate, and precipitating convection averages show the second general type of $\pi\dot{\sigma}$ profile. The net vertical motion is ascending and the ascent profiles have a double maximum. The lower maximum near cloud base occurs not only in the average profiles but is also present in many of the individual profiles. Several other mesoscale

studies have shown this double maximum. It is not present in previous large scale studies. This double maximum in the ω profile may, therefore, be a characteristic feature of deep mesoscale convection.

The $\pi\dot{\sigma}$ profiles calculated over the sloping NHRE terrain are interpreted as being the proper representation of the vertical mass flux to compare to low and mid level ω profiles calculated over level lower boundaries. This interpretation is based on the idea that low and mid level σ surfaces are nearly parallel to the cloud base level. Consequently, $\pi\dot{\sigma}$ is a measure of vertical velocity relative to cloud base level over the NHRE area just as ω approximates vertical motion relative to cloud base level when the lower boundary does not slope.

The convective flux profiles for weak, suppressed convection are studied by expressing F_h and F_{s_ℓ} in terms of a convective transport model developed and used by Ooyama (1971), Betts (1973, 1975), and Yanai, et al (1973). The model is simply the product of a mass flux times a cloud-environment difference of s_ℓ or h. The cloud-environment difference of s_ℓ or h is calculated by using a simple nonentraining parcel model and the convective mass flux is determined by dividing this difference into F_{s_ℓ} or F_h, respectively. The two resulting convective mass flux profiles are independent of each other. The following conclusions (prompted by the discussion presented by Betts (1975)) are drawn from the use of the model.

The general similarity of the two independently calculated convective mass flux profiles indicates an approximate coupling of water and energy transports. One convective mass flux is associated with the transport of both h and s_ℓ. The mass flux, related to the single representative cloud that has been used as a model, decreases with height. The change of this

convective mass flux with height indicates that detrainment is an important feature of the cloud model.

The data of this research are only marginally accurate for use with the above convection model. The calculation of the convective mass flux involves the sensitive division of F_{s_ℓ}, F_h by the cloud excess of s_ℓ, h. The F_{s_ℓ}, F_h fluxes are noisy, and some features of the vertical profiles of s, h, may be smoothed by the averaging.

Cloud storage is modeled for use in the weak, developing convection budget. The model is the product of a time change of fractional cloud area times a typical cloud excess of q_T or s_ℓ. The cloud excess is calculated by using a simple nonentraining parcel model.

Two independent estimates of the change of fractional cloud area are made by assuming the convective fluxes for weak, developing convection equal the convective fluxes for weak, suppressed convection. These estimates of the change of cloud area show good general agreement, and are idealized by a single profile that decreases linearly with height throughout the cloud layer. The cloud base value of this profile is .13/hour.

The idealized profile of the change of cloud area plus the non-entraining parcel model are used to subtract cloud storage from the weak, developing budget. The cloud storage contribution to the budget for developing convection is as large as the convective flux contribution.

This research brings several points forward that deserve consideration for future mesoscale convection experiments. First, the arrangement of the NHRE rawinsonde network in a "ring" with no central site best lends itself to line integration calculations. On the mesoscale, however, sonde drift and rise time considerations suggest the data are more representative of

an area than of a line. The use of a rawinsonde site configuration that yields a field of data instead of a ring of data is suggested.

The good fit of the data by simple plane functions indicates the 50-100 km spacing of the NHRE sondes is a useful horizontal resolution for mesoscale convection studies. The time resolution of about three hours seems to be marginal for use with the four convection classes used in this research. Rawinsondes every 90 minutes would be preferable. The accuracy of the wind system produced reasonable results below 300 mb, but large divergence errors are probably present in the upper level calculations. Much better upper level wind data are needed.

Increased mesoscale radar converage is suggested. The NHRE was designed primarily for intensive hail storm study. Consequently, the radar data over the entire mesoscale area are marginal. The use of 360° scans, stepped at fine increments (for good vertical resolution at large distances) are suggested.

Radar and possibly high resolution satellite data are very important because they are the primary "physical" measure of mesoscale convection that can be compared to convective budgets based on rawinsonde data. They also afford an estimate of the change of cloud storage and the net movement of clouds into or out of the mesoscale area.

Finally, the study of all stages of cumulus convection is suggested. The interpretation of the budget calculations of this research was greatly aided by being able to compare water and energy budgets for several classifications of cumulus convection.

REFERENCES

Arakawa, A., and W. Schubert, 1974: Interaction of a cumulus cloud ensemble with the large-scale environment. Part I., J. Atmos. Sci., 31, pp. 674-701.

Augstein, E., H. Riehl, R. Ostapoff and V. Wagner, 1973: Mass and energy transports in an undisturbed Atlantic trade-wind flow. Mon. Wea. Rev., 101, pp. 101-111.

Betts, A. K., 1970: Cumulus convection. Ph.D. Thesis, Imperial College, University of London, 151 pp.

_____, 1973: Non-precipitating cumulus convection and its parameterization. Quart. J. Roy. Meteor. Soc., 99, pp. 178-196.

_____, 1974: Further comments on "A comparison of the equivalent potential temperature and the static energy". J. Atmos. Sci., 31, pp. 1713-1715.

_____, 1975: Parametric interpretation of trade-wind cumulus budget studies. J. Atmos. Sci., 32, pp. 1934-1945.

_____, 1976: The thermodynamic transformation of the tropical sub-cloud layer by precipitation and downdrafts. (Submitted to J. Atmos. Sci.)

Cho, H.-R., and Y. Ogura, 1974: A relationship between the cloud activity and the low-level convergence as observed in Reed-Recker's composite easterly waves. J. Atmos. Sci., 31, pp. 2058-2065.

Fankhauser, J.C., 1969: Convective processes resolved by a mesoscale rawinsonde network. J. Appl. Met., 8, pp. 778-798.

Fraedrich, D., 1973: On the parameterization of cumulus convection by lateral mixing and compensating subsidence. Part I. J. Atmos. Sci., 30, pp. 408-413.

_____, 1974: Dynamic and thermodynamic aspects of the parameterization of cumulus convection. Part II. J. Atmos. Sci., 31, pp. 1838-1849.

Gray, W. M., 1972: Cumulus convection and large-scale circulations. Part III: Broadscale and mesoscale considerations. Atmos. Sci. Paper No. 190, Colorado State University, Fort Collins, CO.

Henz, J.F., 1975: Verification of numerical simulations of Colorado Plains cumulus clouds - cloud development and precipitation efficiency controls. J. Appl. and Pure Geophys., Sept. 1975, pp.

Holland, J.Z., and E.M. Rasmusson, 1973: Measurements of the atmospheric mass, energy and momentum budgets over a 500-kilometer square of tropical ocean. Mon. Wea. Rev., 101, pp. 44-55.

REFERENCES - Continued

Jalickee, J.B., and E.M. Rasmusson, 1973: An atmospheric budget analysis scheme. Preprint volume of Third Conference on Probability and Statistics in Atmospheric Science, Boulder, Colorado.

Kasahara, A., 1974: Various vertical coordinate systems used for numerical weather prediction. Mon. Wea. Rev., 102, pp. 509-522.

Lettau, H.H., and B. Davidson, 1957: Exploring the atmosphere's first mile. Volumes I and II. Pergamon Press.

Lewis, J.M., 1975: Test of the Ogura-Cho model on a prefrontal squall-line case. Mon. Wea. Rev., 103, pp. 764-778.

Ninomiya, K., 1974: Bulk properties of cumulus convections in the small area over Kurishio Region. J. Meteor. Soc. of Japan, 52, No. 2, pp 188-202.

Nitta, T., 1975: Observational determination of cloud mass flux distributions. J. Atmos. Sci., 32, pp. 73-91.

_____, and S. Esbensen, 1974: Heat and moisture budgets using BOMEX data. Mon. Wea. Rev., 102, pp. 17-28.

O'Brien, J. J., 1970: Alternative solutions to the classical vertical velocity problem. J. Appl. Meteor., 9, pp. 197-203.

Ogura, Y., and H.-R. Cho, 1973: Diagnostic determination of cumulus cloud populations from observed large-scale variables. J. Atmos. Sci., 30, pp. 1276-1286.

Ooyama, K., 1971: A theory of parameterization of cumulus convection. J. Meteor. Soc. of Japan, 29, The Syono Memorial Volume, pp. 744-756.

Paltridge, G. W., 1974: Infrared emissivity, short-wave albedo, and the microphysics of stratiform water clouds. J. Geophys. Res., 79, pp. 4053-4058.

Pearce, R. P., 1968: Vorticity budgets derived from Caribbean data. Part II. Atmospheric Science Paper No. 126, Colorado State University, Fort Collins, CO 80523.

Phillips, N.A., 1957: A coordinate system having some special advantages for numerical forecasting. J. Meteor., 14, pp. 184-185.

Reed, R. J. and E. E. Recker, 1971: Structure and properties of synoptic scale wave disturbances in the equatorial Pacific. J. Atmos. Sci., 28, pp. 1117-1133.

Williams, K. T., 1970: A statistical analysis of satellite-observed trade wind cloud clusters in the western north Pacific. Atmospheric Science Paper No. 161, Colorado State University, 80 pp.

REFERENCES - Continued

Yanai, M., 1971: A review of recent studies of tropical meteorology relevant to the planning of GATE. Experimental design proposal by the International Scientific and Management Group (ISMG).

_____, S. Esbensen and J. Chu, 1973: Determination of average bulk properties of tropical cloud clusters from large-scale heat and moisture budgets. J. Atmos. Sci., 30, pp. 611-627.

APPENDIX A

DATA AND DERIVED QUANTITIES

The data and derived quantities averaged over the various convective periods discussed in the text are presented in Tables A.1 through A.5.

The convective fluxes FF_{q_T}, FF_{s_ℓ}, and FF_h presented in these tables have been set to zero at the highest available data levels. This corresponds to setting $\sigma_T = .13$ in Tables A.1, A.2, A.3 and A.5 and $\sigma_T = .14$ in Table A.4. The convective fluxes can be set to zero at any arbitrary level by subtracting the flux value at the desired zero level from all other flux values. For example, to obtain the F_{q_T} values for weak, suppressed convection (13 July included) used in the text, subtract the value of FF_{q_T} at $\sigma = .50$ ($.476*10^5$gr s^{-3}) from all the FF_{q_T} values in Table A.1.

The quantity T is a virtual temperature and the derived quantities FF_{q_T}, FF_{s_ℓ}, FF_h, Q_1, Q_2, Q_3, s, and h have been calculated using this virtual temperature.

Table A.1 Suppressed Convection. Data and Derived Quantities.
(13 July included)

Level	u m s^{-1}	v m s^{-1}	p mb	T °K	q gr/gr	z m
0			.85871E+03	.29589E+03	.86537E-02	.14290E+04
1	-.12083E+01	-.30243E+01	.85012E+03	.29539E+03	.79264E-02	.15163E+04
2	-.16198E+01	-.35433E+01	.84153E+03	.29431E+03	.74640E-02	.16039E+04
3	-.20440E+01	-.39758E+01	.83295E+03	.29340E+03	.77490E-02	.16922E+04
4	-.23682E+01	-.41697E+01	.82436E+03	.29250E+03	.75899E-02	.17810E+04
5	-.26143E+01	-.41157E+01	.81577E+03	.29171E+03	.74614E-02	.18706E+04
6	-.27494E+01	-.38842E+01	.80718E+03	.29098E+03	.73468E-02	.19609E+04
7	-.28595E+01	-.36675E+01	.79860E+03	.29025E+03	.72019E-02	.20518E+04
8	-.28549E+01	-.33539E+01	.79001E+03	.28953E+03	.70691E-02	.21436E+04
9	-.27727E+01	-.29840E+01	.78142E+03	.28879E+03	.69002E-02	.22361E+04
10	-.26475E+01	-.25876E+01	.77284E+03	.28804E+03	.68374E-02	.23294E+04
11	-.25204E+01	-.22379E+01	.76425E+03	.28731E+03	.67782E-02	.24235E+04
12	-.24147E+01	-.18245E+01	.75566E+03	.28663E+03	.67019E-02	.25184E+04
13	-.22398E+01	-.13121E+01	.74708E+03	.28595E+03	.65868E-02	.26142E+04
14	-.19928E+01	-.70951E+00	.73849E+03	.28521E+03	.64059E-02	.27108E+04
15	-.16338E+01	-.51230E-03	.72990E+03	.28452E+03	.63595E-02	.28084E+04
16	-.12107E+01	.64425E+00	.72131E+03	.28395E+03	.63406E-02	.29068E+04
17	-.70178E+00	.11723E+01	.71273E+03	.28331E+03	.62390E-02	.30062E+04
18	-.41277E-01	.16821E+01	.70414E+03	.28275E+03	.61433E-02	.31067E+04
19	.77958E+00	.21635E+01	.69555E+03	.28230E+03	.60805E-02	.32081E+04
20	.16191E+01	.25377E+01	.68697E+03	.28186E+03	.60446E-02	.33107E+04
21	.22609E+01	.27660E+01	.67838E+03	.28131E+03	.59145E-02	.34144E+04
22	.27484E+01	.28453E+01	.66979E+03	.28072E+03	.57546E-02	.35192E+04
23	.32412E+01	.29832E+01	.66120E+03	.28006E+03	.55126E-02	.36251E+04
24	.36360E+01	.30758E+01	.65262E+03	.27936E+03	.52862E-02	.37321E+04
25	.40532E+01	.30449E+01	.64403E+03	.27854E+03	.50366E-02	.38402E+04
26	.43641E+01	.28469E+01	.63544E+03	.27775E+03	.48415E-02	.39495E+04
27	.47355E+01	.26567E+01	.62686E+03	.27693E+03	.46095E-02	.40599E+04
28	.51142E+01	.25900E+01	.61827E+03	.27612E+03	.43627E-02	.41715E+04
29	.55809E+01	.24958E+01	.60968E+03	.27531E+03	.42160E-02	.42844E+04
30	.62293E+01	.22224E+01	.60109E+03	.27442E+03	.40570E-02	.43985E+04
31	.69577E+01	.18943E+01	.59251E+03	.27350E+03	.38447E-02	.45139E+04
32	.76386E+01	.15325E+01	.58392E+03	.27263E+03	.36842E-02	.46305E+04
33	.80520E+01	.98293E+00	.57533E+03	.27177E+03	.35084E-02	.47485E+04
34	.83441E+01	.31440E+00	.56675E+03	.27096E+03	.33798E-02	.48680E+04
35	.86777E+01	-.94929E-01	.55816E+03	.27007E+03	.32048E-02	.49888E+04
36	.92432E+01	-.20339E+00	.54957E+03	.26920E+03	.29882E-02	.51112E+04
37	.94717E+01	-.24654E+00	.54098E+03	.26840E+03	.27736E-02	.52351E+04
38	.95077E+01	-.21424E+00	.53240E+03	.26752E+03	.25418E-02	.53606E+04
39	.94679E+01	.18646E-01	.52381E+03	.26672E+03	.23220E-02	.54877E+04
40	.94214E+01	.47812E+00	.51522E+03	.26602E+03	.20896E-02	.56165E+04
41	.93632E+01	.94224E+00	.50664E+03	.26519E+03	.18742E-02	.57472E+04
42	.93580E+01	.13984E+01	.49805E+03	.26439E+03	.16581E-02	.58796E+04
43	.93856E+01	.17837E+01	.48946E+03	.26363E+03	.14825E-02	.60140E+04
44	.92472E+01	.18813E+01	.48087E+03	.26281E+03	.13238E-02	.61504E+04
45	.92715E+01	.19222E+01	.47229E+03	.26198E+03	.12347E-02	.62887E+04
46	.93458E+01	.18241E+01	.46370E+03	.26101E+03	.11447E-02	.64291E+04
47	.89671E+01	.13972E+01	.45511E+03	.26011E+03	.10970E-02	.65716E+04
48	.94224E+01	.15333E+01	.44653E+03	.25913E+03	.10395E-02	.67164E+04
49	.10259E+02	.19333E+01	.43794E+03	.25813E+03	.97276E-03	.68633E+04
50	.10186E+02	.19282E+01	.42935E+03	.25713E+03	.88950E-03	.70126E+04

$\sigma = 1.0 - 0.01 * \text{Level}.$

Table A.1 continued.

Level	u m s^{-1}	v m s^{-1}	p mb	T °K	q gr/gr	z m
51	.10344E+02	.21739E+01	.42077E+03	.25605E+03	.83976E-03	.71643E+04
52	.10492E+02	.25708E+01	.41218E+03	.25494E+03	.78064E-03	.73185E+04
53	.10634E+02	.28691E+01	.40359E+03	.25386E+03	.72136E-03	.74752E+04
54	.11499E+02	.31605E+01	.39500E+03	.25277E+03	.64932E-03	.76346E+04
55	.11704E+02	.37326E+01	.38642E+03	.25162E+03	.58575E-03	.77968E+04
56	.11655E+02	.40083E+01	.37783E+03	.25042E+03	.53355E-03	.79619E+04
57	.11866E+02	.45106E+01	.36924E+03	.24920E+03	.47850E-03	.81299E+04
58	.11967E+02	.50078E+01	.36066E+03	.24788E+03	.42684E-03	.83011E+04
59	.12232E+02	.55528E+01	.35207E+03	.24649E+03	.37877E-03	.84754E+04
60	.12341E+02	.58043E+01	.34348E+03	.24510E+03	.34110E-03	.86530E+04
61	.12399E+02	.59635E+01	.33489E+03	.24371E+03	.30353E-03	.88341E+04
62	.12620E+02	.58807E+01	.32631E+03	.24220E+03	.27008E-03	.90187E+04
63	.13244E+02	.59336E+01	.31772E+03	.24066E+03	.24053E-03	.92071E+04
64	.13884E+02	.60665E+01	.30913E+03	.23914E+03	.21106E-03	.93995E+04
65	.14431E+02	.60477E+01	.30055E+03	.23758E+03	.18282E-03	.95960E+04
66	.14734E+02	.57262E+01	.29196E+03	.23602E+03	.16144E-03	.97968E+04
67	.14923E+02	.54481E+01	.28337E+03	.23431E+03	.14244E-03	.10002E+05
68	.15774E+02	.52493E+01	.27478E+03	.23263E+03	.12676E-03	.10212E+05
69	.16631E+02	.51025E+01	.26620E+03	.23097E+03	.11140E-03	.10428E+05
70	.17350E+02	.48512E+01	.25761E+03	.22934E+03	.96707E-04	.10649E+05
71	.17550E+02	.45922E+01	.24902E+03	.22778E+03	.83664E-04	.10875E+05
72	.17983E+02	.43389E+01	.24044E+03	.22634E+03	.73466E-04	.11108E+05
73	.18359E+02	.49464E+01	.23185E+03	.22498E+03	.65066E-04	.11349E+05
74	.18758E+02	.54854E+01	.22326E+03	.22360E+03	.58086E-04	.11596E+05
75	.18722E+02	.54677E+01	.21467E+03	.22223E+03	.51769E-04	.11852E+05
76	.18350E+02	.46083E+01	.20609E+03	.22066E+03	.45360E-04	.12117E+05
77	.17691E+02	.36711E+01	.19750E+03	.21901E+03	.39552E-04	.12390E+05
78	.16957E+02	.27801E+01	.18891E+03	.21756E+03	.35772E-04	.12674E+05
79	.16170E+02	.26833E+01	.18033E+03	.21639E+03	.33338E-04	.12970E+05
80	.15517E+02	.33892E+01	.17174E+03	.21526E+03	.31116E-04	.13278E+05
81	.13959E+02	.46987E+01	.16315E+03	.21426E+03	.29323E-04	.13601E+05
82	.13599E+02	.59132E+01	.15456E+03	.21344E+03	.27539E-04	.13934E+05
83	.15155E+02	.61452E+01	.14598E+03	.21265E+03	.26399E-04	.14295E+05
84	.15142E+02	.63757E+01	.13738E+03	.21136E+03	.27987E-04	.14685E+05
85	.14423E+02	.61687E+01	.12879E+03	.21062E+03	.26983E-04	.15084E+05
86	.11655E+02	.47009E+01	.12020E+03	.21068E+03	.27824E-04	.15505E+05
87	.11254E+02	.44229E+01	.11162E+03	.20940E+03	.25827E-04	.15961E+05
88	.66630E+00	.67295E+01	.10288E+03	.21401E+03	.54435E-04	.16463E+05

σ = 1.0 - 0.01 * Level.

Table A.1 continued

Level	Lq $m^2 s^{-2}$	s $m^2 s^{-2}$	h $m^2 s^{-2}$	$\Pi\dot{\sigma}$ $mb\ s^{-1}$	$\sigma\dot{\Pi}$ $mb\ s^{-1}$
0				0.	.11464E-03
1	.19816E+05	.30906E+06	.32888E+06	-.20072E-03	.90986E-04
2	.19660E+05	.30885E+06	.32851E+06	-.28180E-03	.29646E-04
3	.19373E+05	.30881E+06	.32818E+06	-.28960E-03	-.53072E-04
4	.18975E+05	.30876E+06	.32776E+06	-.25990E-03	-.14041E-03
5	.18654E+05	.30887E+06	.32752E+06	-.21689E-03	-.24283E-03
6	.18367E+05	.30904E+06	.32740E+06	-.16375E-03	-.33381E-03
7	.18005E+05	.30919E+06	.32720E+06	-.10048E-03	-.41073E-03
8	.17673E+05	.30936E+06	.32706E+06	-.46825E-04	-.46223E-03
9	.17250E+05	.30955E+06	.32680E+06	-.18375E-04	-.49416E-03
10	.17094E+05	.30971E+06	.32681E+06	-.16520E-04	-.51258E-03
11	.16946E+05	.30991E+06	.32686E+06	-.37006E-04	-.52072E-03
12	.16755E+05	.31016E+06	.32691E+06	-.78595E-04	-.54728E-03
13	.16467E+05	.31043E+06	.32690E+06	-.13359E-03	-.56664E-03
14	.16015E+05	.31064E+06	.32665E+06	-.18938E-03	-.57698E-03
15	.15899E+05	.31090E+06	.32680E+06	-.24634E-03	-.56776E-03
16	.15852E+05	.31130E+06	.32715E+06	-.31665E-03	-.52544E-03
17	.15598E+05	.31164E+06	.32724E+06	-.41441E-03	-.43232E-03
18	.15358E+05	.31207E+06	.32742E+06	-.55321E-03	-.28735E-03
19	.15201E+05	.31261E+06	.32781E+06	-.71684E-03	-.89143E-04
20	.15112E+05	.31317E+06	.32829E+06	-.87677E-03	.12606E-03
21	.14786E+05	.31365E+06	.32843E+06	-.10322E-02	.29416E-03
22	.14387E+05	.31409E+06	.32847E+06	-.11785E-02	.43259E-03
23	.13782E+05	.31446E+06	.32824E+06	-.13154E-02	.55882E-03
24	.13216E+05	.31481E+06	.32803E+06	-.14532E-02	.65733E-03
25	.12591E+05	.31506E+06	.32765E+06	-.15895E-02	.77870E-03
26	.12104E+05	.31534E+06	.32745E+06	-.17130E-02	.89100E-03
27	.11524E+05	.31561E+06	.32713E+06	-.18336E-02	.10189E-02
28	.10907E+05	.31590E+06	.32680E+06	-.19787E-02	.11261E-02
29	.10540E+05	.31620E+06	.32674E+06	-.21445E-02	.12602E-02
30	.10142E+05	.31642E+06	.32657E+06	-.22806E-02	.14695E-02
31	.96118E+04	.31664E+06	.32625E+06	-.23483E-02	.17019E-02
32	.92104E+04	.31692E+06	.32613E+06	-.23777E-02	.19168E-02
33	.87710E+04	.31722E+06	.32599E+06	-.23856E-02	.20792E-02
34	.84495E+04	.31758E+06	.32603E+06	-.23400E-02	.22224E-02
35	.80220E+04	.31788E+06	.32590E+06	-.22329E-02	.23353E-02
36	.74706E+04	.31821E+06	.32568E+06	-.20677E-02	.24612E-02
37	.69341E+04	.31863E+06	.32557E+06	-.18625E-02	.24863E-02
38	.63546E+04	.31899E+06	.32534E+06	-.16618E-02	.24500E-02
39	.58051E+04	.31943E+06	.32524E+06	-.14610E-02	.23692E-02
40	.52240E+04	.32000E+06	.32522E+06	-.12300E-02	.22604E-02
41	.46856E+04	.32045E+06	.32514E+06	-.10060E-02	.21512E-02
42	.41454E+04	.32095E+06	.32510E+06	-.86172E-03	.20586E-02
43	.37062E+04	.32151E+06	.32522E+06	-.81199E-03	.19849E-02
44	.33095E+04	.32203E+06	.32534E+06	-.80277E-03	.19087E-02
45	.30868E+04	.32256E+06	.32564E+06	-.79988E-03	.18765E-02
46	.28617E+04	.32298E+06	.32584E+06	-.79493E-03	.18708E-02
47	.27426E+04	.32348E+06	.32622E+06	-.82780E-03	.17999E-02
48	.25987E+04	.32392E+06	.32651E+06	-.87043E-03	.18492E-02
49	.24319E+04	.32436E+06	.32678E+06	-.80096E-03	.19470E-02
50	.22238E+04	.32483E+06	.32705E+06	-.72150E-03	.18937E-02

$\sigma = 1.0 - 0.01 * \text{Level}.$

Table A.1 continued

Level	Lq $m^2 s^{-2}$	s $m^2 s^{-2}$	h $m^2 s^{-2}$	$\pi\dot{\sigma}$ $mb\ s^{-1}$	$\sigma\dot{\pi}$ $mb\ s^{-1}$
51	.20994E+04	.32524E+06	.32734E+06	-.72850E-03	.18632E-02
52	.19516E+04	.32564E+06	.32759E+06	-.74004E-03	.18141E-02
53	.18034E+04	.32609E+06	.32790E+06	-.78279E-03	.17770E-02
54	.16233E+04	.32658E+06	.32820E+06	-.83336E-03	.18714E-02
55	.14644E+04	.32702E+06	.32849E+06	-.81213E-03	.18153E-02
56	.13339E+04	.32744E+06	.32878E+06	-.78378E-03	.17434E-02
57	.11963E+04	.32788E+06	.32907E+06	-.75836E-03	.16969E-02
58	.10671E+04	.32824E+06	.32930E+06	-.72609E-03	.16311E-02
59	.94692E+03	.32856E+06	.32951E+06	-.69880E-03	.15894E-02
60	.85275E+03	.32892E+06	.32977E+06	-.61399E-03	.15467E-02
61	.75883E+03	.32931E+06	.33007E+06	-.45039E-03	.15033E-02
62	.67519E+03	.32961E+06	.33029E+06	-.30618E-03	.15071E-02
63	.60113E+03	.32993E+06	.33053E+06	-.22024E-03	.15376E-02
64	.52915E+03	.33030E+06	.33082E+06	-.13147E-03	.15991E-02
65	.45706E+03	.33067E+06	.33113E+06	-.29799E-04	.16344E-02
66	.40361E+03	.33108E+06	.33149E+06	.69765E-04	.16527E-02
67	.35616E+03	.33140E+06	.33175E+06	.15448E-03	.16477E-02
68	.31690E+03	.33178E+06	.33210E+06	.24139E-03	.17217E-02
69	.27851E+03	.33224E+06	.33252E+06	.30212E-03	.17862E-02
70	.24177E+03	.33278E+06	.33302E+06	.31809E-03	.18327E-02
71	.20916E+03	.33345E+06	.33365E+06	.31933E-03	.18104E-02
72	.18356E+03	.33432E+06	.33450E+06	.31654E-03	.17816E-02
73	.16267E+03	.33530E+06	.33546E+06	.28609E-03	.17514E-02
74	.14521E+03	.33635E+06	.33649E+06	.16945E-03	.16961E-02
75	.12942E+03	.33750E+06	.33763E+06	.15880E-04	.16259E-02
76	.11340E+03	.33852E+06	.33863E+06	-.52212E-04	.15662E-02
77	.98904E+02	.33956E+06	.33966E+06	-.28830E-04	.14851E-02
78	.89429E+02	.34090E+06	.34098E+06	-.10051E-04	.13946E-02
79	.83469E+02	.34263E+06	.34272E+06	.31150E-04	.12658E-02
80	.77791E+02	.34452E+06	.34460E+06	.12072E-03	.11224E-02
81	.73308E+02	.34669E+06	.34676E+06	.20468E-03	.89458E-03
82	.68847E+02	.34919E+06	.34926E+06	.21429E-03	.77655E-03
83	.65998E+02	.35189E+06	.35196E+06	.10957E-03	.83125E-03
84	.69967E+02	.35443E+06	.35450E+06	.51042E-04	.78356E-03
85	.67458E+02	.35760E+06	.35767E+06	-.44457E-05	.69590E-03
86	.69559E+02	.36178E+06	.36185E+06	.18906E-04	.54452E-03
87	.64567E+02	.36498E+06	.36505E+06	-.75310E-06	.48141E-03
88	.13609E+03	.37449E+06	.37463E+06	.13706E-04	-.14245E-03

$\sigma = 1.0 - 0.01 * \text{Level}.$

Table A.1 continued.

Level	FF_{q_T} gr s^{-3}	FF_{s_1} gr s^{-3}	FF_h gr s^{-3}	Q_1 m^2 s^{-3}	Q_2 m^2 s^{-3}	Q_3 m^2 s^{-3}
1	.542E+06	-.289E+06	.252E+06			
2	.541E+06	-.301E+06	.240E+06	.10493E-01	.13370E+00	.14420E+00
3	.533E+06	-.317E+06	.217E+06	.83902E-01	.17535E+00	.25924E+00
4	.523E+06	-.334E+06	.189E+06	.11952E+00	.20349E+00	.32300E+00
5	.507E+06	-.354E+06	.154E+06	.17949E+00	.22036E+00	.39985E+00
6	.487E+06	-.373E+06	.114E+06	.23529E+00	.21969E+00	.45099E+00
7	.463E+06	-.389E+06	.744E+05	.26864E+00	.18644E+00	.45508E+00
8	.438E+06	-.402E+06	.352E+05	.29190E+00	.15534E+00	.44723E+00
9	.413E+06	-.415E+06	-.165E+04	.27712E+00	.14413E+00	.42125E+00
10	.388E+06	-.425E+06	-.368E+05	.28578E+00	.11561E+00	.40139E+00
11	.373E+06	-.433E+06	-.603E+05	.17514E+00	.92656E-01	.26780E+00
12	.360E+06	-.440E+06	-.807E+05	.15544E+00	.78050E-01	.23349E+00
13	.344E+06	-.449E+06	-.104E+06	.17135E+00	.98833E-01	.27019E+00
14	.329E+06	-.455E+06	-.126E+06	.18137E+00	.71126E-01	.25250E+00
15	.317E+06	-.459E+06	-.142E+06	.13280E+00	.41670E-01	.17447E+00
16	.303E+06	-.463E+06	-.160E+06	.16064E+00	.50016E-01	.21065E+00
17	.294E+06	-.467E+06	-.173E+06	.10747E+00	.41566E-01	.14903E+00
18	.286E+06	-.470E+06	-.184E+06	.82278E-01	.36058E-01	.11834E+00
19	.287E+06	-.473E+06	-.186E+06	-.19337E-02	.35185E-01	.33251E-01
20	.292E+06	-.475E+06	-.183E+06	-.66115E-01	.26344E-01	-.39772E-01
21	.304E+06	-.475E+06	-.172E+06	-.12573E+00	-.85087E-03	-.12658E+00
22	.308E+06	-.474E+06	-.166E+06	-.49903E-01	-.17120E-01	-.67022E-01
23	.304E+06	-.472E+06	-.169E+06	.48630E-01	-.17193E-01	.32437E-01
24	.294E+06	-.472E+06	-.178E+06	.10834E+00	-.74295E-03	.10760E+00
25	.286E+06	-.472E+06	-.186E+06	.88568E-01	-.37043E-02	.84884E-01
26	.281E+06	-.469E+06	-.188E+06	.58083E-01	-.31437E-01	.26645E-01
27	.272E+06	-.470E+06	-.197E+06	.10249E+00	.45900E-02	.10708E+00
28	.268E+06	-.468E+06	-.200E+06	.46257E-01	-.14936E-01	.31321E-01
29	.263E+06	-.469E+06	-.206E+06	.62592E-01	.37285E-02	.66421E-01
30	.255E+06	-.468E+06	-.214E+06	.95884E-01	-.62230E-02	.89661E-01
31	.249E+06	-.466E+06	-.218E+06	.67639E-01	-.18925E-01	.48714E-01
32	.241E+06	-.465E+06	-.225E+06	.88149E-01	-.11513E-01	.76637E-01
33	.227E+06	-.465E+06	-.237E+06	.15381E+00	-.61972E-02	.14761E+00
34	.210E+06	-.463E+06	-.253E+06	.19902E+00	-.16739E-01	.18228E+00
35	.190E+06	-.464E+06	-.273E+06	.22360E+00	-.55097E-02	.22911E+00
36	.174E+06	-.462E+06	-.288E+06	.18947E+00	-.27034E-01	.16244E+00
37	.166E+06	-.457E+06	-.291E+06	.91553E-01	-.49761E-01	.41793E-01
38	.161E+06	-.454E+06	-.293E+06	.55305E-01	-.35904E-01	.19401E-01
39	.151E+06	-.451E+06	-.300E+06	.11522E+00	-.32110E-01	.83109E-01
40	.142E+06	-.445E+06	-.303E+06	.10633E+00	-.71662E-01	.34666E-01
41	.131E+06	-.440E+06	-.309E+06	.12270E+00	-.59622E-01	.63081E-01
42	.116E+06	-.436E+06	-.320E+06	.17081E+00	-.38688E-01	.13212E+00
43	.995E+05	-.431E+06	-.332E+06	.18765E+00	-.58971E-01	.12868E+00
44	.838E+05	-.426E+06	-.342E+06	.17945E+00	-.63196E-01	.11625E+00
45	.745E+05	-.420E+06	-.346E+06	.10628E+00	-.63016E-01	.43267E-01
46	.698E+05	-.414E+06	-.344E+06	.52689E-01	-.68213E-01	-.15524E-01
47	.651E+05	-.409E+06	-.344E+06	.54228E-01	-.52747E-01	.14810E-02
48	.614E+05	-.407E+06	-.344E+06	.41483E-01	-.27352E-01	.14131E-01
49	.575E+05	-.407E+06	-.349E+06	.45226E-01	-.10171E-02	.44209E-01
50	.530E+05	-.405E+06	-.352E+06	.50968E-01	-.19676E-01	.31292E-01

σ = 1.01 - 0.01 * Level.

Q are layer values (Q (level 2) refers to layer 1-2).

Table A.1 continued

Level	FF_{q_T} gr s^{-3}	FF_{s_1} gr s^{-3}	FF_h gr s^{-3}	Q_1 m^2 s^{-3}	Q_2 m^2 s^{-3}	Q_3 m^2 s^{-3}
51	.476E+05	-.398E+06	-.351E+06	.61971E-01	-.76716E-01	-.14745E-01
52	.423E+05	-.392E+06	-.350E+06	.60382E-01	-.71086E-01	-.10704E-01
53	.366E+05	-.385E+06	-.348E+06	.55099E-01	-.86694E-01	-.21595E-01
54	.315E+05	-.375E+06	-.343E+06	.57926E-01	-.11341E+00	-.55981E-01
55	.284E+05	-.366E+06	-.338E+06	.35271E-01	-.96019E-01	-.60748E-01
56	.262E+05	-.360E+06	-.333E+05	.24943E-01	-.74567E-01	-.49624E-01
57	.232E+05	-.357E+06	-.334E+06	.34269E-01	-.31112E-01	.31568E-02
58	.198E+05	-.352E+06	-.333E+06	.38733E-01	-.49370E-01	-.10638E-01
59	.160E+05	-.347E+06	-.331E+06	.43189E-01	-.62743E-01	-.19554E-01
60	.136E+05	-.341E+06	-.327E+06	.27663E-01	-.70033E-01	-.42369E-01
61	.116E+05	-.337E+06	-.325E+06	.22753E-01	-.42989E-01	-.20236E-01
62	.105E+05	-.333E+06	-.323E+06	.12840E-01	-.39523E-01	-.26683E-01
63	.884E+04	-.329E+06	-.320E+06	.18577E-01	-.47895E-01	-.29317E-01
64	.748E+04	-.322E+06	-.315E+06	.15582E-01	-.80893E-01	-.65312E-01
65	.634E+04	-.318E+06	-.312E+06	.12959E-01	-.47525E-01	-.34566E-01
66	.555E+04	-.316E+06	-.310E+06	.89777E-02	-.26154E-01	-.17176E-01
67	.474E+04	-.314E+06	-.309E+06	.91764E-02	-.17932E-01	-.87554E-02
68	.395E+04	-.314E+06	-.310E+06	.89980E-02	-.54745E-02	.35236E-02
69	.334E+04	-.310E+06	-.307E+06	.70085E-02	-.38736E-01	-.31726E-01
70	.273E+04	-.304E+06	-.301E+06	.69688E-02	-.72023E-01	-.65055E-01
71	.204E+04	-.297E+06	-.295E+06	.78838E-02	-.81616E-01	-.73732E-01
72	.136E+04	-.290E+06	-.289E+06	.77285E-02	-.73700E-01	-.65971E-01
73	.752E+03	-.285E+06	-.285E+06	.69087E-02	-.55931E-01	-.49022E-01
74	.211E+03	-.280E+06	-.280E+06	.61647E-02	-.60546E-01	-.54381E-01
75	-.119E+03	-.267E+06	-.267E+06	.37689E-02	-.15062E+00	-.14685E+00
76	-.301E+03	-.251E+06	-.251E+06	.20709E-02	-.18383E+00	-.18176E+00
77	-.354E+03	-.230E+06	-.231E+06	.60713E-03	-.22998E+00	-.22937E+00
78	-.415E+03	-.208E+06	-.208E+06	.68982E-03	-.25834E+00	-.25765E+00
79	-.486E+03	-.184E+06	-.185E+06	.81249E-03	-.27122E+00	-.27040E+00
80	-.414E+03	-.157E+06	-.157E+06	-.82355E-03	-.31009E+00	-.31092E+00
81	-.261E+03	-.128E+06	-.128E+06	-.17507E-02	-.33218E+00	-.33393E+00
82	-.105E+03	-.985E+05	-.986E+05	-.17762E-02	-.33375E+00	-.33552E+00
83	-.656E+02	-.736E+05	-.737E+05	-.45334E-03	-.28420E+00	-.28465E+00
84	-.168E+03	-.104E+06	-.104E+06	.15138E-03	-.28474E+00	-.28459E+00
85	-.819E+02	-.645E+05	-.646E+05	-.98271E-03	-.45313E+00	-.45411E+00
86	.524E+02	-.396E+05	-.326E+05	-.14461E-02	-.34862E+00	-.35006E+00
87	.105E+03	-.154E+05	-.153E+05	-.60001E-03	-.27712E+00	-.27772E+00
88	.343E+03	.114E+05	.11ME+05	.54232E-03	-.19710E+00	-.19656E+00
	.0	.0	.0	.39252E-02	.13058E+00	.13450E+00

σ = 1.01 - 0.01 * Level.

Q are layer values (Q (level 2) refers to layer 1-2).

Table A.2 Weak, Developing Convection. Data and Derived Quantities.

Level	u m s^{-1}	v m s^{-1}	p mb	T °K	q gr/gr	z m
0			.85643E+03	.30152E+03	.88977E-02	.14577E+04
1	-.61026E+00	.10595E+01	.84787E+03	.29975E+03	.75034E-02	.15462E+04
2	-.87292E+00	.95358E+00	.83930E+03	.29858E+03	.72517E-02	.16351E+04
3	-.79665E+00	.92698E+00	.83074E+03	.29767E+03	.71079E-02	.17246E+04
4	-.70834E+00	.97788E+00	.82218E+03	.29683E+03	.70126E-02	.18144E+04
5	-.62782E+00	.10854E+01	.81361E+03	.29596E+03	.68900E-02	.19056E+04
6	-.47664E+00	.12511E+01	.80505E+03	.29502E+03	.67532E-02	.19971E+04
7	-.23256E+00	.13890E+01	.79649E+03	.29407E+03	.66377E-02	.20893E+04
8	.14074E+00	.14204E+01	.78792E+03	.29324E+03	.64636E-02	.21823E+04
9	.47004E+00	.13446E+01	.77936E+03	.29228E+03	.62480E-02	.22759E+04
10	.67167E+00	.13460E+01	.77080E+03	.29144E+03	.60553E-02	.23703E+04
11	.76098E+00	.11991E+01	.76223E+03	.29060E+03	.60022E-02	.24655E+04
12	.95930E+00	.11354E+01	.75367E+03	.28975E+03	.59235E-02	.25614E+04
13	.11323E+01	.10076E+01	.74511E+03	.28888E+03	.58009E-02	.26582E+04
14	.12112E+01	.79033E+00	.73654E+03	.28801E+03	.56886E-02	.27558E+04
15	.13051E+01	.57354E+00	.72798E+03	.28711E+03	.56358E-02	.28542E+04
16	.15146E+01	.39095E+00	.71942E+03	.28622E+03	.55454E-02	.29535E+04
17	.18077E+01	.44391E+00	.71085E+03	.28536E+03	.54515E-02	.30537E+04
18	.20252E+01	.51761E+00	.70229E+03	.28449E+03	.54321E-02	.31548E+04
19	.21427E+01	.65240E+00	.69373E+03	.28355E+03	.54362E-02	.32568E+04
20	.23218E+01	.60806E+00	.68516E+03	.28256E+03	.53618E-02	.33597E+04
21	.26225E+01	.47810E+00	.67660E+03	.28177E+03	.53202E-02	.34636E+04
22	.31350E+01	.27175E+00	.66804E+03	.28098E+03	.52841E-02	.35685E+04
23	.35483E+01	.20521E+00	.65947E+03	.28011E+03	.51834E-02	.36744E+04
24	.39982E+01	.15463E+00	.65091E+03	.27923E+03	.51420E-02	.37814E+04
25	.44831E+01	-.19922E-01	.64234E+03	.27830E+03	.50635E-02	.38895E+04
26	.49871E+01	-.42157E+00	.63378E+03	.27732E+03	.49017E-02	.39988E+04
27	.54457E+01	-.89700E+00	.62522E+03	.27638E+03	.46888E-02	.41088E+04
28	.58024E+01	-.13298E+01	.61665E+03	.27556E+03	.44859E-02	.42203E+04
29	.63034E+01	-.16473E+01	.60809E+03	.27480E+03	.43232E-02	.43329E+04
30	.67292E+01	-.19242E+01	.59953E+03	.27383E+03	.41170E-02	.44468E+04
31	.72849E+01	-.20462E+01	.59096E+03	.27294E+03	.38290E-02	.45619E+04
32	.78128E+01	-.19993E+01	.58240E+03	.27212E+03	.35392E-02	.46783E+04
33	.82968E+01	-.16283E+01	.57384E+03	.27132E+03	.33504E-02	.47961E+04
34	.85890E+01	-.13170E+01	.56527E+03	.27048E+03	.30574E-02	.49154E+04
35	.88238E+01	-.10296E+01	.55671E+03	.26970E+03	.29169E-02	.50361E+04
36	.90710E+01	-.89469E+00	.54815E+03	.26891E+03	.28120E-02	.51583E+04
37	.91755E+01	-.74478E+00	.53958E+03	.26807E+03	.26479E-02	.52820E+04
38	.91574E+01	-.55627E+00	.53102E+03	.26725E+03	.24758E-02	.54074E+04
39	.92566E+01	-.44465E+00	.52245E+03	.26635E+03	.23050E-02	.55344E+04
40	.92929E+01	-.30150E+00	.51389E+03	.26542E+03	.21745E-02	.56630E+04
41	.93353E+01	-.14927E+00	.50533E+03	.26452E+03	.20320E-02	.57934E+04
42	.91221E+01	-.10636E-01	.49676E+03	.26364E+03	.18296E-02	.59255E+04
43	.90303E+01	.19543E+00	.48820E+03	.26284E+03	.17503E-02	.60595E+04
44	.92052E+01	.87897E-01	.47963E+03	.26211E+03	.15061E-02	.61955E+04
45	.94459E+01	-.23585E+00	.47107E+03	.26124E+03	.12942E-02	.63335E+04
46	.98572E+01	-.33172E+00	.46251E+03	.26031E+03	.12226E-02	.64736E+04
47	.10324E+02	-.29453E+00	.45394E+03	.25937E+03	.11312E-02	.66158E+04
48	.10782E+02	-.91140E-01	.44538E+03	.25840E+03	.10488E-02	.67601E+04
49	.11305E+02	.25925E+00	.43682E+03	.25733E+03	.95909E-03	.69067E+04
50	.11763E+02	.52858E+00	.42825E+03	.25643E+03	.89620E-03	.70557E+04

$\sigma = 1.0 - 0.01 * \text{Level}$.

Table A.2 continued

Level	u m s^{-1}	v m s^{-1}	p mb	T °K	q gr/gr	z m
51	.12048E+02	.71294E+00	.41969E+03	.25531E+03	.78915E-03	.72070E+04
52	.12267E+02	.91989E+00	.41112E+03	.25420E+03	.65786E-03	.73608E+04
53	.12640E+02	.11450E+01	.40256E+03	.25306E+03	.57005E-03	.75171E+04
54	.12956E+02	.14353E+01	.39399E+03	.25185E+03	.52624E-03	.76761E+04
55	.13148E+02	.18174E+01	.38543E+03	.25058E+03	.51763E-03	.78378E+04
56	.13323E+02	.20488E+01	.37687E+03	.24937E+03	.46656E-03	.80022E+04
57	.13234E+02	.23051E+01	.36830E+03	.24799E+03	.42434E-03	.81696E+04
58	.13671E+02	.23325E+01	.35974E+03	.24664E+03	.38877E-03	.83400E+04
59	.14633E+02	.23472E+01	.35117E+03	.24528E+03	.34263E-03	.85136E+04
60	.15111E+02	.28001E+01	.34261E+03	.24384E+03	.38619E-03	.86904E+04
61	.15422E+02	.34021E+01	.33405E+03	.24242E+03	.36535E-03	.88707E+04
62	.16092E+02	.43331E+01	.32548E+03	.24092E+03	.33109E-03	.90545E+04
63	.17132E+02	.51433E+01	.31692E+03	.23950E+03	.29090E-03	.92421E+04
64	.16994E+02	.53426E+01	.30835E+03	.23794E+03	.25782E-03	.94337E+04
65	.16501E+02	.54332E+01	.29979E+03	.23639E+03	.22569E-03	.96294E+04
66	[illegible]	[illegible]	[illegible]	[illegible]	[illegible]	[illegible]
67	.18745E+02	.60498E+01	.29266E+03	.23313E+03	.15178E-03	.10034E+05
68	.19978E+02	.60689E+01	.27409E+03	.23161E+03	.10774E-03	.10244E+05
69	.20807E+02	.57003E+01	.26553E+03	.23007E+03	.81503E-04	.10459E+05
70	.21779E+02	.52254E+01	.25696E+03	.22841E+03	.69015E-04	.10679E+05
71	.23287E+02	.51600E+01	.24840E+03	.22684E+03	.60158E-04	.10905E+05
72	.24507E+02	.47620E+01	.23984E+03	.22539E+03	.52318E-04	.11138E+05
73	.25553E+02	.45081E+01	.23127E+03	.22387E+03	.45192E-04	.11377E+05
74	.27117E+02	.50115E+01	.22271E+03	.22243E+03	.39162E-04	.11624E+05
75	.27114E+02	.43521E+01	.21414E+03	.22116E+03	.34807E-04	.11880E+05
76	.27223E+02	.30000E+01	.20558E+03	.21996E+03	.31849E-04	.12144E+05
77	.27117E+02	.25234E+01	.19701E+03	.21883E+03	.29569E-04	.12418E+05
78	.26745E+02	.21597E+01	.18845E+03	.21794E+03	.27999E-04	.12702E+05
79	.26094E+02	.19537E+01	.17988E+03	.21695E+03	.26633E-04	.12999E+05
80	.24583E+02	.16452E+01	.17132E+03	.21582E+03	.24982E-04	.13309E+05
81	.23720E+02	.21337E+01	.16275E+03	.21474E+03	.23430E-04	.13633E+05
82	.21860E+02	.21888E+01	.15419E+03	.21379E+03	.21797E-04	.13972E+05
83	.18859E+02	.40625E+01	.14562E+03	.21314E+03	.20353E-04	.14330E+05
84	.16717E+02	.50355E+01	.13706E+03	.21256E+03	.19669E-04	.14709E+05
85	.15936E+02	.18113E+01	.12849E+03	.21250E+03	.20336E-04	.15111E+05
86	.13615E+02	-.40859E+00	.11993E+03	.21254E+03	.20812E-04	.15541E+05
87	.97735E+01	-.39713E+01	.11128E+03	.21269E+03	.23150E-04	.15996E+05
88	.81536E+01	-.13991E+01	.10288E+03	.21228E+03	.15339E-04	.16554E+05

σ = 1.0 - 0.01 * Level.

Table A.2 continued

Level	Lq $m^2\ s^{-2}$	s $m^2\ s^{-2}$	h $m^2\ s^{-2}$	$\pi\dot{\sigma}$ $mb\ s^{-1}$	$\sigma\dot{\pi}$ $mb\ s^{-1}$
0				0.	-.44229E-03
1	.18759E+05	.31370E+06	.33246E+06	-.14757E-03	-.55734E-03
2	.18129E+05	.31341E+06	.33154E+06	-.29864E-03	-.63215E-03
3	.17770E+05	.31333E+06	.33115E+06	-.43603E-03	-.58901E-03
4	.17532E+05	.31343E+06	.33096E+06	-.54884E-03	-.55900E-03
5	.17225E+05	.31345E+06	.33068E+06	-.62582E-03	-.54533E-03
6	.16883E+05	.31341E+06	.33029E+06	-.64616E-03	-.51604E-03
7	.16594E+05	.31337E+06	.32996E+06	-.62702E-03	-.44613E-03
8	.16159E+05	.31345E+06	.32961E+06	-.63747E-03	-.30785E-03
9	.15620E+05	.31342E+06	.32904E+06	-.72631E-03	-.17552E-03
10	.15138E+05	.31350E+06	.32864E+06	-.89332E-03	-.92444E-04
11	.15005E+05	.31360E+06	.32861E+06	-.11148E-02	-.29747E-04
12	.14809E+05	.31369E+06	.32850E+06	-.13796E-02	.54269E-04
13	.14502E+05	.31378E+06	.32824E+06	-.16883E-02	.13924E-03
14	.14222E+05	.31386E+06	.32804E+06	-.20341E-02	.20575E-03
15	.14090E+05	.31393E+06	.32802E+06	-.24008E-02	.27643E-03
16	.13863E+05	.31402E+06	.32788E+06	-.27789E-02	.37893E-03
17	.13629E+05	.31415E+06	.32774E+06	-.31677E-02	.46409E-03
18	.13580E+05	.31427E+06	.32785E+06	-.35405E-02	.51814E-03
19	.13590E+05	.31433E+06	.32792E+06	-.38587E-02	.52693E-03
20	.13404E+05	.31436E+06	.32776E+06	-.41346E-02	.58758E-03
21	.13301E+05	.31458E+06	.32788E+06	-.44186E-02	.70135E-03
22	.13210E+05	.31482E+06	.32803E+06	-.47326E-02	.89315E-03
23	.12956E+05	.31500E+06	.32796E+06	-.50254E-02	.10245E-02
24	.12855E+05	.31517E+06	.32803E+06	-.52503E-02	.11603E-02
25	.12659E+05	.31531E+06	.32758E+06	-.54074E-02	.13232E-02
26	.12254E+05	.31539E+06	.32765E+06	-.55164E-02	.15241E-02
27	.11722E+05	.31554E+06	.32726E+06	-.55952E-02	.17175E-02
28	.11215E+05	.31582E+06	.32703E+06	-.56445E-02	.18682E-02
29	.10808E+05	.31617E+06	.32698E+06	-.56648E-02	.20374E-02
30	.10293E+05	.31621E+06	.32660E+06	-.56713E-02	.21734E-02
31	.95726E+04	.31655E+06	.32613E+06	-.56713E-02	.23172E-02
32	.88479E+04	.31688E+06	.32573E+06	-.56587E-02	.24226E-02
33	.83761E+04	.31723E+05	.32561E+06	-.56485E-02	.24643E-02
34	.76434E+04	.31757E+05	.32521E+06	-.56248E-02	.24614E-02
35	.72923E+04	.31798E+06	.32527E+06	-.55518E-02	.24456E-02
36	.70300E+04	.31838E+06	.32541E+06	-.54380E-02	.24536E-02
37	.66197E+04	.31876E+06	.32538E+06	-.53203E-02	.24209E-02
38	.61895E+04	.31917E+06	.32536E+06	-.51698E-02	.23528E-02
39	.57626E+04	.31952E+06	.32528E+06	-.50573E-02	.23245E-02
40	.54362E+04	.31986E+06	.32529E+06	-.49667E-02	.22754E-02
41	.50800E+04	.32023E+06	.32531E+06	-.49324E-02	.22264E-02
42	.45741E+04	.32065E+06	.32523E+06	-.48969E-02	.21191E-02
43	.43759E+04	.32122E+06	.32560E+06	-.47969E-02	.20343E-02
44	.37651E+04	.32178E+06	.32555E+06	-.46576E-02	.20517E-02
45	.32354E+04	.32226E+06	.32550E+06	-.45391E-02	.21088E-02
46	.30565E+04	.32271E+06	.32577E+06	-.44940E-02	.21724E-02
47	.28279E+04	.32317E+06	.32600E+06	-.45223E-02	.22284E-02
48	.26221E+04	.32361E+06	.32623E+06	-.45545E-02	.22599E-02
49	.23977E+04	.32399E+06	.32634E+06	-.45512E-02	.22851E-02
50	.22405E+04	.32455E+06	.32674E+06	-.45457E-02	.23027E-02

$\sigma = 1.0 - 0.01 * \text{Level}.$

Table A.2 continued

Level	Lq $m^2\ s^{-2}$	s $m^2\ s^{-2}$	h $m^2\ s^{-2}$	$\pi\dot{\sigma}$ $mb\ s^{-1}$	$\sigma\dot{\pi}$ $mb\ s^{-1}$
51	.19729E+04	.32492E+06	.32689E+06	-.45376E-02	.22926E-02
52	.16447E+04	.32531E+06	.32696E+06	-.45188E-02	.22674E-02
53	.14251E+04	.32571E+06	.32714E+06	-.45349E-02	.22694E-02
54	.13156E+04	.32607E+06	.32738E+06	-.46161E-02	.22517E-02
55	.12941E+04	.32638E+06	.32768E+06	-.47556E-02	.22002E-02
56	.11664E+04	.32680E+06	.32796E+06	-.49311E-02	.21608E-02
57	.10609E+04	.32706E+06	.32812E+06	-.50895E-02	.20715E-02
58	.97192E+03	.32738E+06	.32835E+06	-.52532E-02	.20968E-02
59	.95658E+03	.32773E+06	.32869E+06	-.55093E-02	.22065E-02
60	.96548E+03	.32803E+06	.32900E+06	-.57850E-02	.21895E-02
61	.91338E+03	.32839E+06	.32930E+06	-.59285E-02	.21319E-02
62	.82773E+03	.32869E+06	.32952E+06	-.59382E-02	.21021E-02
63	.72726E+03	.32911E+06	.32986E+06	-.59170E-02	.21362E-02
64	[illegible]	[illegible]	[illegible]	[illegible]	[illegible]
65	.56423E+03	.32981E+06	.33037E+06	-.57913E-02	.19104E-02
66	.47939E+03	.33016E+06	.33064E+06	-.56865E-02	.19727E-02
67	.37941E+03	.33053E+06	.33091E+06	-.57115E-02	.20549E-02
68	.26934E+03	.33108E+06	.33134E+06	-.58039E-02	.21509E-02
69	.20376E+03	.33165E+06	.33185E+06	-.58734E-02	.22130E-02
70	.17254E+03	.33215E+06	.33233E+06	-.59378E-02	.22911E-02
71	.15039E+03	.33280E+06	.33295E+06	-.60106E-02	.23947E-02
72	.13079E+03	.33363E+06	.33377E+06	-.60308E-02	.24745E-02
73	.11298E+03	.33447E+06	.33459E+06	-.59571E-02	.25165E-02
74	.97906E+02	.33546E+06	.33556E+06	-.58061E-02	.25575E-02
75	.87016E+02	.33669E+06	.33678E+06	-.55787E-02	.24945E-02
76	.79722E+02	.33809E+06	.33817E+06	-.52947E-02	.24792E-02
77	.73923E+02	.33965E+06	.33972E+06	-.49311E-02	.23902E-02
78	.69998E+02	.34158E+06	.34165E+06	-.44352E-02	.22707E-02
79	.66583E+02	.34347E+06	.34354E+06	-.38838E-02	.21202E-02
80	.62456E+02	.34538E+06	.34545E+06	-.32491E-02	.19096E-02
81	.58576E+02	.34748E+06	.34754E+06	-.24947E-02	.17272E-02
82	.54494E+02	.34986E+06	.34992E+06	-.17895E-02	.14988E-02
83	.50881E+02	.35272E+06	.35278E+06	-.11763E-02	.11412E-02
84	.49173E+02	.35566E+06	.35591E+06	-.68429E-03	.90061E-03
85	.50840E+02	.35974E+06	.35979E+06	-.35124E-03	.90267E-03
86	.52029E+02	.36399E+06	.36404E+06	-.78729E-04	.77921E-03
87	.57876E+02	.36861E+06	.36867E+06	.14609E-03	.61995E-03
88	.38346E+02	.37366E+06	.37369E+06	.25534E-04	.42125E-03

$\sigma = 1.0 - 0.01 * \text{Level}.$

Table A.2 continued.

Level	FF_{q_T} gr s^{-3}	FF_{s_1} gr s^{-3}	FF_h gr s^{-3}	Q_1 m^2 s^{-3}	Q_2 m^2 s^{-3}	Q_3 m^2 s^{-3}
1	-.262E+06	-.336E+06	-.598E+06			
2	-.261E+06	-.346E+06	-.607E+06	-.86893E-02	.10914E+00	-.10045E+00
3	-.251E+06	-.355E+06	-.606E+06	-.11720E+00	.10967E+00	-.75231E-02
4	-.244E+06	-.366E+06	-.610E+06	-.80540E-01	.12367E+00	.43130E-01
5	-.241E+06	-.377E+06	-.619E+06	-.29296E-01	.12427E+00	.94979E-01
6	-.240E+06	-.387E+06	-.627E+06	-.14696E-01	.11429E+00	.99594E-01
7	-.241E+06	-.396E+06	-.636E+06	.59043E-02	.98087E-01	.10399E+00
8	-.244E+06	-.403E+06	-.647E+06	.39692E-01	.83630E-01	.12332E+00
9	-.250E+06	-.410E+06	-.660E+06	.62338E-01	.78538E-01	.14088E+00
10	-.261E+06	-.416E+06	-.677E+06	.12866E+00	.66425E-01	.19509E+00
11	-.275E+06	-.423E+06	-.697E+06	.15490E+00	.81314E-01	.23622E+00
12	-.293E+06	-.426E+06	-.720E+06	.21311E+00	.42900E-01	.25601E+00
13	-.314E+06	-.430E+06	-.743E+06	.23671E+00	.34648E-01	.27156E+00
14	-.332E+06	-.433E+06	-.765E+06	.21035E+00	.39662E-01	.25001E+00
15	-.350E+06	-.435E+06	-.785E+06	.20207E+00	.22284E-01	.22436E+00
16	-.364E+06	-.435E+06	-.800E+06	.16211E+00	.49299E-02	.16704E+00
17	-.378E+06	-.440E+06	-.818E+06	.15490E+00	.47968E-01	.20687E+00
18	-.383E+06	-.443E+06	-.826E+06	.59271E-01	.40262E-01	.99533E-01
19	-.390E+06	-.444E+06	-.834E+06			
20	-.396E+06	-.440E+06	-.836E+06	.61266E-01	-.43272E-01	.17994E-01
21	-.401E+06	-.438E+06	-.839E+06	.59722E-01	-.23695E-01	.36027E-01
22	-.416E+06	-.443E+06	-.859E+06	.16754E+00	.59322E-01	.22686E+00
23	-.434E+06	-.449E+06	-.883E+06	.21078E+00	.65839E-01	.27662E+00
24	-.454E+06	-.453E+06	-.907E+06	.23224E+00	.41992E-01	.27423E+00
25	-.482E+06	-.453E+06	-.935E+06	.31020E+00	.61240E-02	.31632E+00
26	-.505E+06	-.450E+06	-.956E+06	.26981E+00	-.32857E-01	.23695E+00
27	-.522E+06	-.449E+06	-.971E+06	.19580E+00	-.20575E-01	.17522E+00
28	-.523E+06	-.445E+06	-.968E+06	.40740E-02	-.36828E-01	-.32754E-01
29	-.517E+06	-.454E+06	-.971E+06	-.71654E-01	.98921E-01	.27267E-01
30	-.513E+06	-.469E+06	-.982E+06	-.46785E-01	.16984E+00	.12305E+00
31	-.486E+06	-.468E+06	-.953E+06	-.30746E+00	-.14587E-01	-.32204E+00
32	-.448E+06	-.479E+06	-.927E+06	-.43513E+00	.13045E+00	-.30468E+00
33	-.422E+06	-.500E+06	-.922E+06	-.29086E+00	.23617E+00	-.54695E-01
34	-.413E+06	-.518E+06	-.932E+06	-.10435E+00	.21491E+00	.11056E+00
35	-.366E+06	-.532E+06	-.899E+06	-.53785E+00	.15988E+00	-.37797E+00
36	-.365E+06	-.551E+06	-.916E+06	-.12388E-01	.20886E+00	.19647E+00
37	-.373E+06	-.565E+06	-.938E+06	.91228E-01	.16269E+00	.25392E+00
38	-.361E+06	-.568E+06	-.929E+06	-.14147E+00	.31211E-01	-.11025E+00
39	-.350E+06	-.579E+06	-.929E+06	-.11897E+00	.12745E+00	.84796E-02
40	-.334E+06	-.581E+06	-.914E+06	-.19102E+00	.19299E-01	-.17172E+00
41	-.333E+06	-.583E+06	-.916E+06	-.81951E-02	.32048E-01	.23853E-01
42	-.332E+06	-.588E+06	-.920E+06	-.15945E-01	.53454E-01	.37509E-01
43	-.302E+06	-.593E+06	-.895E+06	-.33873E+00	.54811E-01	-.28392E+00
44	-.304E+06	-.617E+06	-.921E+06	.17667E-01	.27672E+00	.29438E+00
45	-.262E+06	-.637E+06	-.899E+06	-.47953E+00	.22780E+00	-.25173E+00
46	-.237E+06	-.650E+06	-.888E+06	-.28461E+00	.14483E+00	-.13978E+00
47	-.234E+06	-.657E+06	-.892E+06	-.28919E-01	.88661E-01	.59742E-01
48	-.223E+06	-.659E+06	-.882E+06	-.12576E+00	.19021E-01	-.10674E+00
49	-.209E+06	-.663E+06	-.872E+06	-.16023E+00	.45124E-01	-.11511E+00
50	-.184E+06	-.660E+06	-.844E+06	-.28708E+00	-.33916E-01	-.32100E+00

σ = 1.01 - 0.01 * Level.

Q are layer values (Q (level 2) refers to layer 1-2).

Table A.2 continued.

Level	FF_{q_T} gr s^{-3}	FF_{s_1} gr s^{-3}	FF_h gr s^{-3}	Q_1 m^2 s^{-3}	Q_2 m^2 s^{-3}	Q_3 m^2 s^{-3}
51	-.165E+06	-.675E+06	-.841E+06	-.21532E+00	.17642E+00	-.38892E-01
52	-.131E+06	-.673E+06	-.804E+06	-.38761E+00	-.32963E-01	-.42058E+00
53	-.929E+05	-.677E+06	-.770E+06	-.44060E+00	.55930E-01	-.33467E+00
54	-.674E+05	-.681E+06	-.748E+06	-.29200E+00	.36229E-01	-.25577E+00
55	-.589E+05	-.683E+06	-.742E+06	-.96280E-01	.31120E-01	-.65160E-01
56	-.629E+05	-.677E+06	-.740E+06	.45906E-01	-.67605E-01	-.21699E-01
57	-.527E+05	-.681E+06	-.734E+06	-.11713E+00	.43733E-01	-.73401E-01
58	-.446E+05	-.674E+06	-.719E+06	-.92232E-01	-.83326E-01	-.17556E+00
59	-.392E+05	-.684E+06	-.723E+06	-.61947E-01	.10883E+00	.46881E-01
60	-.456E+05	-.690E+06	-.736E+06	.73525E-01	.77065E-01	.15059E+00
61	-.593E+05	-.691E+06	-.750E+06	.15676E+00	.92255E-02	.16598E+00
62	-.623E+05	-.694E+06	-.756E+06	.33764E-01	.34569E-01	.68333E-01
63	-.559E+05	-.697E+06	-.753E+06	-.72919E-01	.30835E-01	-.42044E-01
64	-.434E+05	-.704E+06	-.748E+06	-.14267E+00	.85735E-01	-.56931E-01
65	-.328E+05	-.693E+06	-.726E+06	-.12104E+00	-.12711E+00	-.24815E+00
66	-.225E+05	-.684E+06	-.707E+06	-.11801E+00	-.10229E+00	-.22031E+00
67	-.122E+05	-.670E+06	-.682E+06	-.11754E+00	-.16352E+00	-.28107E+00
68	-.268E+03	-.658E+06	-.657E+06	-.14303E+00	-.14027E+00	-.28330E+00
69	.132E+05	-.666E+06	-.653E+06	-.14750E+00	.37700E-01	-.25700E-01
70	.178E+05	-.669E+06	-.651E+06	-.52508E-01	.29152E-01	-.23436E-01
71	.170E+05	-.652E+06	-.635E+06	.83622E-02	-.19002E+00	-.18166E+00
72	.151E+05	-.641E+06	-.626E+06	.21723E-01	-.12596E+00	-.10424E+00
73	.133E+05	-.629E+06	-.616E+06	.20692E-01	-.13439E+00	-.11770E+00
74	.116E+05	-.607E+06	-.596E+06	.19966E-01	-.24713E+00	-.22717E+00
75	.996E+04	-.572E+06	-.562E+06	.18524E-01	-.40061E+00	-.38209E+00
76	.838E+04	-.536E+06	-.528E+06	.18080E-01	-.41232E+00	-.39424E+00
77	.708E+04	-.486E+06	-.479E+06	.14906E-01	-.58443E+00	-.55352E+00
78	.588E+04	-.444E+06	-.439E+06	.13684E-01	-.48003E+00	-.46634E+00
79	.484E+04	-.405E+06	-.404E+06	.11934E-01	-.41214E+00	-.40020E+00
80	.396E+04	-.364E+06	-.360E+06	.99970E-02	-.50826E+00	-.49826E+00
81	.334E+04	-.306E+06	-.303E+06	.71588E-02	-.65916E+00	-.65201E+00
82	.276E+04	-.249E+06	-.247E+06	.65800E-02	-.65121E+00	-.64463E+00
83	.222E+04	-.198E+06	-.196E+06	.61314E-02	-.58623E+00	-.58009E+00
84	.172E+04	-.173E+06	-.172E+06	.57201E-02	-.28397E+00	-.27825E+00
85	.132E+04	-.142E+06	-.141E+06	.45652E-02	-.35417E+00	-.34960E+00
86	.966E+03	-.995E+05	-.985E+05	.40815E-02	-.49062E+00	-.48654E+00
87	.816E+03	-.724E+05	-.716E+05	.43853E-02	-.54630E+00	-.54192E+00
88	.928E+03	-.607E+05	-.598E+05	.50810E-02	-.55122E+00	-.54613E+00
	0.0	0.0	0.0	.10612E-01	-.69416E+00	-.68355E+00

σ = 1.01 - 0.01 * Level.

Q are layer values (Q (level 2) refers to layer 1-2).

Table A.3 continued.

Level	FF_{q_T} gr s^{-3}	FF_{s_1} gr s^{-3}	FF_h gr s^{-3}	Q_1 m^2 s^{-3}	Q_2 m^2 s^{-3}	Q_3 m^2 s^{-3}
1	-.381E+06	.674E+06	.293E+06			
2	-.377E+06	.671E+06	.294E+06	-.46908E-01	.36996E-01	-.99118E-02
3	-.363E+06	.665E+06	.302E+06	-.16223E+00	.71106E-01	-.91171E-01
4	-.347E+06	.656E+06	.309E+06	-.17514E+00	.93576E-01	-.81565E-01
5	-.329E+06	.647E+06	.318E+06	-.21117E+00	.10911E+00	-.10205E+00
6	-.312E+06	.636E+06	.324E+06	-.19405E+00	.12457E+00	-.73486E-01
7	-.294E+06	.628E+06	.334E+06	-.19460E+00	.93378E-01	-.10522E+00
8	-.281E+06	.620E+06	.339E+06	-.15317E+00	.91108E-01	-.62062E-01
9	-.266E+06	.610E+06	.344E+06	-.16591E+00	.10751E+00	-.58403E-01
10	-.247E+06	.602E+06	.355E+06	-.21914E+00	.92622E-01	-.12652E+00
11	-.233E+06	.594E+06	.361E+06	-.16410E+00	.93062E-01	-.71037E-01
12	-.224E+06	.584E+06	.360E+06	-.10467E+00	.11615E+00	-.11475E-01
13	-.213E+06	.576E+06	.363E+06	-.12019E+00	.95815E-01	-.24372E-01
14	-.199E+06	.570E+06	.371E+06	-.15819E+00	.66521E-01	-.41064E-01
15	-.190E+06	.561E+06	.371E+06	-.10283E+00	.10145E+00	-.13777E-02
16	-.176E+06	.554E+06	.377E+06	-.16029E+00	.86040E-01	-.74248E-01
17	-.162E+06	.547E+06	.385E+06	-.16366E+00	.77132E-01	-.86529E-01
18	-.152E+06	.535E+06	.377E+06	-.47334E-01	.14083E+00	.95496E-01
19	-.147E+06	.527E+06	.379E+06	-.12192E+00	.90182E-01	-.31743E-01
20	-.142E+06	.519E+06	.376E+06	-.56052E-01	.91552E-01	.35500E-01
21	-.135E+06	.519E+06	.384E+06	-.87746E-01	-.32953E-02	-.91041E-01
22	-.128E+06	.512E+06	.384E+06	-.80550E-01	.84947E-01	.43972E-02
23	-.123E+06	.506E+06	.383E+06	-.50788E-01	.64461E-01	.13694E-01
24	-.129E+06	.498E+06	.370E+06	.62218E-01	.88843E-01	.15106E+00
25	-.136E+06	.489E+06	.353E+06	.84717E-01	.99889E-01	.18461E+00
26	-.155E+06	.476E+06	.321E+06	.22604E+00	.14986E+00	.37191E+00
27	-.179E+06	.465E+06	.286E+06	.27574E+00	.12582E+00	.40155E+00
28	-.191E+06	.455E+06	.263E+06	.13639E+00	.12295E+00	.25934E+00
29	-.195E+06	.442E+06	.247E+06	.39972E-01	.14845E+00	.18442E+00
30	-.188E+06	.433E+06	.244E+06	-.73606E-01	.10421E+00	.30607E-01
31	-.180E+06	.422E+06	.242E+06	-.96055E-01	.12358E+00	.27523E-01
32	-.171E+06	.411E+06	.240E+06	-.10690E+00	.12441E+00	.17513E-01
33	-.152E+06	.398E+06	.247E+06	-.21752E+00	.14232E+00	-.75240E-01
34	-.133E+06	.385E+06	.252E+06	-.21424E+00	.15089E+00	-.63353E-01
35	-.114E+06	.378E+06	.264E+06	-.22005E+00	.84529E-01	-.13552E+00
36	-.922E+05	.365E+06	.273E+06	-.24866E+00	.14572E+00	-.10274E+00
37	-.675E+05	.354E+06	.287E+06	-.28401E+00	.12333E+00	-.16068E+00
38	-.536E+05	.347E+06	.293E+06	-.15999E+00	.86266E-01	-.73720E-01
39	-.502E+05	.337E+06	.287E+06	-.38765E-01	.11390E+00	.75136E-01
40	-.568E+05	.325E+06	.268E+06	.75259E-01	.13585E+00	.21111E+00
41	-.518E+05	.313E+06	.261E+06	-.57118E-01	.14447E+00	.87349E-01
42	-.451E+05	.303E+06	.258E+06	-.77614E-01	.11322E+00	.35600E-01
43	-.409E+05	.292E+06	.251E+06	-.47565E-01	.12284E+00	.75327E-01
44	-.400E+05	.275E+06	.235E+06	-.10703E-01	.19387E+00	.18316E+00
45	-.405E+05	.255E+06	.214E+06	.48967E-02	.23421E+00	.23910E+00
46	-.388E+05	.246E+06	.208E+06	-.19465E-01	.93886E-01	.74420E-01
47	-.380E+05	.236E+06	.202E+06	-.56601E-01	.12006E+00	.63462E-01
48	-.361E+05	.226E+06	.189E+06	.23646E-01	.11930E+00	.14294E+00
49	-.335E+05	.214E+06	.181E+06	-.29348E-01	.19125E+00	.10185E+00
50	-.222E+05	.200E+06	.178E+06	-.13042E+00	.15926E+00	.28839E-01

σ = 1.01 - 0.01 * Level.

Q are layer values (Q (level 2) refers to layer 1-2).

Table A.3 continued.

Level	FF_{q_T} gr s^{-3}	FF_{s_1} gr s^{-3}	FF_h gr s^{-3}	Q_1 m^2 s^{-3}	Q_2 m^2 s^{-3}	Q_3 m^2 s^{-3}
51	-.900E+04	.184E+06	.175E+06	-.15171E+00	.18676E+00	.35046E-01
52	-.309E+04	.168E+06	.165E+06	-.68232E-01	.18473E+00	.11650E+00
53	-.274E+04	.154E+06	.151E+06	-.43751E-02	.15732E+00	.15295E+00
54	-.282E+04	.139E+06	.136E+06	.78320E-03	.17338E+00	.17416E+00
55	-.346E+04	.118E+06	.114E+06	.72964E-02	.24483E+00	.25213E+00
56	.444E+02	.104E+06	.104E+06	-.40305E-01	.15581E+00	.11550E+00
57	.663E+03	.889E+05	.896E+ 5	-.73410E-02	.17269E+00	.16535E+00
58	-.108E+04	.791E+05	.780E+05	.19672E-01	.11254E+00	.13221E+00
59	-.101E+04	.700E+05	.690E+05	-.10543E-02	.10440E+00	.10334E+00
60	-.659E+03	.615E+05	.608E+05	-.41773E-02	.97677E-01	.93500E-01
61	-.648E+03	.544E+05	.537E+05	-.30975E-03	.81882E-01	.81572E-01
62	-.118E+03	.470E+05	.468E+05	-.62917E-02	.84866E-01	.78575E-01
63	-.749E+03	.410E+05	.402E+05	.70452E-02	.68739E-01	.75784E-01
64	-.125E+04	.332E+05	.319E+05	.55388E-02	.89231E-01	.94820E-01
65	-.137E+04	.235E+05	.221E+05	.12208E-02	.11066E+00	.11188E+00
66	-.270E+04	.136E+05	.109E+05	.15176E-01	.11383E+00	.12900E+00
67	-.250E+04	.411E+04	.161E+04	-.24177E-03	.10852E+00	.10610E+00
68	-.183E+04	-.409E+04	-.592E+04	-.76842E-02	.93915E-01	.86231E-01
69	-.142E+04	-.135E+05	-.149E+05	-.47142E-02	.10748E+00	.10277E+00
70	-.122E+04	-.193E+05	-.205E+05	-.23206E-02	.66987E-01	.64666E-01
71	-.940E+03	-.250E+05	-.260E+05	-.32947E-02	.65685E-01	.62390E-01
72	-.667E+03	-.308E+05	-.315E+05	-.31496E-02	.66700E-01	.63550E-01
73	-.290E+03	-.350E+05	-.353E+05	-.43603E-02	.48053E-01	.43693E-01
74	.219E+02	-.394E+05	-.394E+05	-.35979E-02	.50884E-01	.47287E-01
75	.322E+03	-.417E+05	-.413E+05	-.34702E-02	.26426E-01	.22955E-01
76	.524E+03	-.421E+05	-.416E+05	-.23293E-02	.53123E-02	.29830E-02
77	.648E+03	-.425E+05	-.419E+05	-.14403E-02	.58669E-02	.44266E-02
78	.719E+03	-.441E+05	-.434E+05	-.83521E-03	.18339E-01	.17503E-01
79	.759E+03	-.508E+05	-.500E+05	-.47020E-03	.77415E-01	.76944E-01
80	.782E+03	-.552E+05	-.544E+05	-.28685E-03	.51336E-01	.51049E-01
81	.710E+03	-.580E+05	-.572E+05	.81338E-03	.31959E-01	.32772E-01
82	.530E+03	-.576E+05	-.571E+05	.20614E-02	-.32431E-02	-.11817E-02
83	.372E+03	-.442E+05	-.438E+05	.17973E-02	-.15349E+00	-.15170E+00
84	.369E+03	-.395E+05	-.391E+05	.14400E-02	-.20391E+00	-.20247E+00
85	.288E+03	-.382E+05	-.379E+05	.92525E-03	-.14677E-01	-.13752E-01
86	.185E+03	-.326E+05	-.324E+05	.11767E-02	-.63558E-01	-.62381E-01
87	.160E+03	-.360E+05	-.358E+05	.14317E-02	-.21886E+00	-.21743E+00
88	.171E+03	-.162E+05	-.160E+05	.11773E-02	-.35111E+00	-.34993E+00
	.0	.0	.0	.19518E-02	-.18455E+00	-.18260E+00

$\sigma = 1.01 - 0.01 * \text{Level}$.

Q are layer values (Q (level 2) refers to layer 1-2).

Table A.3 continued.

Level	Lq $m^2\ s^{-2}$	s $m^2\ s^{-2}$	h $m^2\ s^{-2}$	$\pi\dot{\sigma}$ $mb\ s^{-1}$	$\sigma\dot{\pi}$ $mb\ s^{-1}$
0				0.	-.67401E-03
1	.20081E+05	.31507E+06	.33515E+06	-.28396E-03	-.96159E-03
2	.19056E+05	.31505E+06	.33410E+06	-.69373E-03	-.11858E-02
3	.18583E+05	.31507E+06	.33366E+06	-.11449E-02	-.13367E-02
4	.18184E+05	.31516E+06	.33334E+06	-.15643E-02	-.13594E-02
5	.17690E+05	.31524E+06	.33293E+06	-.19344E-02	-.12908E-02
6	.17191E+05	.31525E+06	.33244E+06	-.22549E-02	-.12610E-02
7	.16898E+05	.31530E+06	.33220E+06	-.25412E-02	-.12373E-02
8	.16623E+05	.31541E+06	.33203E+06	-.28147E-02	-.11906E-02
9	.16308E+05	.31544E+06	.33175E+06	-.30742E-02	-.11494E-02
10	.16098E+05	.31548E+06	.33157E+06	-.33137E-02	-.11205E-02
11	.15951E+05	.31561E+06	.33156E+06	-.35282E-02	-.10900E-02
12	.15741E+05	.31567E+06	.33141E+06	-.37309E-02	-.10487E-02
13	.15464E+05	.31568E+06	.33114E+06	-.39440E-02	-.98121E-03
14	.15191E+05	.31575E+06	.33094E+06	-.41645E-02	-.94088E-03
15	.14795E+05	.31577E+06	.33057E+06	-.43774E-02	-.75413E-03
16	.14459E+05	.31580E+06	.33029E+06	-.45668E-02	-.67473E-03
17	.14326E+05	.31595E+06	.33028E+06	-.47320E-02	-.58116E-03
18	.14072E+05	.31604E+06	.33011E+06	-.48880E-02	-.49569E-03
19	.13880E+05	.31616E+06	.33004E+06	-.50376E-02	-.40345E-03
20	.13609E+05	.31625E+06	.32986E+06	-.51844E-02	-.33081E-03
21	.13394E+05	.31649E+06	.32988E+06	-.53278E-02	-.29384E-03
22	.13159E+05	.31667E+06	.32983E+06	-.54560E-02	-.24148E-03
23	.12855E+05	.31675E+06	.32961E+06	-.55704E-02	-.15372E-03
24	.12523E+05	.31686E+06	.32938E+06	-.56744E-02	-.21640E-04
25	.12112E+05	.31693E+06	.32905E+06	-.57761E-02	.10567E-03
26	.11843E+05	.31694E+06	.32883E+06	-.58717E-02	.20454E-03
27	.11444E+05	.31710E+06	.32854E+06	-.59329E-02	.32788E-03
28	.11041E+05	.31728E+06	.32832E+06	-.59334E-02	.48750E-03
29	.10594E+05	.31743E+06	.32803E+06	-.58804E-02	.60588E-03
30	.10186E+05	.31764E+06	.32783E+06	-.57985E-02	.68900E-03
31	.98232E+04	.31783E+06	.32766E+06	-.56998E-02	.79317E-03
32	.93754E+04	.31804E+06	.32742E+06	-.55851E-02	.93358E-03
33	.88753E+04	.31825E+06	.32712E+06	-.54565E-02	.10743E-02
34	.83683E+04	.31840E+06	.32677E+06	-.53052E-02	.12268E-02
35	.78251E+04	.31852E+06	.32645E+06	-.51046E-02	.13037E-02
36	.72096E+04	.31885E+06	.32606E+06	-.48705E-02	.13150E-02
37	.68581E+04	.31914E+06	.32600E+06	-.46585E-02	.12653E-02
38	.66967E+04	.31943E+06	.32603E+06	-.45091E-02	.12852E-02
39	.63084E+04	.31979E+06	.32610E+06	-.44004E-02	.13063E-02
40	.58753E+04	.32019E+06	.32606E+06	-.42659E-02	.12497E-02
41	.53370E+04	.32053E+06	.32587E+06	-.41263E-02	.11596E-02
42	.48308E+04	.32087E+06	.32571E+06	-.40352E-02	.10736E-02
43	.42567E+04	.32130E+06	.32556E+06	-.39979E-02	.95777E-03
44	.37539E+04	.32188E+06	.32563E+06	-.40229E-02	.90885E-03
45	.33417E+04	.32231E+06	.32565E+06	-.41003E-02	.89635E-03
46	.31101E+04	.32276E+06	.32587E+06	-.41982E-02	.94618E-03
47	.28089E+04	.32323E+06	.32604E+06	-.43007E-02	.10165E-02
48	.25246E+04	.32373E+06	.32625E+06	-.44273E-02	.11127E-02
49	.22257E+04	.32423E+06	.32646E+06	-.45717E-02	.11205E-02
50	.20521E+04	.32473E+06	.32678E+06	-.46832E-02	.10761E-02

$\sigma = 1.0 - 0.01 * \text{Level}.$

Table A.3 continued.

Level	Lq	s	h	$\pi\dot{\sigma}$	$\sigma\dot{\pi}$
	$m^2\ s^{-2}$	$m^2\ s^{-2}$	$m^2\ s^{-2}$	$mb\ s^{-1}$	$mb\ s^{-1}$
51	.19313E+04	.32518E+06	.32712E+06	-.47375E-02	.10416E-02
52	.18332E+04	.32581E+06	.32744E+06	-.47843E-02	.10193E-02
53	.17383E+04	.32647E+06	.32780E+06	-.48757E-02	.10418E-02
54	.16212E+04	.32657E+06	.32819E+06	-.49600E-02	.10518E-02
55	.14552E+04	.32698E+06	.32843E+06	-.49341E-02	.10413E-02
56	.13545E+04	.32744E+06	.32879E+06	-.48380E-02	.10650E-02
57	.12818E+04	.32775E+06	.32903E+06	-.46965E-02	.10890E-02
58	.11727E+04	.32814E+06	.32931E+06	-.45053E-02	.10957E-02
59	.10663E+04	.32857E+06	.32963E+06	-.43792E-02	.11486E-02
60	.96364E+03	.32896E+06	.32993E+06	-.42980E-02	.12169E-02
61	.83868E+03	.32936E+06	.33020E+06	-.41644E-02	.12609E-02
62	.72507E+03	.32973E+06	.33045E+06	-.40202E-02	.13076E-02
63	.62761E+03	.33014E+06	.33077E+06	-.39021E-02	.13480E-02
64	.53390E+03	.33053E+06	.33107E+06	-.38290E-02	.13640E-02
65	.45988E+03	.33096E+06	.33142E+06	-.38201E-02	.13987E-02
66	.37420E+03	.33143E+06	.33180E+06	-.37621E-02	.13871E-02
67	.30441E+03	.33192E+06	.33222E+06	-.36122E-02	.13651E-02
68	.26257E+03	.33249E+06	.33275E+06	-.34433E-02	.14410E-02
69	.23308E+03	.33303E+06	.33326E+06	-.32946E-02	.15073E-02
70	.20429E+03	.33358E+06	.33378E+06	-.31660E-02	.15318E-02
71	.17896E+03	.33421E+06	.33439E+06	-.29735E-02	.15232E-02
72	.15507E+03	.33486E+06	.33502E+06	-.27109E-02	.15245E-02
73	.13432E+03	.33559E+06	.33573E+06	-.24755E-02	.15401E-02
74	.11475E+03	.33633E+06	.33645E+06	-.22363E-02	.15386E-02
75	.98596E+02	.33716E+06	.33726E+06	-.20041E-02	.14768E-02
76	.85060E+02	.33814E+06	.33822E+06	-.18297E-02	.13559E-02
77	.74991E+02	.33944E+06	.33951E+06	-.17685E-02	.13858E-02
78	.69032E+02	.34131E+06	.34134E+06	-.17177E-02	.13046E-02
79	.63792E+02	.34327E+06	.34333E+06	-.14682E-02	.12024E-02
80	.59133E+02	.34522E+06	.34528E+06	-.10423E-02	.11549E-02
81	.57245E+02	.34748E+06	.34754E+06	-.65047E-03	.10942E-02
82	.54237E+02	.34969E+06	.34975E+06	-.48276E-03	.10359E-02
83	.53353E+02	.35225E+06	.35230E+06	-.38329E-03	.88377E-03
84	.63410E+02	.35602E+06	.35603E+06	-.48960E-03	.63581E-03
85	.60862E+02	.35927E+06	.35933E+06	-.14556E-03	.54283E-03
86	.57970E+02	.36262E+06	.36268E+06	.71777E-04	.56235E-03
87	.47221E+02	.36562E+06	.36567E+06	.10971E-03	.67667E-03
88	.78913E+02	.37433E+06	.37441E+06	-.43230E-04	.39624E-03

$\sigma = 1.0 - 0.01 *Level$

Table A.3 Precipitating Convection. Data and Derived Quantities.

Level	u m s^{-1}	v m s^{-1}	p mb	T °K	q gr/gr	z m
0			.85615E+03	.30225E+03	.94755E-02	.14386E+04
1	-.16861E+01	.10014E+01	.84759E+03	.30131E+03	.80326E-02	.15275E+04
2	-.23132E+01	.91546E+00	.83903E+03	.30040E+03	.76226E-02	.16169E+04
3	-.26306E+01	.10916E+01	.83047E+03	.29954E+03	.74333E-02	.17070E+04
4	-.25712E+01	.11856E+01	.82191E+03	.29873E+03	.72735E-02	.17977E+04
5	-.25228E+01	.11948E+01	.81335E+03	.29792E+03	.70760E-02	.18892E+04
6	-.24131E+01	.13219E+01	.80479E+03	.29702E+03	.68764E-02	.19813E+04
7	-.23337E+01	.14211E+01	.79623E+03	.29616E+03	.67594E-02	.20742E+04
8	-.22323E+01	.14448E+01	.78766E+03	.29534E+03	.66494E-02	.21678E+04
9	-.21507E+01	.14548E+01	.77910E+03	.29445E+03	.65232E-02	.22621E+04
10	-.20770E+01	.15098E+01	.77054E+03	.29355E+03	.64391E-02	.23572E+04
11	-.20368E+01	.14909E+01	.76198E+03	.29274E+03	.63803E-02	.24531E+04
12	-.19256E+01	.15489E+01	.75342E+03	.29185E+03	.62964E-02	.25498E+04
13	-.17770E+01	.15318E+01	.74486E+03	.29090E+03	.61857E-02	.26473E+04
14	-.15671E+01	.12278E+01	.73630E+03	.29001E+03	.60763E-02	.27456E+04
15	-.14525E+01	.10196E+01	.72774E+03	.28905E+03	.59180E-02	.28447E+04
16	-.12800E+01	.95477E+00	.71918E+03	.28810E+03	.57837E-02	.29447E+04
17	-.10310E+01	.94660E+00	.71062E+03	.28726E+03	.57305E-02	.30455E+04
18	-.83236E+00	.87669E+00	.70206E+03	.28634E+03	.56288E-02	.31473E+04
19	-.61743E+00	.78527E+00	.69350E+03	.28545E+03	.55519E-02	.32500E+04
20	-.45359E+00	.69671E+00	.68494E+03	.28452E+03	.54434E-02	.33536E+04
21	-.35682E+00	.68414E+00	.67638E+03	.28373E+03	.53575E-02	.34582E+04
22	-.24387E+00	.61008E+00	.66782E+03	.28287E+03	.52635E-02	.35638E+04
23	-.41511E-01	.48294E+00	.65925E+03	.28191E+03	.51418E-02	.36705E+04
24	.27856E+00	.29354E+00	.65069E+03	.28096E+03	.50093E-02	.37782E+04
25	.62911E+00	.16956E+00	.64213E+03	.27996E+03	.48449E-02	.38869E+04
26	.99158E+00	.16383E+00	.63357E+03	.27894E+03	.47373E-02	.39967E+04
27	.13454E+01	.96202E-01	.62501E+03	.27794E+03	.45774E-02	.41076E+04
28	.17910E+01	-.11894E+00	.61645E+03	.27704E+03	.44164E-02	.42197E+04
29	.21611E+01	-.23688E+00	.60789E+03	.27608E+03	.42377E-02	.43329E+04
30	.24744E+01	-.25287E+00	.59933E+03	.27516E+03	.40744E-02	.44473E+04
31	.28866E+01	-.24547E+00	.59077E+03	.27421E+03	.39293E-02	.45630E+04
32	.34030E+01	-.31028E+00	.58221E+03	.27327E+03	.37502E-02	.46800E+04
33	.39114E+01	-.42309E+00	.57365E+03	.27231E+03	.35501E-02	.47983E+04
34	.44595E+01	-.57528E+00	.56509E+03	.27129E+03	.33473E-02	.49179E+04
35	.49089E+01	-.40909E+00	.55652E+03	.27032E+03	.31300E-02	.50390E+04
36	.51281E+01	-.21894E+00	.54796E+03	.26934E+03	.28839E-02	.51614E+04
37	.51625E+01	.65171E-01	.53940E+03	.26842E+03	.27432E-02	.52854E+04
38	.53816E+01	.17754E+00	.53084E+03	.26748E+03	.26387E-02	.54109E+04
39	.55237E+01	.11831E+00	.52228E+03	.26658E+03	.25234E-02	.55380E+04
40	.54020E+01	.15168E+00	.51372E+03	.26572E+03	.23501E-02	.56668E+04
41	.52728E+01	.44525E+00	.50516E+03	.26478E+03	.21348E-02	.57973E+04
42	.50977E+01	.64085E+00	.49660E+03	.26382E+03	.19323E-02	.59295E+04
43	.48897E+01	.70976E+00	.48804E+03	.26293E+03	.17027E-02	.60636E+04
44	.46889E+01	.92668E+00	.47948E+03	.26217E+03	.15016E-02	.61996E+04
45	.47452E+01	.10046E+01	.47091E+03	.26124E+03	.13367E-02	.63376E+04
46	.50630E+01	.10357E+01	.46235E+03	.26032E+03	.12441E-02	.64777E+04
47	.54113E+01	.92415E+00	.45379E+03	.25939E+03	.11236E-02	.66199E+04
48	.58275E+01	.68028E+00	.44523E+03	.25847E+03	.10099E-02	.67643E+04
49	.59923E+01	.72408E+00	.43667E+03	.25754E+03	.89027E-03	.69109E+04
50	.59780E+01	.90529E+00	.42811E+03	.25657E+03	.82082E-03	.70600E+04

σ = 1.0 - 0.01 * Level.

Table A.3 continued.

Level	u m s^{-1}	v m s^{-1}	p mb	T °K	q gr/gr	z m
51	.59491E+01	.97593E+00	.41955E+03	.25553E+03	.77250E-03	.72114E+04
52	.59738E+01	.10356E+01	.41099E+03	.25445E+03	.73329E-03	.73653E+04
53	.61999E+01	.10309E+01	.40243E+03	.25337E+03	.69533E-03	.75218E+04
54	.63534E+01	.99094E+00	.39386E+03	.25230E+03	.64846E-03	.76810E+04
55	.65373E+01	.12141E+01	.38530E+03	.25112E+03	.58709E-03	.78429E+04
56	.68125E+01	.12333E+01	.37674E+03	.24996E+03	.54179E-03	.80077E+04
57	.70745E+01	.12081E+01	.36818E+03	.24862E+03	.51270E-03	.81755E+04
58	.73159E+01	.13212E+01	.35962E+03	.24733E+03	.46907E-03	.83463E+04
59	.77133E+01	.11675E+01	.35106E+03	.24605E+03	.42652E-03	.85203E+04
60	.83632E+01	.12832E+01	.34250E+03	.24470E+03	.38546E-03	.86977E+04
61	.89687E+01	.15544E+01	.33393E+03	.24333E+03	.33547E-03	.88785E+04
62	.98425E+01	.22539E+01	.32537E+03	.24188E+03	.29003E-03	.90630E+04
63	.10574E+02	.27100E+01	.31681E+03	.24044E+03	.25104E-03	.92513E+04
64	.11080E+02	.29963E+01	.30825E+03	.23894E+03	.21356E-03	.94435E+04
65	.11885E+02	.35734E+01	.29969E+03	.23744E+03	.18395E-03	.96399E+04
66	.12154E+02	.37074E+01	.29113E+03	.23593E+03	.14988E-03	.98407E+04
67	.12384E+02	.38959E+01	.28257E+03	.23440E+03	.12176E-03	.10046E+05
68	.13323E+02	.39834E+01	.27400E+03	.23290E+03	.10503E-03	.10257E+05
69	.14080E+02	.37531E+01	.26544E+03	.23132E+03	.93231E-04	.10472E+05
70	.14530E+02	.34775E+01	.25688E+03	.22970E+03	.81715E-04	.10692E+05
71	.14924E+02	.35525E+01	.24832E+03	.22810E+03	.71584E-04	.10921E+05
72	.15484E+02	.37464E+01	.23976E+03	.22646E+03	.62029E-04	.11154E+05
73	.16427E+02	.43549E+01	.23119E+03	.22483E+03	.53727E-04	.11394E+05
74	.17062E+02	.45754E+01	.22263E+03	.22314E+03	.45900E-04	.11642E+05
75	.16901E+02	.42953E+01	.21407E+03	.22146E+03	.39438E-04	.11897E+05
76	.16355E+02	.44561E+01	.20551E+03	.21984E+03	.34024E-04	.12161E+05
77	.17228E+02	.43548E+01	.19695E+03	.21846E+03	.29996E-04	.12434E+05
78	.16741E+02	.38668E+01	.18838E+03	.21756E+03	.27613E-04	.12717E+05
79	.16104E+02	.36266E+01	.17982E+03	.21661E+03	.25517E-04	.13013E+05
80	.15976E+02	.31616E+01	.17126E+03	.21553E+03	.23653E-04	.13322E+05
81	.15876E+02	.30273E+01	.16270E+03	.21463E+03	.22898E-04	.13645E+05
82	.16440E+02	.40810E+01	.15413E+03	.21351E+03	.21695E-04	.13984E+05
83	.15243E+02	.43976E+01	.14557E+03	.21256E+03	.21341E-04	.14340E+05
84	.13137E+02	.60818E+01	.13692E+03	.21298E+03	.25364E-04	.14683E+05
85	.10967E+02	.86398E+01	.12836E+03	.21229E+03	.24345E-04	.15085E+05
86	.11568E+02	.29431E+01	.11980E+03	.21144E+03	.23188E-04	.15513E+05
87	.11541E+02-.26484E+01		.11107E+03	.20920E+03	.18888E-04	.16047E+05
88	.70767E+01-.23583E+01		.10295E+03	.21414E+03	.31565E-04	.16434E+05

α = 1.0 - 0.01 * Level.

Table A.4 continued

Level	u m/s	v m/s	p mb	T °K	q gr/gr	z m
51	.90479E+01	.35580E+01	.41656E+03	.25487E+03	.74717E-03	.71870E+04
52	.10085E+02	.37021E+01	.40806E+03	.25378E+03	.71179E-03	.73406E+04
53	.10780E+02	.38934E+01	.39956E+03	.25274E+03	.68049E-03	.74966E+04
54	.11556E+02	.43808E+01	.39106E+03	.25158E+03	.68224E-03	.76554E+04
55	.12358E+02	.48110E+01	.38256E+03	.25044E+03	.65645E-03	.78170E+04
56	.13016E+02	.51263E+01	.37406E+03	.24922E+03	.61402E-03	.79814E+04
57	.13168E+02	.53759E+01	.36556E+03	.24794E+03	.55636E-03	.81487E+04
58	.12930E+02	.53757E+01	.35705E+03	.24668E+03	.47320E-03	.83191E+04
59	.13228E+02	.54356E+01	.34855E+03	.24534E+03	.41416E-03	.84928E+04
60	.14431E+02	.50061E+01	.34005E+03	.24394E+03	.37698E-03	.86697E+04
61	.15800E+02	.44214E+01	.33155E+03	.24251E+03	.33155E-03	.88500E+04
62	.15763E+02	.43436E+01	.32305E+03	.24102E+03	.28709E-03	.90339E+04
63	.15539E+02	.44778E+01	.31455E+03	.23948E+03	.25439E-03	.92217E+04
64	.16008E+02	.46481E+01	.30605E+03	.23795E+03	.22886E-03	.94133E+04
65	.16419E+02	.47251E+01	.29755E+03	.23640E+03	.20088E-03	.96089E+04
66	.17157E+02	.47570E+01	.28905E+03	.23488E+03	.17724E-03	.98091E+04
67	.17222E+02	.56022E+01	.28054E+03	.23311E+03	.15285E-03	.10014E+05
68	.17016E+02	.67896E+01	.27204E+03	.23130E+03	.13052E-03	.10223E+05
69	.17461E+02	.72400E+01	.26354E+03	.22952E+03	.11162E-03	.10437E+05
70	.17560E+02	.81081E+01	.25504E+03	.22759E+03	.93622E-04	.10657E+05
71	.17193E+02	.88709E+01	.24654E+03	.22567E+03	.78020E-04	.10882E+05
72	.17920E+02	.86756E+01	.23804E+03	.22397E+03	.66166E-04	.11113E+05
73	.19500E+02	.82127E+01	.22954E+03	.22251E+03	.57813E-04	.11351E+05
74	.19491E+02	.81151E+01	.22103E+03	.22105E+03	.50932E-04	.11597E+05
75	.18749E+02	.80975E+01	.21253E+03	.21957E+03	.45532E-04	.11850E+05
76	.19553E+02	.81196E+01	.20403E+03	.21836E+03	.41627E-04	.12112E+05
77	.20880E+02	.78667E+01	.19553E+03	.21779E+03	.40685E-04	.12384E+05
78	.23391E+02	.66770E+01	.18703E+03	.21772E+03	.43562E-04	.12668E+05
79	.25967E+02	.47877E+01	.17853E+03	.21767E+03	.47058E-04	.12965E+05
80	.24248E+02	.51159E+01	.17002E+03	.21726E+03	.48069E-04	.13276E+05
81	.21502E+02	.50051E+01	.16152E+03	.21693E+03	.48552E-04	.13603E+05
82	.13176E+02	.94015E+01	.15299E+03	.21764E+03	.53441E-04	.13926E+05
83	.13231E+02	.10163E+02	.14449E+03	.21714E+03	.52549E-04	.14291E+05
84	.13809E+02	.10271E+02	.13599E+03	.21619E+03	.49917E-04	.14675E+05
85	.11902E+02	.10015E+02	.12749E+03	.21480E+03	.46134E-04	.15083E+05
86	.80730E+01	.57691E+01	.11814E+03	.21215E+03	.32352E-04	.15575E+05
87	.11995E+02	.34180E+00	.10840E+03	.20836E+03	.90999E-05	.16234E+05

$\sigma = 1.0 - 0.01 * \text{Level}.$

Table A.4 Moderate Convection. Data and Derived Quantities.

Level	u m/s	v m/s	p mb	T °K	q gr/gr	z m
0			.85006E+03	.30028E+03	.78615E-02	.14442E+04
1	-.17163E+01	.43789E+01	.84156E+03	.29953E+03	.72725E-02	.15326E+04
2	-.21994E+01	.48711E+01	.83306E+03	.29871E+03	.71294E-02	.16214E+04
3	-.24787E+01	.53726E+01	.82456E+03	.29767E+03	.69250E-02	.17110E+04
4	-.27071E+01	.58875E+01	.81606E+03	.29677E+03	.67895E-02	.18011E+04
5	-.28403E+01	.58308E+01	.80756E+03	.29595E+03	.66925E-02	.18920E+04
6	-.28411E+01	.59365E+01	.79907E+03	.29503E+03	.64981E-02	.19835E+04
7	-.27198E+01	.59960E+01	.79057E+03	.29418E+03	.63326E-02	.20757E+04
8	-.24880E+01	.58749E+01	.78207E+03	.29327E+03	.62187E-02	.21687E+04
9	-.23040E+01	.57372E+01	.77357E+03	.29231E+03	.61051E-02	.22624E+04
10	-.20541E+01	.54809E+01	.76507E+03	.29135E+03	.59526E-02	.23567E+04
11	-.16850E+01	.53012E+01	.75657E+03	.29048E+03	.58382E-02	.24519E+04
12	-.14572E+01	.53732E+01	.74807E+03	.28960E+03	.57100E-02	.25478E+04
13	-.14160E+01	.55572E+01	.73957E+03	.28865E+03	.55859E-02	.26445E+04
14	-.13034E+01	.54327E+01	.73107E+03	.28774E+03	.55877E-02	.27421E+04
15	-.10243E+01	.51567E+01	.72257E+03	.28697E+03	.54630E-02	.28404E+04
16	-.52716E+00	.47345E+01	.71407E+03	.28596E+03	.52589E-02	.29397E+04
17	-.45743E-01	.45330E+01	.70557E+03	.28514E+03	.52166E-02	.30398E+04
18	.36314E+00	.44370E+01	.69707E+03	.28438E+03	.51972E-02	.31408E+04
19	.80812E+00	.43931E+01	.68857E+03	.28345E+03	.51023E-02	.32428E+04
20	.10640E+01	.41574E+01	.68007E+03	.28248E+03	.50227E-02	.33456E+04
21	.11810E+01	.37436E+01	.67157E+03	.28151E+03	.49046E-02	.34495E+04
22	.13534E+01	.33249E+01	.66307E+03	.28069E+03	.48221E-02	.35543E+04
23	.16123E+01	.28046E+01	.65457E+03	.27973E+03	.46478E-02	.36601E+04
24	.19601E+01	.24221E+01	.64607E+03	.27884E+03	.44383E-02	.37669E+04
25	.22600E+01	.21763E+01	.63757E+03	.27801E+03	.42406E-02	.38749E+04
26	.26999E+01	.18852E+01	.62907E+03	.27715E+03	.41242E-02	.39840E+04
27	.30987E+01	.16291E+01	.62057E+03	.27624E+03	.39755E-02	.40942E+04
28	.35650E+01	.15434E+01	.61207E+03	.27531E+03	.38019E-02	.42055E+04
29	.41378E+01	.15282E+01	.60357E+03	.27447E+03	.36655E-02	.43180E+04
30	.46982E+01	.13138E+01	.59507E+03	.27356E+03	.35185E-02	.44318E+04
31	.50527E+01	.11111E+01	.58657E+03	.27254E+03	.33344E-02	.45468E+04
32	.53597E+01	.10996E+01	.57807E+03	.27161E+03	.31149E-02	.46630E+04
33	.57344E+01	.96121E+00	.56957E+03	.27074E+03	.29797E-02	.47806E+04
34	.58528E+01	.75580E+00	.56107E+03	.26994E+03	.27328E-02	.48996E+04
35	.59132E+01	.81071E+00	.55257E+03	.26913E+03	.25821E-02	.50201E+04
36	.63421E+01	.99936E+00	.54407E+03	.26827E+03	.24369E-02	.51420E+04
37	.66629E+01	.13348E+01	.53557E+03	.26736E+03	.23048E-02	.52654E+04
38	.64550E+01	.13879E+01	.52707E+03	.26653E+03	.21633E-02	.53905E+04
39	.63592E+01	.14757E+01	.51857E+03	.26572E+03	.20173E-02	.55171E+04
40	.61141E+01	.17710E+01	.51007E+03	.26486E+03	.18760E-02	.56455E+04
41	.61963E+01	.20716E+01	.50156E+03	.26389E+03	.16431E-02	.57755E+04
42	.66745E+01	.21683E+01	.49306E+03	.26304E+03	.14882E-02	.59073E+04
43	.71225E+01	.22965E+01	.48456E+03	.26223E+03	.13345E-02	.60410E+04
44	.73254E+01	.24879E+01	.47606E+03	.26158E+03	.12137E-02	.61767E+04
45	.75876E+01	.25676E+01	.46756E+03	.26088E+03	.11260E-02	.63145E+04
46	.78156E+01	.26514E+01	.45906E+03	.26006E+03	.10706E-02	.64544E+04
47	.80997E+01	.28046E+01	.45056E+03	.25919E+03	.96772E-03	.65964E+04
48	.82362E+01	.30950E+01	.44206E+03	.25823E+03	.87641E-03	.67407E+04
49	.84790E+01	.37930E+01	.43356E+03	.25714E+03	.81179E-03	.68872E+04
50	.83310E+01	.36706E+01	.42506E+03	.25600E+03	.77810E-03	.70360E+04

$\sigma = 1.0 - 0.01 * \text{Level}$.

Table A.4 continued.

Level	Lq $m^2 s^{-2}$	s $m^2 s^{-2}$	h $m^2 s^{-2}$	$\Pi\dot{\sigma}$ $mb\ s^{-1}$	$\sigma\dot{\Pi}$ $mb\ s^{-1}$
0				0.	-.14392E-02
1	.18181E+05	.31335E+06	.33153E+06	-.21243E-03	-.17624E-02
2	.17824E+05	.31340E+06	.33123E+06	-.49640E-03	-.20461E-02
3	.17312E+05	.31324E+06	.33056E+06	-.82974E-03	-.22441E-02
4	.16974E+05	.31324E+06	.33021E+06	-.11892E-02	-.23789E-02
5	.16731E+05	.31331E+06	.33004E+06	-.15587E-02	-.24377E-02
6	.16245E+05	.31328E+06	.32953E+06	-.19257E-02	-.24340E-02
7	.15831E+05	.31334E+06	.32917E+06	-.23085E-02	-.23745E-02
8	.15547E+05	.31335E+06	.32890E+06	-.27075E-02	-.22374E-02
9	.15263E+05	.31331E+06	.32857E+06	-.30927E-02	-.21164E-02
10	.14882E+05	.31329E+06	.32817E+06	-.34440E-02	-.19496E-02
11	.14595E+05	.31335E+06	.32794E+06	-.37531E-02	-.17585E-02
12	.14275E+05	.31341E+06	.32769E+06	-.40407E-02	-.16717E-02
13	.13965E+05	.31341E+06	.32737E+06	-.43180E-02	-.16740E-02
14	.13969E+05	.31346E+06	.32743E+06	-.45774E-02	-.15938E-02
15	.13656E+05	.31350E+06	.32722E+06	-.48208E-02	-.14240E-02
16	.13147E+05	.31362E+06	.32677E+06	-.50376E-02	-.11576E-02
17	.13042E+05	.31383E+06	.32687E+06	-.51999E-02	-.94342E-03
18	.12993E+05	.31403E+06	.32702E+06	-.52956E-02	-.77816E-03
19	.12756E+05	.31410E+06	.32686E+06	-.53286E-02	-.61427E-03
20	.12557E+05	.31414E+06	.32669E+06	-.53165E-02	-.48197E-03
21	.12261E+05	.31419E+06	.32645E+06	-.52785E-02	-.36606E-03
22	.12055E+05	.31440E+06	.32645E+06	-.52361E-02	-.23553E-03
23	.11619E+05	.31448E+06	.32610E+06	-.51907E-02	-.63673E-04
24	.11096E+05	.31464E+06	.32574E+06	-.51130E-02	.10829E-03
25	.10602E+05	.31487E+06	.32547E+06	-.49979E-02	.23848E-03
26	.10310E+05	.31509E+06	.32540E+06	-.48772E-02	.41492E-03
27	.99387E+04	.31526E+06	.32520E+06	-.47930E-02	.56816E-03
28	.95046E+04	.31543E+06	.32493E+06	-.47394E-02	.71016E-03
29	.91639E+04	.31569E+06	.32486E+06	-.46829E-02	.86859E-03
30	.87963E+04	.31589E+06	.32469E+06	-.46127E-02	.10492E-02
31	.83359E+04	.31601E+06	.32435E+06	-.45269E-02	.11641E-02
32	.77872E+04	.31622E+06	.32401E+06	-.44262E-02	.12337E-02
33	.74492E+04	.31654E+06	.32399E+06	-.43286E-02	.13385E-02
34	.68308E+04	.31685E+06	.32371E+06	-.42395E-02	.13797E-02
35	.64552E+04	.31725E+06	.32371E+06	-.41259E-02	.13658E-02
36	.60922E+04	.31759E+06	.32368E+06	-.40011E-02	.14289E-02
37	.57619E+04	.31769E+06	.32365E+06	-.39331E-02	.14408E-02
38	.54206E+04	.31829E+06	.32371E+06	-.39356E-02	.13577E-02
39	.50431E+04	.31873E+06	.32377E+06	-.39526E-02	.13007E-02
40	.46899E+04	.31912E+06	.32381E+06	-.39580E-02	.11799E-02
41	.41078E+04	.31944E+06	.32355E+06	-.39745E-02	.11390E-02
42	.37205E+04	.31988E+06	.32360E+06	-.40147E-02	.12180E-02
43	.33361E+04	.32039E+06	.32372E+06	-.40901E-02	.12830E-02
44	.30342E+04	.32106E+06	.32410E+06	-.42279E-02	.12822E-02
45	.28149E+04	.32172E+06	.32454E+06	-.44430E-02	.13082E-02
46	.26764E+04	.32227E+06	.32495E+06	-.47190E-02	.13244E-02
47	.24193E+04	.32280E+06	.32522E+06	-.49947E-02	.13433E-02
48	.21910E+04	.32326E+06	.32545E+06	-.51999E-02	.13137E-02
49	.20245E+04	.32351E+06	.32564E+06	-.52769E-02	.12591E-02
50	.19452E+04	.32393E+06	.32588E+06	-.53207E-02	.12169E-02

$\sigma = 1.0 - 0.01 * \text{Level}$.

Table A.4 *Continued*

Level	Lq $m^2\ s^{-2}$	s $m^2\ s^{-2}$	h $m^2\ s^{-2}$	$\Pi\dot{\sigma}$ $mb\ s^{-1}$	$\sigma\dot{\Pi}$ $mb\ s^{-1}$
51	.18679E+04	.32428E+06	.32615E+06	-.54640E-02	.13452E-02
52	.17795E+04	.32470E+06	.32648E+06	-.56860E-02	.15021E-02
53	.17012E+04	.32520E+06	.32690E+06	-.59245E-02	.15713E-02
54	.17056E+04	.32560E+06	.32730E+06	-.61265E-02	.16410E-02
55	.16411E+04	.32604E+06	.32768E+06	-.63109E-02	.17067E-02
56	.15350E+04	.32644E+06	.32797E+06	-.64856E-02	.17543E-02
57	.13909E+04	.32681E+06	.32820E+06	-.66014E-02	.17164E-02
58	.11830E+04	.32722E+06	.32840E+06	-.66477E-02	.16357E-02
59	.10354E+04	.32759E+06	.32863E+06	-.66652E-02	.16401E-02
60	.94245E+03	.32793E+06	.32887E+06	-.67071E-02	.18333E-02
61	.82888E+03	.32827E+06	.32910E+06	-.67589E-02	.20536E-02
62	.71771E+03	.32859E+06	.32931E+06	-.67283E-02	.20011E-02
63	.63597E+03	.32889E+06	.32953E+06	-.65429E-02	.19038E-02
64	.57216E+03	.32925E+06	.32983E+06	-.62885E-02	.19067E-02
65	.50219E+03	.32962E+06	.33012E+06	-.59285E-02	.19062E-02
66	.44309E+03	.33007E+06	.33051E+06	-.54025E-02	.19503E-02
67	.38211E+03	.33031E+06	.33069E+06	-.48757E-02	.18391E-02
68	.32631E+03	.33050E+06	.33084E+06	-.43695E-02	.16715E-02
69	.27906E+03	.33089E+06	.33117E+06	-.38941E-02	.16423E-02
70	.23406E+03	.33112E+06	.33135E+06	-.35716E-02	.15423E-02
71	.19505E+03	.33142E+06	.33161E+06	-.32432E-02	.13990E-02
72	.16541E+03	.33198E+06	.33215E+06	-.28742E-02	.14450E-02
73	.14453E+03	.33286E+06	.33301E+06	-.26486E-02	.15932E-02
74	.12733E+03	.33381E+06	.33394E+06	-.23981E-02	.15394E-02
75	.11383E+03	.33482E+06	.33494E+06	-.20362E-02	.14080E-02
76	.10407E+03	.33619E+06	.33629E+06	-.16358E-02	.14305E-02
77	.10171E+03	.33826E+06	.33838E+06	-.12827E-02	.15094E-02
78	.10890E+03	.34100E+06	.34110E+06	-.10820E-02	.17262E-02
79	.11764E+03	.34385E+06	.34397E+06	-.96534E-03	.19546E-02
80	.12017E+03	.34649E+06	.34661E+06	-.87117E-03	.17090E-02
81	.12138E+03	.34937E+06	.34949E+06	-.56111E-03	.14186E-02
82	.13360E+03	.35325E+06	.35338E+06	-.41021E-03	.57271E-03
83	.13137E+03	.35632E+06	.35645E+06	-.28070E-03	.51736E-03
84	.12479E+03	.35914E+06	.35927E+06	-.35199E-03	.52211E-03
85	.11533E+03	.36175E+06	.36187E+06	-.22159E-03	.38340E-03
86	.80879E+02	.36393E+06	.36401E+06	.87623E-04	.26606E-03
87	.22750E+02	.36662E+06	.36664E+06	.43144E-03	.61515E-03

$\alpha = 1.0 - 0.01 * \text{Level}$.

Table A.4 continued.

Level	FF_{q_T} gr s^{-3}	FF_{s_1} gr s^{-3}	FF_h gr s^{-3}	Q_1 m^2 s^{-3}	Q_2 m^2 s^{-3}	Q_3 m^2 s^{-3}
1	-.170E+06	.352E+06	.182E+06			
2	-.167E+06	.344E+06	.177E+06	-.33908E-01	.91426E-01	.57519E-01
3	-.171E+06	.333E+06	.162E+06	.50089E-01	.12555E+00	.17564E+00
4	-.174E+06	.323E+06	.149E+06	.34046E-01	.11952E+00	.15357E+00
5	-.173E+06	.312E+06	.137E+06	-.13012E-01	.13018E+00	.11717E+00
6	-.170E+06	.299E+06	.129E+06	-.31385E-01	.15012E+00	.11873E+00
7	-.162E+06	.287E+06	.126E+06	-.91704E-01	.13294E+00	.41240E-01
8	-.155E+06	.273E+06	.118E+06	-.77433E-01	.10417E+00	.86733E-01
9	-.148E+06	.260E+06	.112E+06	-.75107E-01	.14985E+00	.74742E-01
10	-.143E+06	.250E+06	.107E+06	-.59744E-01	.11626E+00	.56514E-01
11	-.135E+06	.239E+06	.104E+06	-.82459E-01	.12476E+00	.42304E-01
12	-.131E+06	.227E+06	.967E+05	-.55430E-01	.13415E+00	.78721E-01
13	-.127E+06	.217E+06	.894E+05	-.34325E-01	.11988E+00	.85558E-01
14	-.132E+06	.208E+06	.766E+05	.51204E-01	.96015E-01	.14722E+00
15	-.148E+06	.196E+06	.483E+05	.15201E+00	.13911E+00	.32512E+00
16	-.135E+06	.183E+06	.484E+05	-.15173E+00	.15127E+00	-.45705E-03
17	-.108E+06	.177E+06	.686E+05	-.30628E+00	.74940E-01	-.23134E+00
18	-.103E+06	.164E+06	.611E+05	-.59700E-01	.14859E+00	.88488E-01
19	-.102E+06	.155E+06	.526E+05	.81504E-03	.99469E-01	.10028E+00
20	-.979E+05	.150E+06	.524E+05	-.50319E-01	.53405E-01	.30861E-02
21	-.932E+05	.147E+06	.535E+05	-.52219E-01	.40049E-01	-.12171E-01
22	-.874E+05	.143E+06	.556E+05	-.85596E-01	.41200E-01	-.24396E-01
23	-.854E+05	.139E+06	.481E+05	-.22729E-01	.10968E+00	.86951E-01
24	-.793E+05	.134E+06	.549E+05	-.68041E-01	-.84669E-02	-.76508E-01
25	-.646E+05	.129E+06	.646E+05	-.16705E+00	.57912E-01	-.10913E+00
26	-.614E+05	.112E+06	.509E+05	-.35212E-01	.19296E+00	.15775E+00
27	-.692E+05	.988E+05	.296E+05	.93108E-01	.15388E+00	.24698E+00
28	-.734E+05	.946E+05	.212E+05	.51012E-01	.48238E-01	.99250E-01
29	-.837E+05	.857E+05	.234E+04	.11[illegible]E+00	.10[illegible]E+00	.22[illegible]E+00
30	-.942E+05	.769E+05	-.173E+05	.12617E+00	.10090E+00	.22737E+00
31	-.103E+06	.669E+05	-.365E+05	.10592E+00	.11361E+00	.21952E+00
32	-.112E+06	.636E+05	-.481E+05	.94613E-01	.37547E-01	.13216E+00
33	-.110E+06	.531E+05	-.573E+05	-.13297E-01	.11951E+00	.10622E+00
34	-.106E+06	.375E+05	-.686E+05	-.47853E-01	.17855E+00	.13120E+00
35	-.106E+06	.210E+05	-.848E+05	-.36356E-02	.18883E+00	.18519E+00
36	-.111E+06	.322E+04	-.107E+06	.54445E-01	.20436E+00	.25920E+00
37	-.108E+06	-.108E+05	-.119E+06	-.25573E-01	.16048E+00	.13191E+00
38	-.111E+06	-.246E+05	-.136E+06	.33944E-01	.15848E+00	.19243E+00
39	-.111E+06	-.444E+05	-.155E+06	.76487E-03	.22681E+00	.22758E+00
40	-.105E+06	-.635E+05	-.168E+06	-.66729E-01	.21776E+00	.15103E+00
41	-.103E+06	-.817E+05	-.185E+06	-.25406E-01	.20963E+00	.18422E+00
42	-.950E+05	-.945E+05	-.190E+06	-.90095E-01	.14731E+00	.57217E-01
43	-.950E+05	-.110E+06	-.205E+06	.26489E-03	.17732E+00	.17759E+00
44	-.916E+05	-.130E+06	-.222E+06	-.42263E-01	.23543E+00	.19316E+00
45	-.872E+05	-.154E+06	-.242E+06	-.51445E-01	.28065E+00	.22921E+00
46	-.844E+05	-.176E+06	-.261E+06	-.31627E-01	.25098E+00	.21935E+00
47	-.816E+05	-.186E+06	-.267E+06	-.31121E-01	.11153E+00	.80405E-01
48	-.806E+05	-.190E+06	-.271E+06	-.10419E-01	.50763E-01	.40344E-01
49	-.824E+05	-.192E+06	-.275E+06	.23496E-01	.18907E-01	.42403E-01
50	-.777E+05	-.191E+06	-.269E+06	-.54698E-01	-.14034E-01	-.68732E-01

σ = 1.01 - 0.01 * Level.

Q are layer values (Q (level 2) refers to layer 1-2).

Table A.4 continued.

Level	FF_{q_T} gr s^{-3}	FF_{s_1} gr s^{-3}	FF_h gr s^{-3}	Q_1 m^2 s^{-3}	Q_2 m^2 s^{-3}	Q_3 m^2 s^{-3}
51	-.722E+05	-.191E+06	-.263E+06	-.63666E-01	-.10085E-01	-.73751E-01
52	-.657E+05	-.194E+06	-.260E+06	-.75362E-01	.36223E-01	-.39139E-01
53	-.588E+05	-.202E+06	-.260E+06	-.79352E-01	.84903E-01	.55517E-02
54	-.549E+05	-.215E+06	-.270E+06	-.46327E-01	.15746E+00	.11113E+00
55	-.548E+05	-.227E+06	-.282E+06	-.44601E-03	.13305E+00	.13251E+00
56	-.526E+05	-.240E+06	-.293E+06	-.25711E-01	.15247E+00	.12676E+00
57	-.495E+05	-.249E+06	-.299E+06	-.34235E-01	.10408E+00	.67843E-01
58	-.463E+05	-.257E+06	-.304E+06	-.37650E-01	.87144E-01	.49494E-01
59	-.387E+05	-.265E+06	-.304E+06	-.87526E-01	.85820E-01	-.17064E-02
60	-.317E+05	-.271E+06	-.303E+06	-.80565E-01	.73223E-01	-.73422E-02
61	-.268E+05	-.276E+06	-.303E+06	-.56857E-01	.56892E-01	.34834E-04
62	-.212E+05	-.279E+06	-.300E+06	-.64502E-01	.26477E-01	-.38025E-01
63	-.158E+05	-.278E+06	-.293E+06	-.62058E-01	-.16787E-01	-.78845E-01
64	-.119E+05	-.271E+06	-.283E+06	-.45034E-01	-.82979E-01	-.12801E+00
65	-.844E+04	-.262E+06	-.270E+06	-.39875E-01	-.10521E+00	-.14509E+00
66	-.462E+04	-.254E+06	-.259E+06	-.43983E-01	-.91516E-01	-.13550E+00
67	-.252E+04	-.253E+06	-.256E+06	-.24258E-01	-.16257E-01	-.40515E-01
68	-.120E+04	-.238E+06	-.239E+06	-.15374E-01	-.17422E+00	-.18960E+00
69	-.448E+03	-.229E+06	-.228E+06	-.86528E-02	-.12391E+00	-.13256E+00
70	-.312E+02	-.210E+06	-.210E+06	-.48197E-02	-.10658E+00	-.11140E+00
71	.435E+03	-.201E+06	-.201E+06	-.54068E-02	-.19878E+00	-.20419E+00
72	.822E+03	-.185E+06	-.184E+06	-.44945E-02	-.19301E+00	-.19750E+00
73	.879E+03	-.177E+06	-.176E+06	-.64917E-03	-.92221E-01	-.92870E-01
74	.798E+03	-.166E+06	-.167E+06	-.92461E-03	-.98660E-01	-.97735E-01
75	.851E+03	-.148E+06	-.147E+06	-.61497E-03	-.23215E+00	-.23277E+00
76	.875E+03	-.125E+06	-.124E+06	-.30849E-03	-.26915E+00	-.26946E+00
77	.512E+03	-.120E+06	-.120E+06	.41545E-02	-.61479E-01	-.57325E-01
78	.306E+02	-.126E+06	-.126E+06	.62046E-02	.57299E-01	.63508E-01
79	-.415E+03	-.126E+06	-.127E+06	.44197E-02	-.11791E-02	.32405E-02
80	-.541E+03	-.109E+06	-.109E+06	.14535E-02	-.20977E+00	-.20832E+00
81	-.456E+03	-.743E+05	-.748E+05	-.94791E-03	-.40092E+00	-.40187E+00
82	-.436E+03	-.555E+05	-.559E+05	-.12119E-02	-.34010E+00	-.34931E+00
83	-.246E+03	-.495E+05	-.499E+05	-.21656E-02	-.68062E-01	-.70228E-01
84	-.393E+02	-.376E+05	-.376E+05	-.23734E-02	-.13884E+00	-.14121E+00
85	.122E+03	-.214E+05	-.213E+05	-.18551E-02	-.18751E+00	-.18936E+00
86	.301E+03	-.203E+05	-.200E+05	-.32233E-03	-.12893E+00	-.12925E+00
87	.134E+02	-.345E+05	-.345E+05	.33836E-02	-.35521E-01	-.32138E-01
	.0	.0	.0	.15747E-03	-.40566E+00	-.40551E+00

σ = 1.01 - 0.01 * Level.

Q are layer values (Q (level 2) refers to layer 1-2).

Table A.5 Suppressed Convection. Data and Derived Quantities.
(13 July excluded.)

Level	u m s^{-1}	v m s^{-1}	p mb	T °K	q gr/gr	z m
0			.85892E+03	.29891E+03	.9495AE-02	.14213E+04
1	.18136E+00	.19958E+00	.85034E+03	.29717E+03	.86105E-02	.15090E+04
2	.29439E+00	.15240E+00	.84175E+03	.29607E+03	.85401E-02	.15972E+04
3	.29049E+00	.81736E-01	.83316E+03	.29523E+03	.84363E-02	.16859E+04
4	.26551E+00	-.74938E-02	.82457E+03	.29439E+03	.82881E-02	.17753E+04
5	.21348E+00	-.11814E+00	.81598E+03	.29357E+03	.81526E-02	.18654E+04
6	.11249E+00	-.14357E+00	.80739E+03	.29282E+03	.80565E-02	.19563E+04
7	.18339E-01	-.16556E+00	.79880E+03	.29207E+03	.78834E-02	.20478E+04
8	.12593E+00	-.36519E-01	.79021E+03	.29129E+03	.76797E-02	.21401E+04
9	.24433E+00	.10393E+00	.78163E+03	.29051E+03	.74399E-02	.22331E+04
10	.43401E+00	.15203E+00	.77304E+03	.28971E+03	.73263E-02	.23270E+04
11	.69535E+00	.19519E+00	.76445E+03	.28892E+03	.71864E-02	.24216E+04
12	.96129E+00	.28458E+00	.75586E+03	.28822E+03	.70807E-02	.25170E+04
13	.12551E+01	.43319E+00	.74727E+03	.28752E+03	.68948E-02	.26133E+04
14	.15285E+01	.63676E+00	.73868E+03	.28671E+03	.65892E-02	.27104E+04
15	.18719E+01	.96568E+00	.73009E+03	.28590E+03	.63946E-02	.28084E+04
16	.22965E+01	.12129E+01	.72150E+03	.28518E+03	.61526E-02	.29074E+04
17	.27694E+01	.12983E+01	.71291E+03	.28439E+03	.58702E-02	.30072E+04
18	.32019E+01	.12709E+01	.70432E+03	.28371E+03	.56025E-02	.31079E+04
19	.35986E+01	.12465E+01	.69574E+03	.28304E+03	.53487E-02	.32097E+04
20	.39971E+01	.12685E+01	.68715E+03	.28243E+03	.51487E-02	.33125E+04
21	.42970E+01	.13640E+01	.67856E+03	.28170E+03	.49264E-02	.34163E+04
22	.45027E+01	.14208E+01	.66997E+03	.28096E+03	.47295E-02	.35212E+04
23	.47126E+01	.13622E+01	.66138E+03	.28023E+03	.45482E-02	.36272E+04
24	.48660E+01	.13708E+01	.65279E+03	.27944E+03	.43413E-02	.37343E+04
25	.51954E+01	.14839E+01	.64420E+03	.27861E+03	.41045E-02	.38424E+04
26	.54885E+01	.15759E+01	.63561E+03	.27777E+03	.39391E-02	.39517E+04
27	.57628E+01	.16021E+01	.62702E+03	.27685E+03	.37200E-02	.40621E+04
28	.60117E+01	.16622E+01	.61844E+03	.27598E+03	.35023E-02	.41737E+04
29	.63397E+01	.15144E+01	.60985E+03	.27508E+03	.33654E-02	.42864E+04
30	.69160E+01	.14245E+01	.60126E+03	.27409E+03	.31813E-02	.44004E+04
31	.75958E+01	.98722E+00	.59267E+03	.27311E+03	.29742E-02	.45156E+04
32	.82587E+01	.66687E+00	.58408E+03	.27214E+03	.28155E-02	.46321E+04
33	.86902E+01	.17949E+00	.57549E+03	.27120E+03	.26902E-02	.47498E+04
34	.90276E+01	-.58767E+00	.56690E+03	.27028E+03	.25818E-02	.48690E+04
35	.95271E+01	-.10424E+01	.55831E+03	.26933E+03	.23970E-02	.49895E+04
36	.10248E+02	-.98578E+00	.54972E+03	.26843E+03	.21215E-02	.51115E+04
37	.10505E+02	-.84622E+00	.54113E+03	.26755E+03	.18309E-02	.52350E+04
38	.10532E+02	-.56270E+00	.53254E+03	.26664E+03	.15822E-02	.53601E+04
39	.10549E+02	-.13351E+00	.52396E+03	.26578E+03	.13421E-02	.54867E+04
40	.10643E+02	.45528E+00	.51537E+03	.26502E+03	.11231E-02	.56151E+04
41	.10882E+02	.10296E+01	.50678E+03	.26413E+03	.92624E-03	.57452E+04
42	.11090E+02	.14728E+01	.49819E+03	.26334E+03	.73644E-03	.58771E+04
43	.11283E+02	.17177E+01	.48960E+03	.26256E+03	.60490E-03	.60109E+04
44	.11151E+02	.17577E+01	.48101E+03	.26173E+03	.49538E-03	.61467E+04
45	.11145E+02	.19764E+01	.47242E+03	.26087E+03	.45188E-03	.62845E+04
46	.11110E+02	.20036E+01	.46383E+03	.25992E+03	.42626E-03	.64242E+04
47	.11109E+02	.19447E+01	.45524E+03	.25901E+03	.41833E-03	.65661E+04
48	.11205E+02	.17891E+01	.44665E+03	.25801E+03	.41675E-03	.67102E+04
49	.11431E+02	.17380E+01	.43806E+03	.25697E+03	.40995E-03	.68565E+04
50	.11739E+02	.20720E+01	.42947E+03	.25589E+03	.39134E-03	.70050E+04

$\sigma = 1.0 - 0.01 * \text{Level}.$

Table A.5 *continued.*

Level	u m s^{-1}	v m s^{-1}	p mb	T K	q gr/gr	z m
51	.11760E+02	.23110E+01	.42089E+03	.25477E+03	.37612E-03	.71560E+04
52	.11724E+02	.28381E+01	.41230E+03	.25359E+03	.35019E-03	.73093E+04
53	.11585E+02	.31884E+01	.40371E+03	.25245E+03	.33037E-03	.74657E+04
54	.12461E+02	.35493E+01	.39512E+03	.25134E+03	.30934E-03	.76237E+04
55	.12757E+02	.43969E+01	.38653E+03	.25012E+03	.28547E-03	.77849E+04
56	.12775E+02	.46607E+01	.37794E+03	.24890E+03	.27179E-03	.79489E+04
57	.13223E+02	.51164E+01	.36935E+03	.24763E+03	.26657E-03	.81159E+04
58	.13386E+02	.56052E+01	.36076E+03	.24624E+03	.25462E-03	.82859E+04
59	.13698E+02	.60778E+01	.35217E+03	.24479E+03	.23604E-03	.84590E+04
60	.13735E+02	.63145E+01	.34358E+03	.24338E+03	.22114E-03	.86353E+04
61	.13755E+02	.64027E+01	.33499E+03	.24197E+03	.20789E-03	.88151E+04
62	.14050E+02	.60765E+01	.32640E+03	.24047E+03	.19260E-03	.89983E+04
63	.14924E+02	.59455E+01	.31781E+03	.23896E+03	.17585E-03	.91854E+04
64	.15817E+02	.59190E+01	.30923E+03	.23746E+03	.15785E-03	.93763E+04
65	.16532E+02	.56518E+01	.30064E+03	.23599E+03	.13959E-03	.95714E+04
66	.16874E+02	.51638E+01	.29205E+03	.23450E+03	.12560E-03	.97709E+04
67	.17016E+02	.47483E+01	.28346E+03	.23290E+03	.11174E-03	.99750E+04
68	.18040E+02	.45331E+01	.27487E+03	.23133E+03	.98546E-04	.10184E+05
69	.18891E+02	.44328E+01	.26628E+03	.22977E+03	.86350E-04	.10398E+05
70	.19697E+02	.42087E+01	.25769E+03	.22828E+03	.75915E-04	.10616E+05
71	.19828E+02	.40697E+01	.24910E+03	.22688E+03	.67112E-04	.10843E+05
72	.20422E+02	.45159E+01	.24051E+03	.22568E+03	.60686E-04	.11076E+05
73	.20995E+02	.48120E+01	.23193E+03	.22456E+03	.56002E-04	.11315E+05
74	.21696E+02	.55752E+01	.22333E+03	.22339E+03	.51829E-04	.11563E+05
75	.21881E+02	.55843E+01	.21474E+03	.22232E+03	.48264E-04	.11818E+05
76	.21208E+02	.43499E+01	.20615E+03	.22090E+03	.43492E-04	.12083E+05
77	.20153E+02	.30310E+01	.19756E+03	.21932E+03	.38687E-04	.12357E+05
78	.18867E+02	.25527E+01	.18897E+03	.21799E+03	.36050E-04	.12641E+05
79	.17584E+02	.36422E+01	.18038E+03	.21692E+03	.34449E-04	.12937E+05
80	.16878E+02	.51955E+01	.17179E+03	.21605E+03	.33335E-04	.13247E+05
81	.15591E+02	.65237E+01	.16320E+03	.21535E+03	.32445E-04	.13570E+05
82	.14909E+02	.70621E+01	.15461E+03	.21499E+03	.31583E-04	.13911E+05
83	.15307E+02	.68295E+01	.14602E+03	.21436E+03	.30621E-04	.14270E+05
84	.14342E+02	.68601E+01	.13756E+03	.21527E+03	.46627E-04	.14605E+05
85	.12503E+02	.74013E+01	.12896E+03	.21467E+03	.45367E-04	.15011E+05
86	.10349E+02	.47353E+01	.12036E+03	.21329E+03	.40199E-04	.15443E+05
87	.61136E+01	.22704E+01	.11176E+03	.21244E+03	.39901E-04	.15904E+05
88	.66630E+00	.67295E+01	.10288E+03	.21401E+03	.54435E-04	.16463E+05

$\sigma = 1.0 - 0.01 * \text{Level}.$

Table A.5 continued.

Level	Lq $m^2\ s^{-2}$	s $m^2\ s^{-2}$	h $m^2\ s^{-2}$	$\pi\dot{\sigma}$ $mb\ s^{-1}$	$\sigma\dot{\pi}$ $mb\ s^{-1}$
0				0.	-.10319E-03
1	.21526E+05	.31076E+06	.33229E+06	-.48445E-04	-.16563E-03
2	.21350E+05	.31054E+06	.33184E+06	-.77040E-04	-.20039E-03
3	.21091E+05	.31057E+06	.33166E+06	-.78311E-04	-.18009E-03
4	.20720E+05	.31061E+06	.33133E+06	-.47789E-04	-.14949E-03
5	.20381E+05	.31067E+06	.33105E+06	-.14869E-04	-.10574E-03
6	.20141E+05	.31082E+06	.33096E+06	.64855E-05	-.58513E-04
7	.19708E+05	.31097E+06	.33064E+06	.10942E-04	-.56902E-05
8	.19199E+05	.31110E+06	.33030E+06	-.17550E-04	.98637E-05
9	.18600E+05	.31123E+06	.32983E+06	-.92382E-04	.27102E-04
10	.18316E+05	.31135E+06	.32967E+06	-.22186E-03	.88915E-04
11	.17966E+05	.31150E+06	.32946E+06	-.39777E-03	.17697E-03
12	.17702E+05	.31173E+06	.32944E+06	-.60995E-03	.25643E-03
13	.17247E+05	.31198E+06	.32922E+06	-.83676E-03	.33201E-03
14	.16473E+05	.31212E+06	.32859E+06	-.10577E-02	.38487E-03
15	.15986E+05	.31228E+06	.32826E+06	-.12664E-02	.44490E-03
16	.15381E+05	.31253E+06	.32791E+06	-.14594E-02	.54217E-03
17	.14675E+05	.31273E+06	.32740E+06	-.16460E-02	.68501E-03
18	.14006E+05	.31303E+06	.32704E+06	-.18438E-02	.83053E-03
19	.13372E+05	.31340E+06	.32677E+06	-.20339E-02	.95947E-03
20	.12872E+05	.31377E+06	.32664E+06	-.21821E-02	.10764E-02
21	.12316E+05	.31406E+06	.32637E+06	-.22951E-02	.11450E-02
22	.11824E+05	.31434E+06	.32616E+06	-.23946E-02	.11878E-02
23	.11366E+05	.31466E+06	.32602E+06	-.24850E-02	.12144E-02
24	.10853E+05	.31496E+06	.32581E+06	-.25609E-02	.12131E-02
25	.10261E+05	.31515E+06	.32541E+06	-.26246E-02	.12785E-02
26	.98479E+04	.31539E+06	.32523E+06	-.26804E-02	.13514E-02
27	.93000E+04	.31555E+06	.32485E+06	-.27380E-02	.14249E-02
28	.87558E+04	.31578E+06	.32453E+06	-.28128E-02	.14755E-02
29	.84136E+04	.31598E+06	.32440E+06	-.29197E-02	.15600E-02
30	.79533E+04	.31612E+06	.32408E+06	-.30297E-02	.17640E-02
31	.74356E+04	.31627E+06	.32371E+06	-.30827E-02	.19969E-02
32	.70387E+04	.31644E+06	.32348E+06	-.30909E-02	.21993E-02
33	.67256E+04	.31667E+06	.32339E+06	-.30955E-02	.23572E-02
34	.64545E+04	.31692E+06	.32337E+06	-.30796E-02	.25256E-02
35	.59936E+04	.31715E+06	.32314E+06	-.30175E-02	.26866E-02
36	.53036E+04	.31745E+06	.32275E+06	-.29839E-02	.28275E-02
37	.45773E+04	.31778E+06	.32236E+06	-.27001E-02	.28312E-02
38	.39554E+04	.31810E+06	.32206E+06	-.25328E-02	.27551E-02
39	.33551E+04	.31849E+06	.32184E+06	-.23545E-02	.26572E-02
40	.28078E+04	.31898E+06	.32179E+06	-.21031E-02	.25593E-02
41	.23156E+04	.31938E+06	.32170E+06	-.18169E-02	.24884E-02
42	.18411E+04	.31988E+06	.32172E+06	-.16130E-02	.24526E-02
43	.15122E+04	.32042E+06	.32193E+06	-.15534E-02	.24253E-02
44	.12385E+04	.32093E+06	.32216E+06	-.15671E-02	.23500E-02
45	.11296E+04	.32142E+06	.32255E+06	-.15860E-02	.22846E-02
46	.10656E+04	.32184E+06	.32291E+06	-.16074E-02	.22355E-02
47	.10458E+04	.32232E+06	.32337E+06	-.16002E-02	.22012E-02
48	.10419E+04	.32274E+06	.32374E+06	-.15878E-02	.21977E-02
49	.10249E+04	.32313E+06	.32416E+06	-.16119E-02	.22086E-02
50	.97836E+03	.32352E+06	.32450E+06	-.16394E-02	.21943E-02

$\sigma = 1.0 - 0.01 * \text{Level}.$

Table A.5 continued.

Level	Lq $m^2\ s^{-2}$	s $m^2\ s^{-2}$	h $m^2\ s^{-2}$	$\pi\dot{\sigma}$ $mb\ s^{-1}$	$\sigma\dot{\pi}$ $mb\ s^{-1}$
51	.94030E+03	.32388E+06	.32482E+06	-.16897E-02	.21317E-02
52	.87547E+03	.32421E+06	.32508E+06	-.17543E-02	.20282E-02
53	.82592E+03	.32460E+06	.32543E+06	-.18392E-02	.19294E-02
54	.77336E+03	.32504E+06	.32582E+06	-.18918E-02	.20154E-02
55	.71368E+03	.32542E+06	.32613E+06	-.18235E-02	.19456E-02
56	.67944E+03	.32580E+06	.32648E+06	-.17650E-02	.18852E-02
57	.66643E+03	.32618E+06	.32684E+06	-.17614E-02	.18798E-02
58	.63654E+03	.32646E+06	.32709E+06	-.17738E-02	.18282E-02
59	.59020E+03	.32671E+06	.32730E+06	-.17810E-02	.17858E-02
60	.55285E+03	.32703E+06	.32758E+06	-.16910E-02	.17272E-02
61	.51972E+03	.32739E+06	.32791E+06	-.14800E-02	.16781E-02
62	.48149E+03	.32769E+06	.32817E+06	-.12818E-02	.17083E-02
63	.43962E+03	.32802E+06	.32846E+06	-.11307E-02	.18033E-02
64	.39462E+03	.32839E+06	.32879E+06	-.95173E-03	.18881E-02
65	.34898E+03	.32885E+06	.32920E+06	-.77697E-03	.19570E-02
66	.31401E+03	.32932E+06	.32963E+06	-.63710E-03	.19838E-02
67	.27934E+03	.32973E+06	.33001E+06	-.50040E-03	.19713E-02
68	.24637E+03	.33021E+06	.33046E+06	-.33397E-03	.20599E-02
69	.21587E+03	.33076E+06	.33097E+06	-.20890E-03	.21110E-02
70	.16979E+03	.33142E+06	.33161E+06	-.15899E-03	.21570E-02
71	.16778E+03	.33224E+06	.33241E+06	-.14179E-03	.21091E-02
72	.15172E+03	.33332E+06	.33347E+06	-.12996E-03	.20766E-02
73	.14001E+03	.33455E+06	.33469E+06	-.14842E-03	.20462E-02
74	.12957E+03	.33561E+06	.33594E+06	-.26576E-03	.19982E-02
75	.12066E+03	.33725E+06	.33737E+06	-.41316E-03	.19361E-02
76	.10873E+03	.33843E+06	.33854E+06	-.41264E-03	.18529E-02
77	.96718E+02	.33954E+06	.33964E+06	-.32144E-03	.17419E-02
78	.90126E+02	.34100E+06	.34109E+06	-.31496E-03	.15733E-02
79	.86122E+02	.34283E+06	.34292E+06	-.28282E-03	.13435E-02
80	.83337E+02	.34501E+06	.34509E+06	-.12044E-03	.11571E-02
81	.81114E+02	.34748E+06	.34756E+06	-.3254E-04	.94577E-03
82	.78957E+02	.35045E+06	.35053E+06	-.11577E-03	.82529E-03
83	.76552E+02	.35335E+06	.35343E+06	-.36527E-04	.81342E-03
84	.11657E+03	.35753E+06	.35765E+06	-.29823E-03	.71648E-03
85	.11342E+03	.36092E+06	.36103E+06	-.12181E-03	.53969E-03
86	.10050E+03	.36378E+06	.36388E+06	.88487E-04	.46178E-03
87	.99751E+02	.36746E+06	.36756E+06	.17569E-03	.27355E-03
88	.13609E+03	.37449E+06	.37463E+06	.13706E-04	-.14245E-03

$\sigma = 1.0 - 0.01 * \text{Level}$.

Table A.5 continued.

Level	FF_{q_T} gr s^{-3}	FF_{s_1} gr s^{-3}	FF_h gr s^{-3}	Q_1 m^2 s^{-3}	Q_2 m^2 s^{-3}	Q_3 m^2 s^{-3}
1	.501E+06	-.153E+06	.347E+06			
2	.504E+06	-.156E+06	.347E+06	-.32566E-01	.32743E-01	.17689E-03
3	.494E+06	-.160E+06	.334E+06	.10754E+00	.43131E-01	.15067E+00
4	.480E+06	-.164E+06	.316E+06	.16569E+00	.41964E-01	.20765E+00
5	.460E+06	-.168E+06	.292E+06	.22290E+00	.50107E-01	.27301E+00
6	.438E+06	-.172E+06	.266E+06	.26618E+00	.44117E-01	.30030E+00
7	.415E+06	-.175E+06	.240E+06	.25773E+00	.37815E-01	.29554E+00
8	.391E+06	-.179E+06	.212E+06	.27443E+00	.40759E-01	.31514E+00
9	.369E+06	-.183E+06	.186E+06	.25862E+00	.41045E-01	.29967E+00
10	.343E+06	-.185E+06	.158E+06	.29710E+00	.31323E-01	.32842E+00
11	.327E+06	-.187E+06	.140E+06	.17551E+00	.22413E-01	.19792E+00
12	.310E+06	-.191E+06	.119E+06	.20136E+00	.41987E-01	.24335E+00
13	.291E+06	-.194E+06	.922E+05	.21900E+00	.85553E-01	.30456E+00
14	.267E+06	-.205E+06	.619E+05	.26851E+00	.76732E-01	.34524E+00
15	.248E+06	-.209E+06	.392E+05	.21530E+00	.44621E-01	.25992E+00
16	.228E+06	-.214E+06	.139E+05	.23275E+00	.55466E-01	.28621E+00
17	.214E+06	-.218E+06	-.378E+04	.15693E+00	.45959E-01	.20289E+00
18	.200E+06	-.221E+06	-.217E+05	.16567E+00	.39348E-01	.20501E+00
19	.191E+06	-.226E+06	-.359E+05	.10525E+00	.56879E-01	.16213E+00
20	.181E+06	-.234E+06	-.524E+05	.10746E+00	.82196E-01	.18966E+00
21	.173E+06	-.239E+06	-.663E+05	.99648E-01	.59757E-01	.15941E+00
22	.165E+06	-.240E+06	-.750E+05	.86092E-01	.13220E-01	.99311E-01
23	.150E+06	-.243E+06	-.928E+05	.16859E+00	.35205E-01	.20379E+00
24	.137E+06	-.246E+06	-.108E+06	.14893E+00	.26796E-01	.17573E+00
25	.128E+06	-.248E+06	-.120E+06	.11066E+00	.24660E-01	.13532E+00
26	.123E+06	-.246E+06	-.123E+06	.50479E-01	-.16833E-01	.33644E-01
27	.118E+06	-.249E+06	-.131E+06	.66301E-01	.29560E-01	.95861E-01
28	.120E+06	-.249E+06	-.128E+06	-.31749E-01	-.99360E-03	-.32743E-01
29	.122E+06	-.251E+06	-.130E+06	-.12211E-01	.26122E-01	.13911E-01
30	.116E+06	-.253E+06	-.137E+06	.62634E-01	.18594E-01	.81228E-01
31	.115E+06	-.252E+06	-.137E+06	.10285E-01	-.86643E-02	.16210E-02
32	.113E+06	-.252E+06	-.140E+06	.29038E-01	.23334E-02	.31371E-01
33	.104E+06	-.253E+06	-.149E+06	.10226E+00	.98034E-02	.11207E+00
34	.875E+05	-.254E+06	-.167E+06	.18580E+00	.11645E-01	.19744E+00
35	.684E+05	-.257E+06	-.189E+06	.21742E+00	.34239E-01	.25216E+00
36	.564E+05	-.257E+06	-.201E+06	.13759E+00	-.84992E-03	.13674E+00
37	.588E+05	-.255E+06	-.196E+06	-.28070E-01	-.23750E-01	-.51819E-01
38	.652E+05	-.256E+06	-.191E+06	-.73518E-01	.15785E-01	-.57733E-01
39	.654E+05	-.258E+06	-.192E+06	-.21046E-02	.19306E-01	.17202E-01
40	.626E+05	-.257E+06	-.195E+06	.31900E-01	-.49182E-02	.26982E-01
41	.567E+05	-.260E+06	-.203E+06	.67723E-01	.23477E-01	.91200E-01
42	.449E+05	-.263E+06	-.218E+06	.13529E+00	.40601E-01	.17589E+00
43	.287E+05	-.262E+06	-.233E+06	.14482E+00	-.11814E-01	.13300E+00
44	.122E+03	-.260E+06	-.248E+06	.14914E+00	-.18565E-01	.13062E+00
45	.491E+04	-.259E+06	-.254E+06	.82813E-01	-.17290E-01	.65522E-01
46	.472E+04	-.258E+06	-.253E+06	.22095E-02	-.11668E-01	-.94555E-02
47	.445E+04	-.257E+06	-.253E+06	.30596E-02	-.57006E-02	-.26410E-02
48	.348E+04	-.260E+06	-.256E+06	.11036E-01	.27326E-01	.38362E-01
49	.230E+03	-.265E+06	-.265E+06	.37029E-01	.60204E-01	.97233E-01
50	.317E+04	-.269E+06	-.272E+06	.38769E-01	.44373E-01	.83142E-01

σ = 1.01 - 0.01 * Level.

Q are layer values (Q (level 2) refers to layer 1-2).

Table A.5 continued.

Level	FF_{q_T} gr s^{-3}	FF_{s_l} gr s^{-3}	FF_h gr s^{-3}	Q_1 m^2 s^{-3}	Q_2 m^2 s^{-3}	Q_3 m^2 s^{-3}
51	-.621E+04	-.270E+06	-.276E+06	.34637E-01	.15133E-01	.49770E-01
52	-.790E+04	-.270E+06	-.278E+06	.19259E-01	.28245E-02	.22083E-01
53	-.862E+04	-.270E+06	-.279E+06	.81398E-02	-.84339E-03	.72965E-02
54	-.843E+04	-.268E+06	-.276E+06	-.22561E-02	-.26561E-01	-.28818E-01
55	-.735E+04	-.266E+06	-.274E+06	-.12443E-01	-.14993E-01	-.27436E-01
56	-.503E+04	-.266E+06	-.271E+06	-.26555E-01	-.10089E-01	-.36657E-01
57	-.319E+04	-.265E+06	-.269E+06	-.21061E-01	.62410E-02	-.14820E-01
58	-.209E+04	-.265E+06	-.267E+06	-.12652E-01	-.11948E-01	-.24592E-01
59	-.216E+04	-.262E+06	-.264E+06	.83505E-03	-.31617E-01	-.30782E-01
60	-.226E+04	-.259E+06	-.262E+06	.98079E-03	-.31502E-01	-.30521E-01
61	-.196E+04	-.259E+06	-.261E+06	-.35003E-02	-.22746E-02	-.57749E-02
62	-.126E+04	-.260E+06	-.261E+06	-.79501E-02	.98705E-02	.19205E-02
63	-.785E+03	-.259E+06	-.260E+06	-.55047E-02	-.78187E-02	-.13323E-01
64	-.568E+03	-.255E+06	-.256E+06	-.25251E-02	-.44148E-01	-.46673E-01
65	-.413E+03	-.252E+06	-.252E+06	-.17069E-02	-.39785E-01	-.41582E-01
66	-.277E+03	-.253E+06	-.253E+06	-.15907E-02	.10335E-01	.87446E-02
67	-.265E+03	-.255E+06	-.255E+06	-.18074E-03	.24667E-01	.24486E-01
68	-.320E+03	-.256E+06	-.257E+06	.60716E-03	.18112E-01	.18719E-01
69	-.383E+03	-.255E+06	-.256E+06	.69238E-03	-.10240E-01	-.95473E-02
70	-.492E+03	-.252E+06	-.252E+06	.12200E-02	-.44855E-01	-.43634E-01
71	-.610E+03	-.245E+06	-.246E+06	.13228E-02	-.70526E-01	-.69203E-01
72	-.770E+03	-.239E+06	-.240E+06	.18079E-02	-.68462E-01	-.66654E-01
73	-.100E+04	-.237E+06	-.238E+06	.26449E-02	-.21711E-01	-.19066E-01
74	-.125E+04	-.235E+06	-.236E+06	.28598E-02	-.25964E-01	-.23104E-01
75	-.137E+04	-.226E+06	-.227E+06	.13398E-02	-.10521E+00	-.10387E+00
76	-.132E+04	-.212E+06	-.213E+06	-.57944E-03	-.16117E+00	-.16175E+00
77	-.115E+04	-.192E+06	-.193E+06	-.19317E-02	-.22574E+00	-.22768E+00
78	-.106E+04	-.168E+06	-.169E+06	-.10842E-02	-.27596E+00	-.27704E+00
79	-.103E+04	-.145E+06	-.146E+06	-.33634E-03	-.26427E+00	-.26461E+00
80	-.844E+03	-.120E+06	-.120E+06	-.21064E-02	-.28465E+00	-.28676E+00
81	-.546E+03	-.901E+05	-.907E+05	-.34048E-02	-.33643E+00	-.33984E+00
82	-.271E+03	-.598E+05	-.601E+05	-.31369E-02	-.34533E+00	-.34847E+00
83	-.171E+03	-.338E+05	-.340E+05	-.11441E-02	-.29644E+00	-.29758E+00
84	-.857E+03	-.739E+05	-.748E+05	.12332E-04	-.21683E+00	-.21682E+00
85	-.591E+03	-.455E+05	-.461E+05	-.30266E-02	-.32525E+00	-.32827E+00
86	-.156E+03	-.202E+05	-.204E+05	-.49630E-02	-.28844E+00	-.29340E+00
87	.156E+03	.686E+03	.842E+03	-.35685E-02	-.23839E+00	-.24196E+00
88	.343E+03	.114E+05	.118E+05	-.18504E-03	-.56774E-01	-.56959E-01
	.0	.0	.0	.39252E-02	.13058E+00	.13450E+00

σ = 1.01 - 0.01 * Level.

Q are layer values (Q (level 2) refers to layer 1-2).

APPENDIX B

DATA NETWORKS USED IN PREVIOUS BUDGET STUDIES

A summary of the data networks used in previous budget studies is presented in Table B.1. The summary is designed to give an overview of the horizontal space resolution, time resolution, and amount of averaging used in earlier budgets. These quantities are of basic importance for the interpretation of budget calculations of unresolved flows.

Table B.1. Summary of Data Networks for Previous Budget Studies.

RESEARCHERS	GENERAL AREA	TIME PERIOD	NUMBER OF CALCULATIONS AVERAGED	RAWINSONDE SPACING (Horizontal)	RAWINSONDE FREQUENCY
Reed and Recker (1971) Cho and Ogura (1974)	Western Pacific 10°N, 165°E	July-Sept. 1967	several hundred (18 disturbances)	composit analysis 3 stations 5-10° spacing	12 hour
Yanai, et al (1973) Ogura and Cho (1973)	Marshall Islands	15 April - 22 July 1956	390 samples	62 x 10^4 km^2 pentagon, 5 sondes	6 hour
Gray (1972) Williams (1970)	Western Pacific and West Indies Belt 5°-25°N	3 summers 1967-1969	several hundred	composit analysis around cloud clusters with 5-10° of latitude sonde spacing	12 hour
Pearce (1968)	10°-25°N 90°-60°W	Aug.-Oct. 1963	5 synoptic periods	5-10° of latitude	12 hour
Augstein, et al (1973)	ATEX 10°N, 37°W	Feb. 1969 undisturbed period	8	750 km	3 hour
Holland & Rasmusson (1973) Nitta and Esbensen (1974) Nitta (1975) Betts (1975)	BOMEX 15°N, 56°W	22-30 June 1969 (3 periods)	30-75	500 km	1.5 hour
Ninomiya (1974)	East China Sea (Kuroshio Region) part of AMTEX	Feb. 1968	6-19	200 km (3 sondes)	12 hour

Table B.1. Continued

RESEARCHERS	GENERAL AREA	TIME PERIOD	NUMBER OF CALCULATIONS AVERAGED	RAWINSONDE SPACING (Horizontal)	RAWINSONDE FREQUENCY
Betts (1973)	VIMHEX I Northeast Venezuela	June-Sept. 1969	50	composit analysis with 1 sonde (400 km^2)	1-2 hour
Fankhauser (1969)	NSSL	28 May 1967	2 case studies	85 km	1.5 hour
Lewis (1975)	200^2 km^2 area Texas, Oklahoma	8 June 1966			
McNab (1976)	NHRE 100^2 km^2 area Northeastern Colorado	June-July 1973	4 sets of ~10	~65 km	2-3 hours

BIBLIOGRAPHIC DATA SHEET	1. Report No. CSU-ATSP-242	2.	3. Recipient's Accession No.

4. Title and Subtitle

MESOSCALE CHARACTERISTICS OF CUMULUS CONVECTION
A Mesoscale Budget Study of Convection in the NHRE Network

5. Report Date: February 1976

6.

7. Author(s): Alan McNab

8. Performing Organization Rept. No. CSU-ATSP-242

9. Performing Organization Name and Address
Department of Atmospheric Science
Foothills Campus
Colorado State University
Fort Collins, Colorado 80523

10. Project/Task/Work Unit No.

11. Contract/Grant No.
NSF OCD72-01406

12. Sponsoring Organization Name and Address
Atmospheric Sciences Section
National Science Foundation
Washington, D. C.

13. Type of Report & Period Covered
Ph.D. Thesis

14.

15. Supplementary Notes

16. Abstracts Water and energy budget descriptions of four broad classifications of summertime cumulus convection occurring over the National Hail Research Experiment (NHRE) area are calculated from NHRE rawinsonde data. A budget equation designed for use with mesoscale data from the NHRE area is derived. The equation uses a normalized pressure coordinate to facilitate calculations at the sloping lower boundary. The environmental variables appear as functions of horizontal position. The change of cloud storage term (usually neglected) is retained for use during intervals of rapid convection development. The budget calculations are based on data for 39 intervals (about three hours long) occurring over 14 days. The data processing takes into account downwind sonde drift and time differences in the data due to sonde rise time and launch time differences. The presence or absence of radar echoes and/or precipitation is used to classify the convection as (1) weak, suppressed; (2) weak, developing; (3) moderate; (4) precipitating. The weak, suppressed average budgets are generally similar to budgets calculated for "undisturbed" synoptic situations. The NHRE vertical velocities, however, are several times larger than the earlier undisturbed values. The weak, developing average budget shows the importance of retaining the change of cloud storage term in the budget equation. The moderate and precipitating average budgets show an introduction of relatively dry air into the subcloud layer. The fluxes show a systematic variation with the trend of the convective classification.

A cloud model is used to show that weak, suppressed convective fluxes can be expressed as the product of a single convective mass flux times a cloud-environment difference. Another cloud model is used to approximate the change of cloud storage, which is as large as the convective flux terms during periods of rapid cumulus convection development. General conclusions are drawn on the quantity and quality of the data needed to generate a useful mesoscale convective budget.

17a. Descriptors

Convective Budgets
Mesoscale Convection
Cumulus Clouds

17b. Identifiers/Open-Ended Terms

NHRE

17c. COSATI Field/Group

18. Availability Statement	19. Security Class (This Report) UNCLASSIFIED	21. No. of Pages 187
	20. Security Class (This Page UNCLASSIFIED	22. Price